University of Leicester

Manganese, Iron and Cobalt Complexes Bearing Multidentate Ligand Sets; Catalysts for Ethylene Oligomerisation/Polymerisation

Thesis submitted for the degree of Doctor of Philosophy

at the University of Leicester

by

Christopher James Davies MChem/USA (Leicester)

Department of Chemistry

University of Leicester

ProQuest LLC
789 East Eisenhower Parkway
P.O. Box 1346
Ann Arbor, MI 48106-1346

Acknowledgments

I would like to take this opportunity to thank first and foremost my PhD supervisor Dr G. A. Solan for his support and constructive input through out the duration of my PhD. Secondly, I would like to thank my industrial supervisor Dr R. Shutt from ExxonMobil for his enthusiastic discussions on Chemistry and related areas.

In addition, I am grateful to Dr J. Fawcett (University of Leicester) for single crystal X-ray crystallography, Dr G. Eaton (University of Leicester) for FAB mass spectra, Dr G. Griffith (University of Leicester) for ^{1}H and ^{13}C NMR spectra recorded on the 400 MHz spectrometer, Dr J. D. Marechal (University of Leicester) for DFT calculations, Mr K. Singh (University of Leicester) for the preparation of several synthetic precursors and Dr A. Harrison (University of Edinburgh) for variable temperature magnetic susceptibility measurements.

The sometimes divided Inorganic Research group at the University of Leicester. But always united in times of need. Thank you.

Mum, Dad and my brother Paul thanks for all your love and support throughout the years.

To my Friends and the remainder of my Family who have always been there. You know who you are. Thank you.

Abstract

In Chapter **One**, an introduction to the field of metal-mediated olefin polymerisation has been undertaken. The major focus in this section has been on non-metallocene systems and, in particular, *NN*-, *NNN*-, *NNNN*-, *NO*-, *NNO*-, *NNOO*-, *PO*-chelates as supports for early-to-late transition metal catalysts.

In Chapter **Two**, the synthesis and coordination behaviour of the aryl-substituted *N*-picolyethylenediamines and *N*-bis(picolyl)ethylenediamines along with bis(2-picolyl)amine, tris(2-picolyl)amine in manganese(II), iron(II) and cobalt(II) complexes are reported. The notable influence of steric effects upon the nuclearity and the binding mode is described. The flexibility of the *N*-picolyl-en systems when coordinated to iron or cobalt is observed by single crystal X-ray diffraction studies, paramagnetic ^{1}H NMR spectroscopy and DFT calculations.

In Chapter **Three**, the reactions of the sterically variable aryl-substituted diethylenetriamines with $CoCl_2$ to afford *NNN*-chelated complexes are reported. Notably, the analogous iron(II) complexes are not produced. The introduction of a picolyl donor affords the ligand set, *N*-picolyldiethylenetriamine, which is capable of coordinating to iron and cobalt in a *pseudo*-tetradentate fashion.

In Chapter **Four**, the *N*-aryl substituted *NNN*-iron(II) and -cobalt(II) complexes are activated by the addition of excess methylaluminoxane for the oligomerisation of ethylene. The activities are low-to-moderate at 1 bar ethylene pressure and the selectivity of the catalysts is dependent on the metal centre with the iron systems forming linear α-olefins while the cobalt systems give a mixture of linear and branched oligomers.

In Chapter **Five**, the versatile preparation of the novel *NNO*-ligand sets anisole-pyidine-imine, phenol-pyridine-imine and phenol-pyridine-amine and their coordination behaviour in aluminium(III), iron(II) and cobalt(II) complexes is described. Preliminary catalytic evaluation studies reveal moderate-to-high activities for the polymerisation of ethylene into moderate-to-high molecular weight polyethylene.

In Chapter **Six**, full details of the experimental procedures along with the spectroscopic, analytical and X-ray data are reported.

Contents

Abbreviations

Polyethylene	**PE**
Polypropylene	**PP**
Low density polyethylene	**LDPE**
Ultra low density polyethylene	**ULDPE**
High density polyethylene	**HDPE**
Linear low, medium density polyethylene	**LLDPE**
Isotactic polypropylene	***i*PP**
Methylaluminoxane	**MAO**
Atactic polypropylene	***a*PP**
Syndiotactic polypropylene	***s*PP**
Isotactic polypropylene	***i*PP**
Weakly coordinated anion	**WCA**
Perfluoro-tetraphenylborate	**$B(Arf)_4^-$**
Perfluoro-triphenylborane	**$B(C_6F_5)_3$ or "Marks reagent"**
Cyclopentadienyl	**Cp**
Constrained geometry catalysts	**CGC**
Transition metal	**TM**
Shell Higher Olefin Process	**SHOP**
Ultra high molecular weight polyethylene	**UHMPE**
Associative displacement	**a.d.**
Methyl acrylate	**MA**
1,4,7-Trimethyl-1,4,7-triazacyclononane	**Cn**
Triazacyclohexane	**Ch**
Actelyacetonate	**acac**
Room temperature	**rt**

Ring opening metathesis polymerisation	**ROMP**
Methyl methacrylate	**MMA**
2-vinyl-1,3,-dioxolane	**VDO**
Terpyridine	**terpy**
bis(2-picolyl)amine	**dpa**
tris(2-picolyl)amine	**tpa**
High-spin	**HS**
Low-spin	**LS**
Relaxation times	T_1
Atom transfer radical polymerisation	**ATRP**

Complexes

[{dpa}FeCl(μ-Cl)]$_2$	**1**
[(dpa)$_2$Fe]Cl$_2$	**2**
[{dpa}CoCl(μ-Cl)]$_2$	**3**
[(dpa)$_2$Co]Cl$_2$	**4**
[{tpa}MnCl$_2$]	**5**
[{tpa}FeCl$_2$]	**6**
[{tpa}CoCl$_2$]	**7**
[{tpa}CoCl][Cl]	**8**
[{tpa}CoCl]$_2$[CoCl$_4$]	**9**
[{**LIa**}FeCl$_2$]	**10a**
[{**LIb**}FeCl$_2$]	**10b**
[{**LIc**}FeCl(μ-Cl)]$_2$	**10c**
[{**LIa**}CoCl$_2$]	**11a**
[{**LIb**}CoCl$_2$]	**11b**
[{**LIc**}CoCl$_2$]	**11c**
[{**LId**}CoCl$_2$]	**11d**
[{**LII**}CoCl$_2$]	**12**
[{**LIII**}CoCl$_2$]	**13**
[{**LIVa**}MnCl(μ-Cl)]$_2$	**14a**
[{**LIVb**}MnCl$_2$]	**14b**
[{**LIVc**}MnCl(μ-Cl)]$_2$	**14c**
[{**LIVa**}FeCl$_2$]	**15a**
[{**LIVb**}FeCl$_2$]	**15b**
[{**LIVc**}FeCl$_2$]	**15c**
[{**LVa**}CoCl$_2$]	**16a**

University of Leicester

Chapter One

Introduction: The Evolution of Olefin Polymerisation Catalysis

1.1. Overview

The development of polyolefins over the course of the 20th century was a significant factor in the consumer revolution of the latter half of the century. The global consumption of polyethylene (PE) amounted to approximately 55 billion metric tons (5.49 x 10^{10} Kg) in 2002 and is predicted to increase to 87 million (8.69x 10^{10} Kg) by 2010.[1] Over the same time scale the demand for polypropylene (PP) is expected to increase from 35 million metric tons (3.5 x 10^{10} Kg) to 60 million (5.99 x 10^{10} Kg) per annum.[1] Increased consumption will require the development of 100 or more new polyolefin plants with a geographical shift towards Asia, the Middle East and developing countries such as those located in Eastern Europe or Latin America.[1]

The three major microstructures of PE are low density polyethylene (LDPE), linear low density polyethylene (LLDPE) and high density polyethylene (HDPE). The free-radical polymerisation of ethylene to form LDPE was discovered in 1933 at ICI. The process employs high pressures, 1000-3000 bar, high temperatures, 100-250 °C and an initiator such as benzoyl peroxide.[2] The LDPE contains short- or long-chain branches with densities in the region of 0.915-0.930 g cm^{-3}.[2] Short chain branches control the crystallinity and melting points (T_m = 105-115 °C) of the polymer whilst long-chain branches broaden the molecular weight distributions resulting in enhanced processing capability of LDPE.[2] Co-polymerisation with functionalised monomers such as vinyl acetate increases the adhesion properties of LDPE. The applications of LDPE include adhesives, consumer packaging, shrink film, heavy-duty sacks, extrusion coating and electrical wire and cables.

LLDPE is a copolymer of ethylene and α-olefins (1-butene, 1-hexene or 1-octene) with a density in the range of 0.915-0.940 g cm^{-3} and a melt temperature of 122-127 °C.[2] It is produced commercially employing the Ziegler type catalysts, constrained geometry catalysts or the Philips catalyst (0.938-0.940 g cm^{-3}).[2] LLDPE is employed in packaging, stretch film, extrusion coating, and electrical wire and cable.

HDPE is a linear, semi-crystalline, ethylene homo-polymer with a density in the range of 0.960-0.970 g cm^{-3} and a melt temperature of 128-135 °C or it is a hetero-polymer (1-butene or 1-hexene as the co-polymers) with a density in the range of 0.940-0.958 g cm^{-3} and a melt temperature of approximately 125-132 °C.[2] The latter was discovered fifty years ago by Ziegler-Natta and consists of a mixture of $TiCl_4$ and $AlEt_2Cl$, to generate the active species, "$TiCl_3$".[3, 4] In addition, the low insertion barrier for α-olefins led to the development of a new polymer, isotactic polypropylene (*i*PP).[5, 6] The former type of HDPE was developed at Phillips and comprises of CrO_3 impregnated silica followed by calcinations in oxygen.[7, 8] The applications of HDPE consist of rotational, injection and blow moulding and food, litter and carry out packaging.

The interest in homogeneous catalysis originates from the inadvertent discovery of methylaluminoxane (MAO) by Sinn and Kaminsky, which led to the "metallocene revolution" of the 1980's.[9] Sinn and Kaminsky found that in the presence of water, Cp_2ZrMe_2 and $AlMe_3$ would catalyse the polymerisation of ethylene with a 10,000-fold increase in activity *via* a Cossee-Arlman type mechanism.[9 - 13] The polymerisation of propylene was also possible, albeit with a lack of stereoselectivity (atactic polypropylene, *a*PP).

The ligand framework of a metallocene can be fine-tuned to develop several multipurpose precatalysts (Figure 1).[14, 15] The rates of ethylene and propylene polymerisation are dependent upon the stabilisation of the electron deficient metal centre, which is controlled by the electronic properties of the ligand framework. The tacticity of polypropylene is controlled by the symmetry of the ligand architecture with a C_{2v} symmetric metallocene **1** producing *a*PP, C_s symmetric metallocenes **8** and **9** yield syndiotactic polypropylene (*s*PP), whilst a C_2 symmetrical framework, **2-7** gives *i*PP *via* enantiomorphic site control.[10, 14, 15] The precatalyst, **5** upon activation with MAO is, the most active catalyst (111,900 g/mmol/h/bar) attributed to the electron donating groups and the delocalisation of the electron density.

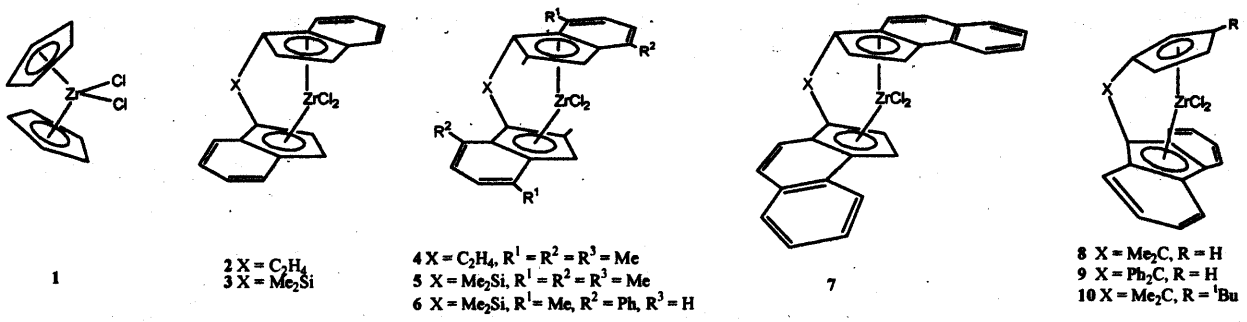

Figure 1 Fine-tuning of the metallocene architecture

Despite the discovery of MAO a quarter of a century ago, there is still uncertainty with regards to its precise structure. It is postulated from spectroscopic evidence to have a molecular weight of 900-1200 with the composition $(MeAlO)_n$, and a structure consisting of linear, cyclic or cross-linked polymers where n is in the range of 4-20.[14] The *cis*-halo precatalyst is widely accepted to be converted into a 14 electron alkylated cationic species upon activation with MAO (Scheme 1).[15 - 17] Throughout the course of the polymerisation MAO acts as a weakly coordinated anion (WCA) to the cationic species and a scavenger to the α-olefin feed preventing poisoning of the catalyst.

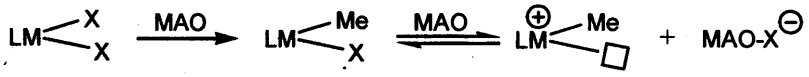

Scheme 1 Activation of the precatalyst with MAO

Alternative WCA's to MAO utilise four essential features: (i) low overall charge, (ii) high degree of charge delocalisation, (iii) very weakly basic sites on the periphery of the anion and (iv) thermodynamic stability.[18] An example of such a WCA is the Turner and Marks anion perfluorotetraphenylborate, $B(C_6F_5)_4^-$ or $B(Arf)_4^-$ anion as it is otherwise known.[19, 20] The π-coordination ability of the anion is reduced by fluoride groups resulting in an increase in the polymerisation rate due to lowering in the barrier to insertion of a α-olefin. Marks and co-workers also discovered that the powerful Lewis acid perfluorotriphenylborane, $B(C_6F_5)_3$ or "Marks reagent" also generates a highly active well-defined catalyst without the additional feature of requiring an alkyl acceptor or a H donor to remove a Me group.[21]

The replacement of a cyclopentadienyl (Cp) donor with a neutral or mono-anionic donor ligand led to the discovery of a novel family of catalysts known as the constrained geometry catalysts (CGC).[22, 23] The trend in activity for the homo-polymerisation of ethylene into linear high molecular weight PE is as follows; **11** (2500 g/mmol/h/bar)[24] ≈ **12** (2050 g/mmol/h/bar)[25] < **13** (4200 g/mmol/h/bar)[25] < **14** (14,800 g/mmol/h/bar).[26, 27] The complexes **12-14** polymerise propylene into *s*PP[28] (**12**) or *a*PP (**13** and **14**).[25 - 27] In addition, the co-polymerisation of ethylene with α-olefins, norbornenes, α,ω-dienes and functionalised protected α,ω-olefins has been reported.[25 – 27, 29 - 31]

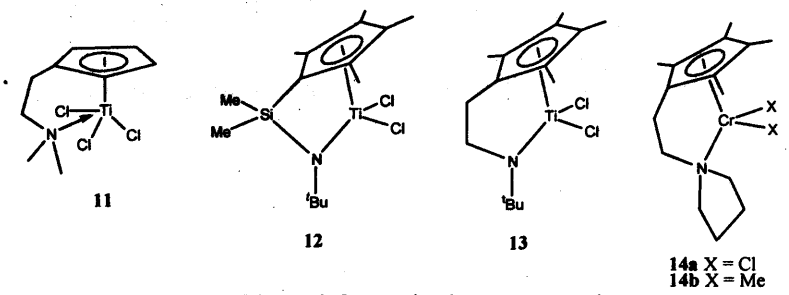

Figure 2 Constrained geometry catalysts

Although homogeneous metallocene-based systems generate lower polydispersities and a more uniform incorporation of α-olefins than their heterogeneous counterparts. Their commercial impact has been less than originally anticipated.

The high oxophilic nature and low functional group tolerance of early transition metals (TMs) prevents the incorporation of polar co-monomers without initial protection of the functional group. The search for novel polymer microstructures led scientists to consider employing late TMs with their low oxophilic nature and high functional group tolerance as alternative active metal centres. The discovery by Keim *et al.* in 1978, showed the capability of non-Cp based ligand supports coordinated to late TMs to polymerise or oligomerise ethylene with or without the incorporation of polar co-monomers and it is utilised to-date in the Shell Higher Olefin Process (SHOP).[32 – 34] Late TM research remained dormant until the mid 90's when Brookhart and co-workers demonstrated how fine-tuning of a non-Cp based ligand architecture can control the molecular weight, the degree of linearity and the

incorporation of polar co-monomers.[35] As a consequence, a chain reaction of both industrial and academic research into late TM olefin polymerisation was born.

The purpose of this introduction is to detail the significant developments of the past ten years, which have fine-tuned several non-Cp ligand architectures in particular, *NN*-, *NNN*-, *NNNN*-, *NO*-, *NNO*-, *NNOO*-, *PO*-chelates as supports for early-to-late TM olefin polymerisation/oligomerisation catalysts. Notably, this review is only intended to cover areas related to the forthcoming Results and Discussion (Chapters 2 - 5). For a more extensive insight into olefin polymerisation by Cp and non-Cp based catalysts see reviews by Mecking,[36] Gibson[37, 38] and Brookhart.[39] In addition, we attempt to demonstrate how the activity is dependent upon the cumulative electronic effects of both the ligand and the metal centre *via* showing trends between a specific ligand family and the various metal centres employed.

The activities are expressed in g/mmol/h/bar for gaseous monomers, such as ethylene and g/mmol/h for reactions carried out in liquid α-olefins such as 1-hexene. They are classified in a similar fashion to the Gibson reviews: very high (>1,000), high (500-1,000), moderate (100-500), low (1-100) and very low (<1). The classification can only be viewed qualitatively, due to the variants of several polymerisation parameters. For example, catalyst lifetimes, run times, temperature, pressure, vessel size, scavengers, stirring rate, nature of solvent and monomer solubility.

Table 1 provides a summary of the types of catalysts discussed within the introduction. It details the activities for the polymerisation of ethylene, polydispersities, microstructure of the PE, the functional group tolerance and co-monomer incorporation.

Table 1 Summary of the types of homogeneous catalysts employed in ethylene polymerisation from 1970's to 2004.

Year	Catalyst type	Activity g/mmol/h/bar	M_w	M_w/M_n	PE microstructure	Functional group tolerance and co-monomer incorporation
1970's	Neutral Ni(II) *PO* complexes	50-100	α-olefin oligomers	Schulz-Flory	linear oligomers	Two-phase process in butandiol
	Cationic metallocene activation with MAO	60,900	6.2×10^5	≈ 2	HDPE	Co-polymerisation of α-olefins
1980's	fine-tuning of metallocene ligand framework	111,900	2.5×10^5	≈ 2	HDPE	Co-polymerisation of α-olefins
	Optimisation of the conditions for neutral Ni(II) PO complexes	100-500	1×10^3 to 4×10^5	2 to 25	Essentially linear	Stable in several polar organic media, copolymerisatiom of functionalised monomers
1995	Cationic α-diimine Ni(II) and Pd (II) Complexes	11, 000 (Ni) 27 (Pd)	3×10^3 to 1×10^6	1.5 to 3	Highly branched to linear, Me, Et, Pr, Bu and longer. Hyperbranched structures (Pd)	Coploymerisation of simple polar monomers, such as acrylates (Pd), stable in esters, acetone or water (Pd)
1998	Cationic pyridine-diimine Fe(II) and Co(II) complexes	20, 600 (Fe*ket*) 555 (Fe*ald*) 1700 (Co*Ket*)	1.6×10^3 to 6×10^5	2.3 to 105	Highly linear sat. *vs.* unsat end groups	Stable in several polar media. No copolymerisation.
	Neutral Ni(II) *NO* complexes	529	5×10^5	1.5 to 3	Moderately branched to linear, predominantly Me also Et, Pr, Bu	Stable to added amounts of polar organic solvents and water, co-polymerisation of functionalised α–olefins and norbornenes.
	Cationic phenoxy-imine Zr(IV) complexes	4,320,000	1.5×10^5	1.88	HDPE	Co-polymerisation of α-olefins
2000	Cationic pyrrolide-imine Ti(IV) complexes	14,100	$\geq 1 \times 10^5$ (M_v)	2	HDPE	Not applicable
	Cationic Ch Cr(III) complexes	717	1×10^4 and trimers of the respective α-olefin	2 to 4	LLDPE	trimerisation of α-olefins
2001	Cationic perfluorinated Phenoxy-Imine Ti(IV) complex	33,960	M_n: 412,000	≈ 1	HDPE	Block co-polymers
2003	Cationic pyridine-diimine Cr(III)	41,400	1×10^3 to 1×10^4	1.3 to 2.17	HDPE	Co-polymerisation of α-olefins

1.2. *NN*-ligand libraries

1.2.1. α-diimine ligand family and derivatives thereof

The capability of the α-diimine ligand set to act as a bidentate donor in organometallic compounds was first described in the early 1980's.[40] However, it was Brookhart and co-workers whom developed nickel(II) and palladium(II) α-diimine compounds for the polymerisation of ethylene.[35] The ligand has been coordinated to both early-to-late TMs (Figure 3) with the activity of the catalyst and the microstructure of the PE being dependent upon the metal centre.[35, 39, 41 – 43] The following trend in activity with respect to the active metal centre is observed: Fe (**21**: 0.01 g/mmol/h/bar)[41] < Sc (**15**)[41] ≈ Zr (**17**)[41] ≈ Cr(II) (**19a**)[41] ≈ Cr(III) (**19b**)[41] ≈ Cu (**24**: 1-10 g/mmol/h/bar)[43] < Ti (**16**: 30 g/mmol/h/bar)[41] ≈ Pd (**23a**: 27 g/mmol/h/bar)[35] < V/Et_2AlCl (**18**: 40 g/mmol/h/bar)[41, 44] < Co (**20**: *Oligomers* 345 g/mmol/h/bar)[41, 42] < < Ni (**22a**: 11,000 g /mmol/h/bar, R = *i*-Pr, R^1 = H).[35]

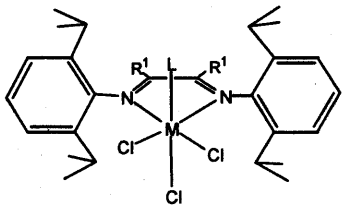

15 M = Sc, L = thf, R^1 = Me
16 M = Ti, L = Cl, R^1 = Me
17 M = Zr, L = Cl, R^1 = Me

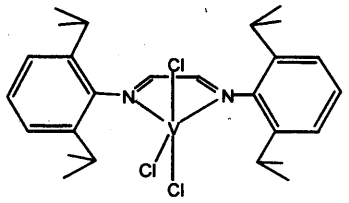

18

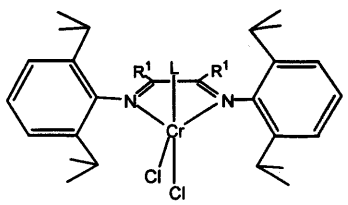

19a L= thf, R^1 = Me
19b L= Cl, R^1 = Me

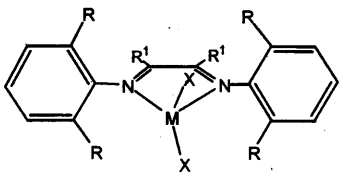

20 M = Co, X= Br, R= *i*-Pr, R^1 = H or Me
21 M = Fe, X = Br, R= *i*-Pr, R^1 = Me
22a M= Ni, R = H or alkyl, R^1 = H or Me
24 M = Cu, X = Cl, R=Ph, R^1 = Me

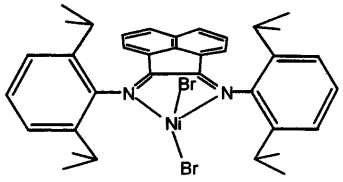

22b

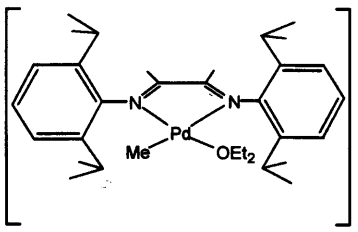

23a

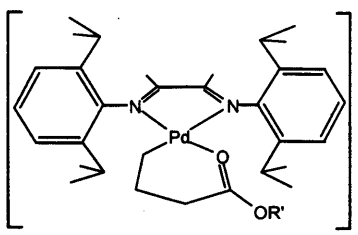

23b

Figure 3 α-diimine compounds

The microstructure obtained for scandium, titanium, zirconium, chromium and iron is that of HDPE,[41] whilst cobalt forms branched oligomers.[42] Vanadium exhibits a dependence on the type of activator employed. With Et_2AlCl utilised as the co-catalyst a relatively stable active species is formed whilst in the presence of MAO facile decomposition of **18** is observed.[44] Medium-to-HDPE is formed with nickel acting as the metal centre. In addition, the microstructure is a function of temperature, ethylene pressure, and the ligand architecture (controls the extent of chain branching and molecular weight of the PE).[35, 39, 45, 46] Palladium gives an amorphous highly branched microstructure (ULDPE, density: 0.85 gcm^{-3}), with the extent of branching being independent of temperature, pressure and fine-tuning of the ligand architecture. However, reduction in steric bulk about the *ortho*-positions of the aryl ring results in a reduction in molecular weight (*cf.* nickel).[39] At moderate-to-high laboratory pressures (5-30 bar) and temperatures (70 °C) ultrahigh molecular weight polyethylene (UHMPE M_w: > 5 x 10^6) is formed with copper employed as the metal centre.[43]

The high d^n configuration of late TM complexes leads to facile β-H elimination and the subsequent formation of dimers and oligomers.[32, 47, 48] The α-diimine ligand framework inhibits β-H elimination *via* two possible mechanisms. Firstly, associative displacement (a.d.) is hindered *via* steric bulk about the *ortho*-position of the aryl ring preventing the incoming monomer from coordinating to the metal centre at the vacant axial coordination sites (Figure 4).[49]

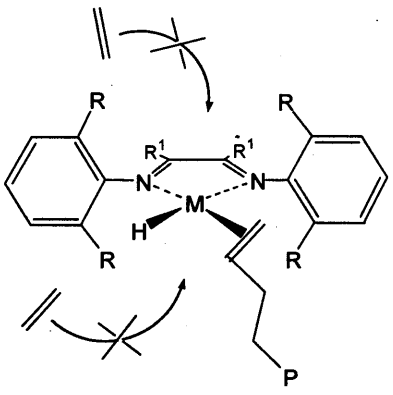

Figure 4 Prevention of a.d. about the vacant axial coordination sites

Secondly, calculations by Ziegler *et al.* have indicated that the barrier for β-H transfer to monomer in the alkyl olefin resting state increases with enhancement of the steric bulk at the *ortho*-position (Scheme 2).[49]

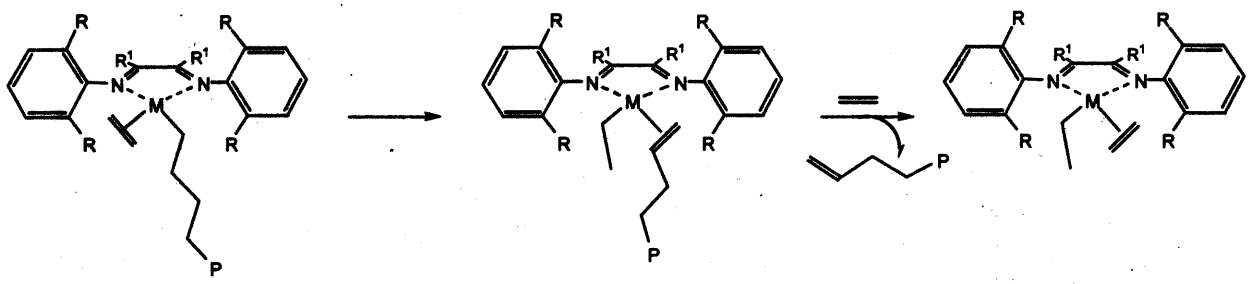

Scheme 2 chain transfer to monomer

The formation of branched PE when utilising **22a**, **22b** and **23a** is attributed to a chain walking mechanism (Scheme 3), which consists of a β-H elimination followed by reinsertion at the opposite carbon atom (1,2 migration).[49, 50] The catalyst resting state is the alkyl ethylene complex, upon insertion a highly dynamic β-agostic alkyl species is formed, which can chain walk to form a 1° or 2° alkyl agostic species, with the latter being more stable.

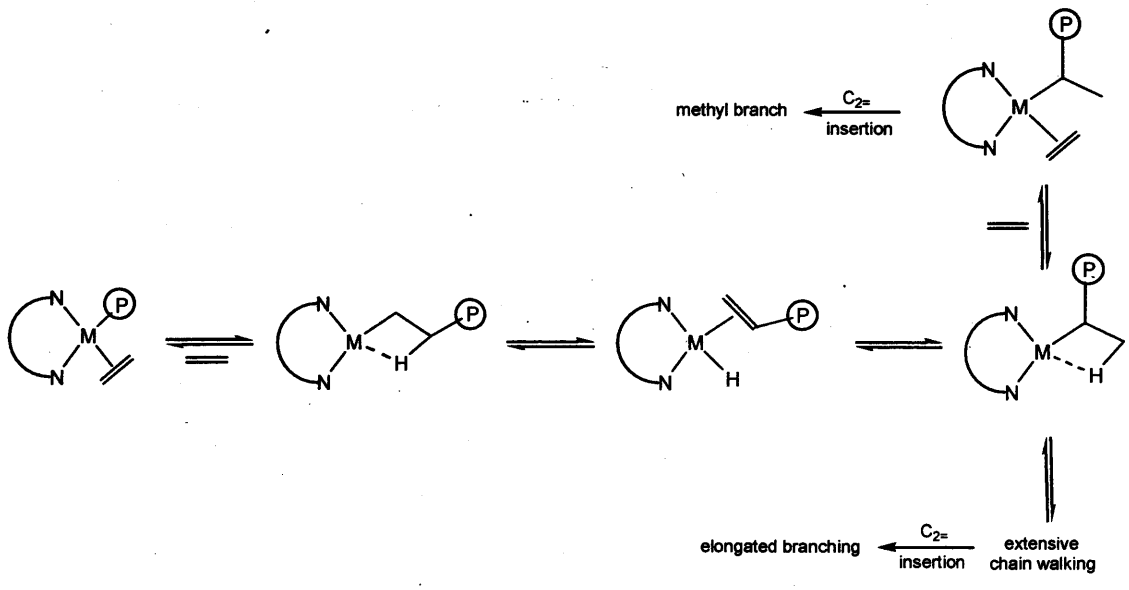

Scheme 3 Proposed mechanism for propagation and chain walking

Despite the high energy insertion barriers for α-olefins, both hetero-block- and homo-polymerisation occurs for **22a** and **22b** (84 g/mmol/h).[51] PP normally contains 333 Me branches per 1000 C atoms, the resultant PP from the α-diimine catalytic system contains

150-250 branches per 1000 C atoms. This is attributed to a possible 1,3-insertion mechanism, which leads to a resultant straightening of the polypropylene chain (Scheme 4).[39]

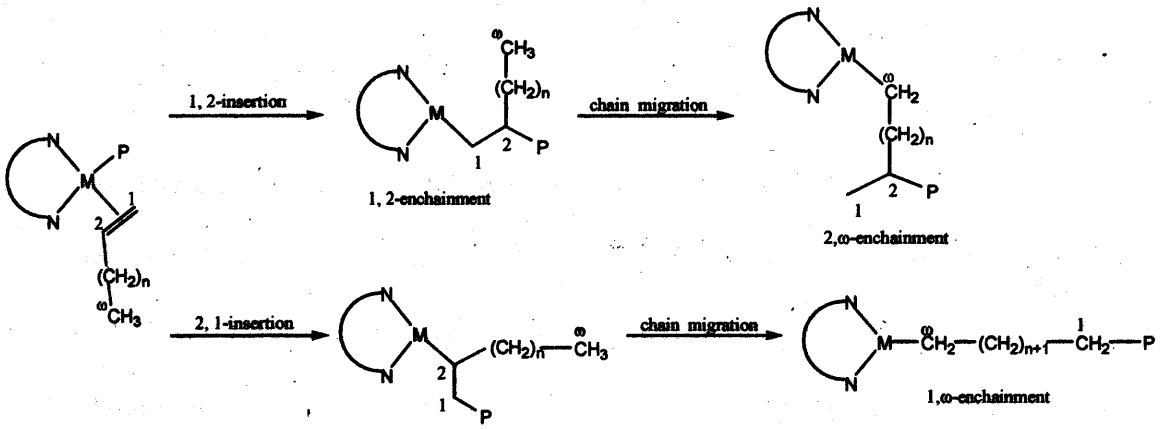

Scheme 4 Chain walking attributable to straightening of the polymer chain

An interesting feature of α-olefin polymerisation is that at low temperature (-10 °C) it is possible to achieve living polymerisation of α-olefins (PDI ≈1).[51] Reducing the temperature even further to –78 °C yields *s*PP attributed to a chain-end control mechanism.[52, 53] The synthesis of C_2 symmetric nickel complexes (unsymmetrical aryl substituents) results in a reduced syndiotacticity attributed to a dual stereodifferentiation mechanism (partly enantiomorphic site control and partly chain-end control).[54]

At low pressure and temperatures **23b** was found to randomly copolymerise ethylene with vinyl acrylates to give high molecular weight, amorphous, highly branched material (*T*g –67 to –77 °C), with *only* end group incorporation of the comonomer.[55] The Pd-O six-membered chelate (**23b**), is also the catalyst resting state.[55, 56] Further evidence for functional group tolerance arises from the polymerisation of ethylene in water.[57] Nickel η^3-allyl/-benzyl complexes in combination with a WCA have been reported to homo-polymerise ethylene, albeit with lower activities than **22a** and **22b**, they are also known to hetero-polymerise ethylene with acrylates.[38, 58, 59]

The notable absence of any steric control in complexes **25**, **26** and **27** (Figure 5) produces moderate (**25**: 124g/mmol/h/bar) to very highly (**26**: 24,320 g/mmol/h/bar) active catalysts with a 90 % selectivity for the dimerisation of ethylene upon activation with Et_2AlCl

(**25**) and oligomerisation of ethylene with $Et_3Al_2Cl_3$ as the co-catalysts (**26**).[60 - 62] Utilising the above characteristic with bipy and its derivatives as the bidentate ligand (**28a**), leads to the oligomerisation of ethylene, with less selectivity for α-olefins than the α-diimine nickel system at 1-bar ethylene pressure.[45] Increasing the pressure to 5-bar and employing derivatives of bipy yields HDPE with moderate to high activities.[63] In addition, **28b** and **29** oligomerise butadiene in the presence (**28b**) or absence (**29**) of oxygen.[64, 65]

Coordination of the pyridinyl-imine ligand to cobalt, nickel and palladium (Figure 5) leads to the following trend in activity for the polymerisation of ethylene: Pd (**33a**) *inactive*[67, 70] < Co (**30a** and **30b**) *trace activity*[67, 68] < Pd (**34**: *oligomers* 17.5 g/mmol/h/bar)[71] ≈ Pd (**33b**: 15.4 g/mmol/h/bar)[70] < Ni (**31b**: 137 g/mmol/h/bar)[72] < Ni (**31a**: 1326 g/mmol/h/bar)[72] < Co (**32**: *oligomers ca.* 3000 g/mmol/h/bar).[66, 69]

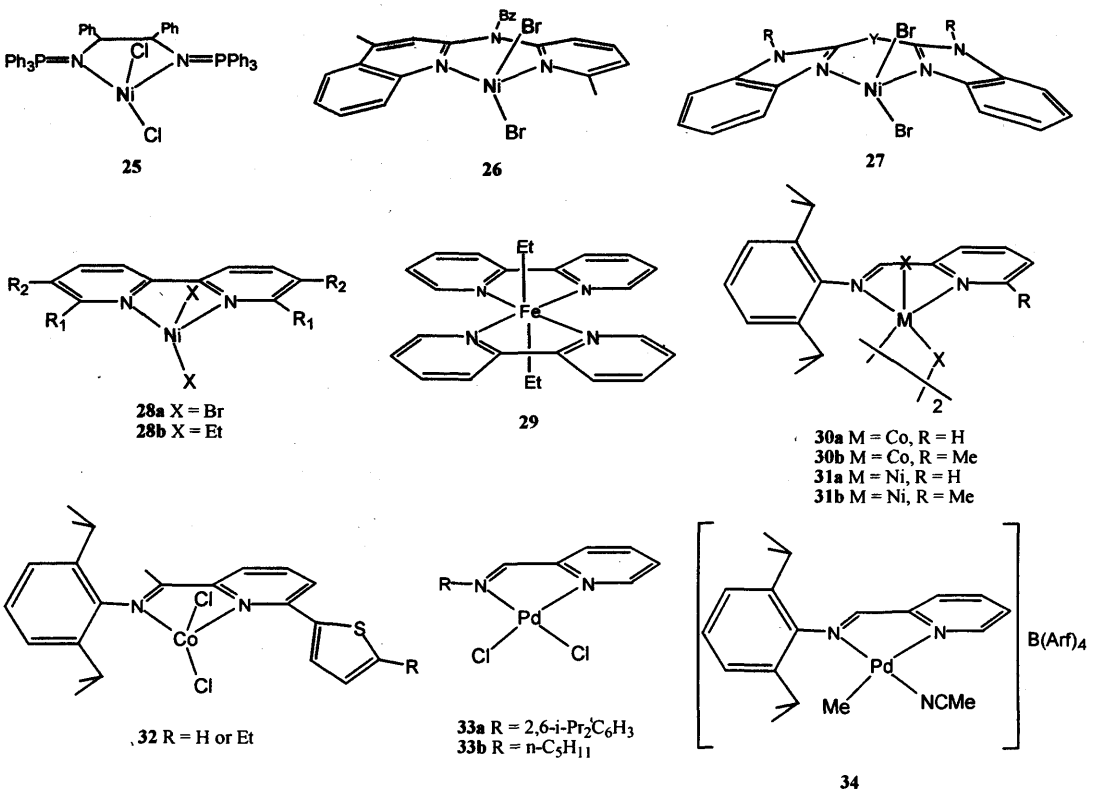

Figure 5 α-diimine derivatives

The introduction of a pendant donor atom in **32** reduces the molecular weight and enhances the activity in relation to **30a** and **30b**.[67 - 69] The *cis*-chloro Pd complex is activated for ethylene polymerisation (HDPE) upon replacing the *N*-aryl ring with an *N*-(n-alkyl) chain

(**33a** *vs.* **33b**) albeit with low activity.[70] The synthesis of a discrete cationic species (**34**) yields a catalyst capable of oligomerising ethylene, propylene and 1-hexene at low activities.[71] Increasing the steric bulk in the *ortho*-position of the pyridinyl ring (**31b**) is deleterious to the catalyst activity.[72] The absence of steric control about the pyridinyl ring for the nickel systems is attributed to the low molecular weight PE produced (*cf.* α-diimine nickel).[72]

1.2.2. Pyrrolide-imine ligand family and derivatives thereof

The utilisation of the pyrrolide-imine ligand set has lead to the design of several compounds, with the intended employment as ethylene polymerisation catalysts (Figure 6). The trend in activity is as follows: Fe (**39**)[77] ≈ Pd (**41**)[81] *inactive* < Cr/MAO (**38**: 5 g/mmol/h/bar)[78] ≈ Zr (**36a**: 12 g/mmol/h/bar)[75] < Zr (**36b**)[75] ≈ Zr (**36c**)[75] ≈ Zr (**37**) (30-50 g/mmol/h/bar)[78] ≈ Co (**40**: *oligomers* 36 g/mmol/h/bar)[70, 73] ≈ Cr/Et_2AlCl (**38**: 70 g/mmol/h/bar)[78] < Ti (**35a**: 6000 g/mmol/h/bar)[74] < Ti (**35b**: 14,100 g/mmol/h/bar).[74]

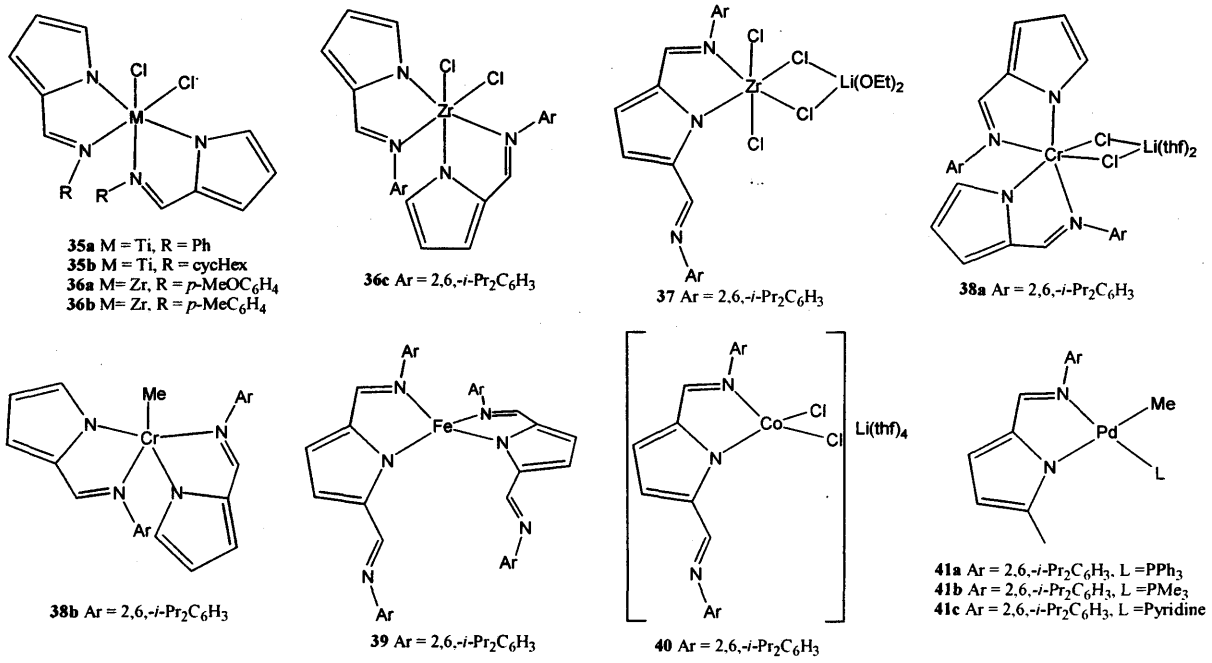

Figure 6 Pyrrolide-imine complexes

It is apparent from diffractometric studies that the dichloro moieties of the *bis*-ligated complexes are bound in a *cis*-configuration.[74 - 78] The *cis*-environment in the cationic species is a prerequisite for propagation and is evident by the observed polymerisations of ethylene.

Further evidence arises from the DFT calculations on a methyl(ethylene) cationic species of **35a** indicating that the *cis*-configuration is present in the active species.[74, 76] The ligand environment is dependent upon the steric bulk at the imino carbon atom, decreasing the steric bulk gives a *trans*-configuration of the pyrrolide donor atoms (**36a-b**), whereas a increase yields a *cis*-pyrrolide relationship (**36c**). When titanium replaces zirconium as the metal centre (**35** *vs.* **36**), there is a dramatic increase in catalytic activity (NOTE: titanium employs short run times). UHMPE is formed albeit with a decline in activity when **36**/$Ph_3CB(Arf)_4$/*i*-Bu_3Al replaces **36**/MAO as the pre-catalyst/co-catalyst mixture.[74, 76]

The introduction of an additional imine donor gives a mono-ligated complex, **37** with comparable activity to **36c**.[77] The activity of **38** is dependent upon the nature of the co-catalyst, with Et_2AlCl enhancing the activity in comparison to MAO.[78] Notably, **38b** is inactive for the polymerisation of ethylene in the absence of an activator. Coordination to iron forms a bis-ligated species with no *cis*-chloro ligands bound thereby rendering the catalyst inactive (**39**).[77] In contrast, cobalt (**40**) forms an active catalyst for the oligomerisation of ethylene albeit with low activity and poor selectivity for α-olefins.[77]

The highly active living hetero-polymerisation of ethylene and norbornene, is possible with **35** producing high molecular weight polymer and approximately 1:1 incorporation ratio of ethylene:norbornene.[79] Complex **41** is inactive for the polymerisation of ethylene and 1-hexene even when polymerisation is carried out in the presence of phosphine scavengers. However, the palladium complex may acts as an initiator in the radical polymerisation of methyl acrylate (MA).[80]

The reduced pyrrolide-amino zirconium complex **42** (Figure 7) exhibits low activity for the polymerisation of ethylene into HDPE, as also observed for the pyrrolide-imine zirconium complexes **36**.[81] Easily accessible related five-membered chelate rings bound to zirconium have been reported in the patent literature and recently reviewed by Gibson (**43** and **44**).[38, 82, 83] The activity of **43** is determined by the steric enhancement at the aryl group, in the following order: 2,6-*i*-$Pr_2C_6H_3$ >> 2,4,6-*t*-$Bu_3C_6H_2$ or Ph. Complex **44** upon activation with

MMAO can give activities of up to 6100 g/mmol/h/bar for the polymerisation of ethylene (*cf.* **36**).

Utilising the indolide-imine ligand as a six-membered chelate ring when bound to titanium (**45**) produces highly active catalysts (short run times) for the polymerisation of ethylene into HDPE, with saturated chain end groups.[84, 85] Increasing the number of fluorine substituents enhances the electrophilicity of the metal centre thereby increasing the activity (**45a**: 480 *vs.* **45b**: 1902 g/mmol/h/bar). In addition, the PE goes from moderate to high molecular weight, with a proportional increase in the polydispersity at room temperature (**45a**: 1.11 *vs.* **45b**: 1.93). **45a** can incorporate 20 mol% propylene in a PE-*b*-poly(ethylene-co-propylene) block co-polymer.[85] Alternative six-membered β-diketiminate type chelates, are complexes **46** and **47**, which respectively produce moderate and low activities for the polymerisation of ethylene.[38]

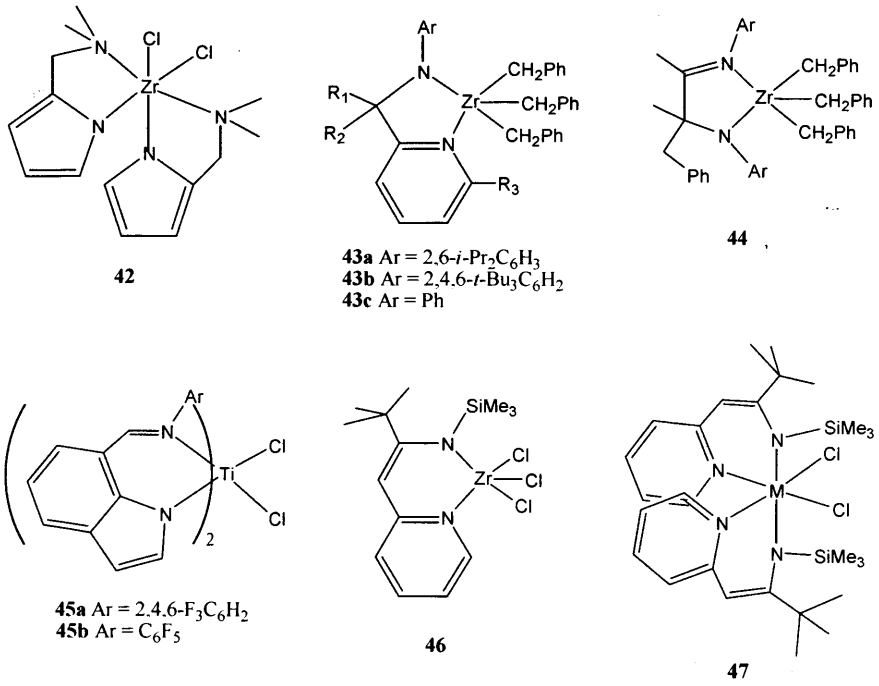

42

43a Ar = 2,6-*i*-$Pr_2C_6H_3$
43b Ar = 2,4,6-*t*-$Bu_3C_6H_2$
43c Ar = Ph

44

45a Ar = 2,4,6-$F_3C_6H_2$
45b Ar = C_6F_5

46

47

Figure 7 Pyrrolide-imine derivatives

1.3. *NNN*-ligand libraries

1.3.1. Neutral tridentate amines

The ligand 1,4,7-trimethyl-1,4,7-triazacyclononane (Cn) may act as a support for scandium alkyls (Figure 8: **48a-c**).[86, 87] Upon reaction with $B(C_6F_5)_3$ a cationic species is generated which is active for the polymerisation of ethylene. The cationic species originating from **48b** is moderately active (220 g/mmol/h/bar) and forms PE with a temperature dependent bimodal molecular weight distribution.[87] Reducing the bite size of the triamine to that of triazacyclohexane (Ch) renders a support suitable for chromium that is active for the polymerisation and trimerisation of ethylene (**49**).[88] Enhanced activity is achieved by introducing long alkyl chains (**49b**) thereby increasing the solubility of the catalyst system (**49a**: 455; **49b**: 717 g/mmol/h/bar). Lower activities are achieved for **49b** when a combination of $[HN(CH_3)_2Ph][B(Arf)]$ and $(i\text{-}Bu)_3Al$ are employed as co-catalysts, whilst the molecular weight and molecular weight distribution remain constant (M_w: *ca.* 40,000; PDI 2-4). Trimerisation is the dominant propagating mechanism when α-olefins act as the monomer or when branched susbstituents such as 3-propyl-heptyl are employed.[38, 89]

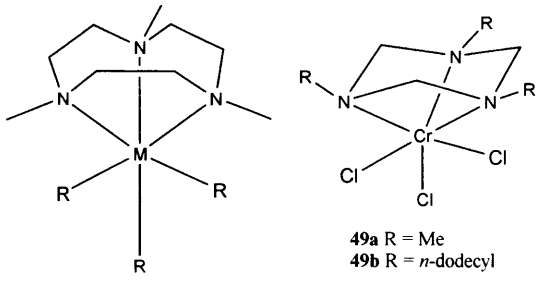

48a M = Sc, R = Me
48b M = Sc, R = CH_2SiMe_3
48c M = Y, R = CH_2SiMe_3

49a R = Me
49b R = *n*-dodecyl

Figure 8 Neutral tridentate amine complexes

The mechanism is postulated to proceed in a analogous fashion to the Phillips type trimerisation catalyst (Scheme 5).[90] Upon activation with MAO and insertion of the α-olefin, the chromium(I) complex is generated via β-H and reductive alkane elimination. Oxidative addition of three α-olefins forms a metallacycloheptane, which undergoes facile β-H and

reductive elimination to yield the trimerisation isomeric products and to regenerate the chromium(I) catalytic species.

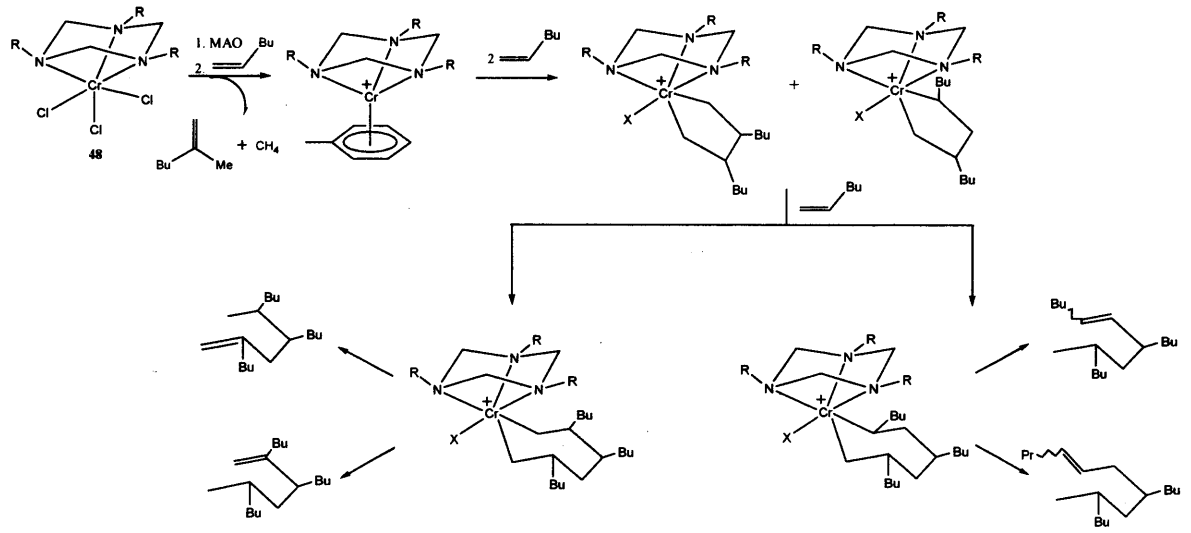

Scheme 5 Postulated trimerisation mechanism and the isomers formed

1.3.2. Pyridine diimine ligand family and derivatives thereof

The pyridine-diimine ligand set has been bound to first and second row early-to-late TMs exclusively in a *meridional*-fashion (Figure 9). The trend in activity for the polymerisation of

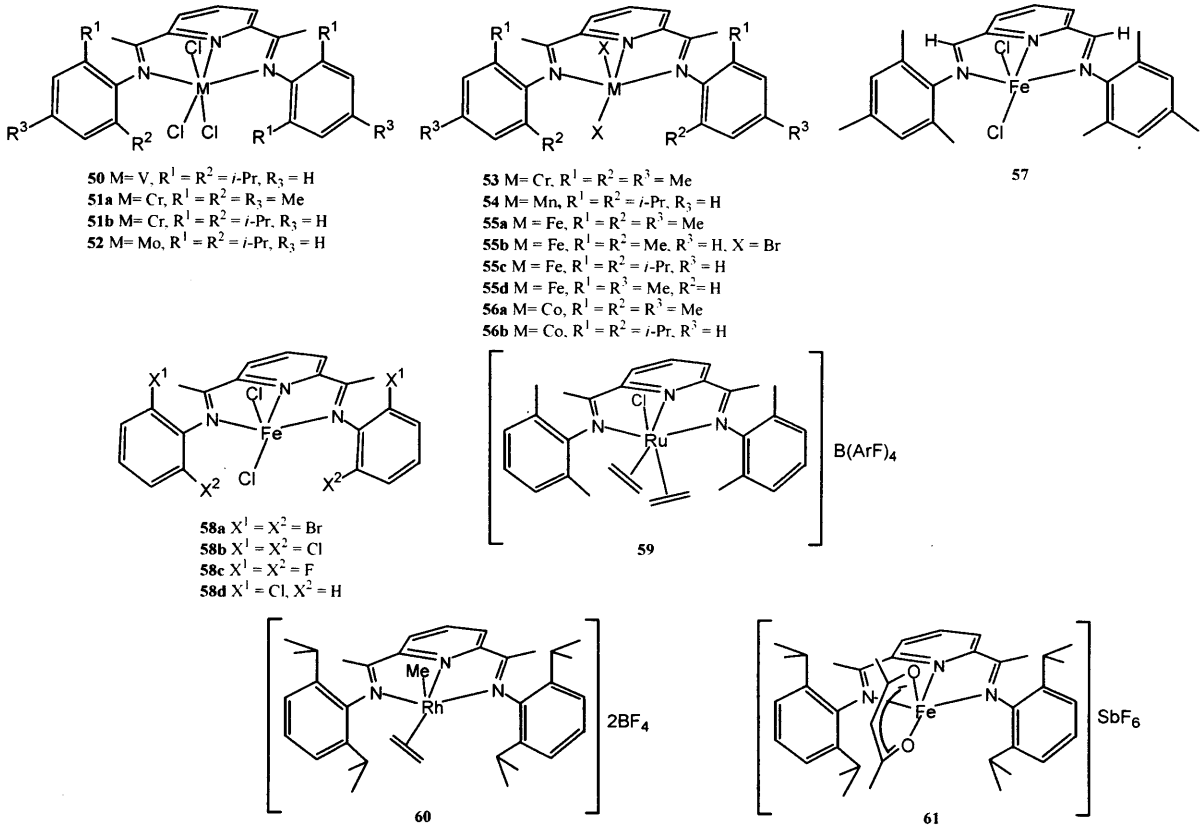

50 M= V, $R^1 = R^2 = i$-Pr, R_3 = H
51a M= Cr, $R^1 = R^2 = R_3$ = Me
51b M= Cr, $R^1 = R^2 = i$-Pr, R_3 = H
52 M= Mo, $R^1 = R^2 = i$-Pr, R_3 = H

53 M= Cr, $R^1 = R^2 = R^3$ = Me
54 M= Mn, $R^1 = R^2 = i$-Pr, R_3 = H
55a M = Fe, $R^1 = R^2 = R^3$ = Me
55b M = Fe, $R^1 = R^2$ = Me, R^3 = H, X = Br
55c M = Fe, $R^1 = R^2 = i$-Pr, R^3 = H
55d M = Fe, $R^1 = R^3$ = Me, R^2 = H
56a M= Co, $R^1 = R^2 = R^3$ = Me
56b M= Co, $R^1 = R^2 = i$-Pr, R^3 = H

57

58a $X^1 = X^2$ = Br
58b $X^1 = X^2$ = Cl
58c $X^1 = X^2$ = F
58d X^1 = Cl, X^2 = H

59

60

61

Figure 9 Pyridine-diimine complexes

ethylene is as follows: Mn (**54**)[109] ≈ Ru (**59**)[110] ≈ Rh (**60**)[110] *inactive* < Mo (**52**: 50 g/mmol/h)[91] < V (**50**: 205 g/mmol/h/bar)[111] < Fe *aldimine* (**57**: 550 g/mmol/h/bar)[95] < Co (**56a**: 1700 g/mmol/h/bar)[95] < Cr(II) (**53**: 17,000 g/mmol/h/bar)[112] < Fe *ketimine* (**55a**: 20, 600 g/mmol/h/bar)[95] < Cr(III) (**51a**: 41,400 g/mmol/h/bar).[113]

Highly active iron and cobalt pyridine-diimine catalysts for the polymerisation of ethylene into HDPE were discovered independently by Gibson, Brookhart and DuPont in 1998.[92 - 94] The overall general trend in activity is that ketimine-based systems are more active than aldimine-based systems (**55** *vs.* **57**) and iron is an order of magnitude higher in activity than cobalt. The productivities, modality (bimodal *vs.* unimodal) and molecular weight are dependent upon the reaction time, pressure, temperature, aluminium concentration or source of aluminium and fine-tuning of the ligand framework. The generally broad molecular weight distribution is attributed to two competing chain termination processes: β-H transfer to monomer or metal (first order dependence on ethylene concentration) and chain transfer to aluminium (Scheme 6).[95]

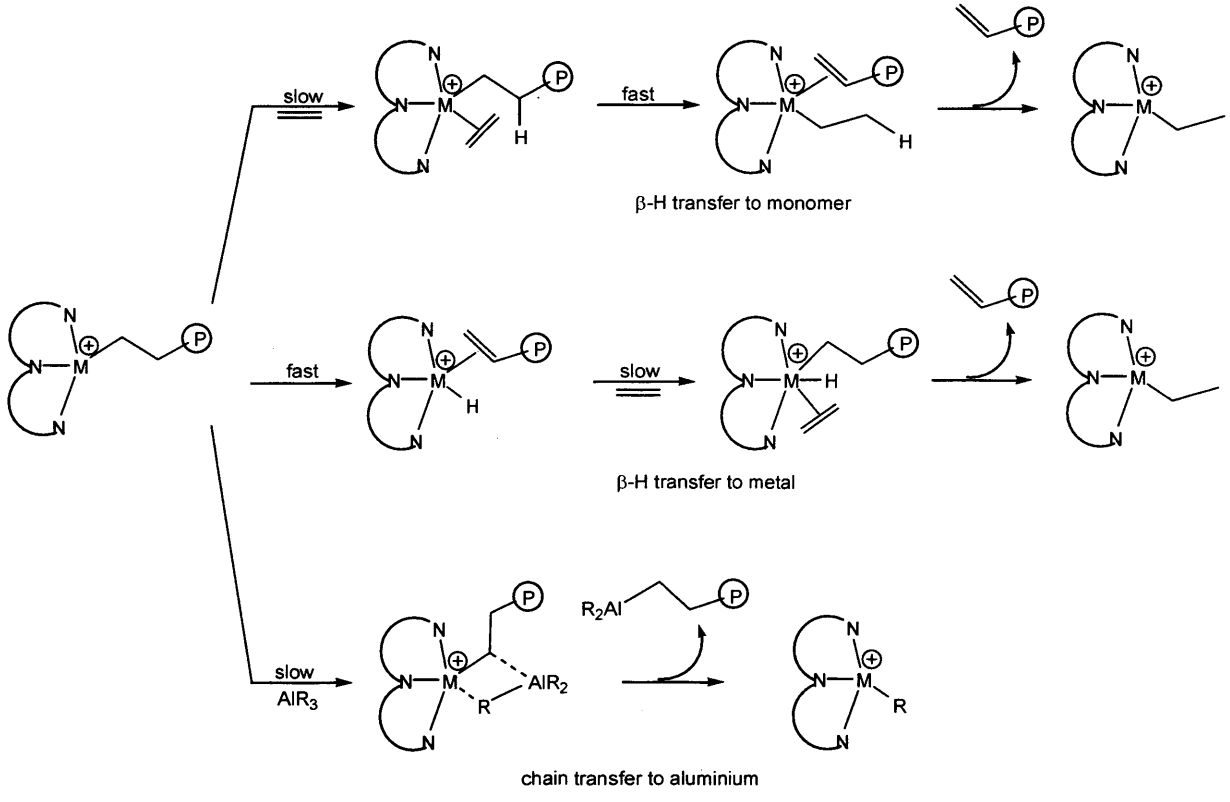

Scheme 6 Possible Chain transfer pathways

The addition of 500 equivalents of $ZnEt_2$ generates a very fast and reversible chain transfer to zinc (Scheme 7).[96] The chain transfer pathway to zinc may involve the formation of an alkyl bridged iron-zinc species, which enables the low molecular weight PE to be exchanged for an ethyl group. The iron-ethyl species is now capable of undergoing propagation (insertion of ethylene into a metal-alkyl bond) followed by chain transfer to zinc. Hydrolysis results in the formation of saturated linear alkanes with a very narrow molecular weight distribution. Alternatively, $Ni(acac)_2$, (actelyacetonate, acac) can be added to catalyse an olefin exchange reaction to give linear α-olefins, with a Poisson distribution.

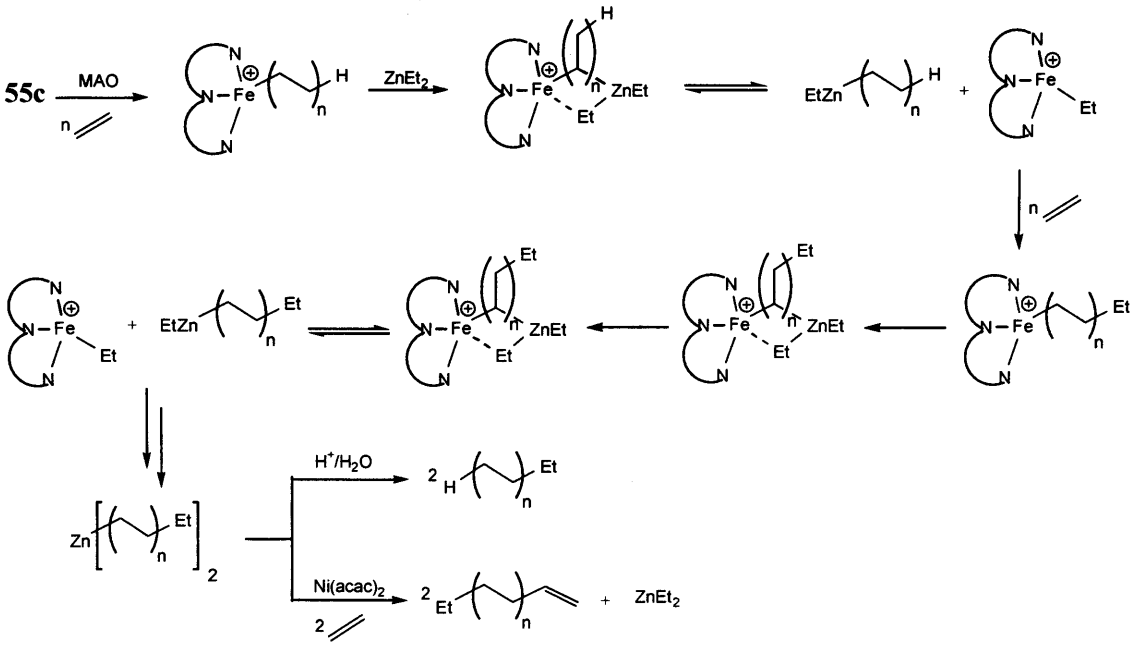

Scheme 7 Chain transfer to zinc

Removal of steric bulk at least one of the *ortho*-positions renders the catalyst highly active for the oligomerisation of ethylene (**55d**: 1040 g/mmol/h/bar), with a ≥ 95% selectivity for α-olefins and a Schulz-Flory distribution of oligomers.[97, 98] The introduction of dihalo substituents (**58a** or **58b**) leads to a catalytic system that exhibits a higher activity than **55c** at 0 °C and 1 atmosphere of ethylene, with an analogous PE microstructure.[99] The increase in activity is possibly attributed to the electron withdrawing effect enhancing the electrophilicity about the iron centre.[99] Employing difluoro (**58c**) and mono halo (**58d**) substituted systems results in the oligomerisation of ethylene with high activities (*cf.* **55d**).[99, 100] Replacing one of the aryl rings with a fluorenyl or an alkyl substituent reduces the steric bulk about one of the

imino groups thereby favouring α-olefin formation.[101, 102] The mono- or di-reduced form of the pyridine-diimine ligand set exhibits low activities for the polymerisation of ethylene when coordinated to iron.[103]

Experimental studies have revealed a cobalt(I) intermediate species in the activation mechanism with MAO as the activator (Scheme 8).[104, 105] The reduction of **56b** is achieved with methyl grignard reagents or alkylating agents (RLi, $ZnEt_2$, Scheme 8). The resulting LCoR species is inactive for the polymerisation of ethylene unless excess MAO is added, whereby activities and microstructures are comparable to that of **56b**. The addition of $B(C_6F_5)_3$ under a nitrogen atmosphere forms the dinitrogen cobalt(I) complex which exhibits a low activity for the polymerisation and yields the ethylene adduct upon consumption of the excess ethylene.

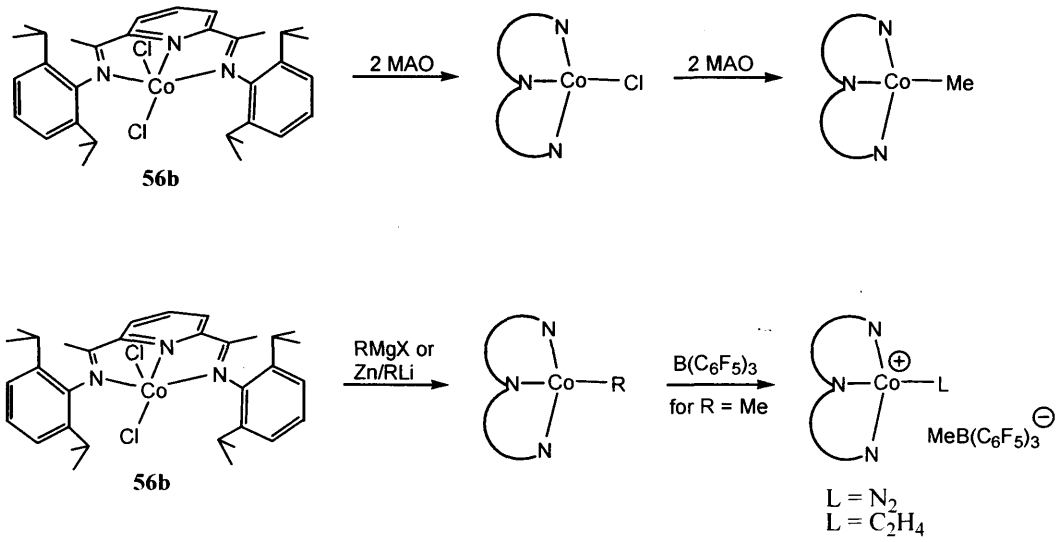

Scheme 8 Generation of intermediate activation species

The similar activities for iron(II) and iron(III) analogous complexes, suggests that the same oxidation state is present in the active species formed from both precatalysts.[95] Activation studies with TMA have been performed by Talzi *et al.* and indicate the formation of a neutral iron(II) complex with TMA in the coordination sphere (Scheme 9a).[106] Upon the addition of $B(C_6F_5)_3$ or $CPh_3.B(C_6F_5)_4$ a cationic species is formed indicative of the WCA role of MAO.[106] EPR and ^1H NMR studies with iron(II) and iron(III) analogous complexes activated with MAO compliment these findings and suggest that a iron(II) species is indeed

the active species.[107] Gibson and co-workers have shown that modification of the pyridine-diimine backbone is possible *via* nucleophilic attack at the pyridine nitrogen (Scheme 9b).[108] This reaction yields a monoanionic *NNN*-ligand, which upon coordination to $FeCl_3$ and activation with MAO affords an ethylene polymerisation catalyst with similar activities to the pyridine-diimine iron systems.[108] The reduction of the iron(III) into iron(II) may be attributed to a one-electron reduction process induced by the monoanionic ligand architecture (*cf.* **50** and **54**).

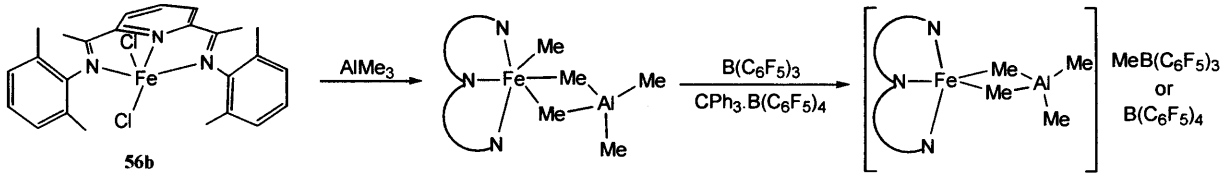

56b

Scheme 9a Activation study with TMA

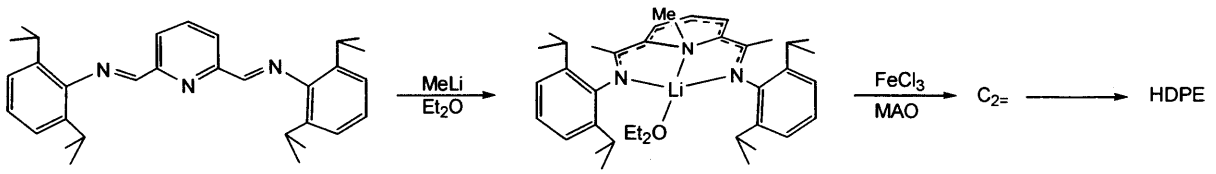

Scheme 9b Nucleophilic attack at pyridine nitrogen atom

Coordination of the pyridine-diimine ligand to manganese (**54**) and the second row TMs, ruthenium and rhodium (**59** and **60**) renders the complexes inactive for the polymerisation of ethylene upon the addition of MAO.[109, 110] When vanadium (**50**) is employed as the metal centre, moderate activities for the polymerisation of ethylene are observed, with no ligand abstraction by aluminium (*cf.* α-diimine system vanadium, **18**).[111] Conflicting results are obtained for chromium(II) (**53**) or chromium(III) (**51a**). When the conditions employed are room temperature (rt) and 1 atmosphere of ethylene, with 70-1000 equivalents of MAO, zero to low activities are observed (chromium(II) *inactive*, chromium(III): 2.6 g/mmol/h/bar).[112] Conversely, at 4 bar ethylene pressure, 70 °C and prolonged MAO activation periods (400 – 2000 equivalents; 30-60 min), the highest activities to date for the pyridine-diimine system are afforded.[113, 114]

Interestingly, with manganese, vanadium or chromium being utilised as the metal centres, a reduction at the metal centre analogous to the cobalt system and in certain cases modification of the ligand architecture are observed (Scheme 10).[109, 111, 112] Alkylation of the pyridine ring at the *ortho* position in **50** forms a monoanionic ligand bound to vanadium(III), which affords comparable activities to **50**. Further addition of MeI yields two products attributed to a ligand mediated two electron reduction process at the vanadium atom, both vanadium(I) species are inactive for the polymerisation of ethylene. Alkylation of the pyridine ring at the *para* position in the case of chromium initiated rearrangement and dimerisation. By varying the alkylating agent it is possible to isolate two types of reduced manganese(I) complexes. The dinuclear species is formed *via* deprotonation of the ketimine methyl group followed by a C-C coupling reaction.

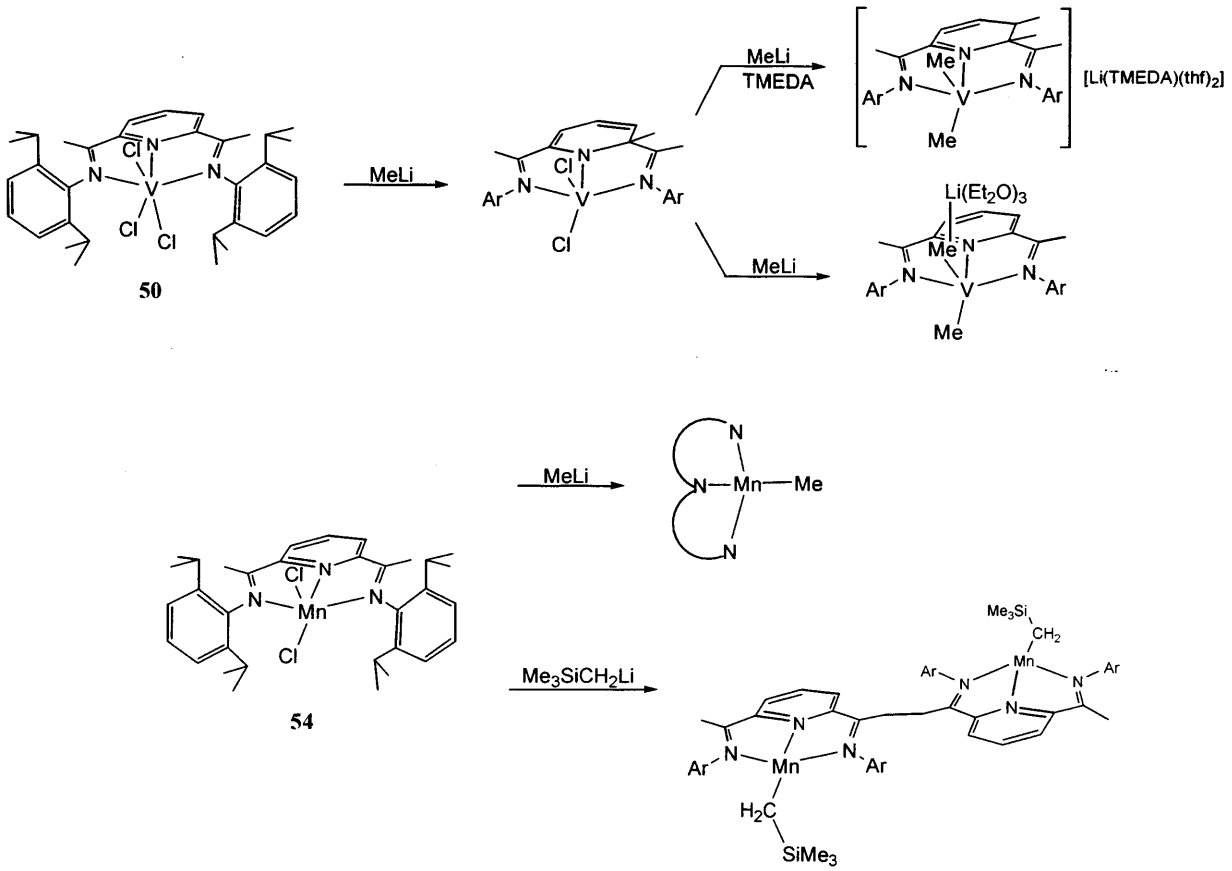

Scheme 10 Metal centre reduction by alkylating agents

With molybdenum as the metal centre HDPE is formed albeit with low activities (**52**).[115] In contrast to the α–diimine system utilising a second row TM does not render the system active for the co-polymerisation of ethylene with norbornene, despite the complexes

high *cis*-selectivity and high yielding ring opening metathesis polymerisation (ROMP) of norbornene.[115] Attempts to co-polymerise ethylene/polar co-monomers with the pyridine-diimine iron system have proven unsuccessful.[116] Even cationic complexes containing a bidentate monoanionic acac ligand (**61**), with their reduced reliance upon an aluminium activator are ineffective for polar co-monomer insertion. However, the homo-polymerisation of ethylene[117] is achieved in the presence of the polar co-monomers MA, Methyl methacrylate (MMA), styrene and 2-vinyl-1,3,-dioxolane (VDO), whilst vinyl acetate, acrolein and acrylonitrile result in deactivation. Co-polymerisation of ethylene/1-hexene has been achieved when the chromium(III) precatalyst **51a** was employed, to give LDPE (T_m = 105 °C) with high productivity.[113]

The precatalyst **62a** is highly active for the polymerisation of ethylene at 0 °C (Figure 10).[118] The activity is enhanced by increasing the chain length (n = 1-3, activity = 24,000-107,000 g/mmol/h/bar) and reduced with an increase in temperature. Self-immobilisation of **62a** is deleterious to the activity attributed to the instability of the activated iron species in the absence of ethylene. Immobilisation onto silica at position S1 or S2 in **62b** produces highly active systems albeit with lower activities than their homogeneous counterparts.[118, 119] The introduction of silica core, polystyrene coated supports at the *para*-position of the aryl ring (S3) also produces an active system for the polymerisation of ethylene.[120] Chain growth is inhibited when employing iron catalysts encapsulated by cyclodextrin and gives activities that are 1000 times lower than the homogeneous iron aldimine system for the polymerisation of ethylene.[121]

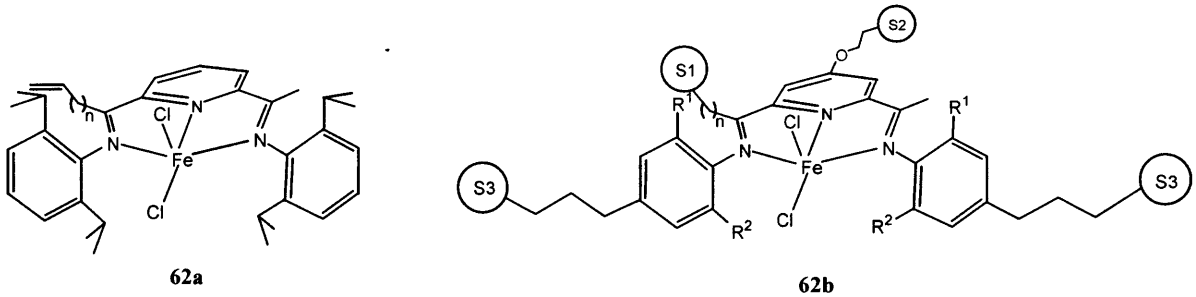

62a **62b**

Figure 10 Heterogenised pyridine-diimine iron system

In contrast to the α-diimine nickel system, the pyridine-diimine iron family are capable of polymerising propylene with high activities at –20 °C into highly regioregular *i*PP (50-70 %), albeit with low molecular weight (*Mw* x10^3).[122] The tacticity is independent of the catalysts symmetry, due to the dominance of a chain-end control mechanism. The system produces *i*PP *via* initially inserting propylene in a 1,2 fashion, followed by successive 2,1 insertions, with the exclusive formation of α-olefin end groups, by β-H elimination (Scheme 11). Removal of steric bulk at least one of the *ortho*-positions renders the catalyst highly active for the linear, head-to-head dimerisation of α-olefins.[123] Replacing iron with cobalt leads to a higher selectivity for the linear dimerisation of α-olefins and a greater tendency towards isomerising the α-olefin feed.[124]

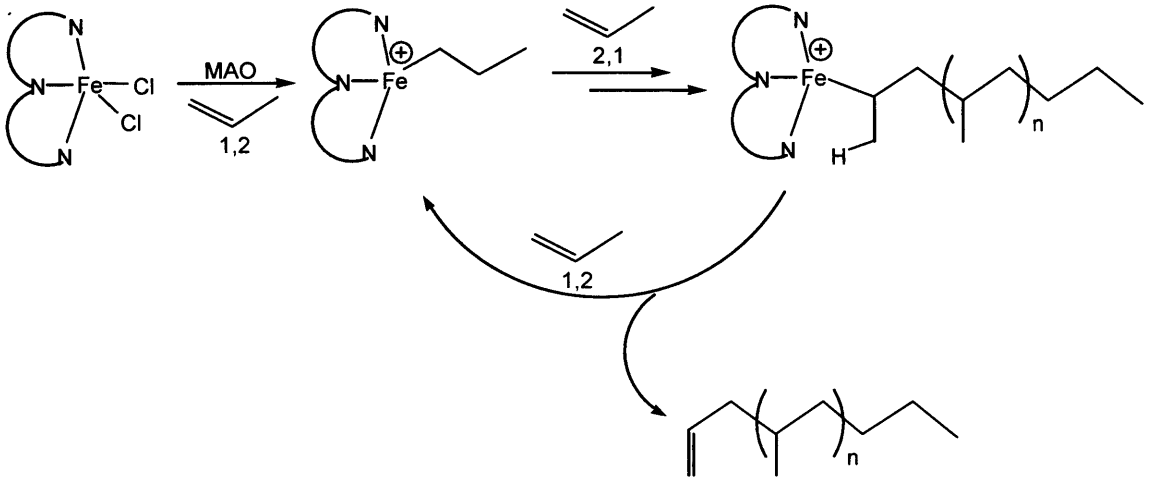

Scheme 11 Mechanism for the generation of *i*PP with α-olefin end groups

Modification of the central pyridine ring with a pyrimidine donor (**63**) results in a reduction in polymerisation activity and an increased proportion of unsaturated end groups upon comparison with the related pyridine-diimine system (Figure 11).[125] Employing triazine (**64**) or a five-membered heterocyclic core, carbazolide donor (**65**) respectively prevents coordination to $FeCl_2$ or affords an inactive system for the polymerisation of ethylene at 1-bar pressure.[125, 126] Replacing one of the imine donors with a pyridine donor (**66**) reduces the steric hindrance at the metal centre thereby producing a catalyst system with high selectivity for the formation of 1-butene and 1-hexene.[127] The steric bulk is not only present to reduce

chain transfer but also as a prerequisite for preventing the formation of the inactive *bis*-ligated cationic complex, **67**.[128]

The pyridine-diiminophosphorane complexes of vanadium, iron and cobalt show a trend in activity for ethylene polymerisation as follows: Fe[129] (**68b** *inactive*) < Fe[130] ≈ Co (**68b** or **68c**: 5-30 g/mmol/h/bar) < V (**68a**: 140 g/mmol/h/bar).[131] In contrast to the pyridine-diimine system UHMPE is formed with a relatively broad unimodal molecular weight distribution when vanadium is acting as the metal centre. Pyridine-diimine iron complexes with the aryl ring replaced by a pyrrolyl (**69**) or a hydrazone (**70**) group exhibit lower activities, lower molecular weight formation and shorter lifetimes than **55** for the polymerisation of ethylene.[132] The molecular weight is dependent upon pressure, at 0.75 bar of ethylene a Schulz-Flory distribution of oligomers and low molecular weight PE is obtained, whilst increasing the pressure to 10-bar yields low molecular weight PE only.[132]

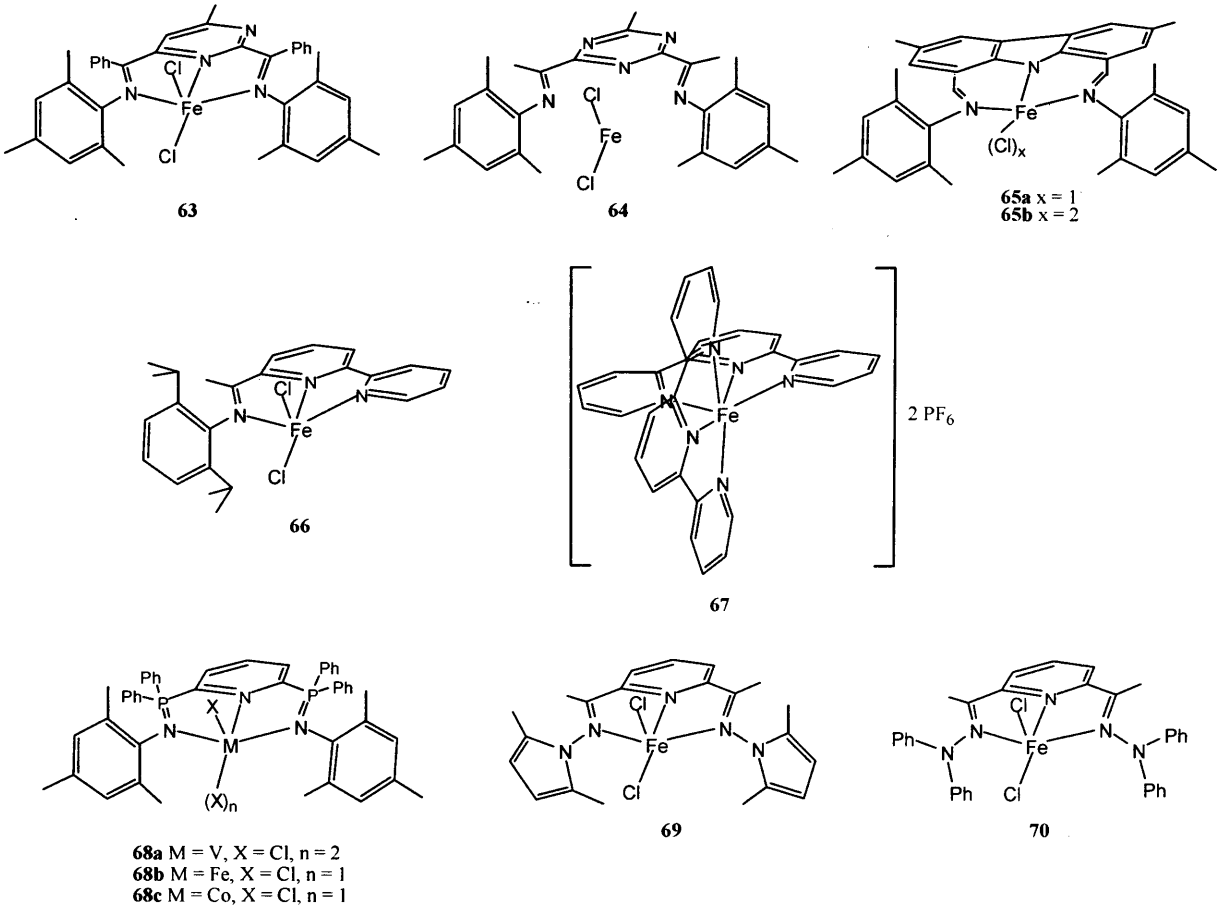

Figure 11 Pyridine-diimine derivatives

1.3.3. Tridentate *NNN*-chelating diamides

Figure 12 depicts the pyridine-diamide ligand family bound in a *meridional*-configuration about the zirconium metal centre (**71**). Activation with MAO yields a highly active (**71a**: 1500 g/mmol/h/bar) and a low activity (**71b**: 2 g/mmol/h/bar) system for the polymerisation of ethylene, which is indicative of the electronic contribution of the substituted aryl ring.[133, 134] Adaptation of the pyridine-diamide donor by employing a tripodal ligand environment centred around a quaternary carbon atom, affords the living polymerisation of 1-hexene at

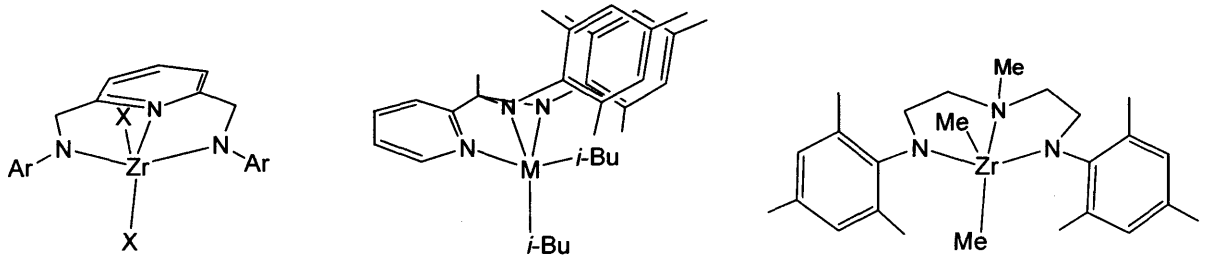

71a Ar = 2,6-i-$Pr_2C_6H_3$, X = Cl
71b Ar = C_6F_5, X = Bz

72a M = Zr
72b M= Hf

73

Figure 12 Tridentate chelating diamides

temperatures below 10 °C when the zirconium and hafnium complexes **72a** and **72b** are activated with $[PhC_3][B(Arf)_4]$.[135, 136] The non-living polymerisation of 1-hexene is achieved by the amino-diamido Zr complex **73** when activated with $[PhNHMe_2][B(Arf)_4]$.[137 - 139] This is attributed to ligand rearrangement about the metal centre (*meridional vs. facial*), followed by catalyst decomposition *via* CH activation of the *ortho*-methyl group and the release of the growing alkyl chain (Scheme 12).[139] Catalyst decomposition can be avoided by utilising chloro-substituents about the 2,6 position of the aryl group.[139]

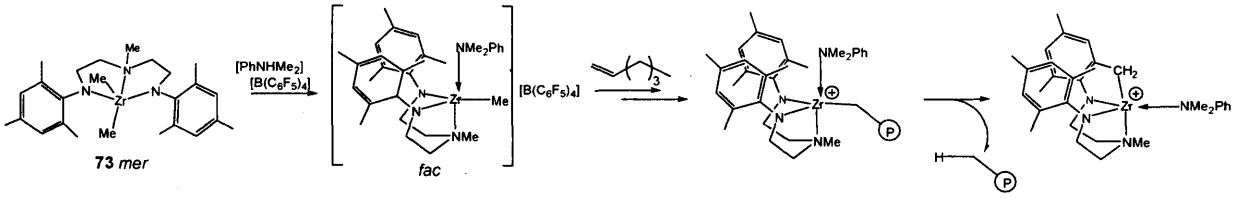

Scheme 12 Catalyst Decomposition of **73**

1.4. Tetradentate *NNNN*-chelating ligand libraries

Complex **74** with the Cn-amido ligand as the support may form a cationic species upon reaction with $[PhNHMe_2][B(Arf)_4]$ (Figure 13).[140] The absence of the additional amido donor affords a cationic species with low activity for the polymerisation of ethylene (**48c**: 10 g/mmol/h/bar).[87] In sharp contrast, the inclusion of the amido donor leads to the production of a highly active system (1790 g/mmol/h/bar), albeit with shorter run times employed. The coordination of the Cn-imido ligand to titanium (**75**) produces an ethylene polymerisation catalyst albeit with low activity.[141, 142] The attempt to isolate the cationic analogue of **76** leads to CH activation of the silicon methyl group thereby deactivating the potential catalytic species (*cf.* **73**).[143]

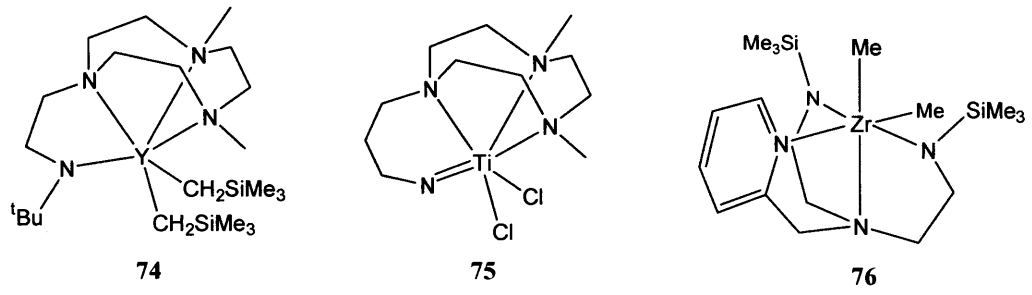

Figure 13 Tetradentate *NNNN*-chelating ligands as supports for group 4 TMs

1.5. *NO*-ligand libraries

1.5.1. Phenoxy-imine ligand set and derivatives thereof

Floriani and co-workers first described the polymerisation of ethylene by the salicylaldiminato-based ligands (phenoxy-imine) with zirconium as the metal centre albeit with very low activities.[144] This concept has been developed to give moderate-to-exceedingly high activities for the polymerisation of ethylene, with group 4, 6 and 10 active metal centres (Figure 14). The following trend in activity with respect to the active metal centre is observed: Cr/MAO (**82a**: < 1 g/mmol/h/bar)[154] < Ti (**81**: 30 g/mmol/h/bar)[153] < Cr/Et_2AlCl (**82a**: 80-96 g/mmol/h/bar)[154] < Ni (**84a**: 537 g/mmol/h/bar)[157] < Cr (**83**: 1760 g/mmol/h/bar)[155] < Ti (**77b**: 33,960 g/mmol/h/bar)[149] < Zr (**78c**: 4,320,000 g/mmol/h/bar).[147]

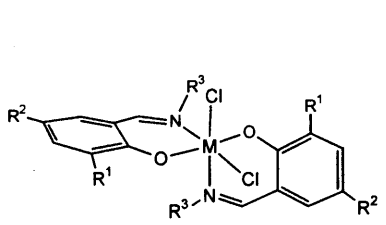

77a M = Ti, R^1 = *t*-Bu, R^2 = H, R^3 = Ph
78a M = Zr, R^1 = *t*-Bu, R^2 = H, R^3 = Ph
78b M= Zr, R^1 = *t*-Bu, R^2 = H, R^3 = Ar
78c M= Zr, R^1 = cumyl, R^2 = Me, R^3 = Cy
79 M = Hf, R^1 = *t*-Bu, R^2 = H, R^3 = Ph

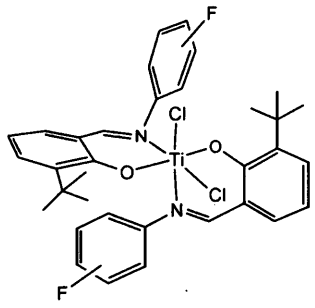

77b

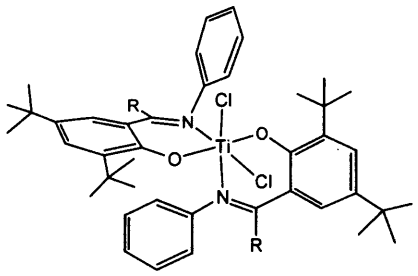

77c R = Me
77d R = Et
77e R = Ph

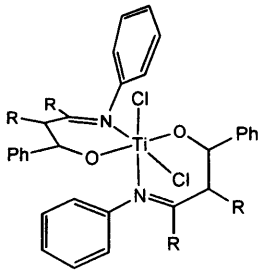

80a R = CF_3
80b R = CH_3

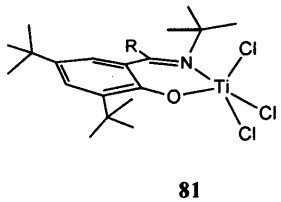

81

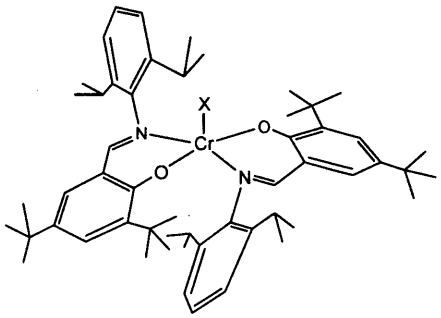

82a X = Cl
82b X = Et

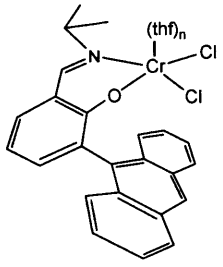

83

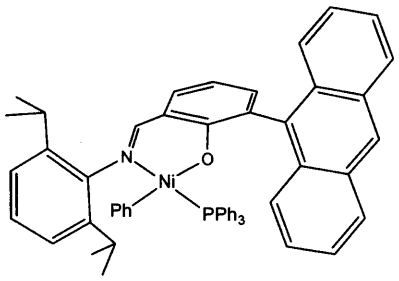

84a

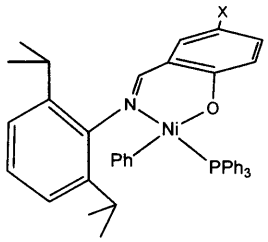

84b X= OMe
84c X= NO_2

Figure 14 Phenoxy-imine complexes

Fujita and co-workers determined that for group 4 TMs, the activity decreases in the order Zr **78** >> Hf **79** > Ti **77a** for the polymerisation of ethylene into HDPE.[145, 146] As for the pyrrolide-imine complexes (**36**) the dichloro moieties adopt a *cis*-configuration in the solid state and DFT calculations indicate that the *cis*-environment is translated into the cationic methyl(ethylene) species.[147] High molecular weight PE can be achieved by employing $[PhC_3][B(Arf)_4]$/*i*-Bu_3Al as the co-catalyst even at moderate temperatures (**78a**). However, with MAO as the co-catalyst exceptionally higher activities are achieved which are even greater than with Cp_2ZrCl_2 under the same conditions. Despite the short run times employed the catalyst lifetime was determined to be at least 30 min long.

Fine-tuning of the ligand architecture can alter the steric and electronic attributes of the metal centre resulting in a deleterious or beneficial effect upon the activity and the microstructure. The introduction of steric bulk at the *ortho*-position of the phenyl substituent adjacent to the imino nitrogen donor leads to a dramatic increase in molecular weight in the following order H << Ph << 2-Me-C_6H_4 < 2-*i*-Pr-C_6H_4 < 2-*t*-Bu-C_6H_4.[147, 148] This trend is achieved *via* reducing the rate of chain transfer. Furthermore, the rate of propagation is reduced thereby diminishing the activities in the reverse order. **78c** is to date the most active phenoxy-imine system. The enhancement in catalytic activity is attributed to the increased steric hindrance *ortho* to the phenoxy donor, which may reduce the interaction of the cationic species and the anionic co-catalyst in addition to protecting the phenoxy donor from electrophilic attack by $AlMe_3$.[145, 147]

The living polymerisation of ethylene with titanium as the metal centre is accomplished even at elevated temperatures by substituting the phenyl group (**77a**) with a pentafluoro aryl ring (**77b**) or by transformation of the imine donor (**77c-e**).[149, 150] Variants of the fluorinated aryl ring and DFT calculations indicate that fluoro-substituents at the *ortho* positions are a necessity for living polymerisation, whilst fluoro-substituents at the *meta* and *para* positions enhance the catalyst activity.[151] The introduction of an electron-withdrawing group at the R position enhances the activity of complex **80** (**80a**: 1320 *vs.* **80b**: 120 g/mmol/h/bar), albeit an order of magnitude less than **77b**.[152] Sterically hindered phenoxy-imines can yield a mono-ligated complex of titanium (**81**) albeit with low activity (30 g/mmol/h/bar), indicative of the importance of *bis*-ligation for the generation of a highly active system.[153]

Complexes **82a** and **82b** show analogous activities and dependence upon the Al co-catalyst as for the pyrrolide-imine Cr complexes (**38**).[154] The addition of an anthracenyl group *ortho* to the phenoxy donor and the replacement of the aryl ring with a small alkyl chain leads to a very highly active *in-situ* generated catalytic system for the polymerisation of ethylene into UHMPE (**83**), even in the presence MAO.[155]

Sterically enhanced phenoxy-imine-based ligands may be employed as supports for nickel to give a mono-ligated neutral catalyst with no requirement for a co-catalyst (**84a**) for the polymerisation of ethylene into medium-to-HDPE.[156, 157] The steric bulk *ortho* to the phenoxy donor not only aids phosphine dissociation and prevents re-coordination, it also hinders ligand disproportionation.[158, 159] The diminishing electrophilicity across a TM series is a contributory factor in the comparatively lower activity observed for **84a** than the optimised chromium and titanium systems **83** and **77b**. Furthermore, the electrophilicity and the activity are also reduced with respect to the cationic α-diimine nickel system **22a**. Both temperature and pressure are capable of controlling the molecular weight of the PE produced (*cf.* **22a** and **106**).[156, 157] Interestingly and in contrast to the DFT calculations the nature of the *para* substituent plays a pivotal role in the activities of complexes **84b** and **84c**. When an electron withdrawing group is present (**84c**) the activity is enhanced despite a prolonged induction period and *vice-versa* for **84b**.[156, 158]

Scheme 13 depicts the phosphine complex as the resting state as determined by experimental and modelling experiments.[157, 158] Chain propagation is assumed to follow a typical Cossee-Arlman mechanism.[11, 12, 13] The stabilised alkyl species orientates the growing polymer chain *trans* to the phenoxy donor.[158] Upon π-coordination of the ethylene molecule

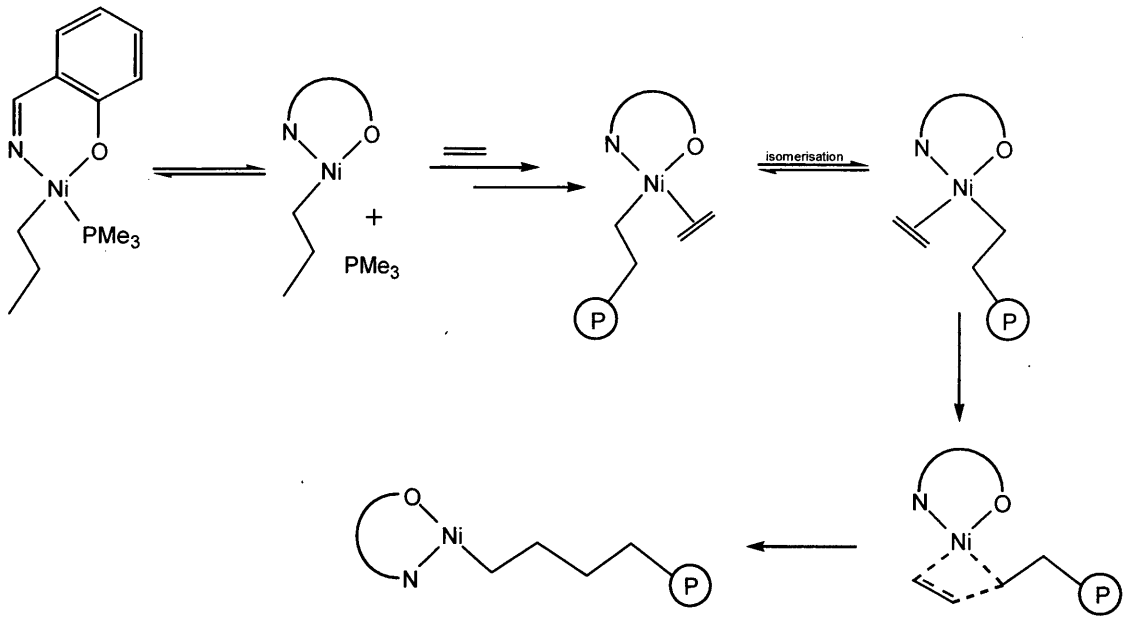

Scheme 13 Postulated propagation pathway

the complex undergoes isomerisation to re-orientate the growing polymer chain *trans* to the imine donor, followed by insertion of the ethylene molecule.[158] The process is repeated until chain transfer occurs *via* β-H transfer to monomer (see Scheme 2 or 6).[158]

Complex **77a** with $[PhC_3][B(Arf)_4]/i\text{-}Bu_3Al$ as the co-catalyst polymerises 1-hexene into high molecular weight atactic poly(1-hexene) with high activity.[160] The ethylene-propylene co-polymerisation by **78a** with MAO or $[PhC_3][B(Arf)_4]/i\text{-}Bu_3Al$ as the co-catalyst is attained with analogous trends to the homo-polymerisation of ethylene.[147] The living polymerisation of propylene at rt into highly stereoregular *s*PP *via* a chain-end control mechanism is achieved by **77b**, albeit with significantly lower activities than the polymerisation of ethylene.[161 – 163] Chain propagation is dominated *via* an initial 1,2 insertion followed by consecutive 2,1 insertions as indicated by chain-end analysis (*cf.* pyridine-diimine iron system, Scheme 12).[162] The sequential addition of ethylene and propylene can lead to the formation of di- (PE-b-PP or PE-b-PE-co-PP) and tri-(PE-b-PE-co-PP-b-PP or PE-b-PE-co-PP-b-PE) block copolymers previously unavailable with the Ziegler-Natta system.[149, 162] In addition, an ethylene/norbornene block copolymer is produced when **80a** is employed as the catalyst.[152]

The self-immobilisation of complex **85** during the polymerisation of ethylene enhances the catalyst activity whilst exhibiting similar functional group tolerance to the homogeneous system.[164, 165]

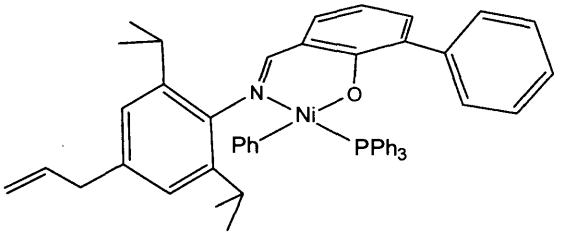

85

Figure 15 Self immobilised Ni Phenoxy-imine system

The reduced oxophilic nature of the neutral late TM complex **84** leads to a greater functional group tolerance than early TM complexes and the cationic α-diimine nickel system. The polymerisation of ethylene in the presence of polar additives such as ethers, ketones and esters produces high molecular weight PE.[157] The tolerance towards water

enables high molecular weight PE to be obtained, albeit at very low activities *via* an emulsion type process.[157, 166] The percentage of incorporation of functionalised α-olefins or norbornenes and non-functionalised α-olefins can be controlled by varying their concentration to produce several functionalised polyolefins ranging from HDPE to LLDPE.[167, 168]

The exocyclic phenoxy-imine derivative with titanium as the metal centre yields a highly active catalyst for the polymerisation of ethylene into high molecular weight PE upon activation with MAO or $[PhC_3][B(Arf)_4]/i\text{-}Bu_3Al$ (**86**: Figure 16).[169] In contrast, replacing the imine donor with a pyridine donor yields only a moderately active system (**87**).[170] DFT calculations show that the *cis*-orientated growing polymer chain and ethylene molecule are *trans* to the phenoxy donors (*cf.* **77**) thereby rendering the steric hindrance *ortho* to the phenoxy donor non-influential on the activity.[170] Upon comparison of complex **88** with **82**, employing the reduced phenoxy-amine-based ligand set does not alter the trend in activity or molecular weight.[171]

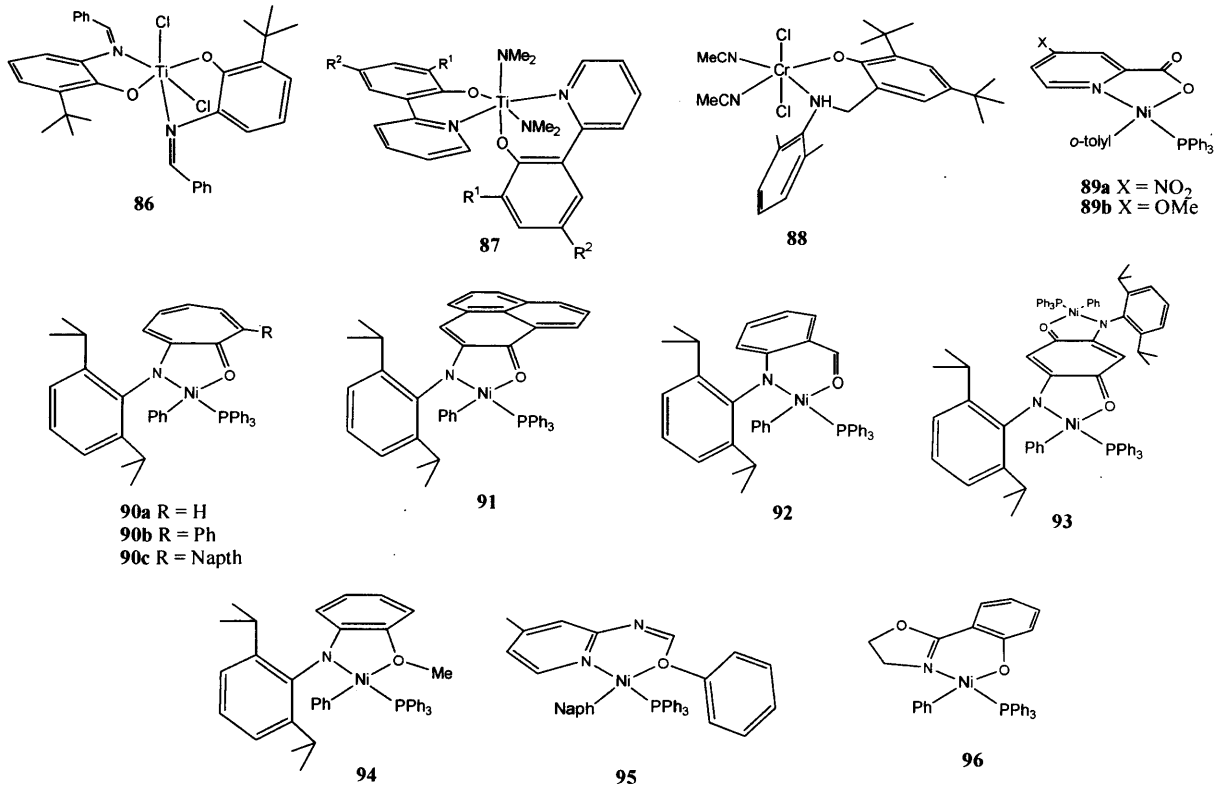

Figure 16 Phenoxy-imine derivatives

Keim and co-workers observe comparative electronic effects to **84** when employing the single-component systems **89a** and **89b** for the polymerisation of ethylene at high ethylene pressure (40-bar).[172] The electron-deficient **89a** produces HDPE with 80-100 % selectivity, whilst the electron-enhanced **89b** gives oligomers as the major product, with 56 % selectivity for linear α-olefins. The five-membered chelate complexes **90** and **91** exhibit similar activities and temperature and pressure dependence upon the microstructure of the PE produced in the absence of a phosphine scavenger as for **84**.[173 - 175] However, the catalyst lifetime is appreciably reduced. In contrast to **84**, steric bulk *ortho* to the oxygen donor does not significantly enhance the catalysts activity and it leads to quasi-living polymerisation at rt.[174] Complex **90** is capable of polymerising ethylene in the presence of ethyl acetate, water, triethylamine and neat thf with comparable activities to those obtained with complex **84**.[173, 174]

The six-membered chelating, amido-aldehyde nickel system **92** reported by Novak *et al.* yields similar activities to **84**.[38] The precursor to the α-diimine nickel η^3-benzyl system is active for the quasi-living polymerisation of ethylene and the co-polymerisation of ethylene with functionalised norbornenes *only* in the presence of $Ni(COD)_2$, which acts as a phosphine scavenger.[176] The novel binuclear single-component system **93** exhibits comparable low activity for the polymerisation of ethylene as for **84** in the absence of steric bulk *ortho* to the phenoxy donor.[157, 177] The molecular weight distribution is notably broader than that observed for **84**. Complex **94** is capable of oligomerising ethylene albeit with low activities in the presence of $B(C_6F_5)_3$.[178] The six-membered chelate complexes **95** and **96** upon activation with MAO or the utilisation of a phosphine scavenger yield short oligomeric chains.[179, 180] The *bis*-imine-phenol ligand may act as a support for cobalt and nickel with one of the imine donors pendant and in a *cisoid* relationship with the other imine donor.[181] The cobalt complexes exhibit 100 % selectivity for the production of butenes albeit with very low activities. In contrast, the nickel complexes are moderately active for the production of butenes and hexenes.

1.6. *NNO*-ligand libraries

In contrast to complex **73**, the cationic species formed from the reaction of **97** with $[PhNHMe_2][B(Arf)_4]$ is stable and acts as a catalyst for the living polymerisation of 1-hexene at 0 °C (Figure 17).[182 - 184] Compound **97** is also a highly active catalyst (810 g/mmol/h/bar) for the polymerisation of ethylene.[182] Replacing the *t*-butyl groups on the amido nitrogen atoms with 2,6-dimethylphenyl, cyclohexyl or *i*-propyl substituents or the employment of the alternative catalyst precursor **98** affords facile chain transfer and the formation of oligomers or low molecular weight poly(1-hexene).[185 - 188] Imposing restrictions upon a 'Berry-type' conformational interconversion in complex **99** is beneficial to the formation of high molecular weight poly(1-hexene) (*cf.* **98**).[189]

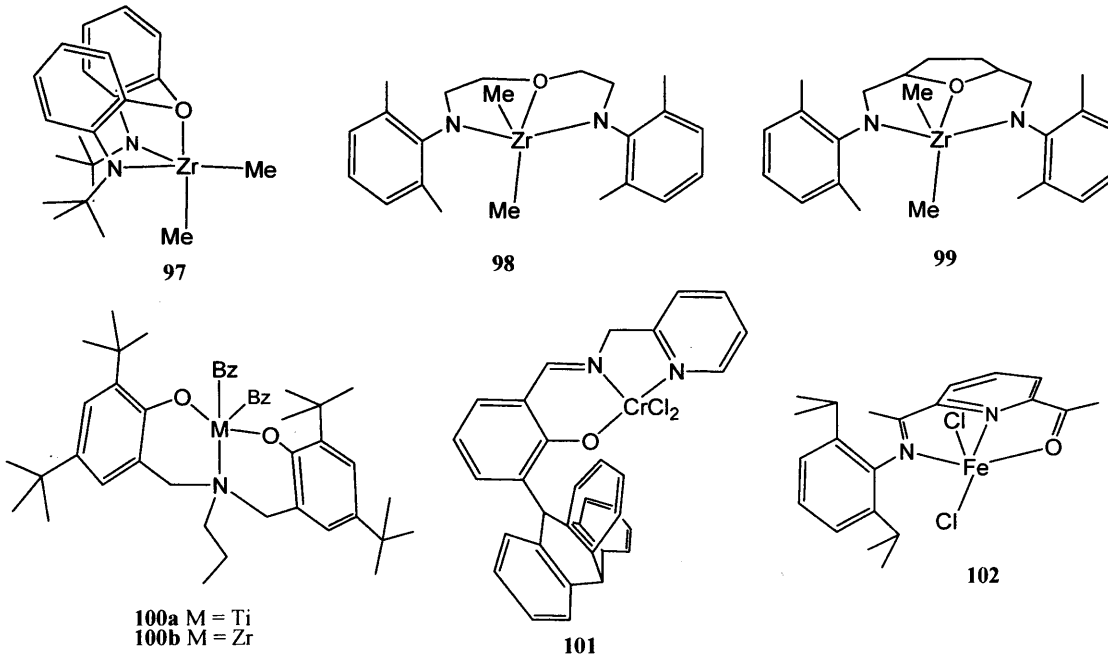

Figure 17 *NNO*-Ligand sets

The titanium complex **100a** exhibits poor activity for the homo-polymerisation of 1-hexene upon activation with $B(C_6F_5)_3$, whilst the zirconium analogue oligomerises 1-hexene with low activity.[190, 191] The additional pyridine donor present in **101** enhances the polymerisation activity of ethylene and is deleterious to the molecular weight upon comparison with the phenoxy-imine chromium system **83**.[155] Complex **102** is highly active for the polymerisation of ethylene. Contradictory results are obtained for the microstructure

with Gomes and co-workers concluding branched PE is formed whilst, Gibson and co-workers observe a mixture of linear α-olefins and linear paraffins.[192, 193]

1.7. *NNOO*-ligand libraries

Low activities for ethylene polymerisation are observed with the tetradentate *bis*-phenoxy-*bis*-imine donor upon coordination to both titanium and zirconium (**103**).[194, 195] The combination of **104** with a borane activator polymerises propylene with high regio- and stereo-selectivity into *i*PP.[196] The postulated mechanism is that of enantiomorphic site control with facile chain transfer to monomer and aluminium. The living polymerisation of 1-hexene is accomplished at 25-40 °C by **105a**/ $B(C_6F_5)_3$ albeit with low activity, whilst the combination of **105b** and $B(C_6F_5)_3$ produces a highly active system for the homo-polymerisation of 1-hexene.[190, 191, 197-199] Upon comparison with **100** it is evident that the forth donor is a prerequisite for enhanced activity and for polymerising 1-hexene in a living fashion when zirconium or titanium are acting as the active metal centre.

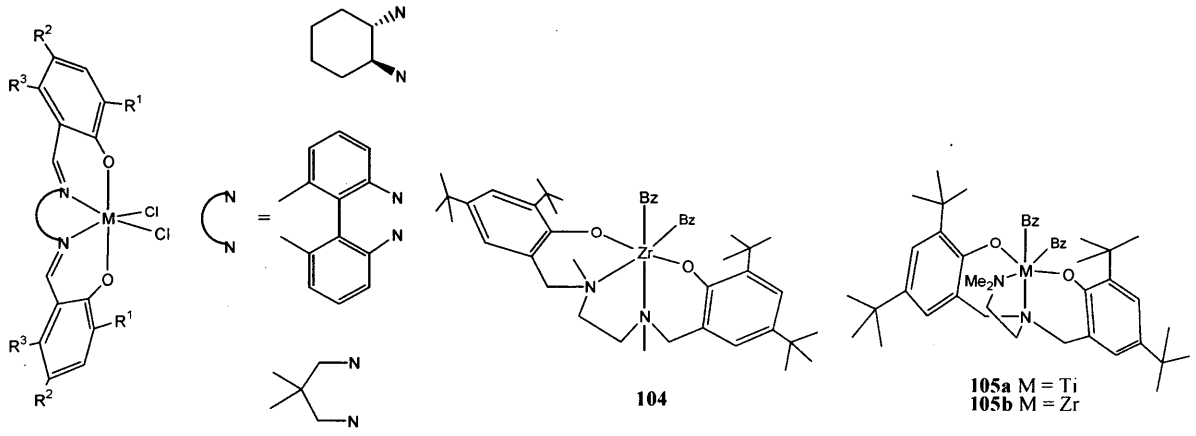

103a M = Ti, $R^1 = R^2$ R^3 = H
103b M = Zr, R^1 = *t*Bu, R^2 = H, R^3 = Me

104

105a M = Ti
105b M = Zr

Figure 18 *NNOO*-Ligand sets

1.8. *PO*-ligand libraries

As stated in the overview Keim and co-workers in 1978 discovered the oligomerisation of ethylene at 50 bar-ethylene pressure and 50 °C into linear α-olefins by employing the phosphorane-phenolate bidentate nickel complex **106a** (Figure 19).[32] Employing *n*-hexane as

opposed to toluene as the solvent leads to the formation of high molecular weight HDPE.[32] The addition of phosphine scavengers to **106a** leads to the formation of low molecular weight PE at moderate ethylene pressure (3.5 - 5 bar).[33, 34] The optimised ligand architecture was found to be that present in **106c** and **106d**.[33, 34] Further enhancement of activity and the non-requirement of a phosphine scavenger can be achieved *via* replacing the strongly co-ordinated phosphine donor with the labile pyridine donor (**106d**) or the readily cleaved μ-oxo dimer (**107**).[33, 34] Functional group tolerance is evident by the polymerisation of ethylene in functionalised organic and aqueous media.[33, 34, 200]

The formation of the inactive *bis*-ligated species can be prevented by enhancing the steric bulk *ortho* to the oxygen donor (*cf.* **84**), which in turn leads to an increase in ethylene polymerisation activity (**106b**: 80 *vs.* **108a**: 1730 g/mmol/h/bar).[201] The co-polymerisation of MMA with ethylene by **108a** and **108b** forms chain-end functionalised PE, which is consistent with MMA insertion into the growing PE chain followed by immediate chain termination (*cf.* **23b**).[202] In addition, high activities are obtained for the oligomerisation of propylene (1350 g/mmol/h) and low activities for the oligomerisation of 1-hexene (15 g/mmol/h) by **108**.[201, 202]

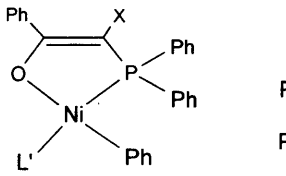

106a X = H, L' = PPh_3
106b X = Ph, L' = PPh_3
106c X = SO_3Na, L' = PPh_3
106d X = SO_3Na, L' = C_5H_5N

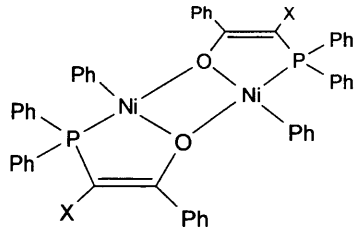

107

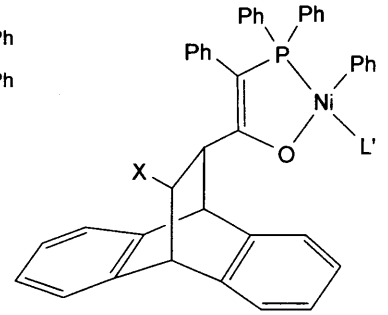

108a X = Me
108b X = C(O)CH(Ph)PPh_3. $Barf_4$

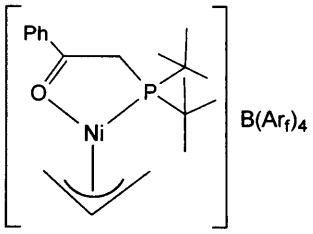

109

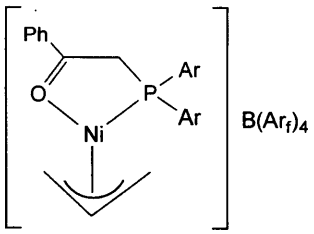

110a Ar = 2,4,6-$Me_3C_6H_2$
110b Ar = C_6H_5

Figure 19 *PO*-ligand sets as supports for Ni complexes

Converting the *PO*-ligand set into a neutral donor enables the formation of the η^3-allyl cationic Ni system **109**, which is highly active for the polymerisation of ethylene (698 g/mmol/h/bar) into moderate molecular weight linear PE.[203] The employment of phenacyldiarylphosphine ligands (**110a**) increases the activity (2473 g/mmol/h/bar) even at low ethylene pressures despite the slower rate of initiation.[204] Reducing the steric bulk of the aryl substituents yields a highly active system (**110b**) for the dimerisation of ethylene to predominantly 1-butene. Complex **109** remains active in the presence of ethyl acetate and is capable of copolymerising ethylene and methyl 10-undecenoate with polar co-monomer incorporation up to *ca.* 5 mol%.[203]

1.9. Summary

The introduction has provided a valuable insight into olefin polymerisation by non-Cp based ligands (*NN*-, *NNN*-, *NNNN*-, *NO*-, *NNO*-, *NNOO*- and *PO*-chelates) acting as supports for early-to-late TM catalysts. It is apparent that the microstructure of PE is dependent on the type of metal centre employed in the catalysis. In general, highly linear PE is produced with groups 4-8, group 9 is intermittent and group 10 affords moderate-to-highly branched PE attributed to a chain-walking mechanism. The α-diimine and pyridine-diimine systems emphasise the importance of the cumulative effects of both the ligand and the metal centre *via* showing high activities for specific metal centres. The initial discoveries by Brookhart, Schrock, McConville and Gibson highlighted the necessity for steric control by employing aryl rings with steric hindrance in the *ortho*-position thereby hindering chain transfer. Further investigation with alternative ligand families has continued to develop the concept of steric control. For example, fine-tuning of the phenoxy-imine ligand architecture enables the system to be moderate-to-highly active for early-to-late TMs. Increasing the steric bulk at the ortho-position of the aryl ring adjacent to the imine nitrogen donor and *ortho* to the phenoxy donor leads to an active mid-to-late TM system (**83** and **84**). This is attributed to a reduction in chain transfer, facile dissociation and hindered re-coordination of the labile ligand and hindered

ligand disproportionation. In contrast, a reduction in steric bulk orientated around the imine and phenoxy donors favours *bis*-ligation, which is deleterious to mid-to-late TMs but advantageous to early TMs bound to a bidentate ligand (**77** and **78** also **35** and **45**).

1.10. Aims and Objectives

Within the proceeding chapters 2 - 6, we are concerned with the synthesis of a range of novel sterically variable *NNN*-, *NNNN*- and *NNO*-ligand sets (**LI** - **LXI**, Figure 20) and their coordination chemistry with mid-late TM divalent metal halides and, in particular, with manganese, iron and cobalt halide precursors. In addition, we probe the ability of some of the resultant complexes, as catalysts for the oligomerisation/polymerisation of ethylene upon activation with MAO.

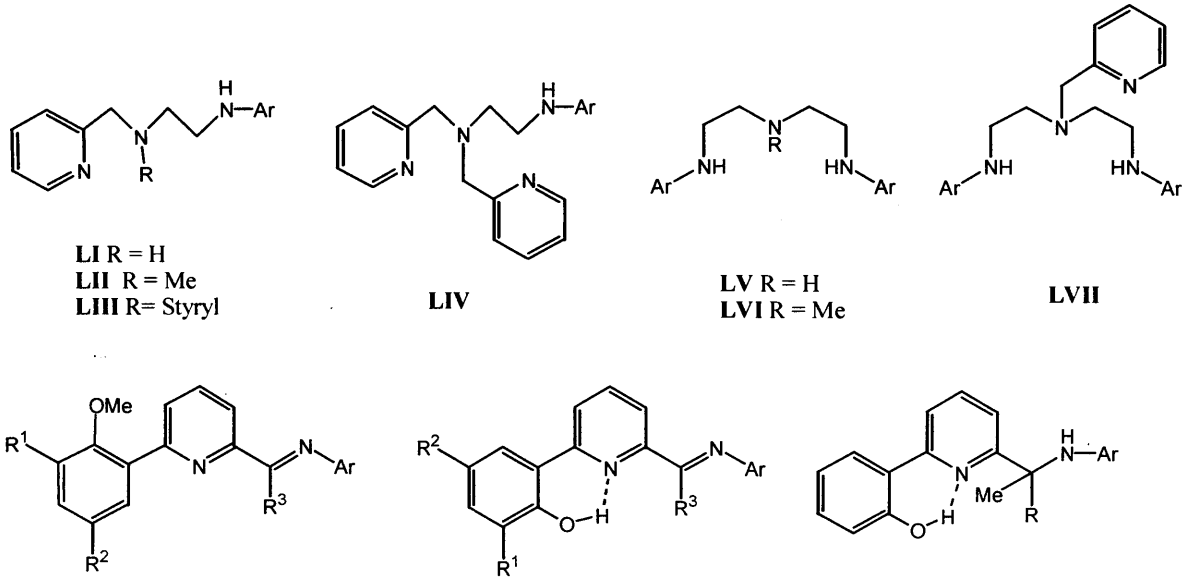

Figure 20 *NNN*-, *NNNN*-, *NNO*-ligand sets

The propensity for *NNN*-systems to form active ethylene polymerisation systems is aided by enhancing the steric bulk around the ligand architecture (section 1.3). For example, modification of the terpyridine (terpy) ligand architecture by replacing one or both of the terminal pyridine donors with *N*-aryl substituted imine moieties yields respectively, a highly selective catalyst for the formation of 1-butene and 1-hexene or a ethylene polymerisation catalyst when coordinated to iron (section 1.3.2). A similar rational can be applied to bis(2-

picolyl)amine (dpa) affording mono- or di- *N*-aryl substituted ethylamine(s) termed *N*-picolyethylenediamines (**LI** and **LII**) and diethylenetriamines (**LV** and **LVI**). Furthermore, the nucleophilicity of the central amine in **LI** and **LV** can be exploited to furnish the novel ligand sets **LII – LIV** and **LVII**, which may potentially act as polymer incorporated ligand supports (**LIII**) or as tetradentate ligands (**LIV** and **LVII**).

The pyridine-diimine ligand set may be modified *via* replacing an *N*-aryl-imine substituent with a phenol group to form the novel ligand family **LIX**. The inclusion of the pyridine donor atom may lead to a suitable tridentate phenoxy-imine-based iron catalyst for the polymerisation of ethylene (*cf.* α-diimine- *vs.* pyridine-diimine- iron systems; sections 1.2 and 1.3). In addition, the versatility of this *NNO*-ligand set can be exploited to afford suitable tridentate donors for early-to-late TMs (**LVIII - LXI**) with the intended application as ethylene polymerisation catalysts.

An overview of the proceeding findings in chapters 2 - 6, are discussed below:

In Chapter **Two**, the synthesis of *N*-aryl substituted multidentate nitrogen donor ligand sets, $(ArNHCH_2CH_2)\{(2\text{-}C_5H_4N)CH_2\}NH$ (**LI**), $\{(2,4,6\text{-}Me_3C_6H_2)NHCH_2CH_2\}\{(2\text{-}C_5H_4N)CH_2\}NMe$ (**LII**), $\{(2,6\text{-}Me_2C_6H_3)NHCH_2CH_2\}\{(2\text{-}C_5H_4N)CH_2\}N(CH_2C_6H_4CH{=}CH_2)$ (**LIII**) and $(ArNHCH_2CH_2)\{(2\text{-}C_5H_4N)CH_2\}_2N$ (**LIV**), is reported as are the reactions of **LI-LIV** with divalent iron- and cobalt- halides. The notable influence of steric effects upon the nuclearity and the binding mode is described. The flexibility of the **LI** systems when coordinated to iron or cobalt is observed by single crystal X-ray diffraction studies, paramagnetic ^1H NMR spectroscopy and DFT calculations. In addition, a study of the reactivity of the well known ligands, dpa and tpa, with divalent manganese-, iron- and cobalt- halides, is described.

In Chapter **Three**, a series of *N*-aryl substituted multidentate nitrogen donor ligand sets, $(ArNHCH_2CH_2)_2NH$ (**LV**), $(ArNHCH_2CH_2)_2NMe$ (**LVI**) and $(ArNHCH_2CH_2)_2\{(2\text{-}C_5H_4N)CH_2\}N$ (**LVII**) are reported. The reaction of **LV** and **LVI** with $CoCl_2$ affords *NNN*-chelated complexes. Notably, the analogous iron(II) complexes are not produced. Conversely,

LVII is capable of coordinating to iron and cobalt in a *pseudo* tetradentate fashion, this is attributable to the pyridyl moiety.

In Chapter **Four**, the *N*-aryl substituted *NNN*-iron(II) and -cobalt(II) complexes are activated by the addition of excess MAO for the oligomerisation of ethylene. The activities are low-to-moderate at 1 bar ethylene pressure and the selectivity of the catalysts is dependent on the metal centre with the iron systems forming linear α-olefins while the cobalt systems give a mixture of linear and branched oligomers.

In Chapter **Five**, the versatile preparation of the novel *NNO*-ligand sets, 2-{(2'-OMe-3'-R^1-5'-R^2)C_6H_2}6-{CR^3N(2,6-*i*-$Pr_2C_6H_3$)}C_5H_3N (**LVIII**), 2-{(2'-OH-3'-R^1-5'-R^2)C_6H_2}6-{CR^3N(2,6-*i*-$Pr_2C_6H_3$)}C_5H_3N (**LIX**), 2-{(2'-OH)C_6H_4}-6-{CMe_2NH(2,6-*i*-$Pr_2C_6H_3$)}C_5H_3N (**LX**) and 2-{(2'-OH)C_6H_4}-6-{CHMeNH(2,6-*i*-$Pr_2C_6H_3$)}C_5H_3N (**LXI**) is described and their coordination behaviour in aluminium(III), iron(II) and cobalt(II) complexes is reported. Preliminary catalytic evaluation studies reveal moderate-to-high activities for the polymerisation of ethylene into moderate-to-high molecular weight polyethylene.

In Chapter **Six**, full details of the experimental procedures along with the spectroscopic, analytical and X-ray data are reported.

References

[1] A. K. Tullo, *Chemical & Engineering News.*, June 2, 2002, 26-27.
[2] K. W. Doak, D. E. James, D. L. Bleach and Yury V. Kissin, *Encyclopedia of Polymer Science and Engineering.*, F. H. Mark., Ed.; John Wiley & Sons: New York, 1986, **6**, 383-490.
[3] K. Ziegler, E. Holzkamp, H. Breil and H. Martin, *Angew. Chem.*, 1955, **67**, 541-544.
[4] K. Ziegler, *Angew. Chem.*, 1964, **76**, 545-553.
[5] G. Natta, *Angew. Chem.*, 1956, **68**, 393-403.
[6] G. Natta, *Angew. Chem.*, 1964, **76**, 553.
[7] J. P. Hogan and R. L. Banks, U.S. Patent 2, **1958**, 825, 721.
[8] M. P. McDaniel, *Adv. Catal.*, 1985, **33**, 47-98.
[9] A. A. Anderson. H. G. Cordes, J. Herwig, W. Kaminsky, A. Merck, R. Mottweiller, J. Pein, H. Sinn and H. J. Vollmer, *Angew. Chem., Int. Ed. Engl.*, 1976, **15**, 630-632.
[10] W. Kaminsky, *J. Chem. Soc., Dalton Trans.*, 1998, 1413-1418.
[11] P. Cossee, *J. Catal.*, 1964, **3**, 80-88.
[12] E. J. Arlman, *J. Catal.*, 1964, **3**, 89-98.
[13] E. J. Arlman and P. Cossee, *J. Catal.*, 1964, **3**, 99-104.
[14] M. Bochmann, *J. Chem. Soc., Dalton Trans.*, 1996, 255-270.
[15] H. H. Brintzinger, D. Fischer, R. Mulhpaupt, B. Rieger and R. M. Waymouth, *Angew. Chem., Int. Ed. Engl.*, 1995, **34**, 1143-1170.
[16] R. F. Jordan, W. E. Dasher and S. F. Echols, *J. Am. Chem. Soc.*, 1986, **108**, 1718-1719.
[17] Y. Koide, S. G. Bott and A. Barron, *Organometallics*, 1996, **15**, 2213-2226.
[18] S. H. Strauss, *Chem. Rev.*, 1993, **93**, 927-942.
[19] G. G. Hlatky, D. J. Upton and H. W. Turner, US Pat. Appl., 1990, 459921.
[20] X. Yang, C. L. Stern and T. J. Marks, *Organometallics*, 1991, **10**, 840-842.
[21] X. Yang, C. L. Stern and T. J. Marks, *J. Am. Chem. Soc.*, 1991, **113**, 3623-3625.
[22] J. C. Stevens, F. J. Timmers, D. R. Wilson, G. F. Schmidt, P. N. Nickias, R. K. Rosen, G. W. Knight and S. Y. Lai, (DowChemical Co., USA)., Eur. Patent EP416815, 1991, Chem. Abtsr., 1991, **115**, 93163.
[23] J. A. M. Cannich, (Exxon Chemical Patents, Inc., USA)., Eur. Patent EP420436, 1991., *Chem. Abtsr.*, 1991, **115**, 184145
[24] J. C. W. Chien, Z. T. Zu, M. M. Marques, J. C. Flores and M. D. Rausch, *J. Polym. Sci. Polym. Chem.*, 1998, **36**, 319-328.
[25] D. van Leusen, D. J. Beetstra, B. Hessen and J. H. Teuben, *Organometallics*, 2000, **19**, 4084-4089
[26] R. Eimrich, O. Heinemann, R. W. Jolly, C. Krüger and G. P. J. Verhovnik, *Organometallics*, 1997, **16**, 1511-1513.
[27] A. Döhring, J. Göhre, P. W. Jolly, B. Kryger, J. Rust and G. P. J. Verhovnik, *Organometallics*, 2000, **19**, 388-402.
[28] A. L. McKnight, Md. A. Masood, R. M. Waymouth and D. A. Straus, *Organometallics*, 1997, 16, 2879-2285.
[29] Y-X. Chen and T. J. Marks, *Organometallics*, 1997, **16**, 3649-3657.
[30] J. M. Santos, M. R. Ribeiro, M. F. Portela, H. Cramail, A. Deffieux, A. Antinolo, A. Otero and S. Prashar, *Macromol. Chem. Phys.*, 2002, **203**, 139-145.
[31] M. M. Marques, S. G. Correia, J. R. Ascenso, A. F. G. Ribeiro, P. T. Gomes, A. R. Dias, P. Foster, M. D. Rausch J. C. W. Chien, *J. Polym. Sci. Polym. Chem.*, 1999, **37**, 2457-2469.
[32] W. Keim, F. H. Kowaldt, R. Goddard and C. Krüger, *Angew. Chem., Int. Ed. Engl.*, 1978, **17**, 466-467.
[33] U. Klabunde and S. D. Ittel, *J. Mol. Catal.*, 1987, **41**, 123-134.
[34] U. Klabunde, R. Mulhaupt, T. Herskovitz, A. H. Janowicz, J. Calabrese and S. D. Ittel, *J. Polym. Sci. Polym. Chem.*, 1987, **25**, 1989-2003.
[35] L. K. Johnson, M. C. Killian and M. Brookhart, *J. Am. Chem. Soc.*, 1995, **117**, 6414-6415.
[36] S. Mecking, *Angew. Chem., Int. Ed. Engl.*, 2001, **40**, 534-540.
[37] G. J. P. Britovsek, V. C. Gibson and D. F. Wass, *Angew. Chem., Int. Ed. Engl.*, 1999, **38**, 419-447.
[38] V. C. Gibson and S. K. Spitzmesser, *Chem. Rev.*, 2003, **103**, 283-315.
[39] S. D. Ittel, L. K. Johnson and M. Brookhart, *Chem. Rev.*, 2000, **100**, 1169-1203.
[40] G. van Koten and K. Vrieze, *Adv. Organomet. Chem.*, 1982, 21, 151-239.
[41] L. K. Johnson, C. M. Killian, S. D. Arthur, J. Feldman, E. McCord, S. J. McLain, K. A. Kreutzer, M. A. Bennett, E. B. Coughlin, S. D. Ittel, A. Parthasarathy, D. Tempel and M. Brookhart, (UNC-Chapel-Hill/DuPont), WO 9623010, 1996., *Chem. Abstr.*, 1996, **125**, 222773t.
[42] T. V. Laine, M. Klinga, A. Maaninen, E. Aitola and M. Leskela, *Acta. Chem. Scand.*, 1999, **53**, 968-973.
[43] V. C. Gibson, A. Tomov, D. F. Wass, A. J. P. White and D. J. Williams, *J. Chem. Soc., Dalton Trans.*, 2002, 2261-2262.
[44] S. Milione, G. Cavallo, C. Tedesco and A. Grassi, *J. Chem. Soc., Dalton Trans.*, 2002, 1839-1846.
[45] M. C. Killian, L. K. Johnson and M. Brookhart, *Organometallics*, 1997, **16**, 2005-2007.
[46] S. A. Svejda and M. Brookhart, *Organometallics*, 1999, **18**, 65-74.
[47] S. P. Muthukumaru, M. Ravindranathan and S. Sivaram, *Chem. Rev.*, 1986, **86**, 353-399.
[48] J. Skupińska, *Chem. Rev.*, 1991, 91, 613-648.

[49] D. P. Gates, S. A. Svejda, E. Oñate, C. M. Killian, L. K. Johnson, P. S. White and M. S. Brookhart, *Macromolecules*, 2000, **33**, 2320-2334.
[50] L. H. Shultz, D. J. Tempel and M. Brookhart, *J. Am. Chem. Soc.*, 2001, **123**, 11539-11555.
[51] C. M. Killian, D. J. Tempel, L. K. Johnson and M. Brookhart, *J. Am. Chem. Soc.*, 1996, **118**, 11664-11665.
[52] C. Pellecchia and A. Zambelli, *Macromol. Rapid. Commun.*, 1996, **17**, 333-338.
[53] C. Pellechia, A. Zambelli, M. Mazzeo and D. Pappalardo, *J. Mol. Catal. A: Chem.*, 1998, **128**, 229-237.
[54] D. Pappalardo, M. Mazzeo, S. Antinucci and C. Pellecchia, *Macromolecules*, 2000, **33**, 9483-9487.
[55] L. K. Johnson, S. Mecking and M. Brookhart, *J. Am. Chem. Soc.*, 1996, **118**, 267-268.
[56] A. C. Gottfried and M. Brookhart, *Macromolecules*, 2003, **36**, 3085-3100.
[57] A. Held, F. M. Bauers and S. Mecking, *Chem. Commun.*, 2000, 301-302.
[58] B. Y. Lee, G. C. Bazan, J. Vela, Z. J. A. Komon and X. Bu, *J. Am. Chem. Soc.*, 2001, **123**, 5352-5353.
[59] V. Fassina, C. Ramminger, M. Seferin, R. S. Mauler, R. F. de Souza and A. L. Montiero, *Macromol. Rapid. Commun.*, 2003, **24**, 667-670.
[60] M. Sauthier, F. Leca, R.F. de Souza, K. Bernardo-Gusmão, L. F. T. Queiroz, L. Toupet and R. Réau, *New. J. Chem.*, 2002, **26**, 630-635.
[61] T. Schareina, G. Hillerbrand, H. Fuhrmann and R. Kempe, *Eur. J. Inorg. Chem.*, 2001, 2421-2426.
[62] R. T. Stibrany, M. G. Matturo, S. Zushma and A. O. Patil (ExxonMobil Research and Engineering Co., USA). PCT Int. Appl., WO01174743, 2001, *Chem. Abstr.*, 2001, **135**, 289188.
[63] T. J. J. Kinnunen, M. Haukka, T. T. Pakkanen and T. Pakkanen, *J. Organomet. Chem.*, 2000, **613**, 257-262.
[64] A. Yamamoto, K. Morifuji, S. Ikeda, T. Saito, Y. Uchida and A. Misono, *J. Am. Chem. Soc.*, 1965, 4652-4653.
[65] T. Yamamoto, A. Yamamoto and S. Ikeda, *Bull. Chem. Soc. Jap.*, 1972, **45**, 1104-1110.
[66] 4.62 x 10^5 TOF (mol of C_2H_4 converted/mol of Co/h) converted into 3128 g/mmol/h/bar
[67] T. V. Laine, M. Klinga and M. Leskela, *Eur. J. Inorg. Chem.*, 1999, 959-964.
[68] T. V. Laine,K. Lappalainen, J. Liimatta, E. Aitola, B. Lofgren and M. Leskela, *Macromol. Rapid Commun.*, 1999, **20**, 487-491.
[69] C. Bianchini, G. Mantovani, A. Meli and F. Migliaci, *Organometallics*, 2003, **22**, 2545-2547.
[70] R. Chen, J. Bacsa and S. F. Mapolie, *Polyhedron*, 2003, **22**, 2855-2861.
[71] S. P. Meneghetti, P. J. Lutz and J. Kress, *Organometallics*, 1999, **19**, 2734-2737.
[72] T. V. Laine, U. Piironen, K. Lappalainen, M. Klinga, E. Aitola, M. Leskela, *J. Organomet. Chem.*, 2000, **606**, 112-114.
[73] 21.4 TO/min (mol of C_2H_4 converted/mol of Co/min) converted into 36 g/mmol/h/bar
[74] Y. Yoshida, S. Matsui, Y. Takagi, M. Mitani, M. Nitabaru, T. Nakano, H. Tanaka and T. Fujita, *Chem. Lett.*, 2000, 1270-1271.
[75] Y. Matsuo, K. Mashima and K. Tani, *Chem. Lett.*, 2000, 1114-1115.
[76] Y. Yoshida, S. Matsui, Y. Takagi, M. Matini, T. Nakano, H. Tanaka, N. Kashiwa and T. Fujita, *Organometallics*, 2001, **20**, 4793-4799.
[77] D. M. Dawson, D. A. Walker, M. Thornton-Pett and M. Bochmann, *J. Chem. Soc., Dalton Trans.*, 2000, 459-466.
[78] V. C. Gibson, P. J. Maddox, C. Newton, C. Redshaw, G. A. Solan, A. J. P. White and D. J. Williams, *Chem. Commun.*, 1998, 1651-1652;
[79] Y. Yoshida, J. Saito, M. Mitani, Y. Takagi, S. Matsui, S. Ishii, N. Kashiwa and T. Fujita, *Chem. Commun.*, 2002, 1298-1299.
[80] G. Tian, H. W. Boone and B. M. Novak, *Macromelcules*, 2001, **34**, 7656-7663.
[81] J-H. Huang, L-S. Chi, R-C. Yu, G. J. Jiang, W-T. Yang, G-H. Lee and S-M. Peng, *Organometallics*, 2001, **20**, 5788-5791.
[82] R. E. Murray, (Union Carbide Chemicals & Plastic Technology Corp., USA)., PCT Int. Appl., WO9901460, 1999, *Chem. Abstr.*, 1999, **130**, 125530.
[83] R. E. Murray, (Union Carbide Chemicals & Plastic Technology Corp., USA)., PCT Int. Appl., *WO 99/01481*, 1999; R. E. Murray, *Chem. Abstr.*, 1999, **130**, 125531.
[84] T. Matsugi, S. Matsui, S. Kojoh, Y. Takagi, Y. Inoue, T. Nakano, T. Fujita and N. Kashiwa, *Chem. Lett.*, 2001, 566-567.
[85] T. Matsugi, S. Matsui, S-i. Kojoh, Takagi, Y. Inoue, T. Nakano, T. Fujita and N. Kashiwa, *Macromolecules*, 2002, **35**, 4880-4887.
[86] S. Hajela, W.P. Schaefer and J. E. Bercaw, *J. Organomet. Chem.*, 1997, **532**, 45-53.
[87] S. C. Lawrence, B. D. Ward, S. R. Dubberley, C. M. Kozak and P. Mountford, *Chem. Commun.*, 2003, 2880-2881.
[88] R. D. Köhn, M. Haufe, S. Mihan and D. Lilge, *Chem. Commun.*, 2000, 1927-1928.
[89] R. D. Köhn, M. Haufe, G. Kociok-Köhn, S. Grimm, P. Wasserscheild and W. Keim, *Angew. Chem., Int. Ed. Engl.*, 2000, **39**, 4337-4339.
[90] J. R. Briggs, *J. Chem. Soc., Chem. Commun.*, 1989, 674-675.
[91] K. Hiya, Y. Nakayama and H. Yasuda, *Macromolecules*, 2002, **36**, 7916-7922. *Ethylene pressure not quoted for polymerisation evaluation.*
[92] G. J. P. Britovsek, V. C. Gibson, B. S. Kimberley, P. J. Maddox, S. J. McTavish, G. A. Solan, A. J. P. White and D. J. Williams, *Chem. Commun.*, 1998, 849-850.

[93] B. L. Small, M. Brookhart and A. M. A, Bennett, *J. Am. Chem. Soc.*, 1998, **120**, 4049-4050.
[94] A. M. A. Bennett, *World Pat., WO 98/27124* (DuPont), 1998; A. M. A. Bennett, *Chem. Abstr.*, 1998, **129**, 122973.
[95] G. J. P. Britovsek, M. Bruce, V. C. Gibson, B. S. Kimberley, P. J. Maddox, S. Mastroianni, S. J. McTavish, C. Redshaw, G. A. Solan, S. Strömberg, A. J. P. White and D. J. Williams, *J. Am. Chem. Soc.*, 1999, **121**, 8728-8740.
[96] G. J. P. Britovsek, S. A. Cohen, V. C. Gibson, P. J. Maddox and M. van Meurs, *Angew. Chem., Int. Ed. Engl.*, 2002, **41**, 489-491.
[97] B. L. Small and M. Brookhart, *J. Am. Chem. Soc.*, 1998, **120**, 7143-7144.
[98] G. J. P. Britovsek, S. Mastroianni, G. A. Solan, S. P. D. Baugh, C. Redshaw, V. C. Gibson, A. J. P. White, D. J. Williams and M. R. J. Elsegood, *Chem. Eur. J.*, 2000, **6**, 2221-2231.
[99] Y. Chen, R. Chen, C. Qian, X. Dong and J. Sun, *Organometallics*, 2003, **22**, 4312-4321.
[100] Y. Chen, C. Qian and J. Sun, *Organometallics*, 2003, **22**, 1231-1236.
[101] Z. M, W-H, Sun, Z-L. Li, C-X. Shao, Y-L. Hu and X-H. Li, *Polym. Int.*, 2002, 51, 994-997.
[102] C. Bianchini, G. Mantovani, A. Meli, F. Migliacci, F. Zanobini, F. Laschi and A. Sommazzi, *Eur. J. Inorg. Chem.*, 2003, 1620-1631.
[103] G. J. P. Britovsek, V. C. Gibson, S. Mastroianni, D. C. H. Oakes, C. Redshaw, G. A. Solan, A. J. P. White and D. J. Williams, *Eur. J. Inorg. Chem.*, 2001, 431-437.
[104] V. C. Gibson, M. J. Humphries, K. P. Tellmann, D. F. Wass, A. J. P. White and D. J. Williams, *Chem. Commun.*, 2001, 2252-2253.
[105] T. M. Kooistra, Q. Knojinenburg, J. M. M. Snits, A. D. Horton, P. H. M. Budzelaar and A. W. Gal, *Angew. Chem., Int. Ed. Engl.*, 2001, **40**, 4719-4722.
[106] E. P. Talzi, D. E. Babushkin, N. V. Semikolenova, V. N. Zudin and V. A. Zakharov, *Kinetics* and *Catal.*, 2001, **42**, 147-153.
[107] K. P. Bryliakov, N. V. Semikolenova, V. N. Zudin, V. A. Zakharov and E. P. Talsi, *Catal. Commun.*, 2004, **5**, 45-48.
[108] G. K. B. Clebson, P. B. Hitchcock, B. S. Kimberley and C. W. Rees, *Chem. Commun.*, 2002, 1498-1499.
[109] D. Reardon, G. Aharonian, S. Gambarotta and G. P. A. Yap, *Organometallics*, 2002, **21**, 786-788.
[110] E. L. Dias, M. Brookhart and P. S. White, *Organometallics*, 2000, **19**, 4995-5004.
[111] D. Reardon, F. Conan, S. Gambarotta, G. Yapp and Q. Wang, *J. Am. Chem. Soc.*, 1999, **121**, 9318-9325.
[112] H. Sugiyama, G. Aharonian, S. Gambarotta, G. P. A. Yap and P. H. M. Budzselaar, *J. Am. Chem. Soc.*, 2002, **124**, 12268-12274.
[113] M. A. Esteruelas, A. M. López, L. Méndez, M. Oliván and E. Oñate, *Organometallics*, 2003, **22**, 395-406.
[114] High temperatures are a contributional factor in the low *Mw* achieved. However, in contrast to pyridine-diimine Fe systems low molecular weight distributions are obtained (*Mw*/*Mn* 1.31-1.86).
[115] K. Hiya, Y. Nakayama and H. Yasuda, *Macromolecules*, 2003, **36**, 7916-7922.
[116] G. J. P. Britovsek, V. C. Gibson, S. K. Spitzmesser, K. P. Tellmann, A. J. P. White and D. J. Williams, *J. Chem. Soc., Dalton Trans.*, 2002, 1159-1171.
[117] In the absence of polar co-monomer the polymerisation of ethylene with the cationic precatalysts reduces the molecular weight distribution significatanly in relation to the neutral *cis*-chloro precataysts. This is attributed to the notable absence of vast quantities of Al.
[118] F. A. Kaul, G. T. Puchta, H. Schneider, F. Bielert, D. Mihalios and W. A. Hermann, *Organometallics*, 2002, **21**, 74-82.
[119] H. Kim, B. H. Han, C-S. Ha, J-K, Kim and H. Suh, *Macromolecules*, 2003, **18**, 6689-6691.
[120] C. Liu and G. Jin, *New. J. Chem.*, 2002, **26**, 1485-1489.
[121] D. Armspach, D. Matt, F. Peruch and P. Lutz, *Eur. J. Inorg. Chem.*, 2003, 805-809.
[122] B. L. Small and M. Brookhart, *Macromolecules*, 1999, **32**, 2120-2130.
[123] C. Pellechia, M. Mazzeo and D. Pappalardo, *Macromol. Rapid Commun.*, 1998, **19**, 651-655.
[124] B. L. Small, *Organometallics*, 2003, **22**, 3178-3183.
[125] G. J. P. Britovsek, V. C. Gibson, O. D. Hoarau, S. K. Spitzmesser, A. J. P. White and D. J. Williams, *Inorg. Chem.*, 2003, **42**, 3454-3465.
[126] V. C. Gibson, S. K. Spitzmesser, A. J. P. White and D. J. Williams, *J. Chem. Soc., Dalton Trans.*, 2003, 2718-2727.
[127] G. J. P. Britovsek, S. P. D. Baugh, O. Hoarau, V. C. Gibson, D. F. Wass, A. J. P. White and D. J. Williams, *Inorg. Chim. Acta.*, 2003, **345**, 279-291.
[128] B. De Bruin, E. Bill, E. Brothe, T. Weyhermüller and K. Wieghardt, *Inorg. Chem.*, 2000, **39**, 2936-2947.
[129] Reaction conditions: 1-bar ethylene pressure, 50°C reactor temperature and MAO as the co-catalyst.
[130] Reaction conditions: 10-bar ethylene pressure, 50°C reactor temperature and MAO as the co-catalyst.
[131] S. Al-Benna, M. J. Sarsfield, M. Thornton-Pett, D. L. Ormsby, P. J. Maddox, P. Brés and M. Bochmann, *J. Chem. Soc., Dalton Trans.*, 2000, 4247-4257.
[132] G. J. P. Britovsek, V. C. Gibson, B. S. Kimberley, S. Mastroianni, C. Redshaw, G. A. Solan, A. J. P. White and D. J. Williams, *J. Chem. Soc., Dalton Trans.*, 2001, 1639-1644.
[133] F. Guerin, D. H. McConville and J. J. Vittal, *Organometallics*, 1996, **15**, 5586-5590.
[134] Z. Ziniuk, I. Goldberg, M. Kol, *Inorg. Chem. Commun.*, 1999, **2**, 549-551.

[135] P. Mehrkhodavandi, P. J. Bonitatebus and R. R. Schrock, *J. Am. Chem. Soc.*, 2000, **122**, 7841-7842.
[136] P. Mehrkhodavandi and R. R. Schrock, *J. Am. Chem. Soc.*, 2001, **123**, 10746-10747.
[137] L-C. Liang, R.R. Schrock, W. M. Davis and D.H. McConville, *J. Am. Chem. Soc.*, 1999, **121**, 5797-5798.
[138] R.R. Schrock, A. L. Caado, J. T. Goodman, L-C. Liang, P. J. Bonitatebus Jr and W. M. Davis, *Organometallics*, 2000, **19**, 5325-5341.
[139] Y. Schrodi, R. R. Schrock and P. J. Bonitatebus Jr, *Organometallics*, 2001, **20**, 3560-3573.
[140] S. Bambirra, D. van Leusen, A. Meetsma, B. Hessen and J. H. Teuben, *Chem. Commun.*, 2001, 637-638.
[141] N. A. H. Male, M. E. G. Skinner, P. J. Wilson, P. Mountford and M. Schröder, *New. J. Chem.*, 2000, **24**, 575-577.
[142] N. A. H. Male, M. E. G. Skinner, S. Y. Bylikin, P. J. Wilson, P. Mountford and M. Schröder, *Inorg. Chem.*, 2000, **39**, 5483-5491.
[143] M. E. G. Skinner, D. A. Cowhig and P. Mountford, *Chem. Commun.*, 2000, 1167-1168.
[144] P. G. Cozzi, E. Gallo, C. Floriani, A. Chiesivilla and C. Rizzoli, *Organometallics*, 1995, **14**, 4994-4996.
[145] S. Matsui and T. Fujita, *Catal. Today.*, 2001, **66**, 63-73.
[146] S. Matsui. Y. Inoue and T. Fujita, *J. Synth. Org. Chem. Jpn.*, 2001, **59**, 232-240.
[147] S. Matsui, M. Mitani, J. Saito, Y. Tohi, H. Makio, N. Matsukawa, Y. Takagi, K. Tsuru, M. Nitabaru, T. Nakano, H. Tanaka, N. Kashiwa and T. Fujita, *J. Am. Chem. Soc.*, 2001, **123**, 6847-6856.
[148] J. Strauch, T. H. Warren, G. Erker, R. Frohlich and P. Saarenketo, *Inorg. Chim. Acta.*, 2000, **300**, 810-821.
[149] J. Saito, M. Mitani, J. Mohri, Y. Yoshida, S. Matsui, S. Ishii, S. Krojoh, N. Kashiwa and T. Fujita, *Angew. Chem., Int. Ed. Engl.*, 2001, **40**, 2918.
[150] S. Reinartz, A. F. Mason, E. B. Lobkovsky and G. W. Coates, *Organometallic*, 2003, **22**, 2542-2544.
[151] M. Mitani, J-I. Mohri, Y. Yoshida, J. Saito, S. Ishii, K. Tsuru, S. Matsui, R. Furuyama, T. Nakano, H. Tanaka, S-I. Kojoh, T. Matsugi, N. Kashiwa and T. Fujita, *J. Am. Chem. Soc.*, 2002, **124**, 3327-3336.
[152] X-F. Li, K, Dai, W-P. Ye, L. Pan and Y-S, Li, *Organometallics*, 2004, **23**, 1223-1230.
[153] D. Owiny, S. Parkin and F. T. Ladipo, *J. Organomet. Chem.*, 2003, **678**, 134-141.
[154] V. C. Gibson, S. Mastroianni, C. Newton, C. Redshaw, G. A. Solan, A. J. P. White and D. J. Williams, *J. Chem. Soc., Dalton Trans.*, 2000, 1969-1971.
[155] D. J. Jones, V. C. Gibson, S. Green and P. J. Maddox, *Chem. Commun.*, 2002, 1038-1039.
[156] C. M. Wang, S. Friedrich, T. R. Younkin, R. T. Li, R. H. Grubbs, D. A. Banselben and M. W. Day, *Organometallics*, 1998, **17**, 3149-3151.
[157] T. R. Younkin, E. F. Connor, J. I. Henderson, S. K. Friedrich, R. H. Grubbs and D. A. Bansleben, *Science*, 2000, **287**, 460.
[158] M. S. W. Chan, L. Q. Deng and T. Ziegler, *Organometallics*, 2000, **19**, 2741-2750.
[159] E. F. Connor, T. R. Younkin, J. I. Henderson, A. W. Waltman and R. H. Grubbs, *Chem. Commun.*, 2003, 2272-2273.
[160] J. Saito, M. Mitani, S. Matsui, N. Kashiwa and T. Fujita, *Macromol. Rapid Commun.*, 2000, **21**, 1333-1336.
[161] J. Saito, M. Mitani, J. Mohri, S. Ishii, Y. Yoshida, T. Matsugi, S. Kojoh, N. Kashiwa and T. Fujita, *Chem. Lett.*, 2001, 576-577.
[162] M. Mitani, J-I. Mohri, Y. Yoshida, J. Saito, S. Ishii, K. Tsuru, S. Matsui, R. Furuyama, T. Nakano, H. Tanaka, S-I, Kojoh, T. Matsugi, N. Kashiwa and T. Fujita, *J. Am. Chem. Soc.*, 2002, **124**, 3327-3336.
[163] J. Tian, P. D. Hustard and G. W. Coates, *J. Am. Chem. Soc.*, 2001, **123**, 5134-5135.
[164] D. Zhang, G-X. Jin and N. Hu, *Chem. Commun.*, 2002, 574-575.
[165] D. Zhang, G-X. Jin and N-H. Hu, *Eur. J. Inorg. Chem.*, 2003, 1570-1576.
[166] F. M. Bauers and S. Mecking, *Angew. Chem., Int. Ed. Engl.*, 2001, **40**, 3020-3022.
[167] E. F. Connor, T. R. Younkin, J. I. Hendersen, S. Hwang, R. H. Grubbs, W. P. Roberts and J. J. Litzau, *J. Polym. Sci. Polym. Chem.*, 2002, **40**, 2842-2854.
[168] G. J. Fatou, I. G. Marco, M. A. Gomez, J. M. Arribas, A. Fonetecha, M. Aroca and M. C. J. Martinez, *J. Mater. Sci.*, 1996, **31**, 3095-3107.
[169] Y. Suzuki, N. Kashiwa and T. Fujita, *Chem. Lett.*, 2002, 358-359.
[170] Y. Inoue, T. Nakano, H. Tanaka, N. Kashiwa and T. Fujita, *Chem. Lett.*, 2001, 1060-1061.
[171] V. C. Gibson, C. Newton, C. Redshaw, G. A. Solan, A. J. P. White and D. J. Williams, *J. Chem. Soc., Dalton Trans.*, 1999, 827-829.
[172] S. Y. Desjardins, K. J. Cavell, J. L. Hoare, B. W. Skelton, A. N. Sobolev, A. H. White and W. Keim, *J. Organomet. Chem.*, 1997, **544**, 163-174.
[173] F. A. Hicks and M. Brookhart, *Organometallics*, 2001, **20**, 3217-3219.
[174] F. A. Hicks, J. C. Jenkins and M. Brookhart, *Organometallics*, 2003, **22**, 3533-3545.
[175] J. C. Jenkins and M. Brookhart, *Organometallics*, 2003, **22**, 250-256.
[176] S. J. Diamanti, P. Ghosh, F. Shimizu and G. C. Bazan, *Macromolecules*, 2003, **36**, 9731-9735.
[177] D. Zhang and G-X. Jin, *Organometallics*, 2003, **22**, 2851-2854.
[178] S. A. Guram, A. M. Lapointe, H. W. Turner and T. Uno, (Symyx Technologies, USA). PCT Int. Appl., WO0020377, 2000, *Chem. Abstr*, 2000, **132**, 287733.
[179] W-H. Sun, W. Zhang, T. Gao, X. Tang, L. Chen, Y. Li and X. Jin, *J. Organomet. Chem.*, 2004, **689**, 917-929.
[180] Y. Qian, W. Zhao and J. Huang, *Inorg.* Chem. *Commun.*, 2004, 7, 459-461.
[181] L. Wang, W-H. Sun, L. Han, Z. Li, Y. Hu, C. He and C. Yan, *J. Organomet. Chem.*, 2002, **650**, 59-64.

[182] R. Baumann, W. M. Davis and R. R. Schrock, *J. Am. Chem. Soc.*, 1997, **119**, 3830-3831.
[183] R. Baumann and R. R. Schrock, *J. Organomet. Chem.*, 1998, **557**, 69-75.
[184] R. R. Schrock, R. Baumann, S. M. Reid, J. T. Goodman, R. Stumpf and W. M. Davis, *Organometallics*, 1999, **18**, 3649-3670.
[185] R. Baumann, R. Strumpf, W. M. Davis, L-C. Liang and R.R. Schrock, *J. Am. Chem. Soc.*, 1999, **121**, 7822-7836.
[186] L-C. Liang, R. R. Schrock and W. M. Davis, *Organometallics*, 2000, **19**, 2526-2531.
[187] R. R. Schrock, F. Schattenmann, M. Aizenburg and W. M. Davis, *Chem. Commun.*, 1998, 199-200.
[188] M. Aizenberg, L. Turculet, W. M. Davis, F. Schattenmann and R. R. Schrock, *Organometallics*, 1998, **17**, 4795-4812.
[189] M. A. Flores, M. R. Manzoni, R. Baumann, W. M. Davis and R. R. Schrock, *Organometallics*, 1999, **18**, 3220-3227.
[190] E. Y. Tshuva, I. Goldberg, M. Kol, and Z. Goldschmidt, *Inorg. Chem. Commun.*, 2000, **3**, 611-614.
[191] E. Y. Tshuva, I. Goldberg, M. Kol, H. Weitman and Z. Goldschmidt, *Chem. Commun.*, 2000, 379-380.
[192] S. Fernandes, R. M. Bellabarba, A. F. G. Ribeiro, P. T. Gomes, J. R. Ascenso, J. F. Mano, A. R. Dias and M. M. Marques, *Polym. Int.*, 2002, **51**, 1301-1303.
[193] V. C. Gibson, C. Redshaw, G. A. Solan, A. Tomov, A. J. P. White and D. J. Williams, 2004 manuscript in preparation.
[194] J. P. Corden, W. Errington, P. Moore and M. G. H. Wallbridge, *Chem. Commun.*, 1999, 323-324.
[195] P. D. Knight, A. J. Clarke, B. S. Kimberley, R. A. Jackson and P. Scott, *Chem. Commun.*, 2002, 352-353.
[196] V. Busico, R. Cipullo, S. Ronca and P. H. M. Budzelaar, *Macromol. Rapid. Commun.*, 2001, **22**, 1405-1410.
[197] E. Y. Tshuva, S. Groysman, I. Goldberg, M. Kol and Z. Goldschmidt, *Organometallics*, 2002, **21**, 662-670.
[198] E. Y. Tshuva, I. Goldberg, M. Kol, and Z. Goldschmidt, *Chem. Commun.*, 2001, 2120-2121.
[199] E. Y. Tshuva, I. Goldberg, M. Kol, and Z. Goldschmidt, *Organometallics*, 2001, **20**, 3017-3028.
[200] S. Mecking, A. Held and F. M. Bauers, *Angew. Chem., Int. Ed. Engl.*, 2002, **41**, 544-561.
[201] V. C. Gibson, A. Tomov, A. J. P. White and D. J. Williams, *Chem. Commun.*, 2001, 719-720.
[202] V. C. Gibson and A. Tomov, *Chem. Commun.*, 2001, 1964-1965.
[203] W. Lui, J. M. Malinoski and M. Brookhart, *Organometallics*, 2002, **21**, 2836-2838.
[204] J. M. Malinoski and M. Brookhart, *Organometallics*, 2003, **22**, 5324-5335.

University of Leicester

Chapter Two

The Origin of the Flexible *N*-picolyl-en Ligand Family; Functionalisation of the Central Amine, Coordination Behaviour in Manganese, Iron and Cobalt complexes

Abstract

The reaction of dpa with an equimolar amount of MCl_2 in *n*-BuOH at 90 °C afforded $[\{dpa\}MCl(\mu\text{-}Cl)]_2$ (M = Fe **1**, Co **3**) as the sole product. Alternatively, 2 equivalents of dpa, alters the product selection to favour the sole formation of the bis-ligated complexes $[\{dpa\}_2M][Cl]_2$ (M = Fe **2**, Co **4**). The reaction of tpa with one equivalent of MCl_2 in *n*-BuOH at elevated temperatures affords the six-coordinate complexes $[\{tpa\}MCl_2]$ (M = Mn **5**, Fe **6**, Co **7**) and, in the case of $CoCl_2$, the five-coordinate chloride salt $[\{tpa\}CoCl][Cl]$ (**8**). The addition of an excess of $CoCl_2$ in the latter reaction leads to $[\{tpa\}CoCl]_2[CoCl_4]$ (**9**) as the only product. Single crystal X-ray diffraction studies are reported for **1**, **2**, **4**, **5**, **6**, **7**, **8** and **9**. Substitution of one of the picolyl groups in dpa with *N*-aryl substituted ethylamines, to give $(ArNHCH_2CH_2)\{(2\text{-}C_5H_4N)CH_2\}NH$ (**LIa**: Ar = 2,6-$Me_2C_6H_3$, **LIb**: 2,4-$Me_2C_6H_3$, **LIc**: 2,4,6-$Me_3C_6H_2$, **LId**: 2,4,6-*i*-$Pr_3C_6H_2$), is reported. Functionalisation of the central amine in **LI** has been achieved to give, $\{(2,4,6\text{-}Me_3C_6H_2)NHCH_2CH_2\}\{(2\text{-}C_5H_4N)CH_2\}NMe$ (**LII**), $\{(2,6\text{-}Me_2C_6H_3)NHCH_2CH_2\}\{(2\text{-}C_5H_4N)CH_2\}N(CH_2C_6H_4CH{=}CH_2)$ (**LIII**) and $(ArNHCH_2CH_2)\{(2\text{-}C_5H_4N)CH_2\}_2N$ (**LIVa**: Ar = 2,6-$Me_2C_6H_3$, **LIVb**: 2,4-$Me_2C_6H_3$, **LIVc**: 2,4,6-$Me_3C_6H_2$). Treatment of MCl_2 with **LI**, **LII**, **LIII** and **LIV** affords $[\{LI\}FeCl_2]_n$ (**LIa**: n = 1 **10a**, **LIb**: n = 1 **10b**, **LIc**: n =2 **10c**), $[\{LI\}CoCl_2]$ (**LIa**: **11a**, **LIb**: **11b**, **LIc**: **11c**, **LId**: **11d**), $[\{LII\}CoCl_2]$ (**12**), $[\{LIII\}CoCl_2]$ (**13**), $[\{LIV\}MnCl_2]_n$ (**LIVa**: n = 2 **14a**, **LIVb**: n = 1 **14b**, **LIVc**: n =2 **14c**) and $[\{LIV\}FeCl_2]$ (**LVa**: **15a**, **LVb**: **15b**, **LVc**: **15c**). The single crystal X-ray structure determination of **10a**, **10c**, **11a**, **11c** and **12** reveal, the *NNN*-chelate in **10a** to adopt a *meridional* configuration with a distorted square pyramidal geometry at the iron centre, while the bis(μ-chloro) dimeric complex **10b** contains the *NNN*-chelate bound in *facial* fashion. A facial coordination mode of the *NNN*-chelate is also observed for the complexes **11a**, **11c** and **12**, with a distorted trigonal bipyramidal environment at the cobalt centre. Solution state studies are indicative of a facile *mer-fac* isomerisation process at room temperature. DFT calculations performed on **10a** and **11a** reveal low ΔG^0 values indicative of the co-existence of the *meridional* and *facial* configurations for **10a** and **11a**. The solid state

structural analysis of **14a**, **14b**, **15a** and **15b** reveals the nuclearity and the binding mode to be dependant upon the steric bulk at the *ortho*-position of the *N*-aryl substituent. Solution state studies may be indicative of the solid state coordination modes existing in the solution state.

2.1. Introduction

The ligands dpa, tpa and their substituted pyridine analogues, have been shown to act as suitable polydentate supports for mid-late TM compounds (Figure 1). Such compounds have been employed extensively as models for biologically important systems[1 - 3] or as candidates for exhibiting high-spin (HS) low-spin (LS) crossover phenomena.[4 - 9]

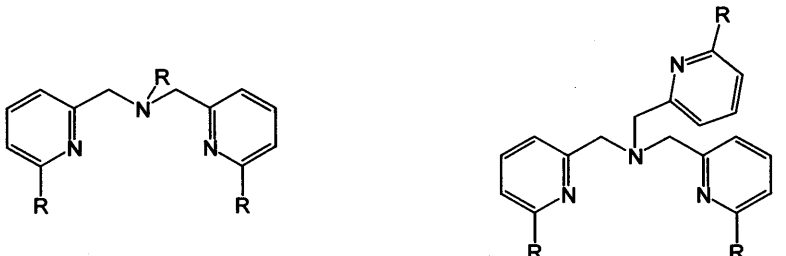

dpa (R = H)
$R_n$dpa (R = hydrocarbyl, n = 1 - 3)

tpa (R = H)
$R_n$tpa (R = halide, hydrocarbyl, n = 1 - 3)

Figure 1 dpa and tpa ligands and their derivatives

Despite the importance of these tri- and tetra-dentate ligand architectures, crystallographically characterised examples of metal(II) halide complexes remain scarce. For example, the *cis*-dichloro-iron(II) tpa complex and the *cis*-dichloro-manganese(II)- and -iron(II)- hydrocarbyl substituted tpa complexes of the formula $LMCl_2$ have only recently been described,[10, 11] whilst for cobalt reports are limited to cationic $[LCoCl]^+$ species.[11, 12] In the case of dpa, the neutral complexes $LMCl_2$ (M = Fe, Co) have only been reported for the more sterically hindered derivatives (*e.g.* 6-Me_2DPA),[12, 13] whereas the well-studied $[L_2Fe]Cl_2$ system has not been structurally characterised.[4]

As already discussed in Chapter 1 (section 1.3), the propensity for *NNN*-systems to form active ethylene polymerisation systems is aided by enhancing the steric bulk around the ligand architecture. For example, modification of the terpy ligand architecture by replacing one or both of the terminal pyridine donors with *N*-aryl substituted imine moieties yields respectively, a highly selective catalyst for the formation of 1-butene and 1-hexene[14] or a ethylene polymerisation catalyst[15 - 17] when coordinated to iron (Figure 2). A similar rational can be applied to dpa affording mono- or di- *N*-aryl substituted ethylamine(s) termed *N*-picolyethylenediamines (**LI**) and diethylenetriamines (**LV**).

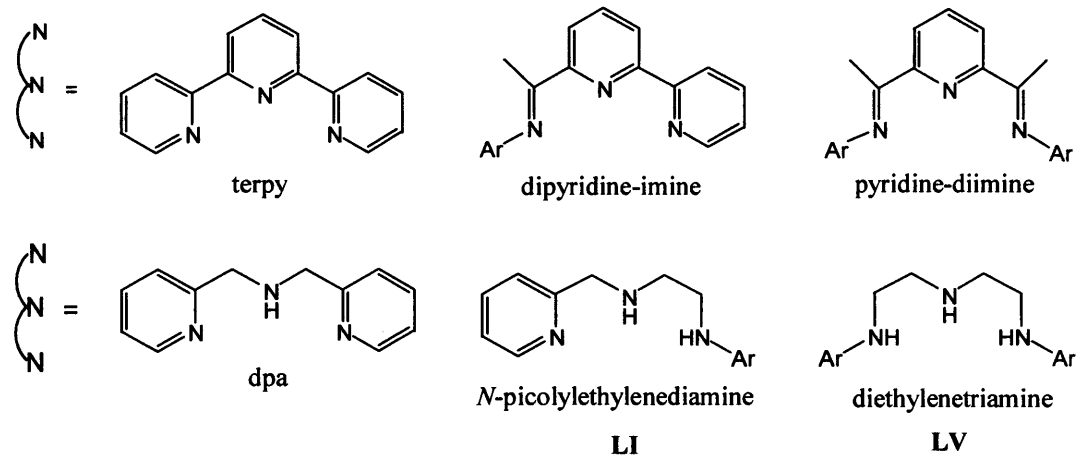

Figure 2 *NNN*-ligand design

Within this chapter we will be focussing on the new sterically variable **LI** ligand family. As is observed in group IV *NNN*-systems (see Chapter 1; section 1.3.3), the flexibility of the *N*-aryl-substituted ethylamine should lend complexes containing **LI** to either adopt the *facial* or the *meridional* geometrical isomers (Figure 3).[18, 19]

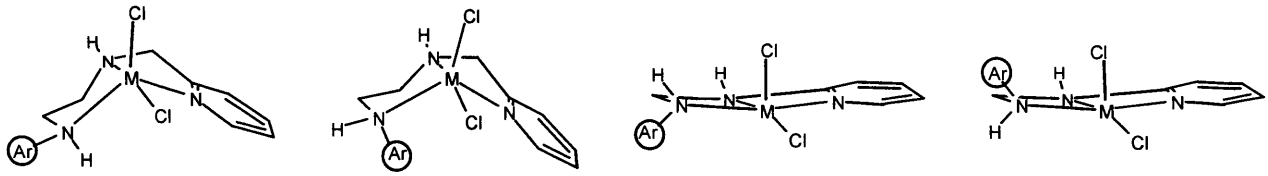

Figure 3 Possible isomeric structures of complexes containing **LI**

In addition, the stereochemistry about the central and terminal amines may increase the number of possible isomeric structures. The nucleophilicity of the central amine in **LI** can be exploited to furnish novel ligand sets (Figure 4), which may potentially act as polymer incorporated ligand supports (**LIII**) or as tetradentate ligands (**LIV**).

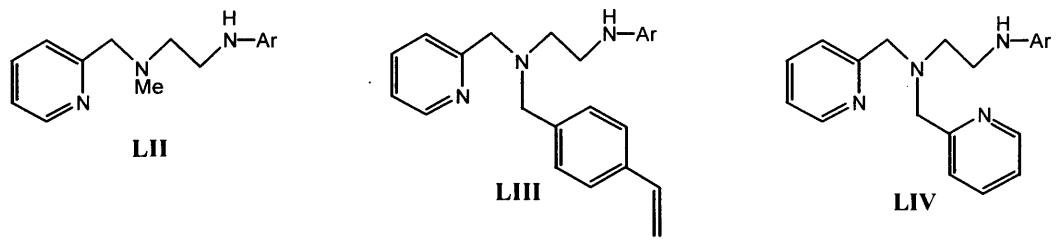

Figure 4 Functionalisation of the central amine in **LI**

In this study, we are concerned with the solid state properties of manganese(II), iron(II) and cobalt(II) halide complexes containing the well-known dpa and tpa ligands and, the novel

NNN- (**LI-LIII**) or *NNNN*- (**LIV**) ligand sets and the importance of steric control upon the nuclearity and the binding mode. In addition, the nature of the solution state is investigated *via* ^{1}H NMR spectroscopy and with the exception of manganese the systematic assignment of the spectra can be achieved despite the paramagnetic nature of the complexes.

2.2. Reactions of MCl_2 (M = Fe, Co) with dpa

The absence of steric bulk about the dpa ligand architecture enables the formation of a mono- and a bis-ligated complex. Addition of 1 equivalent of dpa to a solution of MCl_2 at 90 °C gave the bis(μ-chloro) dimeric complexes $[\{dpa\}MCl(\mu\text{-}Cl)]_2$ (M = Fe **1**, Co **3**) in high yield as the sole product. Indeed, under milder reaction conditions a complex of the composition $[\{dpa\}CoCl_2]$ has also been reported,[12] which has also not been characterised by single crystal X-ray diffraction studies. In contrast, the presence of 1.5 equivalents of dpa afforded the quantitative formation of the complexes $[\{dpa\}FeCl(\mu\text{-}Cl)]_2$ (**1**) and $[\{dpa\}_2Fe][Cl]_2$ (**2**). Upon addition of 2 equivalents of dpa, the product selection favours the sole formation of the bis-ligated complexes (**2** or **4**) in high yield.

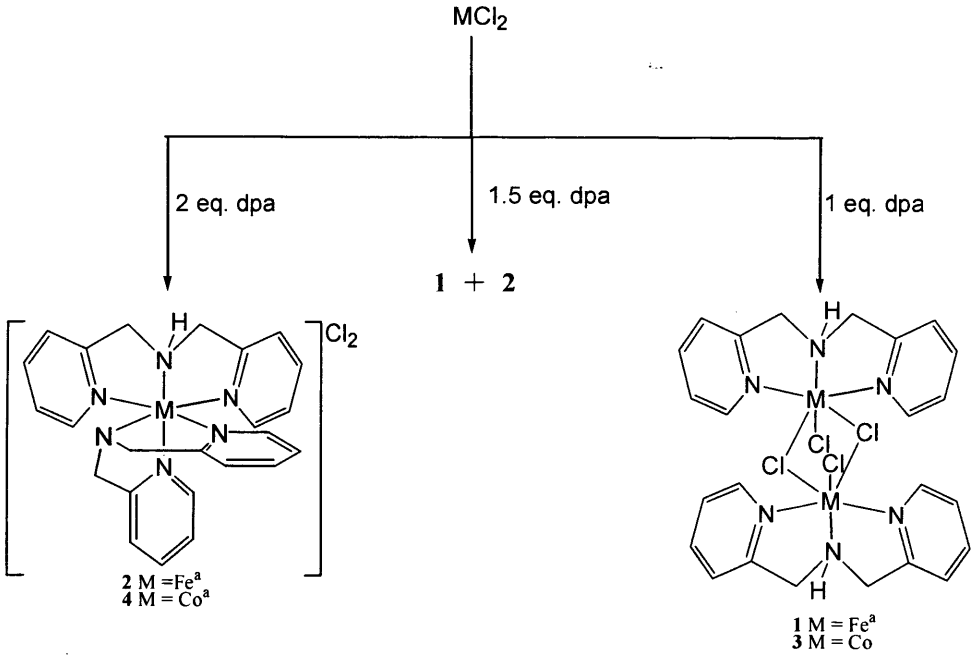

Scheme 1 *Reagents and conditions*: *n*-BuOH, MCl_2, heat
[a] Isolated from single crystal X-ray diffraction studies

With the exception of complex **3**, all products have been characterised by FAB mass spectrometry, magnetic susceptibility, solid state IR spectroscopy and by elemental analysis.

In addition, crystals of **1**, **2** and **4** were grown from slow cooling of a hot acetonitrile solution or dichloromethane at rt and subject to single crystal X-ray diffraction studies. The molecular structures of **1**, **2** and **4** are represented in Figures 5 and 6 and selected bond distances and bond angles are listed in Tables 1 and 2. Crystal data and data collection refinement parameters are presented within Chapter 6; section 6.8.

Table 1 Selected bond distances (Å) and angles (°) for **1**.1⅔CH_2Cl_2

Fe(1)-N(1)	2.174(3)	Fe(2)-N(4)	2.143(3)
Fe(1)-N(2)	2.181(3)	Fe(2)-N(5)	2.167(3)
Fe(1)-N(3)	2.185(2)	Fe(2)-N(6)	2.175(3)
Fe(1)-Cl(1)	2.499(1)	Fe(2)-Cl(1)	2.500(1)
Fe(1)-Cl(2)	2.501(1)	Fe(2)-Cl(2)	2.490(1)
Fe(1)-Cl(3)	2.306(1)	Fe(2)-Cl(4)	2.315(1)
Fe(1)...Fe(2)	3.713(1)		
N(1)-Fe(1)-N(2)	89.28(9)	N(4)-Fe(2)-N(5)	85.06(9)
N(1)-Fe(1)-Cl(1)	89.38(7)	N(4)-Fe(2)-Cl(1)	90.25(7)
N(1)-Fe(1)-Cl(3)	96.23(8)	N(4)-Fe(2)-Cl(4)	98.06(8)
N(1)-Fe(1)-N(3)	76.77(10)	N(4)-Fe(2)-N(6)	76.99(10)
N(1)-Fe(1)-Cl(2)	163.96(8)	N(4)-Fe(2)-Cl(2)	160.98(8)
N(2)-Fe(1)-Cl(1)	163.28(7)	N(5)-Fe(2)-Cl(1)	166.05(7)
N(2)-Fe(1)-Cl(3)	93.79(7)	N(5)-Fe(2)-Cl(4)	95.31(7)
N(2)-Fe(1)-N(3)	76.22(9)	N(5)-Fe(2)-N(6)	77.20(10)
N(2)-Fe(1)-Cl(2)	93.14(7)	N(5)-Fe(2)-Cl(2)	96.28(7)
N(3)-Fe(1)-Cl(1)	87.26(7)	N(6)-Fe(2)-Cl(1)	88.95(7)
N(3)-Fe(1)-Cl(2)	88.40(7)	N(6)-Fe(2)-Cl(2)	84.79(7)
N(3)-Fe(1)-Cl(3)	167.71(7)	N(6)-Fe(2)-Cl(4)	171.26(7)
Cl(1)-Fe(1)-Cl(2)	83.76(3)	Cl(1)-Fe(2)-Cl(2)	83.96(3)
Cl(1)-Fe(1)-Cl(3)	102.92(3)	Cl(1)-Fe(2)-Cl(4)	98.35(3)
Fe(1)-Cl(1)-Fe(2)	93.87(3)	Fe(2)-Cl(2)-Fe(1)	94.07(3)

The molecular structure of **1** consists of a dimeric unit in which the iron(II) centres are bridged by two chloride ligands (Figure 5). Each iron atom is also bound to a terminal chloride and a dpa ligand in a *facial* configuration to give a distorted octahedral geometry with an N3Cl3 donor set at each metal centre. The *facial* coordination mode of the dpa ligand imposes geometry restraints such that the central secondary amines are *trans* to a terminal chloride and the pyridyl groups are *trans* to the bridging chlorides. The Fe-μ-Cl bond distances are similar [2.501(1), 2.499(1), 2.500(1), 2.490(1) Å] and fall at the top end of the range found for related complexes; [{Etdpa}FeCl(μ-Cl)]$_2$,[13] [{2, 2'-dithiazolyl-

disulphide}FeCl(μ-Cl)]$_2$,[20] [{diamine}FeCl(μ-Cl)]$_2$,[21] [{2-(2'-pyridyl)quinoxaline}FeCl(μ-Cl)]$_2$[22] and [{pyridine-imine}FeCl(μ-Cl)]$_2$.[23] The bond distances of the terminal Fe-Cl [Fe(1)-Cl(3) 2.306(1), Fe(2)-Cl(4) 2.315(1)Å] are expectedly shorter than the Fe-μ-Cl bonds in **1** but at the top end of the scale observed in structurally related complexes.[13, 20 - 23] The Fe...Fe distance is 3.713(1) Å and is amongst the longest for previously characterised diferrous complexes with Fe_2Cl_2 cores.[13, 20 - 23] Notably, the Fe-$N_{amine/pyridyl}$ bond lengths are characteristic of a iron(II) complex exhibiting HS behaviour.[13, 20 - 23] Interestingly, the nuclearity of the complex can be altered to favour the formation of a mononuclear species by introducing steric bulk in the 6-position of the pyridyl ring.[13]

Table 2 Selected bond distances (Å) and angles (°) for **2**.3MeCN and **4**.3MeCN

	M = Fe (**2**.3MeCN)	M = Co (**4**.3MeCN)
M(1)-N(3)	1.986(2)	2.140(1)
M(1)-N(2)	2.020(3)	2.149(1)
M(1)-N(1)	1.981(2)	2.124(1)
N(1)-M(1)-N(2)	83.3(1)	80.0(1)
N(2)-M(1)-N(3)	83.2(1)	79.9(1)
N(1)-M(1)-N(3)	86.0(1)	85.7(1)

The molecular structures of **2** and **4** are similar and will be discussed together (Figure 6). The metal(II) centres exhibit pseudo-octahedral geometry with the two tridentate dpa ligands coordinated in a *facial* configuration. The dpa ligands are *facially* coordinated such that the two central amines are mutually *trans* in each complex (*trans-facially* coordinated). This is in contrast to previously reported complexes [{dpa}$_2$Fe][BF_4]$_2$,[24] [{Medpa}$_2$Fe][ClO_4]$_2$,[25] and divalent [{dpa}$_2$M][ClO_4]$_2$ (M = Mn, Zn, Cd, Ni),[26] [{Medpa}$_2$Ni][ClO_4]$_2$[27] and [{dpa}$_2$Cd][Cl]$_2$[26] which all exhibit a *cis-facial* coordination mode. The two chloride anions are weakly coordinated to the [{dpa}$_2$M]$^{2+}$ units *via* hydrogen-bonding with the secondary amine donors of the dpa ligands [H(2)---Cl(1) 2.313 Å (**2**), 2.269 Å (**4**) or N(2)---Cl(1) 3.184 Å (**2**), 3.174 Å (**4**)]. The differences in the Fe-N bond distances are associated with the two types of nitrogen donors present. In both cases the M-N_{amine} bond distances [M(1)-N(2) 2.020(3) (**2**), 2.149(1) Å (**4**)] are longer than the M-$N_{pyridyl}$ bond

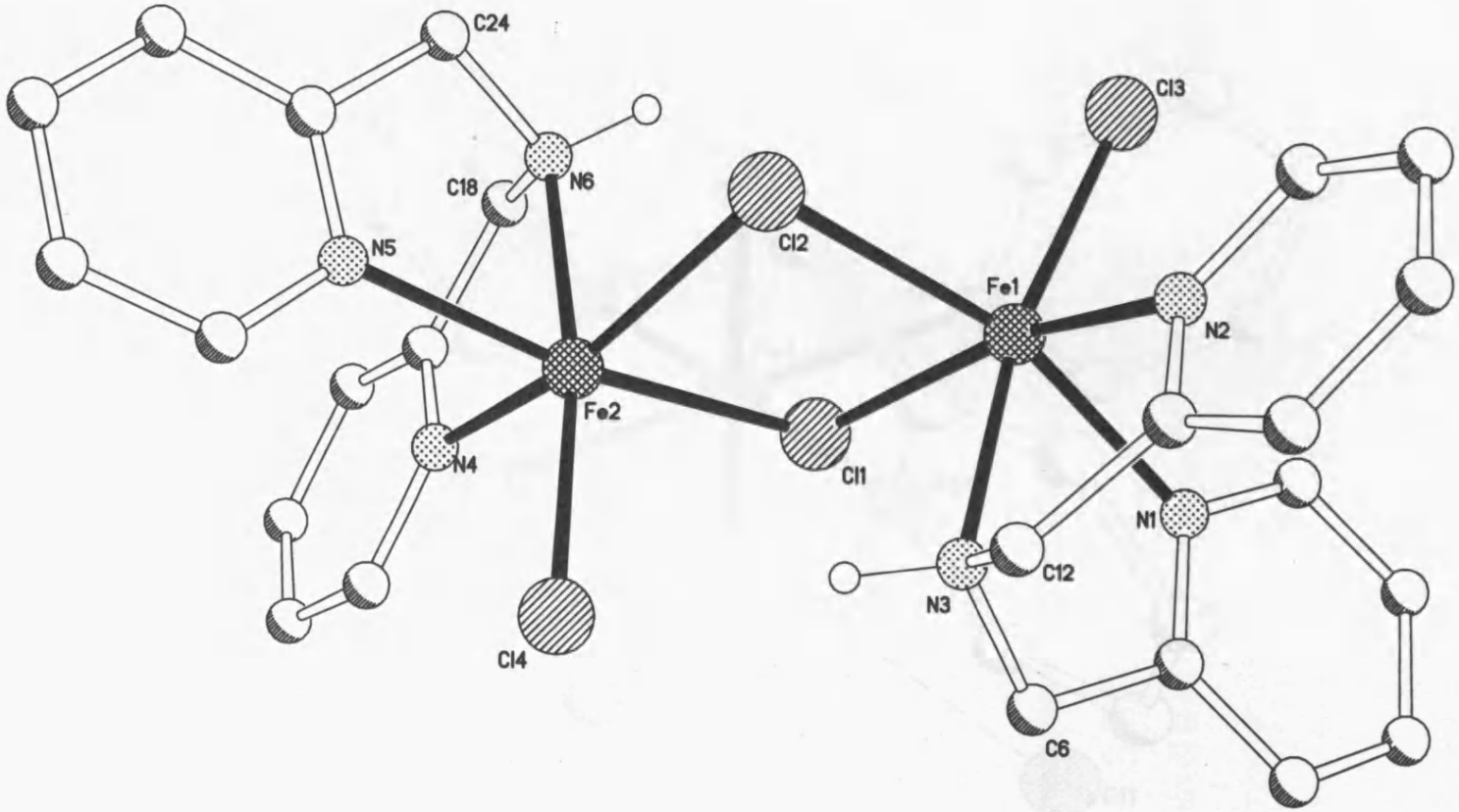

Figure 5 Molecular structure of [{dpa}FeCl(μ-Cl)]$_2$ (**1**) (All the hydrogen atoms apart from H3 and H6 have been omitted for clarity)

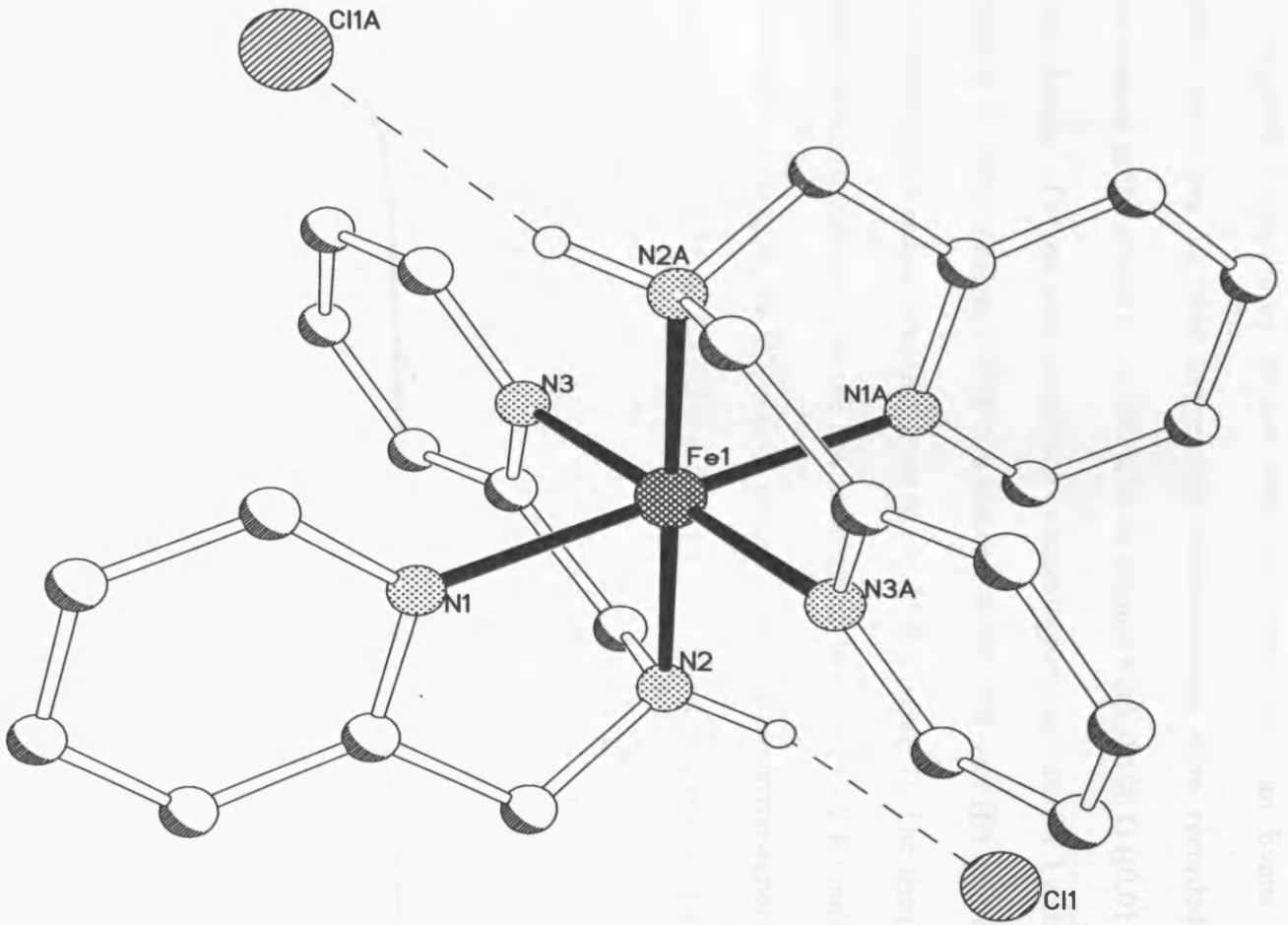

Figure 6 Molecular structure of $[\{dpa\}_2Fe][Cl]_2$ (**2**) (All the hydrogen atoms apart from H2 and H2A have been omitted for clarity). Molecular structure of $[\{dpa\}_2Co][Cl]_2$ (**4**) reveals a similar coordination geometry

distances [Fe(1)-N(1) 1.981(2), Fe(1)-N(3) 1.986 (2) (**2**); Co(1)-N(1) 2.140(1), Co(1)-N(3) 2.124(1) Å (**4**)]. This may be attributable to the sp^2 hybridisation of the latter, which enables dπ–pπ overlap between the metals and the pyridyl nitrogen atoms to occur. In addition, the Fe-$N_{amine/pyridyl}$ bond lengths in **2** are characteristic of a LS iron(II) complex,[24] whilst in **4** the Fe-$N_{pyridyl}$ distances are indicative of a HS cobalt(II) complex.[28, 29]

Magnetic susceptibility studies were performed using an Evans Balance (Johnson Matthey) at rt and variable temperature measurements were recorded using a SQUID magnetometer in the region of 2 - 300 K in an applied field of 100 G ((0.01 T) see appendices for calculations). The variable temperature magnetochemical data for **1** exhibits a rt magnetic moment at 7.4 BM consistent with two non-interacting HS iron (II) centres $^5T_2$ (^5D, $S = 2$), which essentially remains constant down to *ca.* 75 K (Figure 7). The temperature-dependent decrease of the susceptibility in the low temperature region (75 - 2 K) indicates the presence of zero-field splitting of the HS iron(II) ground state[30] or antiferromagnetic coupling. The rt magnetic moment of **3** is at 5.73 BM and is characteristic of two non-interacting HS cobalt(II) centres $^4T_1$ (^4F, $S = 3/2$).

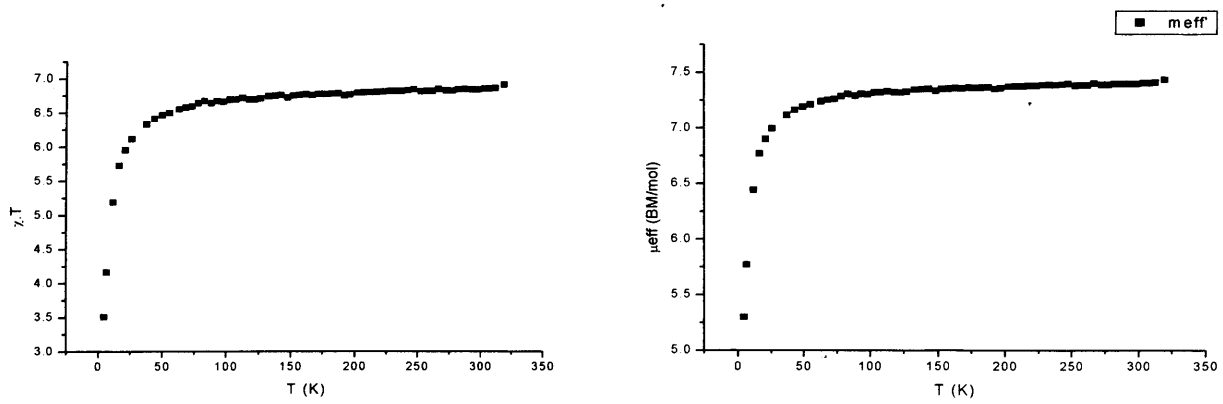

Figure 7 Variable temperature magnetochemical data for **1**

As previously reported by Nelson and Rodgers complex **2** adopts a LS configuration $^1A_1$ (^1S, $S = 0$) and the non-zero value for the magnetic moment can be attributed to paramagnetic impurities of which iron(III) are the most important (Figure 8).[4] Above 50 K and up to 275 K the susceptibility is essentially independent of temperature (*ca.* 0.98 BM). At

275 K the susceptibility begins to increase attributable to the LS-HS crossover transition ($^1A_1 \leftrightarrow {}^5T_2$). In contrast, the high value for the rt magnetic moment (4.44 BM) in **4** suggests a HS configuration $^4T_1$ (^4F, S = 3/2). As already stated, the Fe-N bond distances provide valuable insight into the spin configuration at the iron(II) metal centre. For example, the average Fe-N distance in **1** is *ca.* 0.2 Å longer than in **2**, characteristic of **1** being HS and **2** being LS.

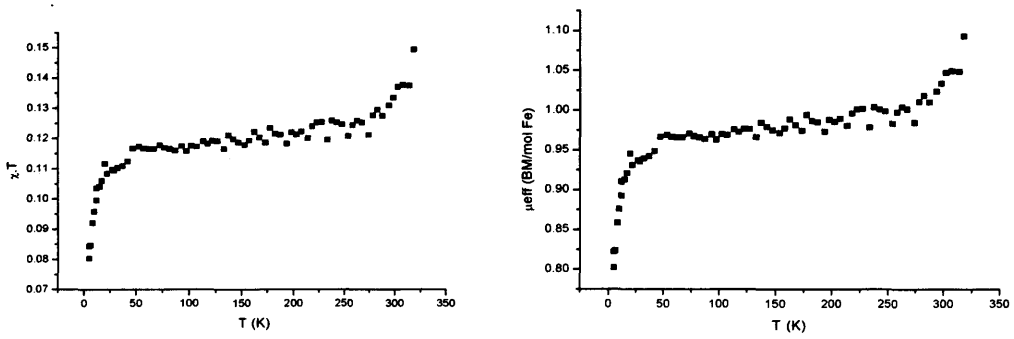

Figure 8 Variable temperature magnetochemical data for **2**

Further insight into the magnetic properties of the complexes **1** - **4** originates from the ^{1}H NMR spectra in CD_3CN at rt. The ^{1}H NMR spectra for complexes **2** and **4** are unassignable due in part to the HS-LS spin transitions and the characteristic paramagnetic shifts and peak broadening (Appendices: Figures 1 and 2). Complete assignment of the ^{1}H NMR spectra of **1** and **3** is possible on comparison with previously reported HS polypyridyl iron(II) and cobalt(II) compounds (Figure 9).[6, 7, 10, 12] Indeed, the spectrum of **3** is similar to the spectrum reported by Gal and co-workers.[12] Therefore, only the spectrum of **1** will be described in detail. The PyCH_α of the coordinated pyridyl arms are found at δ = 116.5 and the secondary amine NH at δ = 107.0, with a T_1 (relaxation time) value of 1.3 ms. The methylene protons are present at δ = 70.8, with a T_1 value of 1.1 ms. The Py$CH_{\beta/\beta'}$ of the coordinated pyridyl donors are found at δ = 54.7 and 51.8 (T_1 = 10.1 and 9.1 ms) and the PyCH_γ at δ = 7.8.

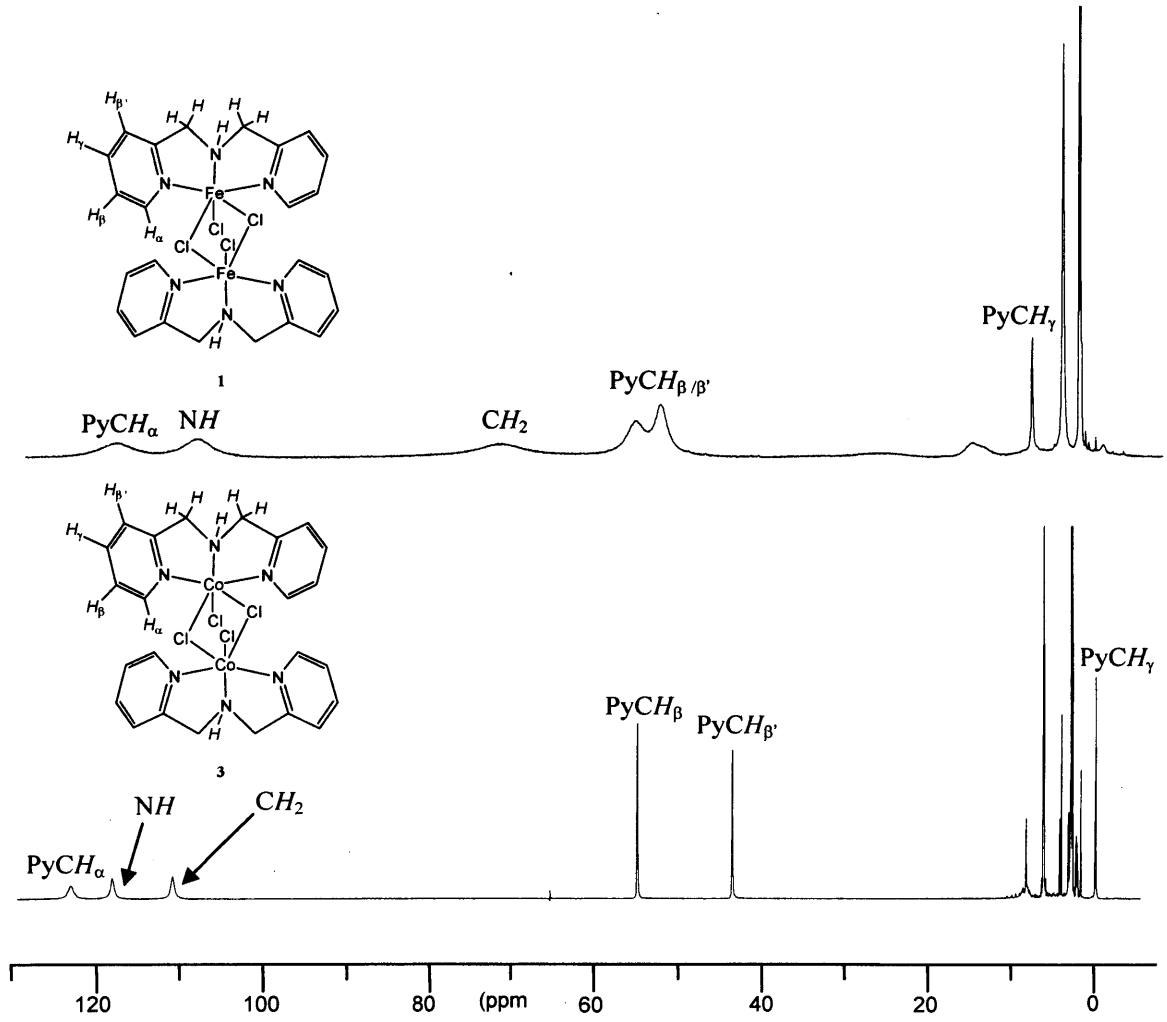

Figure 9 ^{1}H NMR spectra of complexes **1** and **3** in CD_3CN at rt

2.3. Reactions of MCl_2 (M = Mn, Fe, Co) with tpa

Treatment of anhydrous MCl_2 with 1 equivalent of tpa in *n*-BuOH at 90 °C afforded [{tpa}MCl_2] (M = Mn **5**, Fe **6**, Co **7**) in good yield (Scheme 2), as previously reported by Canary and co-workers albeit under different reaction conditions.[31] In addition, with cobalt as the metal centre [{tpa}CoCl][Cl] (**8**) was also isolated; while employing 1.5 equivalents of $CoCl_2$ yields the discrete dicationic unit $[\{tpa\}CoCl]_2^{2+}$ and the anion $[CoCl_4]^{2-}$ as complex **9**. In contrast to the above, the formation of **9** as the sole product has also been achieved *via* the reaction of $CoCl_2$ with 1 - 1.2 equivalents of tpa in methanol or ethanol at rt.[10, 11]

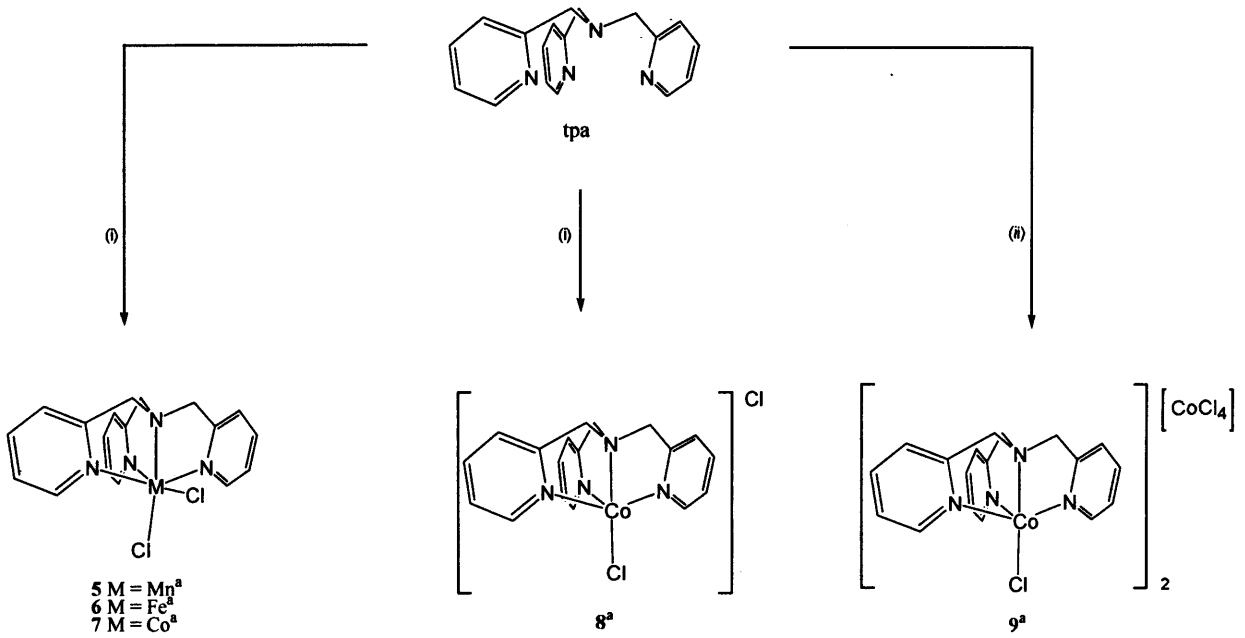

Scheme 2 *Reagents and conditions*: (i) MCl_2, *n*-BuOH, heat; (ii) $CoCl_2$ (1.5 equiv.), *n*-BuOH, heat
[a] Isolated from single crystal X-ray diffraction studies

All products have been characterised by FAB mass spectrometry, magnetic susceptibility, solid state IR spectroscopy and by elemental analysis. Furthermore, crystals of **5** - **9** were grown from slow cooling of a hot acetonitrile solution and subject to single crystal X-ray diffraction studies. The molecular structures of **5** - **8** are represented in Figures 10 and 11 and selected bond distances and bond angles are listed in Tables 3 and 4. Crystal data and data collection refinement parameters are presented within Chapter 6; section 6.8.

Mandon and co-workers[10] have previously reported the molecular structure of **6** with the notable absence of solvated molecules in the crystalline lattice. The molecular structures of **5** - **7** are similar and will be discussed together. The metal(II) centre in each complex is in a distorted octahedral environment ligated by three pyridyl nitrogens and one tertiary amine of the tripodal ligand and two chlorides, affording a N4Cl2 coordination sphere. The geometry constraints applied by the tripodal ligand impose a *cis*-disposition on the bound chloride ligands, with Cl(1) *trans* to the tertiary amine [N(1)] and Cl(2) *trans* to one of the pyridyl moieties [N(4)]. Such constraints leave the pyridyl donor atoms N(2) and N(3) in a *trans* arrangement. The distortion from a ideal octahedron geometry arises from the tripodal ligand, for example the average N_{amine}-M-$N_{pyridyl}$ [72.65° (Mn), 75.22° (Fe), 77.76° (Co)] and the N(2)-

M-N(3) [144.45(5)° (Mn), 149.29(6)° (Fe), 154.74(6)° (Co)] angles are lower than 90 and 180° respectively. Furthermore, the angles between Cl(1) and its *cis*-neighbours are significantly larger than 90° [Cl(1)-M(1)-N(2) 107.38(4)° (Mn), 107.20(5)° (Fe), 101.86(4)° (Co); Cl(1)-M(1)-N(3) 105.02(4)° (Mn), 102.18(5)° (Fe), 102.65(4)° (Co); Cl(1)-M(1)-N(4) 91.16(4)° (Mn), 93.80(5)° (Fe), 93.86(4)° (Co); Cl(1)-M(1)-Cl(2) 101.58(3)° (Mn), 97.86(3)° (Fe), 96.579(17)° (Co)].

Table 3 Selected bond distances (Å) and angles (°) for **5** - **7**

	M = Mn (**5**)	M = Fe (**6**.MeCN)	M = Co (**7**)
M(1)-N(1)	2.407(2)	2.284(2)	2.219(1)
M(1)-N(2)	2.297(2)	2.189(2)	2.136(1)
M(1)-N(3)	2.289(2)	2.191(2)	2.120(2)
M(1)-N(4)	2.349(2)	2.216(2)	2.169(2)
M(1)-Cl(1)	2.438(1)	2.343(1)	2.355(1)
M(1)-Cl(2)	2.463(1)	2.457(1)	2.450(1)
N(1)-M(1)-N(2)	72.65(6)	74.97(7)	78.57(5)
N(1)-M(1)-N(3)	72.18(6)	74.53(6)	76.31(6)
N(1)-M(1)-N(4)	73.13(6)	76.17(6)	78.39(6)
N(2)-M(1)-N(3)	144.45(5)	149.29(6)	154.74(6)
N(2)-M(1)-N(4)	81.51(6)	83.29(6)	82.74(5)
N(3)-M(1)-N(4)	83.60(7)	86.10(6)	89.59(6)
N(1)-M(1)-Cl(1)	164.20(4)	169.54(5)	172.15(4)
N(2)-M(1)-Cl(1)	107.38(4)	107.20(5)	101.86(4)
N(3)-M(1)-Cl(1)	105.02(4)	102.18(5)	102.65(4)
N(4)-M(1)-Cl(1)	91.16(4)	93.80(5)	93.86(4)
N(1)-M(1)-Cl(2)	94.14(5)	92.32(5)	91.24(4)
N(2)-M(1)-Cl(2)	94.24(5)	90.38(5)	91.70(4)
N(3)-M(1)-Cl(2)	93.26(5)	94.33(4)	91.50(5)
N(4)-M(1)-Cl(2)	167.25(4)	167.96(4)	169.00(4)
Cl(1)-M(1)-Cl(2)	101.58(3)	97.86(3)	96.579(17)

The M-N bond distances (>2.0 Å) are characteristic of a metal(II) centre with a HS configuration ranging from 2.297(2)-2.407(2) Å (Mn), 2.189(2)-2.284(2) Å (Fe) and 2.120(2)-2.219(1) Å (Co).[6, 7, 10, 11] The M-N_{amine} bond distance [M(1)-N(2) 2.407(2) Å (Mn), 2.284(2) Å (Fe), 2.219(1) Å (Co)] is the most elongated in each case, attributable to the tertiary amine being the weakest donor atom of tpa. Amongst the three M-$N_{pyridyl}$ bond distances, the pyridyl group *trans* to Cl(2) has the longest bond distance [M(1)-N(4) 2.349(2) Å (Mn), 2.216(2) Å (Fe), 2.169(2) Å (Co)]. The difference in the *trans* arrangement of the chloride ligands results in the M-Cl bond distances being asymmetric with M(1)-Cl(2) bond

distance being the longest in each case [2.463(1) Å (Mn), 2.457(1) Å (Fe), 2.450(1) Å (Co)]. Notably, in the non-solvated form of **6**,[10] the pyridyl moiety in a *trans* arrangement with a chloride ligand possesses a marginally longer Fe-N bond distance than the tertiary amine distance.

Table 4 Selected bond distances (Å) and angles (°) for **8**

	M = Co (**8**)
Co(1)-N(1)	2.212(2)
Co(1)-N(2)	2.065(1)
Co(1)-N(2A)	2.065(1)
Co(1)-N(2B)	2.065(1)
Co(1)-Cl(1)	2.276(1)
N(1)-M(1)-N(2)	77.19(3)
N(2)-M(1)-N(2A)	115.23(2)
N(1)-M(1)-Cl(1)	180.00(7)
N(2)-M(1)-Cl(1)	102.81(3)

The molecular structure of **8** reveals a discrete cationic unit along with a chloride counteranion. The cobalt(II) centre in the cationic unit is in a C_{3v} symmetric pseudo-trigonal bipyramidal coordination environment, with the three symmetrical pyridyl donors in the equatorial plane and the tertiary amine [N(2)-Co(1)-N(2A) 115.23(2)°] and the chloride ligands in the axial positions [N(1)-Co(1)-Cl(1) 180.00(7)°]. As for complexes **5** - **7** the Co-N_{amine} bond distance [Co(1)-N(1) 2.212(2) Å] is longer than the Co-$N_{pyridyl}$ bond distances [Co(1)-N(2) 2.065(1) Å], which are all identical as a consequence of the high symmetry. Notably, the M-N_{amine} bond distance is *ca.* 0.04 Å longer than that reported in the dicationic complex $[\{tpa\}Co(MeCN)]^{2+}$ attributed to the larger *trans* effect of a chloride *vs.* an acetonitrile.[32] The cationic unit in **8** resembles closely the five coordinate geometries found in the independent cations in $[\{tpa\}CoCl]_2[CoCl_4]$ (**9**) and indeed, the Co-ligand bond distances are identical within experimental error.[12] The molecular structure of **9** is discussed in detail by Gal and co-workers.[12]

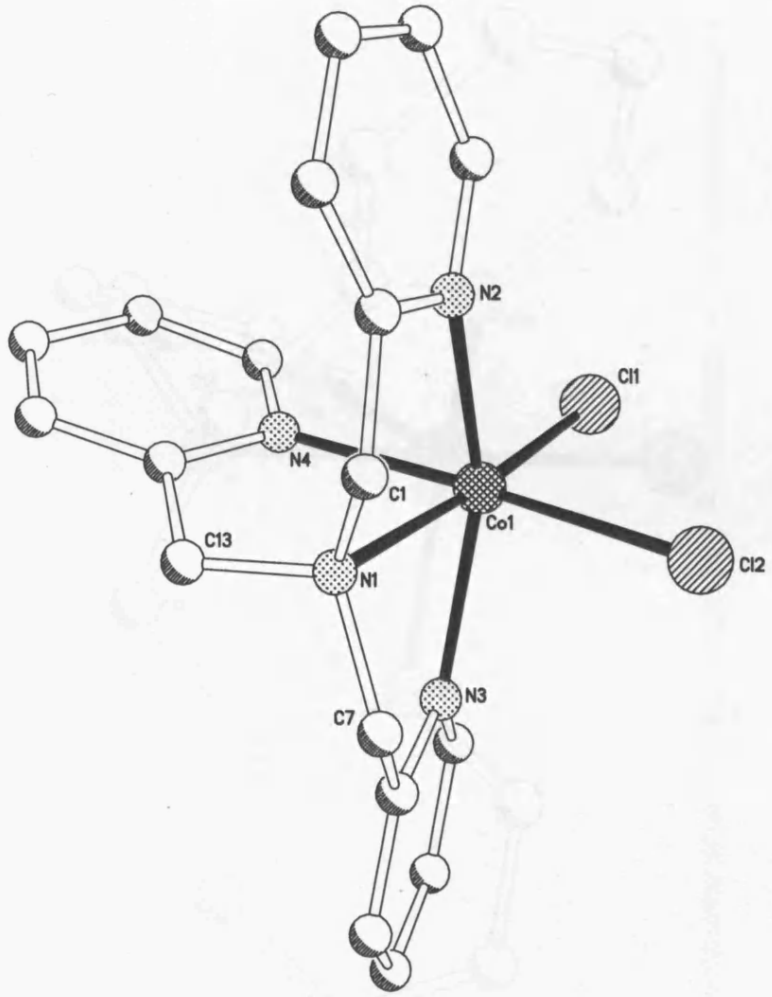

Figure 10 Molecular structure of [{tpa}$CoCl_2$] (**7**) (All the hydrogen atoms have been omitted for clarity). Molecular structures of [{tpa}MCl_2] (M = Mn **5**, Fe **6**) reveal a similar coordination geometry

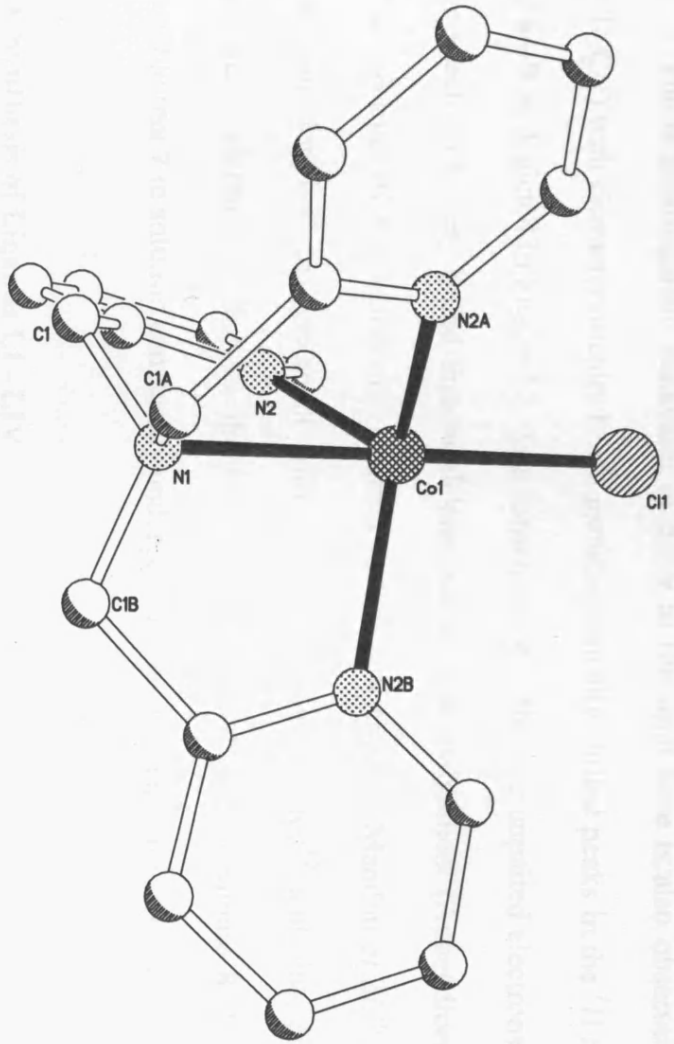

Figure 11 Molecular structure of the cationic unit in [{tpa}CoCl][Cl] (**8**) (All the hydrogen atoms have been omitted for clarity)

The solid state IR spectra of complexes **5** - **9** exhibit characteristic pyridyl ring deformation bands at *ca.* 1600 cm^{-1},[11, 33] indicative of the coordination modes determined by single crystal X-ray diffraction studies. The rt magnetic moments were determined using a Evans Balance (Johnson Matthey) and are characteristic of a metal(II) HS configuration, in accordance with the crystal structure analysis. For example, the manganese(II) complex (**5**) affords a magnetic moment of 5.52 BM, consistent with five unpaired electrons ($S = 5/2$), the iron(II) complex (**6**) affords a magnetic moment of 4.82 BM, consistent with four unpaired electrons ($S = 2$) and the cobalt(II) complexes (**7** - **9**) afford magnetic moments in the range of 3.70 - 4.39 BM, consistent with three unpaired electrons ($S = 3/2$).

The rt paramagnetic behaviour of **5** - **9** in the solid state is also observed in solution (CD_3CN) with characteristically broad paramagnetically shifted peaks in the ^1H NMR spectra of **6** - **9** as depicted in Figure 12. As a consequence of the five unpaired electrons present in **5** the spectrum is very broad thereby deleterious to peak assignment (Appendices: Figure 3). The spectrum of **6** is essentially identical to that described by Mandon *et al.*[10] Equally, the spectrum for **9** is in agreement with that previously reported[12] and, interestingly, it is essentially identical to that for the six-coordinate **7** and five-coordinate **8**. It would seem possible that **7** in solution can readily undergo chloride dissociation to form **8**.

2.4. Synthesis of Ligands LI - LIV

The new *N*-aryl substituted *N*-picolyethylenediamines ligands **LIa - d** were prepared in high yield by a palladium catalysed N-C(aryl) coupling reaction of *N*-picolyethylenediamine (prepared by treating 2-chloroethylamine with excess 2-(aminomethyl)pyridine) with one equivalent of the corresponding aryl bromide using experimental procedures established by Hartwig and Buchwald (Scheme 3).[34] Notably, increasing the steric bulk in the *ortho*-position of the aryl ring is detrimental to the reaction. For example, when 2,4,6-tri-*t*-butylphenyl bromide is utilised in the reaction no conversion is observed. This may be attributable to the steric hindrance preventing either oxidative addition of the aryl bromide to the Pd(0) metal

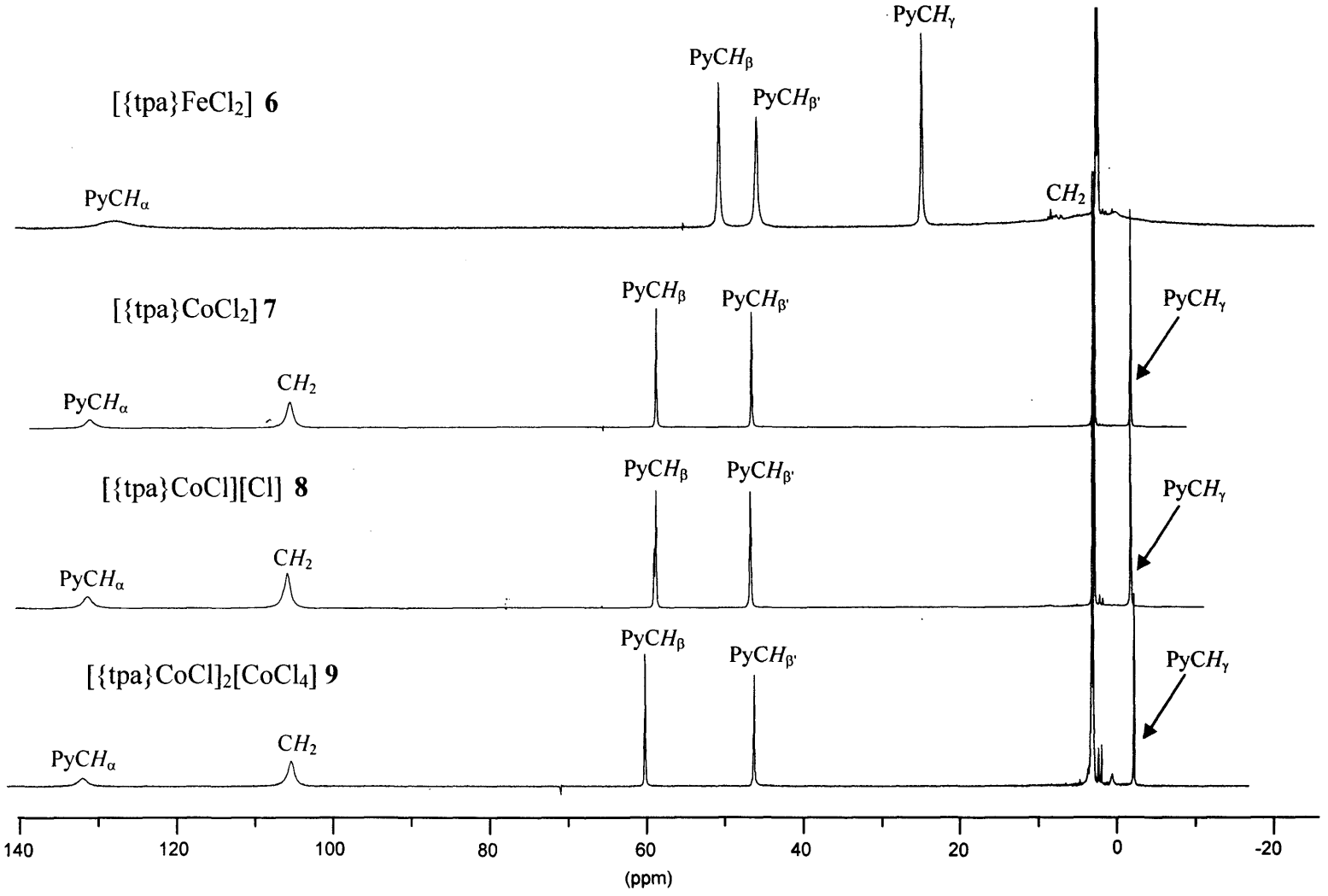

Figure 12 ^{1}H NMR spectra of complexes **6** - **9** in CD_3CN at rt

centre or reductive elimination of the (amido)(aryl)Pd(II) complex.[34, 35] **LIa - d** have been characterised by IR, ^{1}H and ^{13}C NMR spectroscopy and ES mass spectrometry (see Chapter 6; section 6.2.2).

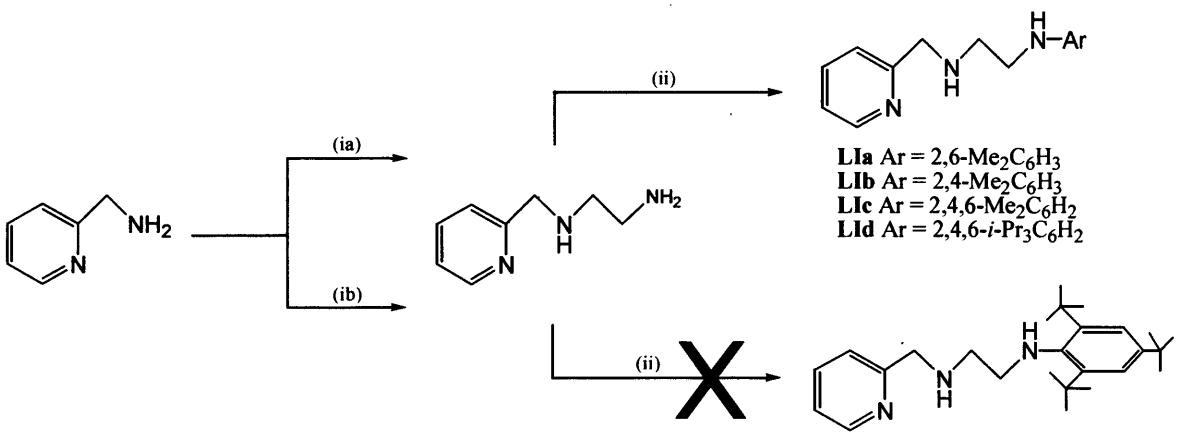

Scheme 3 *Reagents and conditions*: (i) NaOH, $H_2NCH_2CH_2Cl.HCl$, EtOH, heat; (ii) Ar-Br, NaO^tBu, $Pd_2(dba)_3$, *rac*-BINAP, toluene, heat

The nucleophilicity of the central secondary amine in **LI** can be exploited to yield the new ligand sets **LII - LIV** *via* the treatment of **LI** with the respective electrophile and excess K_2CO_3 (Scheme 4). The products **LII - LIV** were purified by column chromatography in order to remove the ammonium salts. Alternatively, **LIV** was prepared analogously to **LI** by

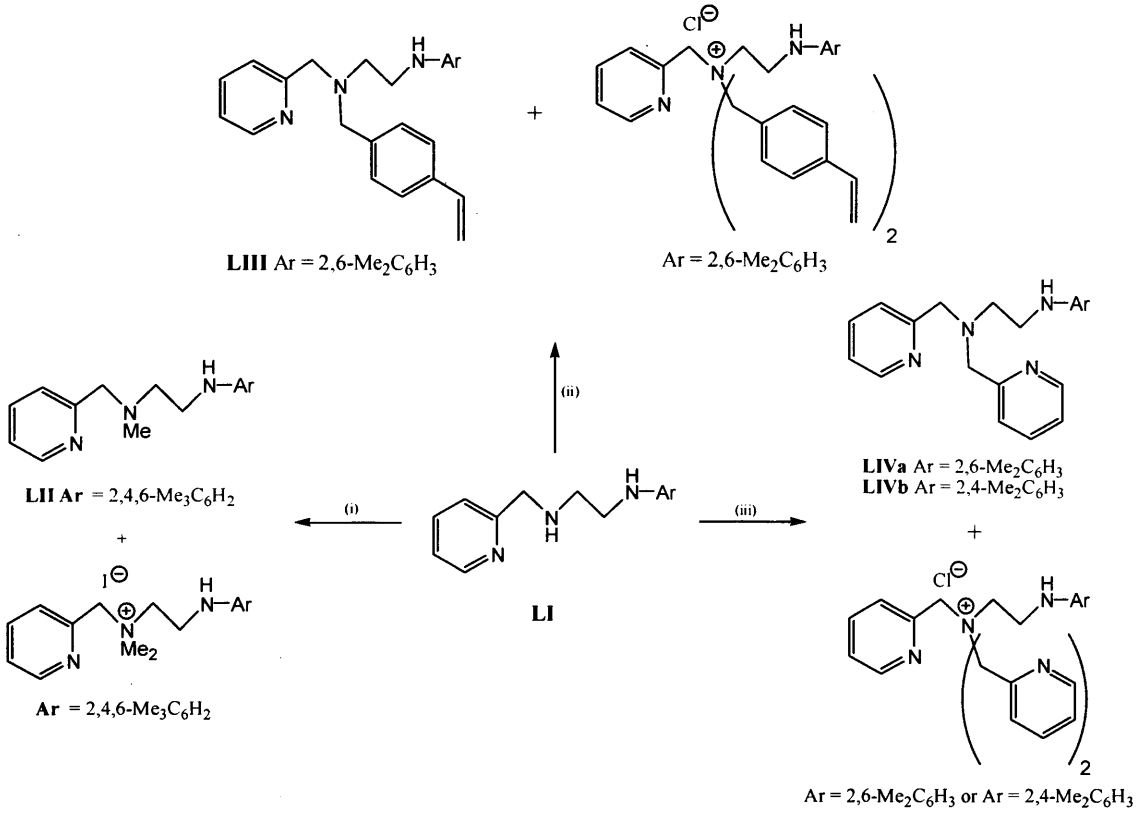

Scheme 4 *Reagents and conditions:* (i) xs K_2CO_3, MeI, MeCN; (ii) xs K_2CO_3, C_8H_9Cl, MeCN, heat; (iii) xs K_2CO_3, $C_6H_7NCl.HCl$, MeCN, heat

the palladium catalysed N-C(aryl) coupling reaction of dpea (prepared by reacting dpa with *N*-tosylaziridine; followed by treating (*N*-tosyl-2-aminoethyl)bis(2-picolyl)amine with conc. H_2SO_4) with one equivalent of the corresponding aryl bromide (Scheme 5). The ligand sets **LII - LIV** have been characterised by IR, ^1H and ^{13}C NMR spectroscopy and ES mass spectrometry (see Chapter 6; sections 6.2.3 - 6.2.7).

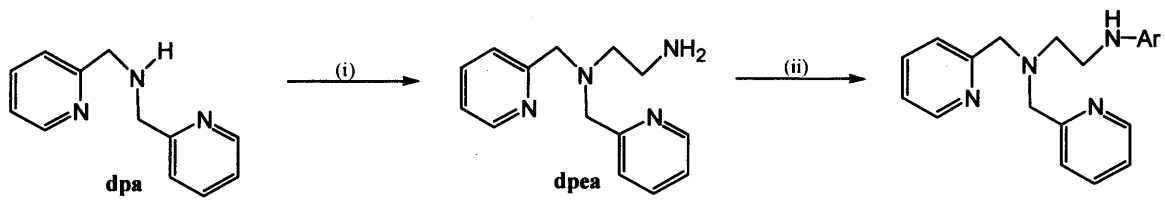

LIVa Ar = 2,6-$Me_2C_6H_3$
LIVb Ar = 2,4-$Me_2C_6H_3$
LIVc Ar = 2,4,6-$Me_3C_6H_2$

Scheme 5 *Reagents and conditions*: (i) *N*-tosylaziridine, CH_3CN, heat, followed by conc. H_2SO_4, heat; (ii) Ar-Br, NaO^tBu, $Pd_2(dba)_3$, *rac*-BINAP, toluene, heat

2.5. Reaction of MCl_2 (M = Fe, Co) with LI

The treatment of anhydrous MCl_2 with 1 equivalent of **LIa - d** in *n*-BuOH at 90 °C afforded the complexes [{**LIa**}MCl_2] (M = Fe **10a**, Co **11a**), [{**LIb**}MCl_2] (M = Fe **10b**, Co **11b**), [{**LIc**}$FeCl(\mu\text{-}Cl)]_2$ (**10c**), [{**LIc**}$CoCl_2$] (**11c**) and [{**LId**}$CoCl_2$] (**11d**), in high yield (Scheme 6).

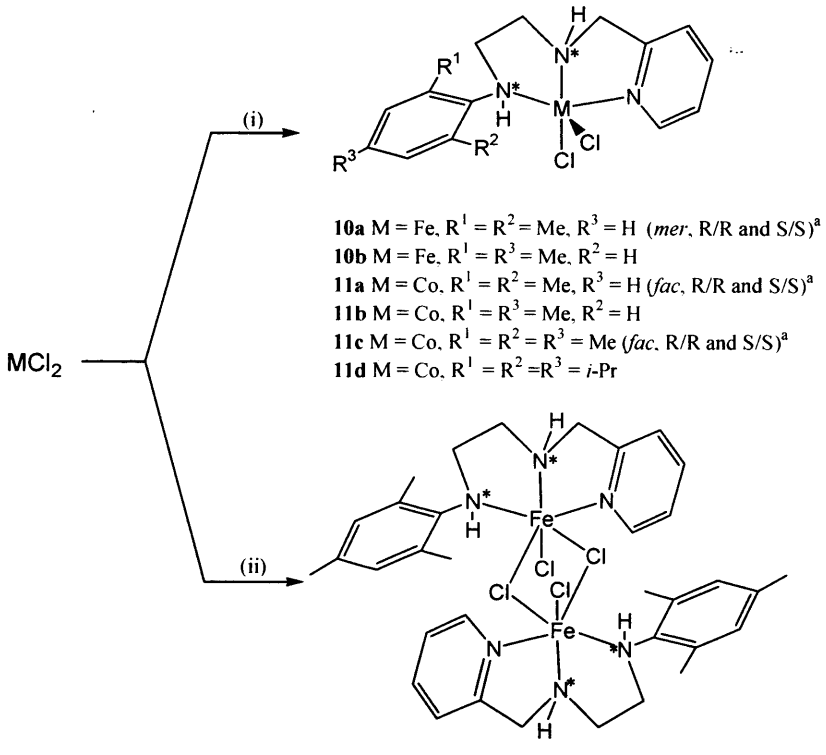

10a M = Fe, $R^1 = R^2 = Me$, $R^3 = H$ (*mer*, R/R and S/S)[a]
10b M = Fe, $R^1 = R^3 = Me$, $R^2 = H$
11a M = Co, $R^1 = R^2 = Me$, $R^3 = H$ (*fac*, R/R and S/S)[a]
11b M = Co, $R^1 = R^3 = Me$, $R^2 = H$
11c M = Co, $R^1 = R^2 = R^3 = Me$ (*fac*, R/R and S/S)[a]
11d M = Co, $R^1 = R^2 = R^3 = i$-Pr

10c M = Fe (*fac*, R/S and S/R)[a]

Scheme 6 *Reagents and conditions*: (i) **LI**, *n*-BuOH, 90 °C; (ii) **LIc**, *n*-BuOH, 90 °C.
[a] Isolated from single crystal X-ray diffraction studies

In contrast to the reaction of dpa with MCl_2 the presence of excess ligand (2 equivalents) does not yield a *bis*-ligated species, this is attributable to the presence of steric hindrance around the substituted aryl amine. All the compounds have been characterised by FAB mass spectrometry, magnetic susceptibility measurements, solid state IR spectroscopy and elemental analysis (except for **11d**). Insight into the coordination geometry around the metal centre and the propensity to form isomeric structures was provided by single crystal X-ray diffraction studies performed on complexes **10a**, **10c**, **11a** and **11c**.

The crystal growth of **10a**, **10c**, **11a** and **11c** was achieved from the layering of an acetonitrile solution with hexane at rt to give golden crystals for **10** and dark blue crystals for **11**. The molecular structures of **10a**, **10c**, **11a** and **11c** are represented in Figures 13 - 15 and selected bond distances and bond angles are listed in Tables 5 and 6. Crystal data and data collection refinement parameters are presented within Chapter 6; section 6.8.

Table 5 Selected bond distances (Å) and angles (°) for **10a**, **11a** and **11c**.MeCN

	M = Fe (**10a**)	M = Co (**11a**)	M = Co (**11c**.MeCN)
M(1)-N(1)	2.178(2)	2.082(1)	2.088(2)
M(1)-N(2)	2.185(2)	2.188(1)	2.189(2)
M(1)-N(3)	2.296(2)	2.168(1)	2.214(2)
M(1)-Cl(1)	2.398(1)	2.347(1)	2.361(1)
M(1)-Cl(2)	2.285(1)	2.296(1)	2.283(1)
N(1)-M(1)-N(2)	75.56(6)	76.64(5)	77.96(8)
N(1)-M(1)-N(3)	153.28(6)	105.72(5)	109.37(7)
N(2)-M(1)-N(3)	77.75(5)	79.14(5)	78.80(7)
N(1)-M(1)-Cl(1)	101.16(4)	105.79(4)	108.00(6)
N(2)-M(1)-Cl(1)	99.92(4)	87.42(3)	85.39(5)
N(3)-M(1)-Cl(1)	84.72(4)	141.63(4)	135.00(5)
N(1)-M(1)-Cl(2)	98.19(4)	98.71(4)	98.65(6)
N(2)-M(1)-Cl(2)	150.84(4)	168.22(4)	171.49(6)
N(3)-M(1)-Cl(2)	104.46(4)	91.95(3)	95.19(5)
Cl(1)-M(1)-Cl(2)	109.24(2)	104.30(2)	103.11(3)

The geometry at the iron(II) centre in complex **10a** may be regarded as being distorted square pyramidal with a N3Cl2 coordination sphere. The square basal plane consists of the *NNN*-chelate [N(1), N(2) and N(3)] and the chloride ligand Cl(2), with Fe(1) deviating from this plane by 0.018 Å and leaving Cl(1) as the apical atom. The *NNN*-chelate is bound in a *meridional* configuration as indicated by the N(1)-Fe(1)-N(3) angle being 153.28(6)° and as

two five-membered chelate rings [N(1)-Fe(1)-N(2) 75.56(6)°; N(2)-Fe(1)-N(3) 77.75(5)°]. The *N*-aryl group is oriented such that the *ortho*-methyl groups [C(15) and C(16)] are positioned above and below the square basal plane [*tors*: C(10)-C(9)-N(3)-Fe(1) 57.6(2)°] with one *ortho*-methyl [C(15)] notably pointing in a similar direction to Cl(1). The sp^3 hybridisation of N3 results in an inclination of the aryl substituent at an angle of 69.18° to the plane as observed in the pyridine-diamine and pyridine-imine-amine iron(II) complexes.[36] This deviation from orthogonallity may affect the steric control imposed on the metal centre by the ligand architecture (see Chapter 4). The Fe-N bond distances are inequivalent with the distance to the pyridyl donor being the shortest [Fe-N(1) 2.178(2) Å] and to the *N*-aryl amine the most elongated [Fe-N(1) 2.296(2) Å]. Furthermore, the Fe-N bond lengths are characteristic of a HS iron(II) configuration.[36] The Fe-Cl bond distances differ by *ca.* 0.1 Å with Fe-Cl(1) being the longest [2.398(1) Å]. The Cl-Fe-Cl angle at 109.24(2)° falls in the lower-range for the corresponding angle in related complexes.[36 - 38] Due to the centric nature of the space group, both R/R and S/S forms are present for the two chiral centres at N(2) and N(3) in the crystal of **10a**.

The cobalt(II) complexes **11a** and **11c** also possess a N3Cl2 coordination sphere but in a distorted trigonal bipyramidal environment, the lack of rigidity within the ligand architecture appears to facilitate the formation of an isomeric structure to **10a**. The structures of **11a** and **11c** are essentially identical and will be discussed together. The axial sites consist of N(2) and Cl(2) [N(2)-Co(1)-Cl(2) 168.22(4)° (**11a**), 171.49(6)° (**11c**)] and the equatorial plane is defined as N(1), N(3), Cl(1) [N(1)-Co(1)-N(3) 105.72(5)° (**11a**), 109.37(7)° (**11c**); N(1)-Co(1)-Cl(1) 105.79(4)° (**11a**), 108.00(6)° (**11c**); N(3)-Co(1)-Cl(1) 141.63(4)° (**11a**), 135.00(5)° (**11c**)]. The *NNN*-ligand is bound in a *facial* configuration and as two five-membered chelate rings as indicated by the bond angles N(1)-Co(1)-N(2) [76.64(5)° (**11a**), 77.96(8)° (**11c**)] and N(2)-Co(1)-N(3) [79.14(5)°(**11a**), 78.80(7)° (**11c**)]. The *N*-aryl group is oriented such that the *ortho*-methyl groups [C(15) and C(16)] are positioned above and below the plane defined by N(3)-N(2)-Co(1) [*tors.*: C(10)-C(9)-N(3)-Co(1) 50.0(2)° (**11a**), 45.5(3)°

(**11c**)] with one *ortho*-methyl [C(15)] notably pointing in a similar direction to Cl(1). In addition, the aryl substituent is inclined at an angle of 73.89(5)° (**11a**) and 69.02(7)° (**11c**) to the N(3)-N(2)-Co(1) plane. As expected, the average Co-N_{amine} bond distance [2.178(1) Å (**11a**), 2.202(1) Å (**11c**)] is longer than the Co-$N_{pyridine}$ bond distance [2.082(1) Å (**11a**), 2.088(2) Å (**11c**)]. Similarly, the Co-Cl bond lengths differ, with the equatorial chloride [2.347(1) Å (**11a**), 2.361(1) Å (**11c**)] being longer than the axial chloride [2.296(1) Å (**11a**), 2.283(1) Å (**11c**)]. The Cl-Co-Cl angle at 103.11(3)° lies below the range found in pyridine-diimine cobalt(II) halide complexes,[37, 38] but compares well with the less rigid *NNN*-chelated five-coordinate cobalt dichloride complexes.[39 - 43] As with **10a**, both R/R and S/S forms of the complexes are present within the crystal of **11a** and **11c** due to the centric nature of the space group.

Table 6 Selected bond distances (Å) and angles (°) for **10c**

Fe(1)-N(1)	2.168(2)	Fe(1)-Cl(2)	2.310(1)
Fe(1)-N(2)	2.218(2)	Fe(1)-Cl(1A)	2.546(1)
Fe(1)-N(3)	2.334(2)	Fe(1)...Fe(1A)	3.600(1)
Fe(1)-Cl(1)	2.509(1)		
Cl(1)-Fe(1)-N(3)	81.06(6)	Cl(2)-Fe(1)-Cl(1A)	96.56(3)
Cl(1)-Fe(1)-Cl(2)	94.41(2)	N(3)-Fe(1)-N(1)	103.43(7)
Cl(1)-Fe(1)-N(1)	162.93(6)	N(3)-Fe(1)-N(2)	77.24(7)
Cl(1)-Fe(1)-Cl(1A)	89.19(2)	N(3)-Fe(1)-Cl(1A)	162.33(5)
Cl(1)-Fe(1)-N(2)	87.88(5)	N(1)-Fe(1)-N(2)	77.27(7)
Cl(2)-Fe(1)-N(1)	101.05(6)	N(1)-Fe(1)-Cl(1A)	81.94(5)
Cl(2)-Fe(1)-N(3)	98.84(5)	N(2)-Fe(1)-Cl(1A)	87.76(6)
Cl(2)-Fe(1)-N(2)	175.13(6)	Fe(1)-Cl(1)-Fe(1A)	90.81(2)

The molecular structure of **10c** differs from **10a**, **11a** and **11c** thereby forming another isomeric structure. Complex **10c** is binuclear with a C_2 symmetry passing through the centre of the Fe_2Cl_2 bridging core, which enables the R/S and S/R configurations to be adopted within the crystal structure. Each iron(II) atom is bound by a *NNN*-chelate in a *facial* bonding mode [N(3)-Fe(1)-N(1) 103.43(7)°], two bridging chlorides and one terminal chloride yielding a distorted octahedron geometry. The *facial* configuration of the *NNN*-chelate imposes geometry restraints such that the central amine is *trans* to a terminal chloride and the pyridyl donor and the *N*-aryl amine are *trans* to bridging chlorides. The two Fe-μ-Cl bond

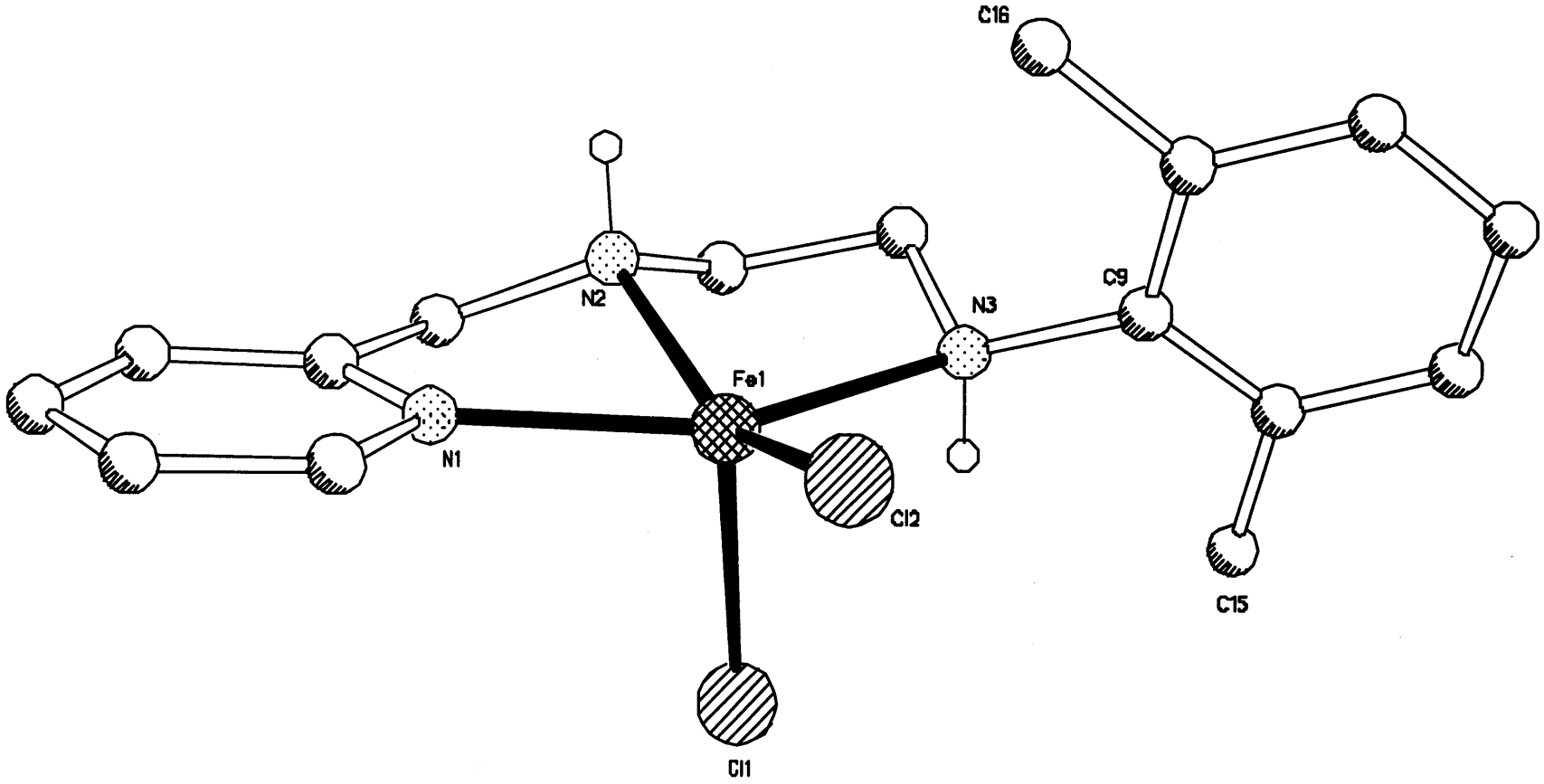

Figure 13 Molecular structure of [{**LIa**}$FeCl_2$] (**10a**) (All the hydrogen atoms apart from H2 and H3 have been omitted for clarity)

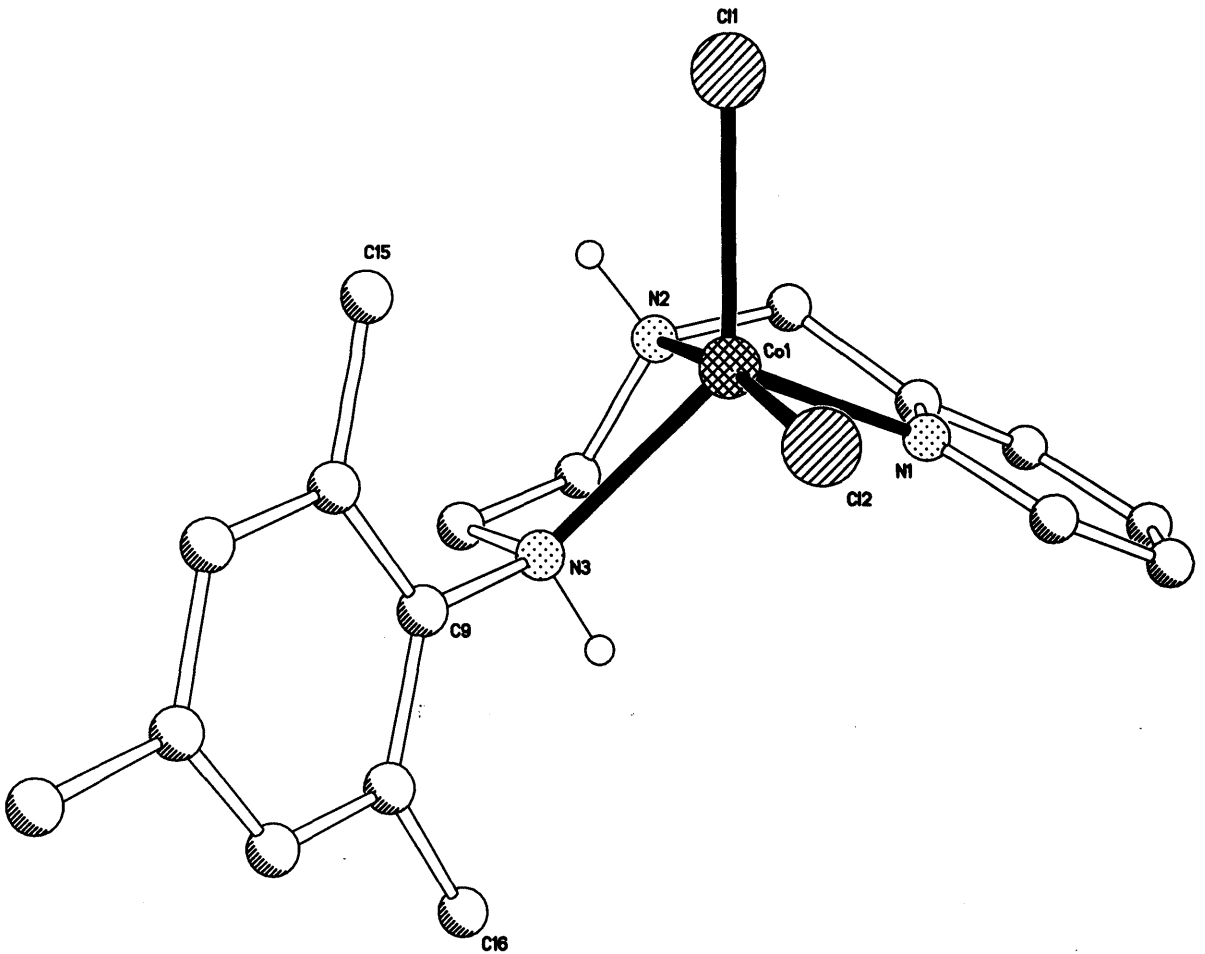

Figure 14 Molecular structure of [{**LIb**}$CoCl_2$] (**11c**) (All the hydrogen atoms apart from H2 and H3 have been omitted for clarity). Molecular structure of [{**LIa**}$CoCl_2$] (**11a**) reveals a similar coordination geometry

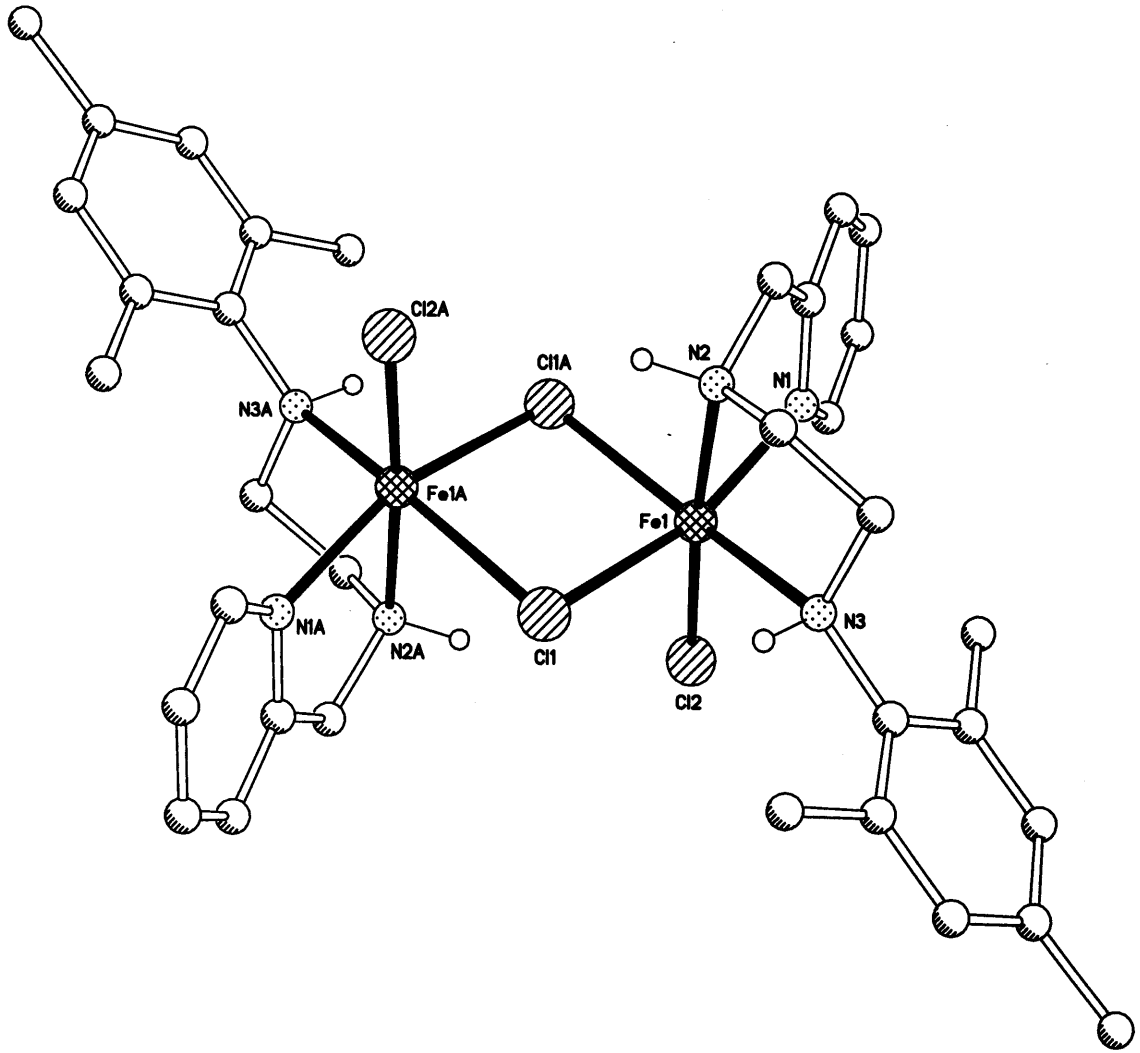

Figure 15 Molecular structure of [{**LIb**}FeCl(μ-Cl)]$_2$ (**10c**) (All the hydrogen atoms apart from H2 and H3 have been omitted for clarity)

distances are slightly different [Fe-Cl(1) 2.509(1) Å, Fe(1)-Cl(1A) 2.546(1) Å] and as expected they are longer than the terminal Fe-Cl bond distances [Fe(1)-Cl(2) 2.310(1) Å] (*cf.* [{dpa}FeCl(μ-Cl)]$_2$ (**1**)). The Fe...Fe separation is 3.600(1) Å and is in the mid-range for previously characterised diferrous complexes with Fe_2Cl_2 cores.[13, 20 - 23] In comparison to **10a** the Fe-N bond distances are inequivalent with the aryl amine distance [Fe(1)-N(3) 2.334(2) Å] being the longest and the pyridyl nitrogen [Fe(1)-N(1) 2.168(2) Å] the shortest. In addition, the Fe-$N_{amine/pyridyl}$ bond lengths are characteristic of a iron(II) complex exhibiting a HS configuration.[13, 20 - 23]

The FAB mass spectrometric data for complexes **10** and **11** show characteristic mass and isotope distribution patterns consistent with a monomeric species and in each case minor peaks attributable to a dimeric species. In accordance with the crystal structure analysis, the solid state IR spectra reflect the ligand coordination modes within the complexes by exhibiting characteristic pyridyl ring deformation bands at *ca.* 1600 cm^{-1},[11, 33] and N-H stretching frequencies at *ca.* 3200 cm^{-1}.[44] The rt magnetic susceptibility measurements are characteristic of HS behaviour, which agrees with the M-N bond lengths obtained from the diffractometric studies. For example, **10a** and **10b** reveal a magnetic moment of *ca.* 4.9 BM, consistent with a mononuclear iron(II) HS configuration (S = 2), whilst the dimeric species **10c** shows a magnetic moment of 7.76 BM, characteristic of two non-interacting HS iron(II) centres. Furthermore, variable temperature magnetochemical studies performed on **10c** reveal the magnetic susceptibility to be essentially independent of temperature down to *ca.* 50 K (Figure 16). The increase in magnetic susceptibility at *ca.* 50K indicates possible

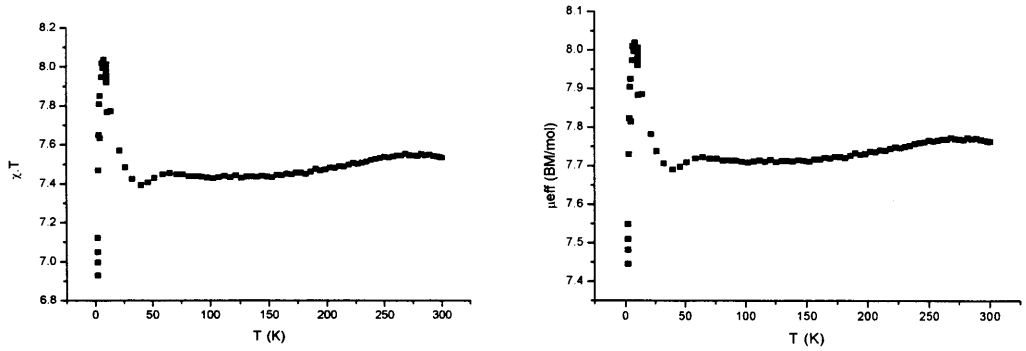

Figure 16 Variable temperature magnetochemical data for **10c**

ferromagnetic coupling between the two HS iron (II) centres.[45] The magnetic moments of **11a-d** (*ca.* 3.87 BM) are consistent with a mononuclear cobalt(II) centre containing three unpaired electrons.

Solution state studies performed on complexes **10** and **11** reveal broad paramagnetically shifted ^{1}H NMR spectra in the range of δ = –40 to 140 (Figures 17 and 18). Interpretation of the paramagnetic ^{1}H NMR spectra can be achieved by comparison with related metal(II) complexes **1, 3** and **6 - 9** where the pyridyl (PyCH_α, PyC$H_{\beta/\beta'}$ and PyCH_γ) and methylene protons have characteristic chemical shifts (Tables 7 and 8). Assignment has also been achieved on the basis of T_1 and *via* direct comparison with related spectra (**10a** *vs.* **10c** and **11a** *vs.* **11c**).

For complexes **10a** and **10c** the PyCH_α of the coordinated pyridyl arm is shifted downfield the most at δ = 130.4 for **10a** and δ = 129.6 (T_1 = 0.9 ms) for **10c**. The PyC$H_{\beta/\beta'}$ appear as sharp signals at δ = 58.8 and 57.4 (T_1 = 16.4, 14.6 ms) for **10a**, whilst for **10c** they are found at δ = 58.6 and 56.6 (T_1 = 13.2 and 11.2 ms). PyCH_γ is the most upfield at δ = 15.8 (T_1 = 37.1 ms) for **10a** and δ = 16.8 (T_1 = 90.3 ms) for **10c**. The methylene protons are broad and shifted downfield at δ = 104.9, 80.9 and 62.9 (T_1 = 0.96, 0.73 and 0.9 ms **10a**) and δ = 108.1, 82.4 and 63.9 (T_1 = 1.7, 1.1 and 0.7 ms **10c**). The aromatic region can be assigned by direct comparison of the two spectra to give ArMe_o at δ = 6.6 (T_1 = 2.0 ms) and ArCH_m at δ = 12.3 (T_1 = 34.2 ms) for **10a** and ArMe_o at δ = 7.39 (T_1 = 2.5 ms), and ArCH_m at δ = 11.6 (T_1 = 27.8 ms) for **10c**. Notably, the *para*-substituent can be informative with the ArCH_p in **10a** appearing at δ = -5.4, whilst in **10c** this signal is absent but replaced by ArMe_p at δ = 15.7 (T_1 = 29.1 ms).

Complexes **11a** and **11c** have been assigned in a similar fashion affording PyCH_α at δ = 113.8 (T_1 = 4.1 ms) for **11a** and 116.7 (T_1 = 9.3 ms) for **11c**. PyC$H_{\beta/\beta'}$ resonate at δ = 45.7 and 42.5, (T_1 = 15.9, 25.9 ms) for **11a**, whilst for **11c** they appear at δ = 46.6 and 44.0 (T_1 = 15.0 and 23.2 ms). The PyCH_γ are found at δ = –3.6 for **11a** and –3.0 (T_1 = 52.6 ms) for **11c**, whilst

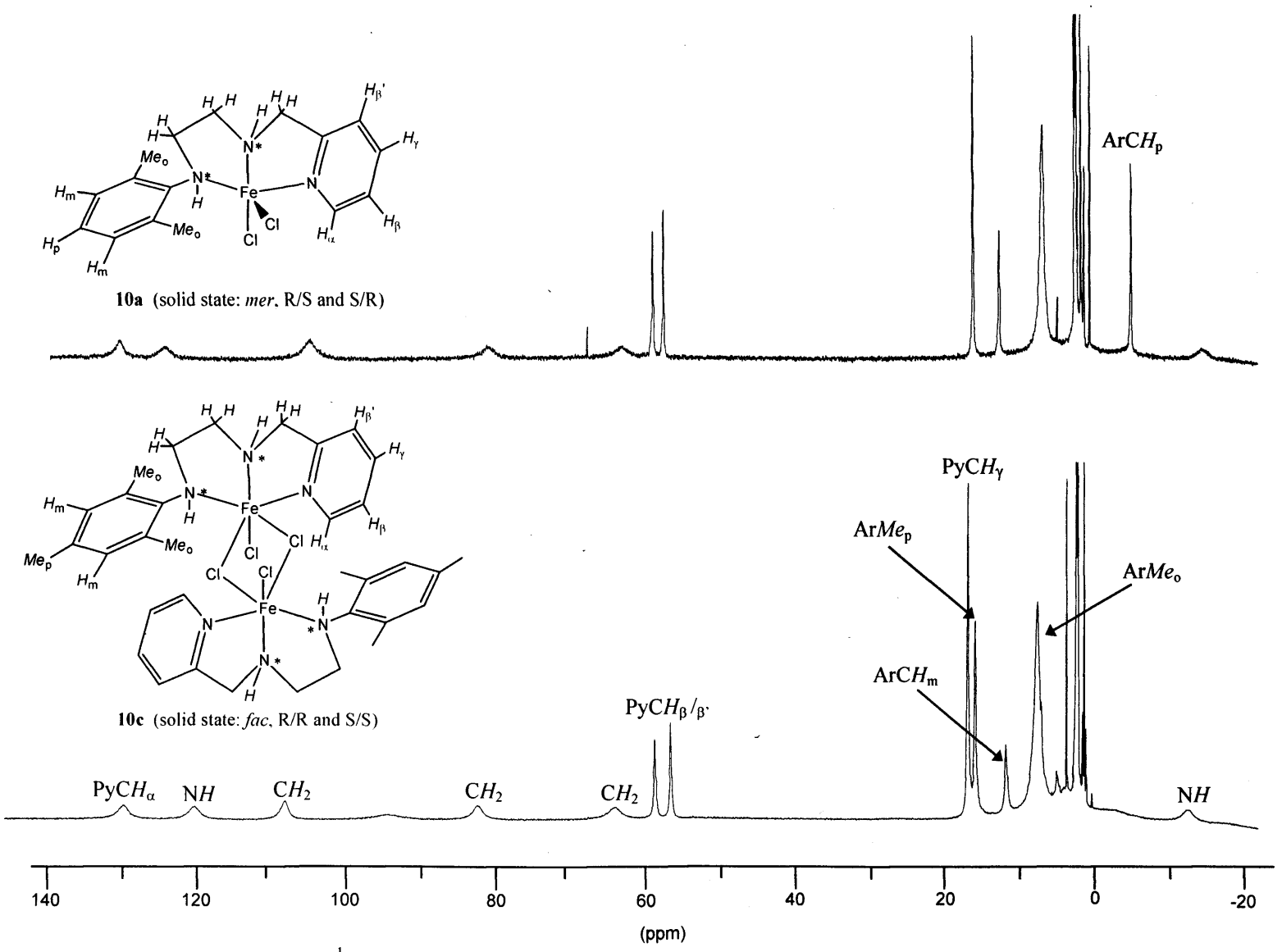

Figure 17 ^{1}H NMR spectra of complexes **10a** and **10c** in CD_3CN at rt

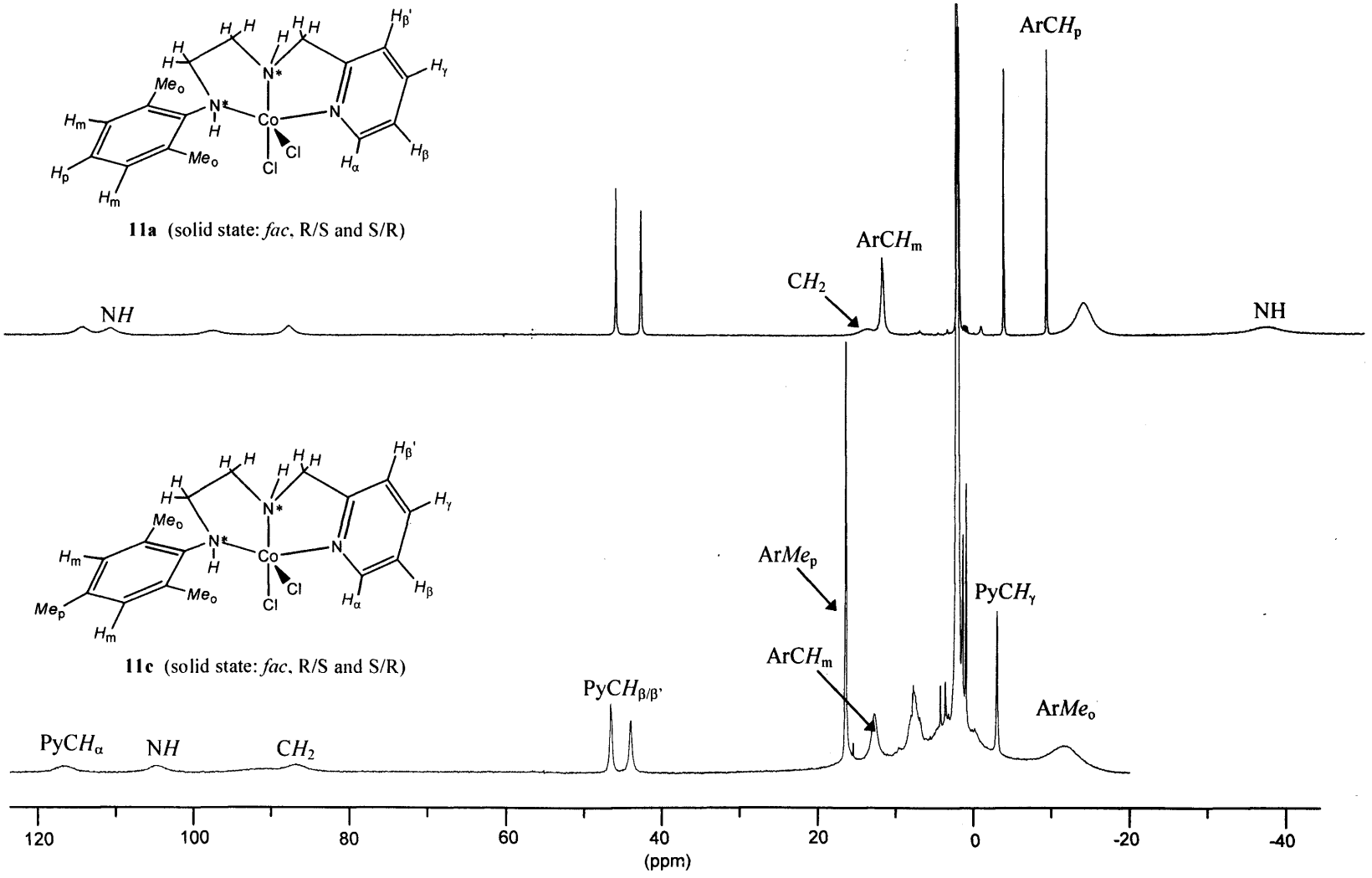

Figure 18 ^{1}H NMR spectra of complexes **11a** and **11c** in CD_3CN at rt

Table 7 ^{1}H NMR chemical shifts (δ) and relaxation times (T_1) for complexes **10a** and **10c** in CD_3CN at rt[a]

	δ / (T_1 ms)						
Complex	PyCH_α	PyC$H_{\beta/\beta'}$	PyCH_γ	CH_2	ArC*H*	Ar*Me*	N*H*
1	116.5	54.7 (10.1), 51.8 (9.1)	7.8	70.8 (1.1)	NA	NA	107.0 (1.3)
6	127.8	50.5 (9.8), 45.8 (8.1)	24.5 (25.0)	-10 to 10 (very broad)	NA	NA	NA
10a	130.4	58.8 (16.4), 57.4 (14.6)	15. 8 (37.1)	104.9 (0.96), 80.9 (0.73), 62.9 (0.9)	12.3 (34.2, ArCH_m), -5.4 (ArCH_p)	6.6 (2.0, ArMe_o),	124.1 (3.8, NH), -15.01 (15.3, NH)
10c	129.6 (0.9)	58.6 (13.2), 56.6 (11.2)	16.8 (90.3),	108.1 (1.7), 82.4 (1.1), 63.9 (0.7)	11.6 (27.8, ArCH_m)	15.7 (29.1, ArMe_p), 7.39 (2.5, ArMe_o)	120.0 (1.9), -12.74 (4.0)

[a] Complexes **1** and **6** included for comparison

Table 8 ^{1}H NMR chemical shifts (δ) and relaxation times (T_1) for complexes **11a** and **11c** in CD_3CN at rt[a]

	δ / (T_1 ms)						
Complex	PyCH_α	PyC$H_{\beta/\beta'}$	PyCH_γ	CH_2	ArCH	ArMe	NH
3	122.8 (1.3)	54.5 (30.4), 43.1 (19.7)	-0.9	110.6 (2.0 ms)	NA	NA	118.0 (1.9),
7	130.8	58.3 (17.9) 46.2 (10.0)	-2.7 (29.3)	105.3 (1.1)	NA	NA	NA
11a	113.8 (4.1)	45.7 (15.9), 42.5 (25.9),	-3.6	97.0 (0.8), 87.3 (1.1), 13.5 (2.9),	11.8 (43.2, ArCH_m), -9.1 (ArCH_p)	-14.1 (ArMe_o)	110.1 (1.0), -40
11c	116.7 (9.3)	46.6 (15.0), 44.0 (23.2)	-3.0 (52.6)	≈ 90 (very broad), 86.9 (0.9)	12.5 (45.3, ArCH_m)	16.4 (ArMe_p), -11.8 (2.2, ArMe_o)	104.6 (1.5)

[a] Complexes **3** and **7** included for comparison

the methylene protons are present at δ = 97.0, 87.3 and 13.5 (T_1 = 0.8, 1.1 and 2.9 ms) for **11a** and δ ≈ 90 (very broad) and 86.9 (T_1 = 0.9 ms) for **11c**. The aromatic region can be assigned to give Ar*Me*$_o$ at δ = –14.1 and ArC*H*$_m$ at δ = 11.8 (T_1 = 43.2 ms) for **11a** and Ar*Me*$_o$ at –11.8 (T_1 = 2.2 ms) and ArC*H*$_m$ at δ = 12.5 (T_1 = 45.3 ms) for **11c**. In analogous manner to **10a** and **10c** the ArC*H*$_p$ signal at δ = –9.1 in **11a** is replaced by a Ar*Me*$_p$ signal at δ = 16.4 in **11c**.

From the crystallographic studies we have observed both *meridional* and *facial* configurations with differing stereochemical relationships with either a iron(II) or cobalt(II) centre. In addition, despite the differences in the solid state structures of **10a** and **10c** both behave similarly in solution. Scheme 7 shows a series of equilibria that may explain the apparent dynamic behaviour of **10** and **11** in particularly, that of **10a** and **10c**.

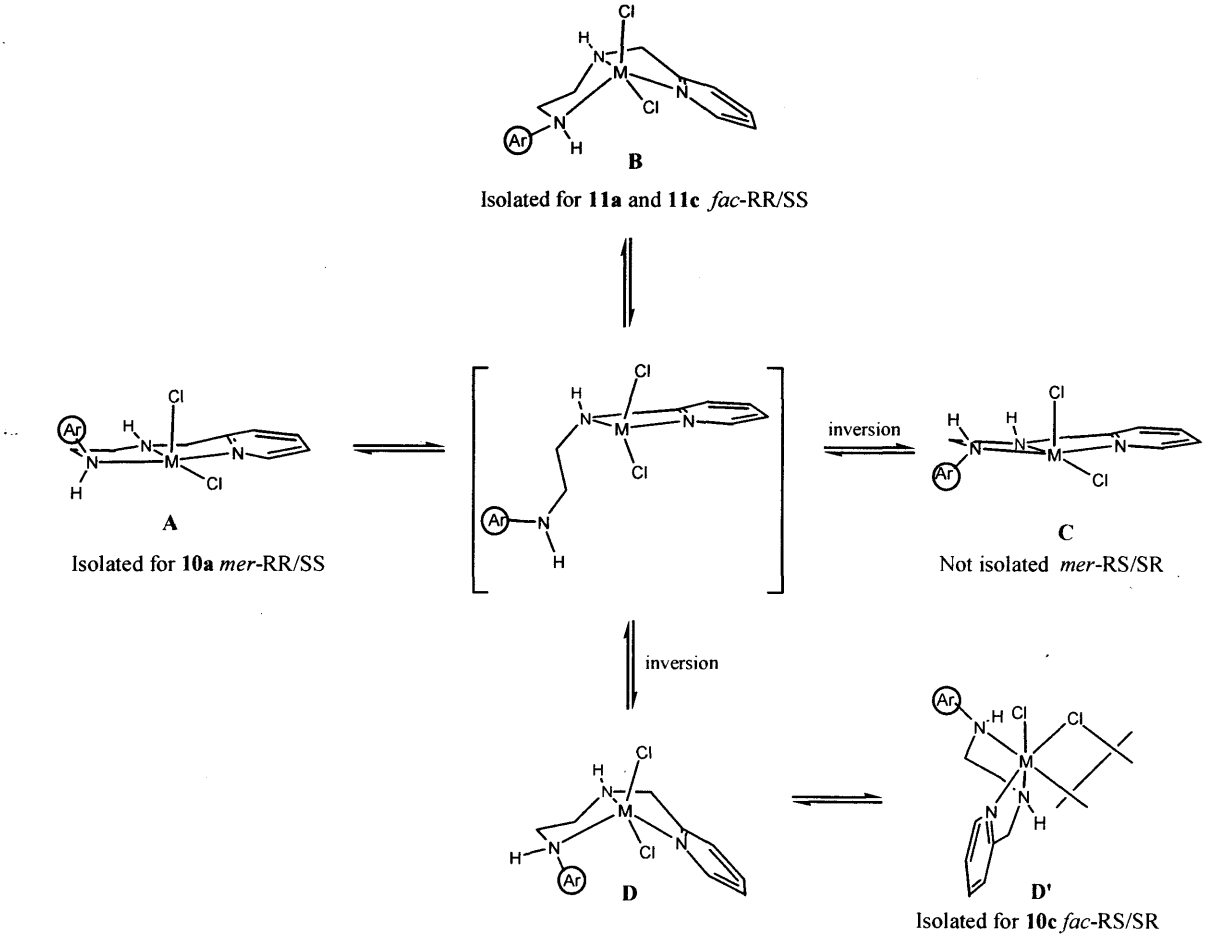

Scheme 7 Isomeric interconversion pathway

Dissociation of the *N*-aryl amine arm of the ligand in species **A** could generate a four coordinate iron complex containing a pendant *N*-aryl amine group. Reorganisation of the coordinated ligand around the metal centre followed by recoordination could afford the *facial*

NNN-chelated species **B**. The stereoisomers may be interconverted *via* inverting the stereochemistry at the pendant *N*-aryl amine followed by recoordination and in the particular case of species **A** yielding species **C** or **D**. The bulky aryl group in species **D** is now remote from the chloride ligands, dimerisation can therefore occur to give a *facially NNN*-chelated bis(μ-chloro) dimeric complex. Some experimental evidence for the postulated lability of the *N*-aryl amine arm is given on inspection of the M-N bond distances in particular for **10a** and **10c**, in which the corresponding Fe-N bond distances are *ca.* 0.1 Å longer than the other Fe-N bond distances. Alternatively a Berry *pseudo*-rotational type process may account for the interconversion of species **A** into species **B** or species **C** into **D**. Further evidence for a 'Berry-type' or a dissociation-inversion process arises from the employment of a *NNN*-, *NON*- or *XNX*- (X = S, O)-chelate in a five-coordinate group 4 or 14 system.[46 - 48]

In order to investigate the relative stabilities of the possible *meridional* and *facial* isomers for **10** and **11**, DFT (B3LYP) calculations have been performed. The geometries of the *mer*-RR and *fac*-RR configurations of both **10a** and **11a** have been optimised taking into account the HS state of the metal(II) centre [*S* = 2 (Fe), 3/2 (Co)]. Different electronic configurations of the metals *d*-orbitals have been considered for both **10a** and **11a** and the lowest energetic ones were selected for geometry optimisation. Optimised structures of the *meridional* and *facial* complexes for **10a** and **11a** are depicted in Figure 19 and the geometrical parameters are listed in Table 9.

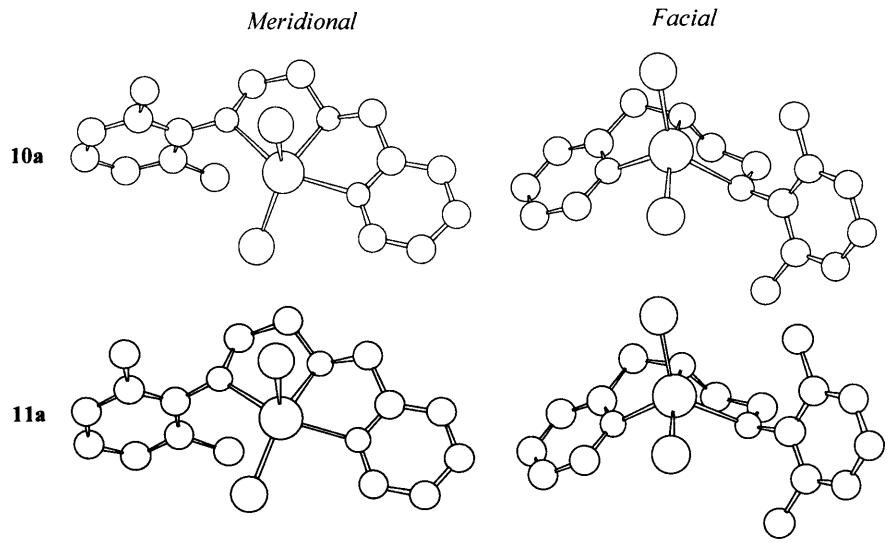

Figure 19 B3LYP optimised structures of *mer* and *fac* isomers of **10a** and **11a**

Table 9 Selected bond distances (Å) and angles (°) for *mer*-RR and *fac*-RR complexes of **10a** and **11a**

	meridional-RR configurations			*facial*-RR configurations		
	Diffractometric M = Fe (**10a**)	Calculated M = Fe (**10a**)	Calculated M = Co (**11a**)	Diffractometric M = Co (**11a**)	Calculated M = Fe (**10a**)	Calculated M = Co (**11a**)
M(1)-N(1)	2.1782(15)	2.24	2.18	2.082(1)	2.23	2.19
M(1)-N(2)	2.1849(15)	2.23	2.23	2.188(1)	2.30	2.25
M(1)-N(3)	2.2956(15)	2.37	2.27	2.168(1)	2.35	2.26
M(1)-Cl(1)	2.2851(5)	2.29	2.30	2.347(1)	2.35	2.34
M(1)-Cl(2)	2.3983(5)	2.41	2.37	2.296(1)	2.34	2.33
N(1)-M(1)-N(2)	75.56(6)	75.0	73.7	76.64(5)	73.5	74.7
N(1)-M(1)-N(3)	153.28(6)	152.2	146.9	105.72(5)	108.8	114.4
N(2)-M(1)-N(3)	77.75(5)	77.2	76.7	79.14(5)	74.8	76.4
N(1)-M(1)-Cl(1)	98.19(4)	95.4	96.3	105.79(4)	106.9	108.8
N(2)-M(1)-Cl(1)	150.84(4)	137.1	150.8	87.42(3)	84.3	84.1
N(3)-M(1)-Cl(1)	104.46(4)	106.0	102.5	141.63(4)	130.9	125.4
N(1)-M(1)-Cl(2)	101.16(4)	95.0	104.1	98.71(4)	95.7	95.0
N(2)-M(1)-Cl(2)	99.92(4)	92.6	90.0	168.22(4)	153.8	157.3
N(3)-M(1)-Cl(2)	84.72(4)	84.6	90.3	91.95(3)	86.8	90.1
Cl(1)-M(1)-Cl(2)	109.24(2)	130.2	119.2	104.30(2)	121.8	118.3

As indicated in Table 9 the gas-phase calculated bond parameters and the diffractometric data are generally in good agreement for both *mer*-**10a** and *fac*-**11a**. Notably, the optimised M-N bond distances are slightly elongated on comparison to the diffractometric values; typical of high spin systems studied by B3LYP.[49] The most significant anomaly between the calculated and diffractometric data is the Cl(1)-M(1)-Cl(2) angle with discrepancies of 14° in *fac*-**11a** (computed 118.3° *vs.* diffractometric 104.3°) to 21° in *mer*-**10a** (computed 130.2° *vs.* diffractometric 109.3°). Interestingly, the optimised values of the Cl(1)-M(1)-Cl(2) angle are closer to the diffractometric values exhibited by **16a** and **16b** (see Chapter 3; 114.4° and 113.3° respectively). The apparent deviation from the diffractometric Cl(1)-M(1)-Cl(2) angle may be related to the rotational behaviour of the aryl ring (and to a lesser extent the pyridine ring) about its N-C bond. Despite the *fac*-**10a** and *mer*-**11a** complexes not being isolated by single crystal X-ray diffraction studies, qualitative analysis of their optimised structures with those of *mer*-**10a** and *fac*-**11a** indicate the stability of both configurations when the *NNN*-chelate is coordinated to either iron or cobalt.

Determining the difference in Gibbs free energy between the *meridional* and the *facial* configurations of the *NNN*-chelate in both **10a** and **11a** enables the relative stabilities of the two optimised geometries at each metal centre to be determined [$\Delta G^0 = G^0_{mer} - G^0_{fac}$]. For **10a**, $\Delta G^0 = -2.41$ kcal/mol and for cobalt(II) complex **11a**, $\Delta G^0 = +1.04$ kcal/mol. Indeed, the low ΔG^0 values for both **10a** and **11a** indicate that both the *meridional* and *facial* configurations are very close in energy. However, for **10a** the *meridional* configuration is *ca.* 2.5 kcal/mol more stable than the *facial*, whilst for **11a**, the *facial* configuration is *ca.* 1 kcal/mol more stable than the *meridional*.

In summary, the ΔG^0 values for the optimised geometries in the gas phase reflect the geometrical environments that have been isolated from single crystal X-ray diffraction studies. Furthermore, the low energy difference between *facial* and *meridional* structures for both iron and cobalt would suggest an equilibrium to be likely in solution, as confirmed by the

paramagnetic ^{1}H NMR studies of **10**. However, these calculations do not take into account the possible mechanistic pathway involved in the transition from one configuration to the other.

2.6. Reaction of $CoCl_2$ with LII and LIII

The reaction studies performed with **LII** and **LIII** are indicative of the formation of the tridentate *NNN*-cobalt systems **12** and **13** (Scheme 8). The FAB mass spectrometric data exhibits characteristic mass and isotope distribution patterns for a monomeric dichloro complex and minor peaks for a dimeric species. The solid state IR spectra exhibit characteristic pyridyl ring deformation bands at *ca.* 1600 cm^{-1},[11, 33] and N-H stretching frequencies at *ca.* 3200 cm^{-1} indicative of coordination of the ligand sets to the metal centre.[44] In addition, complex **13** exhibits a C=C stretching frequency at 1629 cm^{-1}, which is comparative to that observed in the free ligand (1628 cm^{-1}). The rt magnetic moments are characteristic of a cobalt(II) HS configuration, consistent with three unpaired electrons (S = 3/2).

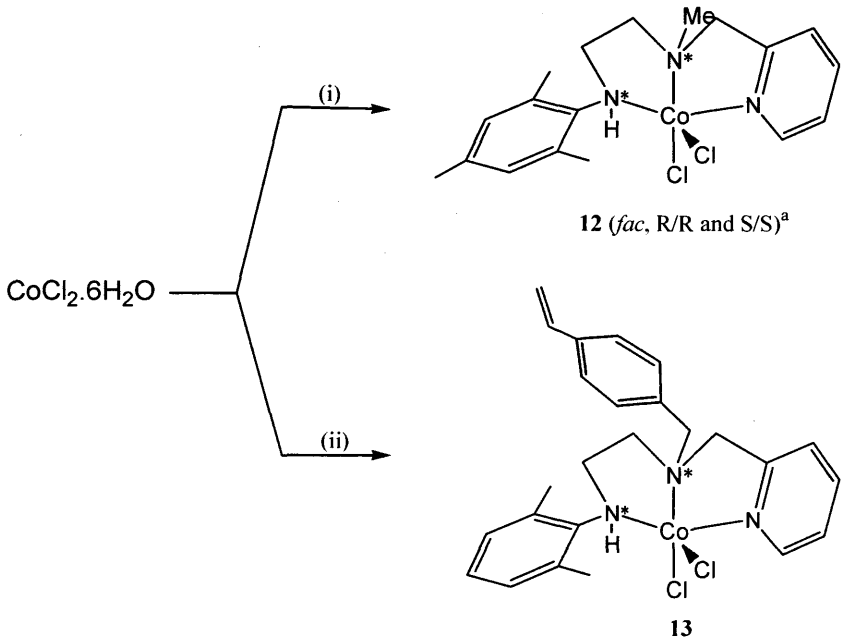

12 (*fac*, R/R and S/S)[a]

13

Scheme 8 *Reagents and conditions*: (i) **LII**, thf, rt; (ii) **LIII**, thf, rt
[a] Isolated from single crystal X-ray diffraction studies

In addition, purple crystals of **12** were grown from slow cooling of a hot acetonitrile solution and subject to a single crystal X-ray diffraction study. The molecular structure of **12** is depicted in Figure 20 and selected bond distances and bond angles are listed in Table 10.

Crystal data and data collection refinement parameters are presented within Chapter 6; section 6.8.

Table 10 Selected bond distances (Å) and angles (°) for **12**

Co(1)-N(1)	2.093(4)
Co(1)-N(2)	2.254(4)
Co(1)-N(3)	2.170(4)
Co(1)-Cl(1)	2.316(2)
Co(1)-Cl(2)	2.311(2)
N(1)-Co(1)-N(2)	76.42(17)
N(1)-Co(1)-N(3)	104.82(16)
N(2)-Co(1)-N(3)	79.45(16)
N(1)-Co(1)-Cl(1)	110.09(13)
N(2)-Co(1)-Cl(1)	89.59(12)
N(3)-Co(1)-Cl(1)	139.68(12)
N(1)-Co(1)-Cl(2)	97.73(13)
N(2)-Co(1)-Cl(2)	166.88(12)
N(3)-Co(1)-Cl(2)	90.95(12)
Cl(1)-M(1)-Cl(2)	103.48(6)

In a similar fashion to **11a** and **11c** the molecular structure of **12** adopts a distorted trigonal bipyramidal geometry with the *NNN*-chelate bound in *facial* configuration. The equatorial plane is defined as N(1), N(3), Cl(1) [N(1)-Co(1)-N(3) 104.82(16)°, N(1)-Co(1)-Cl(1) 110.09(13)°, N(3)-Co(1)-Cl(1) 139.68(12)°] and the axial sites consist of N(2) and Cl(2) [N(2)-Co(1)-Cl(2) 166.88(12)°]. The *N*-aryl group is oriented such that the *ortho*-methyl groups [C(16) and C(18)] are positioned above and below the plane defined by N(3)-N(2)-Co(1) [*tors.*: C(10-C(9)-N(3)-Co(1) 57.1(6)°] with one *ortho*-methyl group [C(18)] pointing in a similar direction to Cl(1). In addition, the aryl substituent is inclined at an angle of 82.6(2)° to the N(3)-N(2)-Co(1) plane. The Co-N(2) bond distance of 2.254(4) Å, is longer than the Co-N(3) bond distance of 2.170(4) Å, which is in contrast to **11c** and more appreciable than that observed in **11a**. Notably, the Co-$N_{pyridyl}$ bond distance [2.093(4) Å] remains the shortest and unlike in **11a** and **11c** the Co-Cl bond lengths are almost identical [Co(1)-Cl(1) 2.316(2) Å, Co(1)-Cl(2) 2.311(2) Å]. The Cl-Co-Cl angle at 103.48(6)° lies below the range found in pyridine-diimine cobalt(II) halide complexes,[37, 38] but compares well with the less rigid *NNN*-chelated five-coordinate cobalt dichloride complexes.[39 - 43] As with

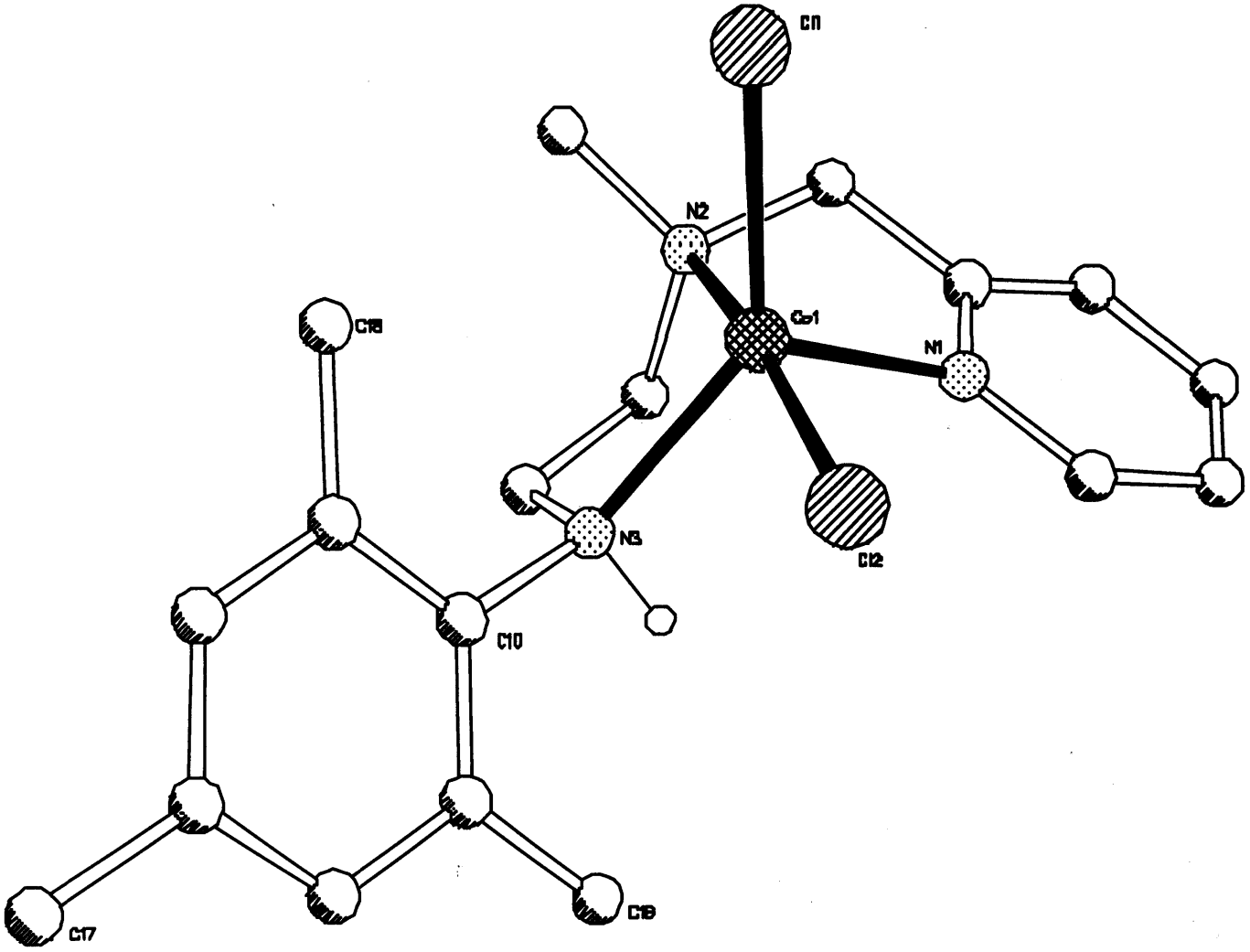

Figure 20 Molecular structure of [{**LII**}$CoCl_2$] (**12**) (All the hydrogen atoms apart from H3 have been omitted for clarity)

11a and **11c**, both R/R and S/S forms are present attributable to the centric nature of the space group.

2.7. Reaction of MCl_2 (M = Mn, Fe) with LIV

As illustrated in Scheme 9 the reaction of anhydrous MCl_2 with 1 equivalent of **LIVa - c** at elevated temperatures gives the complexes [{**LIV**}MnCl(μ-Cl)]$_2$ (**14a** and **14c**), and [{**LIV**}MCl_2] (M = Mn **14b** and Fe **15a - c**) in good yield. All the compounds have been

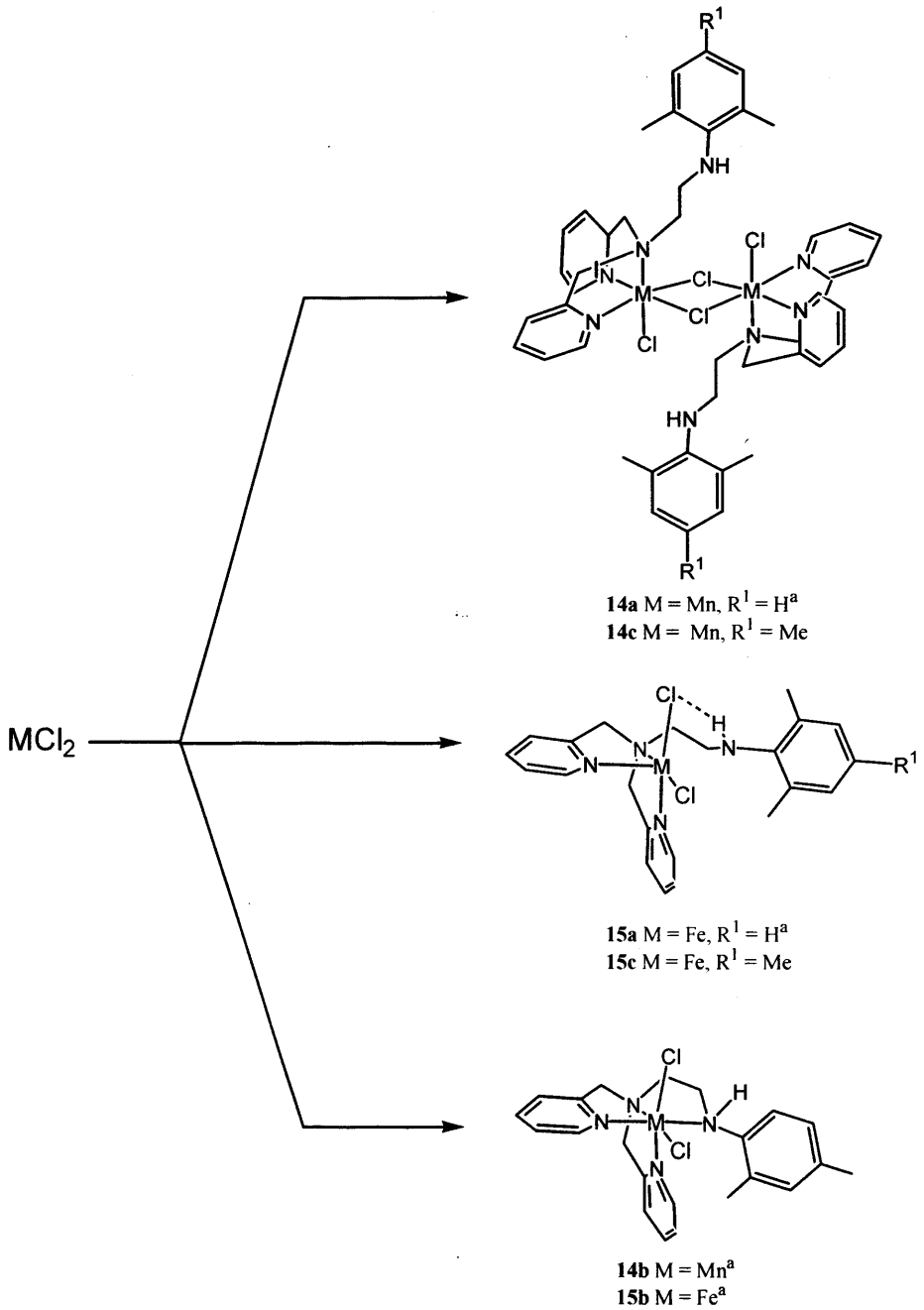

Scheme 9 *Reagents and conditions*: **LIV**, *n*-BuOH , heat
[a] Isolated from single crystal X-ray diffraction studies

characterised by FAB mass spectrometry, magnetic susceptibility measurements, solid state IR spectroscopy and elemental analysis (except for **14c** and **15c**). Insight into the coordination geometry around the metal centre was provided by single crystal X-ray diffraction studies performed on complexes **14a**, **14b**, **15a** and **15b**.

The layering of an acetontrile solution of **14a**, **14b** and **15a** with hexane gave clear crystals for **14a** and **14b** and golden crystals for **15a** suitable for single crystal X-ray diffraction studies. In addition, the slow cooling of a hot acetonitrile solution afforded golden crystals of **15b**, which were also analysed by single crystal X-ray diffraction. The molecular structures of **14a**, **14b**, **15a** and **15b** are represented in Figures 21 - 23 and selected bond distances and bond angles are listed in Tables 11 and 12. Crystal data and data collection refinement parameters are presented within Chapter 6; section 6.8.

Table 11 Selected bond distances (Å) and angles (°) for **14a**

Mn(1)-N(1)	2.286(1)	Mn(1)-Cl(2)	2.531(1)
Mn(1)-N(2)	2.391(1)	Mn(1)-Cl(2A)	2.568(1)
Mn(1)-N(3)	2.222(1)	Mn(1)...Mn(1A)	3.800(1)
Mn(1)-Cl(1)	2.427(1)		
N(1)-Mn(1)-N(3)	97.13(4)	N(3)-Mn(1)-Cl(2)	160.64(3)
N(1)-Mn(1)-N(2)	70.35(4)	N(1)-Mn(1)-Cl(2A)	168.10(3)
N(2)-Mn(1)-N(3)	72.62(4)	N(2)-Mn(1)-Cl(2A)	100.89(3)
N(1)-Mn(1)-Cl(1)	93.71(3)	N(3)-Mn(1)-Cl(2A)	87.51(3)
N(2)-Mn(1)-Cl(1)	157.91(3)	Cl(1)-Mn(1)-Cl(2)	103.06(1)
N(3)-Mn(1)-Cl(1)	95.16(3)	Cl(1)-Mn(1)-Cl(2A)	96.783(14)
N(1)-Mn(1)-Cl(2)	88.26(3)	Cl(2)-Mn(1)-Cl(2A)	83.931(13)
N(2)-Mn(1)-Cl(2)	91.97(3)	Mn(1)-Cl(2)-Mn(1A)	96.07(1)

The molecular structure of **14a** contains two equivalent manganese atoms bridged by a pair of chloride donors to give a Mn_2Cl_2 diamond core, with a C_2 symmetry passing through the centre. In addition, each manganese atom is bound by a *facially* coordinated *NNN*-chelate [N(1)-Mn(1)-N(3) 97.13(4)°] with a pendant *N*-aryl ethylamine arm and a terminal chloride to give a distorted octahedral geometry. In an analogous fashion to $[\{Etdpa\}MnCl(\mu\text{-}Cl)]_2$,[50] the central tertiary amines are *trans* to a terminal chloride and the pyridyl groups are *trans* to the bridging chlorides. As expected the $Mn\text{-}N_{amine}$ bond distance [Mn(1)-N(2) 2.391(1) Å] is elongated in comparison to the $Mn\text{-}N_{pyridyl}$ bond distances [Mn(1)-N(1) 2.286(1), Mn(1)-N(3)

2.222(1) Å]. The two Mn-μ-Cl bond distances are slightly different [Mn-Cl(2) 2.531(1), Mn(1)-Cl(2A) 2.568(1) Å] and longer than the terminal Mn-Cl bond distances [Mn(1)-Cl(1) 2.427(1) Å]. The Mn...Mn separation is 3.800(1) Å, which together with the rt magnetic moment (S = 5/2 per Mn) precludes the existence of a strong Mn-Mn interaction. Finally, these structural features are similar to other structurally characterised bis(μ-chloro) dimanganese(II) complexes.[50 - 52]

Table 12 Selected bond distances (Å) and angles (°) for **14b**.MeCN, **15a**.MeCN and **15b**.MeCN

	M = Mn (**14b**.MeCN)	M = Fe (**15a**.MeCN)	M = Fe (**15b**.MeCN)
M(1)-N(1)	2.272(7)	2.171(2)	2.191(7)
M(1)-N(2)	2.343(7)	2.264(2)	2.249(6)
M(1)-N(3)	2.278(7)	2.188(2)	2.169(7)
M(1)-N(4)	2.403(7)	NA[a]	2.303(6)
M(1)-Cl(1)	2.400(2)	2.320(1)	2.337(2)
M(1)-Cl(2)	2.472(2)	2.463(1)	2.468(2)
N(1)-M(1)-N(2)	71.7(2)	74.91(6)	74.2(2)
N(1)-M(1)-N(3)	93.8(2)	91.02(6)	95.0(2)
N(1)-M(1)-N(4)	146.8(2)	NA	150.9(2)
N(2)-M(1)-N(3)	74.4(2)	77.81(6)	76.7(2)
N(2)-M(1)-N(4)	75.4(2)	NA	77.2(2)
N(3)-M(1)-N(4)	81.5(2)	NA	83.6(2)
N(1)-M(1)-Cl(1)	101.37(18)	103.12(5)	100.28(18)
N(2)-M(1)-Cl(1)	163.85(17)	171.15(4)	167.69(19)
N(3)-M(1)-Cl(1)	91.94(18)	93.68(5)	93.02(18)
N(4)-M(1)-Cl(1)	111.62(16)	NA	108.82(16)
N(1)-M(1)-Cl(2)	91.97(18)	92.72(4)	90.55(18)
N(2)-M(1)-Cl(2)	93.16(17)	91.53(4)	91.99(17)
N(3)-M(1)-Cl(2)	163.80(18)	167.38(5)	165.55(18)
N(4)-M(1)-Cl(2)	85.37(17)	NA	85.08(16)
Cl(1)-M(1)-Cl(2)	101.77(8)	97.20(2)	99.15(8)

[a] M(1)...N(4) 2.558 Å

When iron is acting as the metal centre a monomeric complex is isolated by single crystal X-ray diffraction (**15a**). The iron(II) centre may be regarded as being in a *pseudo*-octahedral environment bound to two pyridyl nitrogen donors, and one central amine donor atom of the tripodal ligand and two chlorides. In addition, the *N*-aryl substituted donor atom of **LIVa** is loosely bound [Fe(1)...N(4) 2.558 Å] to give a *pseudo*-N4Cl2 coordination sphere, this is attributable to the hydrogen-bonding interaction between H(4) and Cl(2) [2.358

Å]. Notably, the Fe...N(4) separation is *ca.* 0.3 Å greater than the iron *N*-aryl amine bond distances in complexes **10a**, **10c** and **15b**. But comparable to the iron *N*-aryl amine bond separation present in the *pseudo*-octahedral structure of complex **18a** [Fe...N(4) 2.597 Å: Chapter 3; section 3.4]. Evidently, the steric bulk in the two *ortho*-positions of the aryl substituent, are preventing the ligand from acting as a genuine *NNNN*-chelate (*cf.* **15b**). The two chlorides are coordinated in a *cis*-disposition [Cl(1)-Fe(1)-Cl(2) 97.20(2)°] with Cl(1) *trans* to the central amine [N(2)-Fe(1)-Cl(1) 171.15(4)°] and Cl(2) *trans* to the pyridyl moiety N(3) [N(3)-Fe(1)-Cl(2) 167.38(5)°]. Such geometry constraints leave the loosely bound *N*-aryl substituted donor atom N(4) in a *trans* arrangement with the pyridyl donor atom N(1).

The Fe-N bond distances (>2.0 Å) are characteristic of a HS configuration ranging from 2.171(2) – 2.264(2) Å.[6, 7, 10, 11] The Fe(1)-N(2) distance of 2.264(2) Å is the most elongated, attributable to the tertiary amine being the weakest donor atom. The differing *trans* effect imposed on the two chloride ligands leads to inequivalent Fe-Cl bond distances, with Fe(1)-Cl(2) being the most elongated at 2.463(1) Å.

The structures of **14b** and **15b** are essentially identical and will be discussed together. Notably, the unit cells contain two independent molecules. The selected bond distances (Å) and angles (°) in Table 12 are representative of one of the unique molecules. The metal(II) centre in each complex is in a distorted octahedral environment ligated by two pyridyl nitrogens, one tertiary amine and one *N*-aryl substituted donor atom of the tripodal ligand and two chlorides, affording a N4Cl2 coordination sphere. The geometry constraints applied by the *NNNN*-chelate impose a *cis*-disposition on the bound chloride ligands, with Cl(1) *trans* to the tertiary amine [N(2)] and Cl(2) *trans* to one of the pyridyl moieties [N(3)]. Such constraints leave the *N*-aryl substituted donor atom N(4) in a *trans* arrangement with the pyridyl moiety N(1).

The distortion from an ideal octahedral geometry arises from the *NNNN*-chelate, for example the angles N(1)-M(1)-N(2) [71.7(2)° (Mn), 74.2(2)° (Fe)] and N(1)-M(1)-N(4) [146.8(2)° (Mn), 150.9(2)° (Fe)] are lower than 90 and 180° respectively. Furthermore, the

angles between Cl(1) and its *cis*-neighbours are greater than 90° [Cl(1)-M(1)-N(1) 101.37(18)° (Mn), 100.28(18)° (Fe); Cl(1)-M(1)-N(3) 91.94(18)° (Mn), 93.02(16)° (Fe); Cl(1)-M(1)-N(4) 111.62(16)° (Mn), 108.82(16)° (Fe); Cl(1)-M(1)-Cl(2) 101.77(8)° (Mn), 99.15(8)° (Fe)]. In the case of **15b** the *cis*-arrangement of the pyridyl donors is in contrast to the *trans*-configuration observed for [{dpea}Fe(NCS)$_2$].[53] The *N*-aryl amine-metal bond length [M-N(4) 2.403(7) (Mn); 2.303(6) (Fe) Å] is predictably the most elongated and the M-$N_{pyridyl}$ the shortest [M-$N_{pyridyl\ ave.}$ 2.275 (Mn); 2.180 (Fe) Å]. The M-Cl bond distances are inequivalent due to the differing *trans* effect imposed on each chloride atom with M(1)-Cl(2) bond distance being the longest in each case [2.472(2) (Mn), 2.468(2) Å (Fe)].

The solid state IR spectra reflect the ligand coordination modes within the complexes by exhibiting characteristic pyridyl ring deformation bands at *ca.* 1600 cm^{-1},[11, 33] and N-H stretching frequencies in the region of 3312 – 3238 cm^{-1}. Interestingly, for **14a** – **c** two N-H stretching frequencies are observed, in **14a** they appear at 3312 and 3261 cm^{-1} with an approximate ratio of 3:1, whilst in **14b** they appear at 3311 and 3261 cm^{-1} with an approximate ratio of 1:4. The lower frequency is typical of a coordinated amine atom[44] and the higher frequency may reflect the pendant nature of the *N*-aryl ethylamine substituent. Notably, for **14a** and **14b** the approximate ratio of the two N-H bands, are in favour of the species isolated by single crystal X-ray diffraction studies. Conversely, **15a** – **c** exhibit a single N-H stretching frequency, which is *ca.* 100 cm^{-1} lower in frequency than the free-ligand. The rt magnetic susceptibility measurements are characteristic of HS behaviour with five-unpaired electrons per manganese atom and four-unpaired electrons per iron atom.

The ^{1}H NMR spectra were recorded for complexes **14** and **15** at rt in CD_3CN. Unsurprisingly (*cf.* complex **5**), the ^{1}H NMR spectra obtained for complexes **14a** and **14b** are very broad thereby preventing comprehensive peak assignment (Appendices: Figures 5 and 6). In contrast, the ^{1}H NMR spectra of complexes **15a** and **15b** are assignable by comparison with related metal(II) complexes **1**, **6** and **10a** (Figure 24 and Table 13). Assignment has also

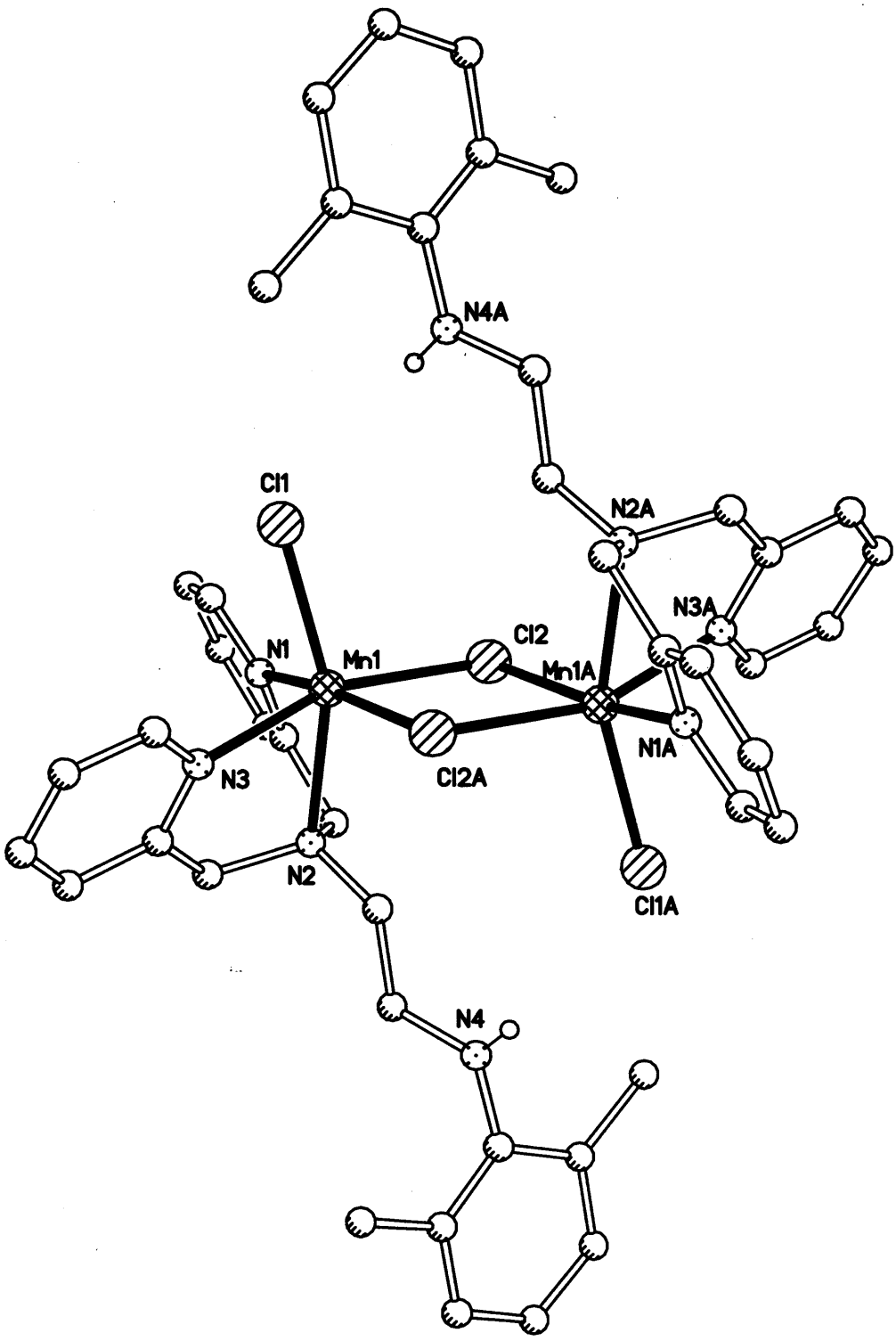

Figure 21 Molecular structure of [{**LIVa**}MnCl(μ-Cl)]$_2$ (**14a**) (All the hydrogen atoms apart from H4 have been omitted for clarity)

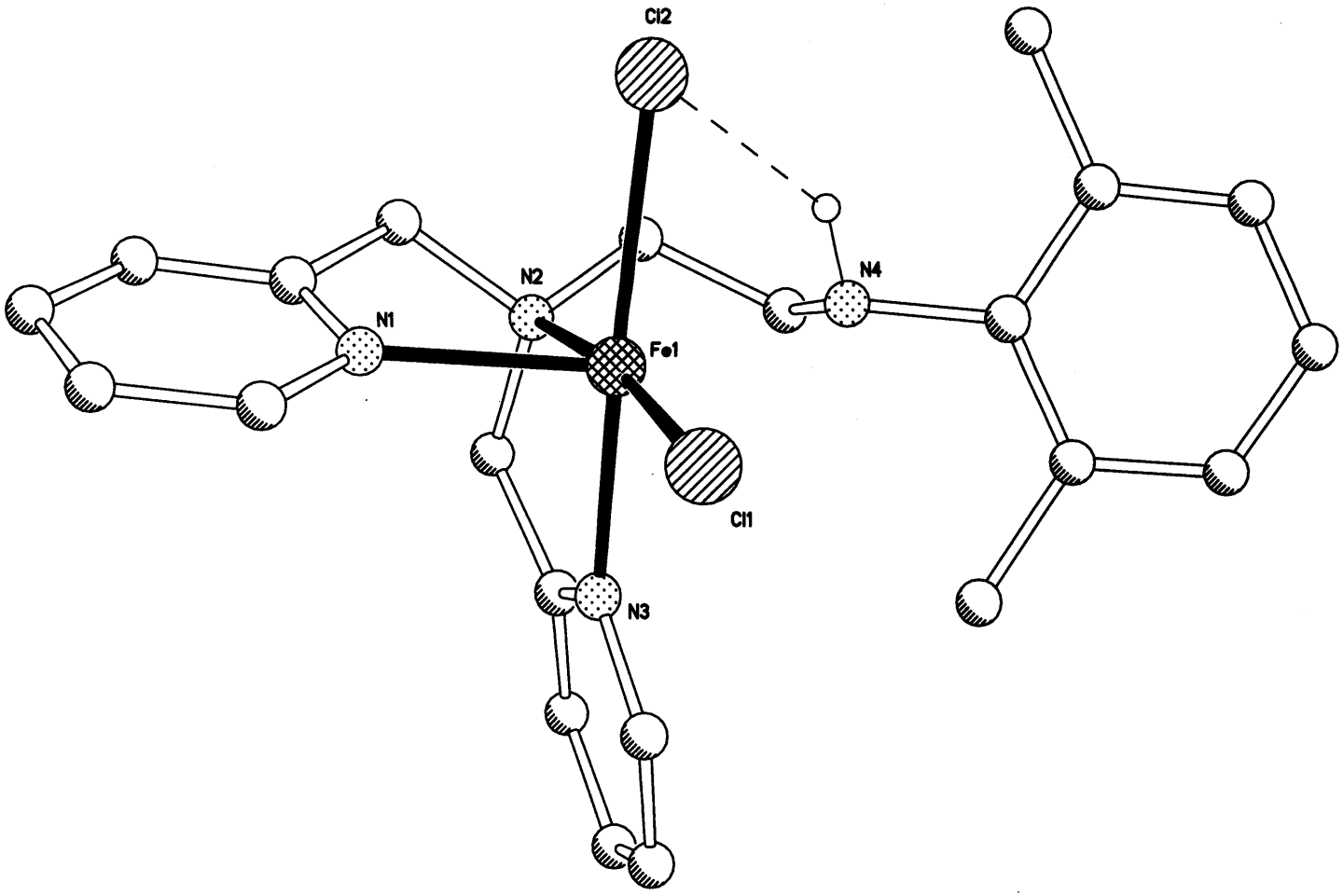

Figure 22 Molecular structure of [{**LIVa**}$FeCl_2$] (**15a**) (All the hydrogen atoms apart from H4 have been omitted for clarity)

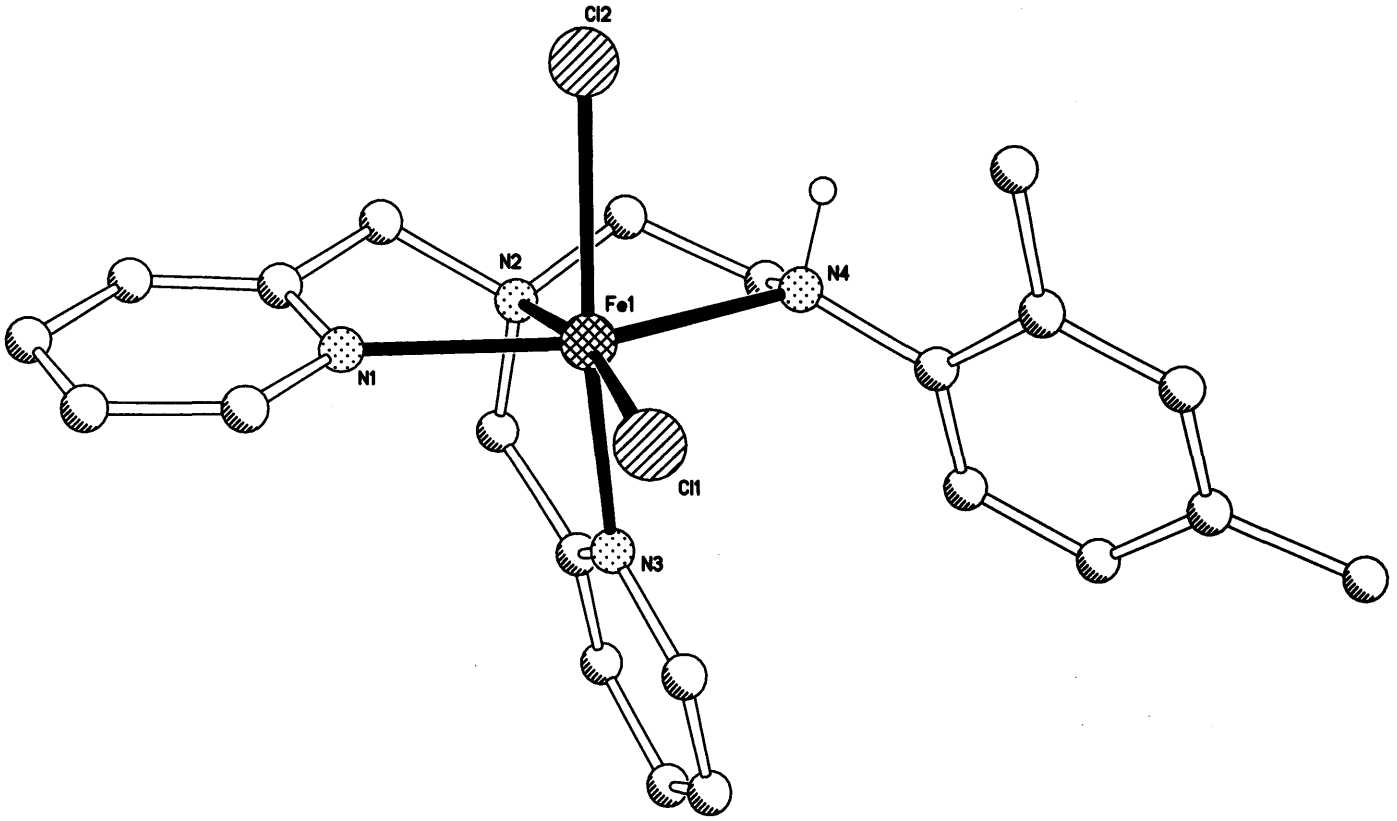

Figure 23 Molecular structure of one of the two unique molecules [{**LIVb**}$FeCl_2$] (**15b**) (All the hydrogen atoms apart from H4 have been omitted for clarity). Molecular structure of [{**LIVb**}$MnCl_2$] (**14b**) reveals a similar coordination geometry

been achieved on the basis of T_1 and *via* direct comparison with one another.

The PyCH_α of the coordinated pyridyl arms are characteristically the furthest downfield at δ = 120.2 and 139.1 for complexes **15a** and **15b** respectively. The Py$CH_{\beta/\beta'}$ and PyCH_γ appear at δ = 51.9, 51.1 and 19.3 (T_1 = 11.4, 9.3 and 26.3 ms) for **15a**, whilst for **15b** they are found at δ = 53.0 (T_1 = 11.7 ms), 45.5 and 27.6 (T_1 = 37.9 ms). All four methylene protons are assigned for **15a** at δ = 73.5 (T_1 = 1.3 ms), *ca.* 72 (shoulder of δ = 73.5), 28.7 (T_1 = 1.0 ms) and 12.2 (T_1 = 1.7 ms). In contrast, for **15b** only one very broad methylene peak is assigned at *ca.* δ = 46. In each case the aromatic peaks are shifted further downfield than their free ligand diamagnetic counterparts (**LIVa** and **LIVb**) and in **15b** they are shifted more than in **15a**. This may be indicative of the solid state coordination modes existing in the solution state for **15a** and **15b**.

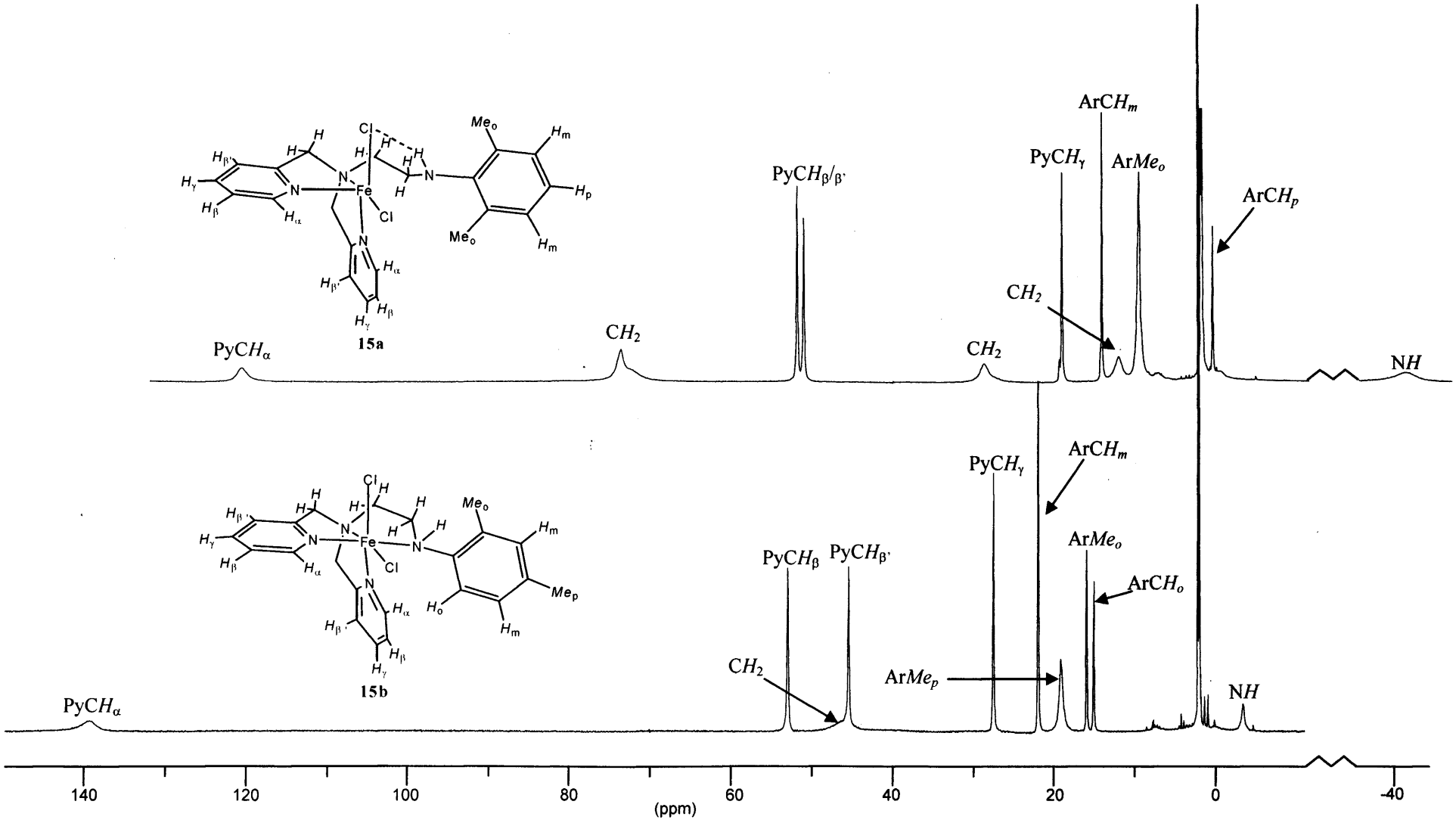

Figure 24 ^{1}H NMR spectra for complexes **15a** and **15b** in CD_3CN at rt

Table 13 ^{1}H NMR chemical shifts (δ) and relaxation times (T_1) for complexes **15a** and **15b** in CD_3CN at rt[a]

	δ / (T_1 ms)						
Complex	PyCH_α	PyC$H_{\beta/\beta'}$	PyCH_γ	CH_2	ArCH	Ar*Me*	NH
1	116.5	54.7 (10.1), 51.8 (9.1)	7.8	70.8 (1.1)	NA	NA	107.0 (1.3)
6	127.8	50.5 (9.8), 45.8 (8.1)	24.5 (25.0)	-10 to 10 (very broad)	NA	NA	NA
10a	130.4	58.8 (16.4), 57.4 (14.6)	15. 8 (37.1)	104.9 (0.96), 80.9 (0.73), 62.9 (0.9)	12.3 (34.2, ArCH_m), -5.4 (ArCH_p)	6.6 (2.0, Ar*Me*$_o$),	124.1 (3.8, NH), -15.01 (15.3, NH)
15a	120.2	51.9 (11.4), 51.1 (9.3),	19.3 (26.3)	73.5 (1.3), 28.7 (1.0), 12.2 (1.7)	14.5 (31.9, ArCH_m), 0.62 (ArCH_p)	9.7 (3.1, Ar*Me*$_o$)	-42.5
15b	139.1 (0.5)	53.0 (11.7), 45.5	27.6 (37.9)	*ca.* 46	21.9 (ArCH_m), 15.1 (29.6, ArCH_o)	19.1 (2.0, Ar*Me*$_p$), 16.1 (Ar*Me*$_o$)	-3.4

[a] Complexes **1**, **6** and **10a** included for comparison

2.8. Conclusions

In summary, we have characterised several new high yielding metal(II) dichloride complexes coordinated to the well known dpa and tpa ligands and the novel ligand sets **LI-LIV**. When dpa is acting as the *NNN*-chelate the absence of steric control enables the formation of a mono- and a bis-ligated species with the former present as dimeric species. Variation in the molar quantity of dpa in the reaction mixture is found to alter the product distribution. In the case of tpa the ligand is found to bind to the metal centres in a tetradentate fashion and the tendency to form chloride salts is evident with cobalt as the metal centre.

The new ligand sets **LI-LIV** have been synthesised *via* utilising established experimental protocols and exploiting the nucleophilicity of the central amine in **LI**. The flexibility of the *NNN*-chelate **LI** when coordinated to iron or cobalt is observed by X-ray crystallography, paramagnetic ^{1}H NMR spectroscopy and DFT calculations. Indeed, the apparent dynamic behaviour in solution may be accountable for, *via* a 'Berry-type' or a dissociation-inversion process. The single crystal X-ray diffraction study performed on **LII** when coordinated to cobalt exhibits analogous geometrical arrangement to the **LI** cobalt dichloride complexes. The *N*-aryl amine coordination mode in **LIV** when bound to manganese or iron is dependent upon the steric bulk in the *ortho*-positions of the *N*-aryl substituent as is observed by X-ray crystallography and paramagnetic ^{1}H NMR spectroscopy.

References

[1] K. Chen, M. Costas and L. Que, Jr., *J. Chem. Soc., Dalton Trans.*, 2002, 672-679.
[2] E.I. Solomon, T.C. Brunold, M.I. Davis, J.N. Kemsley, S.-K. Lee, N. Lehnert, F. Neese, A.J. Skulan, Y.S. Yang, J. Zhou, *Chem. Rev.*, 2000, **100**, 235-349.
[3] B.J. Wallar and J.D. Lipscomb, *Chem. Rev.*, 1996, **96**, 2625-2658.
[4] S. M. Nelson and J. Rodgers, *J. Chem. Soc. A.*, 1968, 272-276
[5] A.W. Addison, S.Burman, C.G. Wahlgren, O.A. Rajan, T.M. Rowe and E. Sinn, *J. Chem. Soc., Dalton Trans.*, 1987, 2621-2630.
[6] Y. Zang, J. Kim, Y. Dong, E. C. Wilkinson, E. H. Appelman and L. Que, Jr., *J. Am. Chem. Soc.*, 1997, **119**, 4197-4205.
[7] A. Diebold and K.S. Hagen, *Inorg. Chem.*, 1998, **37**, 215-223.
[8] P. Gutlich, Y. Garcia and H.A. Goodwin, *Chem. Soc., Rev.*, 2000, **29**, 419-427.
[9] P. Gutlich, A. Hauser and H. Spiering, *Angew. Chem., Int. Ed. Engl.*, 1994, **33**, 2024-2054.
[10] D. Mandon, A. Machkour, S. Goetz and R. Welter, *Inorg. Chem.*, 2002, **41**, 5364-5372.
[11] Z. He, D. C. Craig and S. B. Colbran, *J. Chem. Soc., Dalton Trans.*, 2002, 4224-4235.
[12] T. M. Kooistra, K.F.W. Hekking, Q. Knijnenburg, B. de Bruin, P. H.M. Budzelaar, R. de Gelder, J.M.M. Smits and A. W. Gal, *Eur. J. Inorg. Chem.*, 2003, 648-655.
[13] M.Ito, Y. Takita, K. Sakai and T. Tubomura, *Chem. Lett.*, 1998, 1185-1186.
[14] G. J. P. Britovsek, S. P. D. Baugh, O. Hoarau, V. C. Gibson, D. F. Wass, A. J. P. White and D. J. Williams, *Inorg. Chim. Acta.*, 2003, **345**, 279-291.
[15] G. J. P. Britovsek, V. C. Gibson, B. S. Kimberley, P. J. Maddox, S. J. McTavish, G. A. Solan, A. J. P. White and D. J. Williams, *Chem. Commun.*, 1998, 849-850.
[16] B. L. Small, M. Brookhart and A. M. A, Bennett, *J. Am. Chem. Soc.*, 1998, **120**, 4049-4050.
[17] A. M. A. Bennett, *World Pat., WO 98/27124* (DuPont), 1998; A. M. A. Bennett, *Chem. Abstr.*, 1998, **129**, 122973.
[18] H.C.S. Clark, F.G.N. Cloke, P.B. Hitchcock, J.B. Love and A.P. Wainwright, *J. Organomet. Chem.*, 1995, **501**, 333-340.
[19] Y. Schrodi, R. R. Schrock and P. J. Bonitatebus Jr, *Organometallics*, 2001, **20**, 3560-3573.
[20] E.S. Raper, A. Miller, T. Glowiak and M. Kubiak, *Transition Met. Chem.*, 1989, **14**, 319-320.
[21] D.A. Handley, P.B. Hitchcock, T.-H. Lee and G.J. Leigh, *Inorg. Chim. Acta.*, 2001, **314**, 14-21.
[22] S. Kasselouri, A. Garoufis, S.P. Perlepes, F. Lutz, R. Bau, S. Gourbatsis and N. Hadjiliadis, *Polyhedron*, 1998, **17**, 1281-1288.
[23] V.C. Gibson, R.K. O'Reilly, D.F. Wass, A.J.P. White and D.J. Williams, *J. Chem. Soc., Dalton Trans.*, 2003, 2824-2830.
[24] R. J. Butcher and A. W. Addison, *Inorg. Chim. Acta.*, 1989, **158**, 211-215.
[25] A. Hazell, C. J. McKenzie and L. P. Nielsen, *Polyhedron*, 2000, **19**, 1333-1338 and references therein.
[26] J. Glerup, P.A. Goodson, D.J. Hodgson, K. Michelsen, K.M. Nielsen and H. Weike, *Inorg. Chem.*, 1992, **31**, 4611-4616.
[27] M. Velusamy, M. Palaniandavar and K.R.J. Thomas, *Polyhedron*, 1998, **17**, 2179-2186.
[28] W. Henke and S. Kremer, *Inorg. Chim. Acta.*, 1982, **65**, L115-L117.
[29] F. Takusagawa, P. G. Yohannes and K. B. Mertes, *Inorg. Chim. Acta.*, 1986, **114**, 165-169.
[30] G. S. Matouzenko, A. Bousseksou, S. Lecocq, P. J. van Koningbruggen, M. Perrin, O. Kahn and A. Collet, *Inorg. Chem.*, 1997, **36**, 2975-2981.
[31] C. S. Allen, C. L. Chuang, M. Cornebise and J. W. Canary, *Inorg. Chim. Acta.*, 1995, **239**, 29-37.
[32] A. Nanthakumar, S. Fox, N. N. Murthy and K. D. Karlin, *J. Am. Chem. Soc.*, 1997, **119**, 3898-3906.
[33] M. M. da Mota, J. Rodgers and S. M. Nelson, *J. Chem. Soc. A.*, 1969, 2036-2044.
[34] J. P. Wolfe, S. Wagaw and S. L. Buchwald, *J. Am. Chem. Soc.*, 1996, **118**, 7215-7216.
[35] J. P. Wolfe and S. L. Buchwald, *J. Org. Chem.*, 2000, **65**, 1144-1157.
[36] G. J. P. Britovsek, V. C. Gibson, S. Mastroianni, D. C. H. Oakes, C. Redshaw, G. A. Solan, A. J. P. White and D. J. Williams, *Eur. J. Inorg. Chem.*, 2001, 431-437.
[37] G. J. P. Britovsek, M. Bruce, V. C. Gibson, B. S. Kimberley, P. J. Maddox, S. Mastroianni, S. J. McTavish, C. Redshaw, G. A. Solan, S. Strömberg, A. J. P. White and D. J. Williams, *J. Am. Chem. Soc.*, 1999, **121**, 8728-8740.
[38] G. J. P. Britovsek, S. Mastroianni, G. A. Solan, S. P. D. Baugh, C. Redshaw, V. C. Gibson, A. J. P. White, D. J. Williams and M. R. J. Elsegood, *Chem. Eur. J.*, 2000, **6**, 2221-2231.
[39] N. di Vaira and P.L. Orioli, *Inorg. Chem.*, 1969, **8**, 2729-2734.
[40] Z. Dori, R. Eisenberg and H.B. Gray, *Inorg. Chem.*, 1967, **6**, 483-486.
[41] M. Gerloch, *J. Chem. Soc. A.*, 1966, 1317-1325.
[42] S.J. Shieh, C.-C. Chou, G.-H. Lee, C.-C. Wang and S.-M. Peng, *Angew. Chem., Int. Ed. Engl.*, 1997, **36**, 56-59.
[43] S.-C. Sheu, M.-J. Tien, M.-C. Cheng, T.-I. Ho, S.M. Peng and Y.-C. Lin, *J. Chem. Soc., Dalton Trans.*, 1995, 3503-3510.
[44] Upon coordination the N-H stretching frequency decreases by *ca.* 100 cm^{-1}

[45] Y. Zang, H. G. Jang, Y. M. Chiou, M. P. Hendrich and L. Que, Jr., *Inorg. Chim. Acta.*, 1993, **213**, 41-48.
[46] H.C.S. Clark, F.G.N. Cloke, P.B. Hitchcock, J.B. Love and A.P. Wainwright, *J. Organomet. Chem.*, 1995, **501**, 333-340.
[47] M. Aizenberg, L. Turculet, W. M. Davis, F. Schattenmann and R. R. Schrock, *Organometallics*, 1998, **17**, 4795-4812.
[48] (a) K. Jurkschat, C. Mügge, A. Tzschach and A. Zschunke, *J. Organomet. Chem.*, 1977, **139**, 279-282; (b) C. Mügge, K. Jurkschat, A. Tzschach and A. Zschunke, *J. Organomet. Chem.*, 1979, **164**, 135-139; (c) R. G. Swisher and R. R. Holmes, *Organometallics*, 1984, **3**, 365-369.
[49] J.D. Maréchal, G. Barea, F. Maseras, A. Llenos, L. Mouawad, D. Perahia, *J. Comp. Chem.*, 1999, **21**, 283-294.
[50] I. Romero, M-N. Collomb, A. Deronzier, A. llobet, E. Perret, J. Pecaut, L. Le Pape and J-M. Latour, *Eur. J. Inorg. Chem.*, 2001, 69-72.
[51] E. Sinn, *J. Chem. Soc., Dalton Trans.*, 1976, 162-165.
[52] D. I. Arnold, F. A. Cotton, D. J. Maloney and J. H. Matonic, *Polyhedron*, 1997, **16**, 133-141.
[53] G. S. Matouzenko, A. Bousseksou, S. Lecocq, P. J. van Koningbruggen, M. Perrin, O. Kahn and A. Collet, *Inorg. Chem.*, 1997, **36**, 2975-2981.

University of Leicester

Chapter Three

The Synthesis of the *NN*-diaryl diethylenetriamine Ligand Family, Functionalisation of the Central Amine and Coordination Behaviour of Iron and Cobalt Complexes

Abstract

The substitution of two of the picolyl groups in dpa with *N*-aryl substituted ethylamines, to give $(ArNHCH_2CH_2)_2NH$ (**LVa**: Ar = 2,6-$Me_2C_6H_3$, **LVb**: 2,4,6-$Me_3C_6H_2$, **LVc**: 2,4-$Me_2C_6H_3$,) and the functionalisation of the central amine to afford $(ArNHCH_2CH_2)_2NMe$ (**LVIa**: 2,6-$Me_2C_6H_3$, **LVIb**: 2,4,6-$Me_3C_6H_2$) and $(ArNHCH_2CH_2)_2\{(2\text{-}C_5H_4N)CH_2\}N$ (**LVIIa**: Ar = 2,4,6-$Me_3C_6H_2$, **LVIIb**: Ar = 2,4-$Me_2C_6H_3$) has been performed. The complexation of **LV** or **LVI** with $CoCl_2$ in *n*-BuOH at elevated temperatures yields the complexes [{**LV**}$CoCl_2$] (**LVa**: **16a** and **LVb**: **16b**) and [{**LVI**}$CoCl_2$] (**LVIa**: **17a** and **LVIb**: **17b**). Notably, no reaction occurred with $FeCl_2$. The treatment of **LVII** with MCl_2 affords the iron species [{**LVII**}$FeCl_2$] (**LVIIa**: **17a**, **LVIIb**: **17b**) and the cobalt complexes [{**LVII**}$CoCl_2$] (**LVIIa**: **18a**, **LVIIb**: **18b**). The single crystal X-ray structure determination of **16a**, **16b** and **17a**, reveal five-coordinate complexes with the *NNN*-chelate adopting a *meridional* configuration. Single crystal X-ray diffraction studies performed on **18a** and **19a** show **LVIIa** to be bound in a *pseudo*-tetradentate coordination mode with the *N*-aryl substituted amines being inequivalent. Paramagnetic ^1H NMR studies reveal that the inequivalence of the *N*-aryl substituted amines observed in the solid state for **18a** and **19a** does not exist in the solution state.

3.1. Introduction

Within this chapter we are concerned with the modification of the dpa ligand architecture *via* the replacement of the two pyridyl moieties with *N*-aryl-substituted ethylamines to form the *NN*-diaryl diethylenetriamine ligand sets **LV** and **LVI** (Figure 1). Notably, the inclusion of steric bulk may enhance the *NNN*-systems ability to form an active ethylene polymerisation catalyst when coordinated to a metal(II) centre (see Chapter 2; section 2.1). Furthermore, the coordination behaviour of the *NNN-cis*-dichloro-cobalt(II) complexes will be investigated, with **LV** and **LVI** acting as a neutral donors. In an analogous manner to **LI** (Chapter 2; section 2.4) the nucleophilicity of the central amine in **LV** can be exploited to furnish the novel ligand set **LVII**, which possesses a suitable ligand environment for coordination to both iron(II) and cobalt(II).

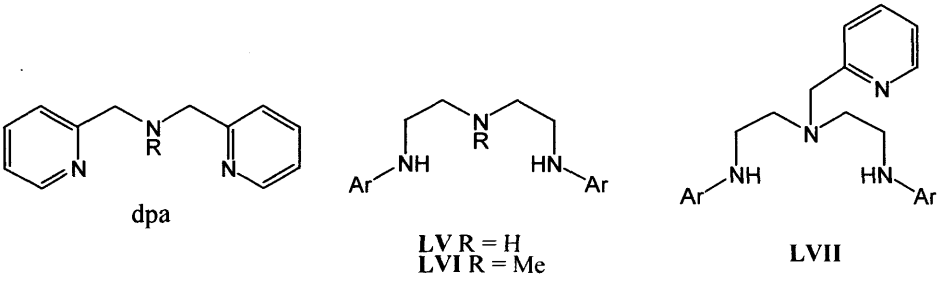

Figure 1 Ligand design

Indeed, the *NNN*-chelating capabilities of **LV** and derivatives thereof (Figure 2) have been exploited in TMs and main group chemistry in which the ligand support is acting as a diamido donor (Chapter 1; section 1.3.3). For example, scandium(III),[1] titanium (III/IV),[2, 3] zirconium(IV),[4 - 8] vanadium(III),[9 - 12] molybdenum(IV),[13 - 15] zinc(II)[16] and aluminium(III)[17, 18] have been utilised as the central atom. The diversified functionalisation of the unsubstituted diethylenetriamine has led to a range of ligand supports in which R = alkyl, silyl aryl or a combination thereof. In many cases, ligand synthesis involves firstly the introduction of two R groups to the two terminal nitrogen atoms followed by the addition of a third R group at the central secondary amine.

Figure 2 LV and derivatives thereof (R = alkyl, silyl, aryl or a combination thereof)

3.2. Ligand Synthesis

The modification of the literature procedure established by Hofmann *et al.*[19] affords aminediethylenediamine(methyl)amine without the requirement for further purification (Scheme 1). The *NN*-diaryl-substituted ligands **LVa** (Ar = 2,6-dimethylphenyl, R = H), **LVb** (Ar = 2,4,6-trimethylphenyl, R = H),[5] **LVc** (Ar = 2,4-dimethylphenyl, R = H), **LVIa** (Ar = 2,6-dimethylphenyl, R = Me) and **LVIb** (Ar = 2,4,6-trimethylphenyl, R = Me) were prepared in high yield by the palladium catalysed N-C(aryl) coupling reaction of diethylenetriamine or diethylenediamine(methyl)amine with two equivalents of the corresponding aryl bromide using an experimental protocol established by Hartwig and Buchwald.[20]

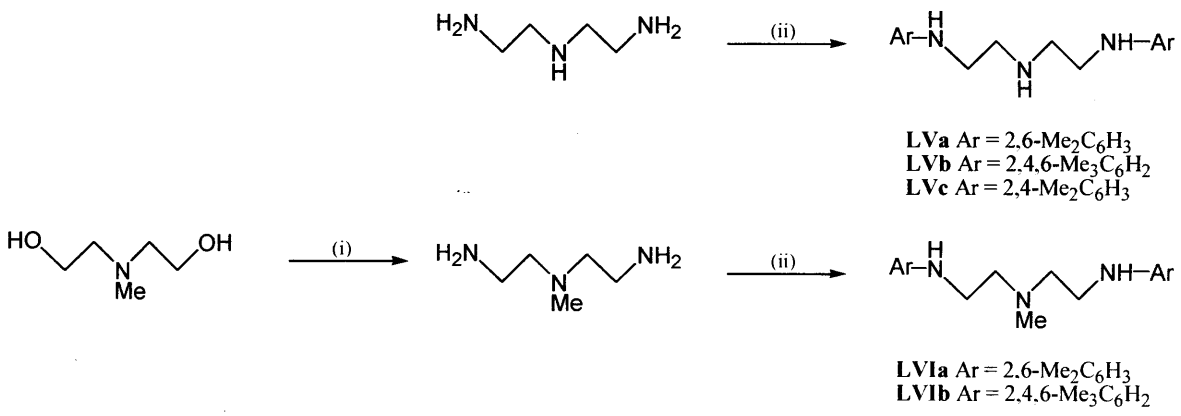

Scheme 1 *Reagents and conditions*: (i) molten phthalimide (2 equiv.) and NaOH (aq); (ii) Ar-Br (2 equiv.), NaO^{t}Bu, $Pd_2(dba)_3$, *rac*-BINAP, toluene, heat

Schrock and co-workers have previously reported the preparation of **LVIb** by an alternative pathway, which involves treating **LVb** with methyl iodide in the presence of excess base and at rt (Scheme 2 *cf.* **LII** Chapter 2; section 2.4).[6, 8] The product requires further purification in order to remove the ammonium salt, which is in contrast to the phthalimide procedure in Scheme 1. **LVII** was prepared *via* the nucleophilic substitution reaction between **LVb** or **LVc** and 2-picolyl chloride in the presence of excess base and at elevated temperature

(*cf.* **LIV** Chapter 2, section 2.4). As expected the product required purification in order to extract **LVII** from the ammonium salt.

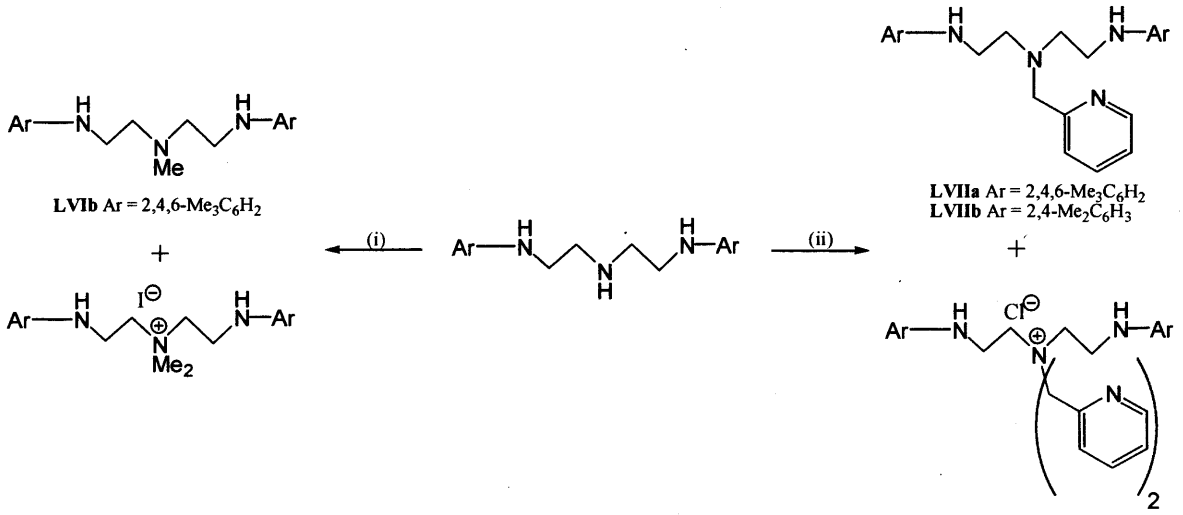

Scheme 2 *Reagents and Conditions*: (i) xs K_2CO_3, MeI, MeCN, rt;[6, 8] (ii) xs K_2CO_3, $C_6H_7NCl.HCl$, MeCN, heat

An alternative reaction pathway for the synthesis of **LVII** was attempted, which involved the reaction of 2-(aminomethyl)pyridine with two equivalents of *N*-tosylaziridine, followed by deprotection with conc. H_2SO_4 (Scheme 3).[21, 22] The resultant free-amine was intended to undergo a palladium catalysed N-C(aryl) coupling reaction[20] with two equivalents of the corresponding aryl bromide. However, we have been unsuccessful in reproducing the previously described procedure for the synthesis of the free-amine.[21, 22] All the new ligands have been characterised by IR, ^1H and ^{13}C NMR spectroscopy and ES mass spectrometry (see Chapter 6; sections 6.3.1 - 6.3.3).

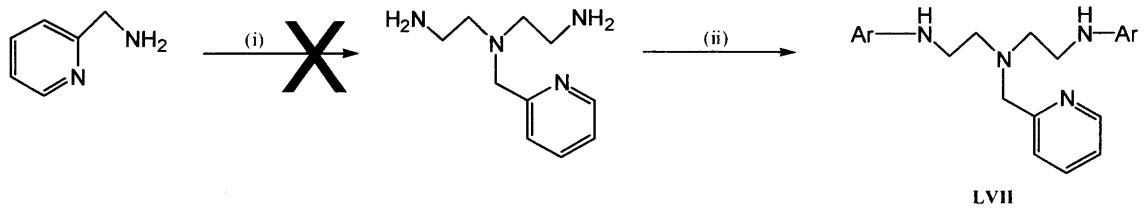

Scheme 3 *Reagents and conditions*: (i) *N*-tosylaziridine (2 equiv.), CH_3CN, heat, followed by conc. H_2SO_4, heat; (ii) Ar-Br (2 equiv.), NaO^tBu, $Pd_2(dba)_3$, *rac*-BINAP, toluene, heat

3.3. Reaction of $CoCl_2$ with LV and LVI

The reaction of anhydrous $CoCl_2$ with 1 equivalent of **LVa** or **LVb** or **LVIa** or **LVIb** in *n*-BuOH at elevated temperature afforded the complexes [{**LVa** or **LVb**}$CoCl_2$] (**16a** and **16b**) and [{**LVIa** or **LVIb**}$CoCl_2$] (**17a** and **17b**) in high yield (Scheme 4). All the compounds have been characterised by FAB mass spectrometry, magnetic susceptibility measurements, solid state IR spectroscopy and elemental analysis (except for **17b**). Insight into the coordination geometry was provided by single crystal X-ray diffraction studies performed on complexes **16a**, **16b** and **17a**. Notably, the reaction of $FeCl_2$ with **LV** or **LVI** under mild or forcing conditions gave only the unreacted starting materials after workup.

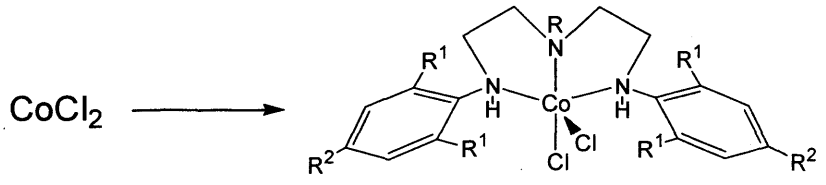

16a R = R^2 = H, R^1 = Me[a]
16b R = H, R^1 = R^2 = Me[a]
17a R = R^1 = Me, R^2 = H[a]
17b R = R^1 = R^2 = Me

Scheme 4 *Reagents and Conditions*: n-BuOH, **LV** or **LVI**, heat
[a] Isolated from single crystal X-ray diffraction studies

The crystals of **16a**, **16b** and **17a** were grown from a hexane layered acetonitrile solution at rt to give pale blue crystals. The molecular structures of **16a** and **16b** are represented in Figure 3, whilst the molecular structure of **17a** is illustrated in Figure 4. Selected bond distances and bond angles are listed in Table 1 for **16a**, **16b** and **17a**. Crystal data and data collection refinement parameters are presented within Chapter 6; section 6.8.

The molecular structures of **16a** and **16b** are essentially the same and only **16a** will be discussed in detail. The geometry at the cobalt(II) centre may be regarded as square pyramidal with a N3Cl2 coordination sphere. The basal plane consists of the *NNN*-chelate [N(1), N(2) and N(3)] and the chloride ligand Cl(1), with Co(1) deviating from this plane by 0.066 Å. The apical position is occupied by the chloride ligand Cl(2). The *NNN*-chelate is bound in a *meridional* configuration with the N(1)-Co(1)-N(3) angle being 160.08(7)° and as two five-membered chelate rings [N(1)-Co(1)-N(2) 80.45(8)°, N(2)-Co(1)-N(3) 80.23(8)°]. The two *N*-

aryl substituents are inclined at an angle of *ca.* 80° to the square basal plane. The *ortho*-methyl groups of the *N*-aryl substituents are positioned above and below the square basal plane [*tors*: C(2)-C(1)-N(1)-Co(1) 66.09°, C(12)-C(11)-N(3)-Co(1) 66.81°] with C6A and C16A pointing in a similar direction to the apical Cl(2) atom. The central amine-cobalt bond distance [Co(1)-N(2) 2.082(2) Å] is shorter than the terminal amine-cobalt bond lengths [Co(1)-N(1) 2.219(3) Å, Co(1)-N(3) 2.243(2) Å]. The two Co-Cl bond distances are asymmetric with Co-Cl(2) being *ca.* 0.08 Å longer than Co-Cl(1). The Cl(1)-Co(1)-Cl(2) bond angle of 114.91(4)° is in the mid-range for those found in pyridine-diimine cobalt(II) halide complexes.[23, 24] As is observed for complexes **11** (Chapter 2; section 2.5), both **16a** and **16b** possess two stereogenic centres, in this case located on the two *N*-aryl substituents. In contrast to **11**, both **16a** and **16b** are achiral by virtue of a symmetry plane through the Co(1)-N(2) bond.

Table 1 Selected bond distances (Å) and angles (°) for **16a**, **16b** and **17a**

	(16a)	**(16b)**	**(17a)**
Co(1)-N(1)	2.219(3)	2.221(4)	2.274(4)
Co(1)-N(2)	2.082(2)	2.066(4)	2.088(3)
Co(1)-N(3)	2.243(2)	2.265(4)	2.289(4)
Co(1)-Cl(1)	2.269(1)	2.256(2)	2.247(2)
Co(1)-Cl(2)	2.350(1)	2.313(2)	2.314(2)
N(1)-Co(1)-N(2)	80.45(8)	80.96(17)	80.25(13)
N(1)-Co(1)-N(3)	160.08(7)	160.00(16)	156.93(12)
N(2)-Co(1)-N(3)	80.23(8)	79.07(17)	80.48(12)
N(1)-Co(1)-Cl(1)	98.82(7)	100.51(13)	100.49(10)
N(2)-Co(1)-Cl(1)	145.33(6)	144.40(14)	132.82(10)
N(3)-Co(1)-Cl(1)	99.79(7)	96.39(13)	101.88(9)
N(1)-Co(1)-Cl(2)	90.50(7)	93.79(12)	87.09(10)
N(2)-Co(1)-Cl(2)	99.76(7)	102.01(14)	108.45(10)
N(3)-Co(1)-Cl(2)	88.06(7)	89.26(13)	87.09(9)
Cl(1)-Co(1)-Cl(2)	114.91(4)	113.29(7)	118.72(6)

The geometry at the cobalt(II) centre in **17a** may be regarded as distorted trigonal bipyramidal with a N3Cl2 coordination sphere. The equatorial plane consists of N(2), Cl(1) and Cl(2) [N(2)-Co(1)-Cl(1) 132.82(10)°, N(2)-Co(1)-Cl(2) 108.45(10)°] and the axial sites are defined as N(1) and N(3) [N(1)-Co(1)-N(3) 156.93(12)°]. The *NNN*-chelate is bound in a *meridional* configuration and as two five-membered chelate rings, which results in the bond

angles 80.25(13) and 80.48(12)°, respectively for N(1)-Co(1)-N(2) and N(2)-Co(1)-N(3). The *ortho*-methyl groups of the *N*-aryl substituents are positioned above and below the plane defined by N(1)-Co(1)-N(3) [*tors*: C(6)-C(1)-N(1)-Co(1) 65.78°, C(16)-C(11)-N(3)-Co(1) 73.57°] with C2A and C12A pointing in a similar direction to Cl(2). In addition, the aryl substituents are inclined at an angle of *ca.* 80° to the N(1)-Co(1)-N(3) plane. There is a difference in the Co-N bond lengths with the central Co-N being shorter than the terminal Co-N bond lengths [Co(1)-N(2) 2.088(3) Å *vs.* Co(1)-N(1) 2.274(4) Å, Co(1)-N(3) 2.289(4) Å]. The two Co-Cl bond distances are asymmetric with Co-Cl(2) being *ca.* 0.07 Å longer than Co-Cl(1). The Cl(1)-Co(1)-Cl(2) bond angle of 118.72(6)° is in the top range for those found in pyridine-diimine cobalt(II) complexes.[23, 24] **17a** possess two stereogenic centres located on the two *N*-aryl substituents, with the relative configurations of the chiral centres being distinct as is observed for both **16a** and **16b**. Notably, the five-coordinate geometry may also be described as square pyramidal with N(1), N(2), N(3) and Cl(1) forming the basal plane, leaving Cl(2) to occupy the apical site.

The FAB mass spectrometric data for complexes **16a**, **16b**, **17a** and **17b** reveals characteristic mass and isotope distribution patterns for a monomeric species with a molecular ion and fragmentation peaks corresponding to the loss of a chloride ion. In contrast, to complexes **10** and **11** (Chapter 2; section 2.5) no minor peaks are observed for a dimeric species. In the solid state IR spectra the N-H stretching frequency is at *ca.* 3290 cm^{-1} and is *ca.* 100 cm^{-1} lower in frequency than the free-ligand. The rt magnetic susceptibility measurements afforded magnetic moments of *ca.* 3.90 BM, characteristic of a HS cobalt(II) configuration (S = 3/2). Attempts to acquire assignable ^1H NMR spectra in CD_3CN at rt proved unsuccessful.

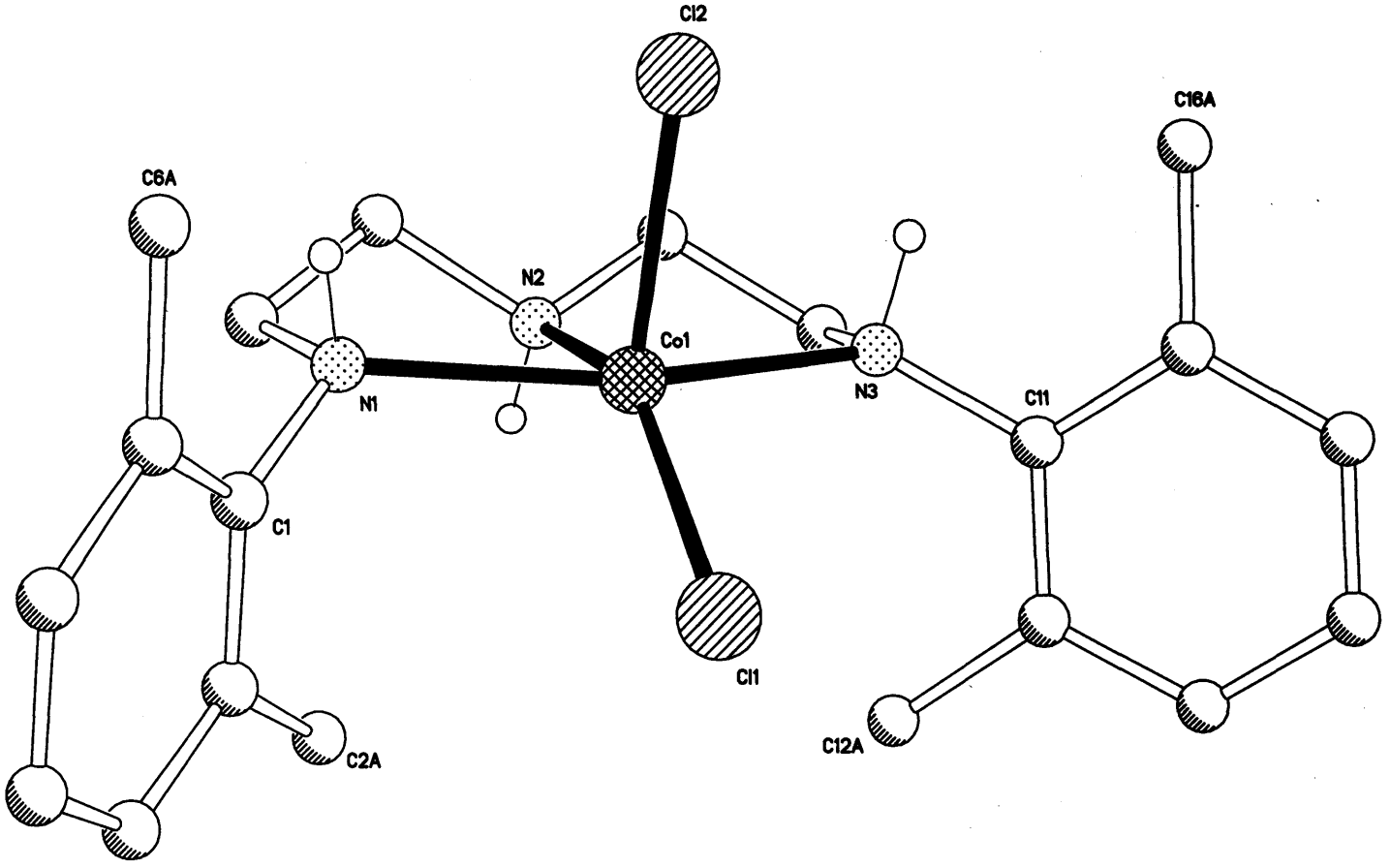

Figure 3 Molecular structure of [{**LVa**}$CoCl_2$] (**16a**) (All the hydrogen atoms apart from H1, H2 and H3 have been omitted for clarity). Molecular structure of [{**LVb**}$CoCl_2$] (**16b**) reveals a similar coordination geometry

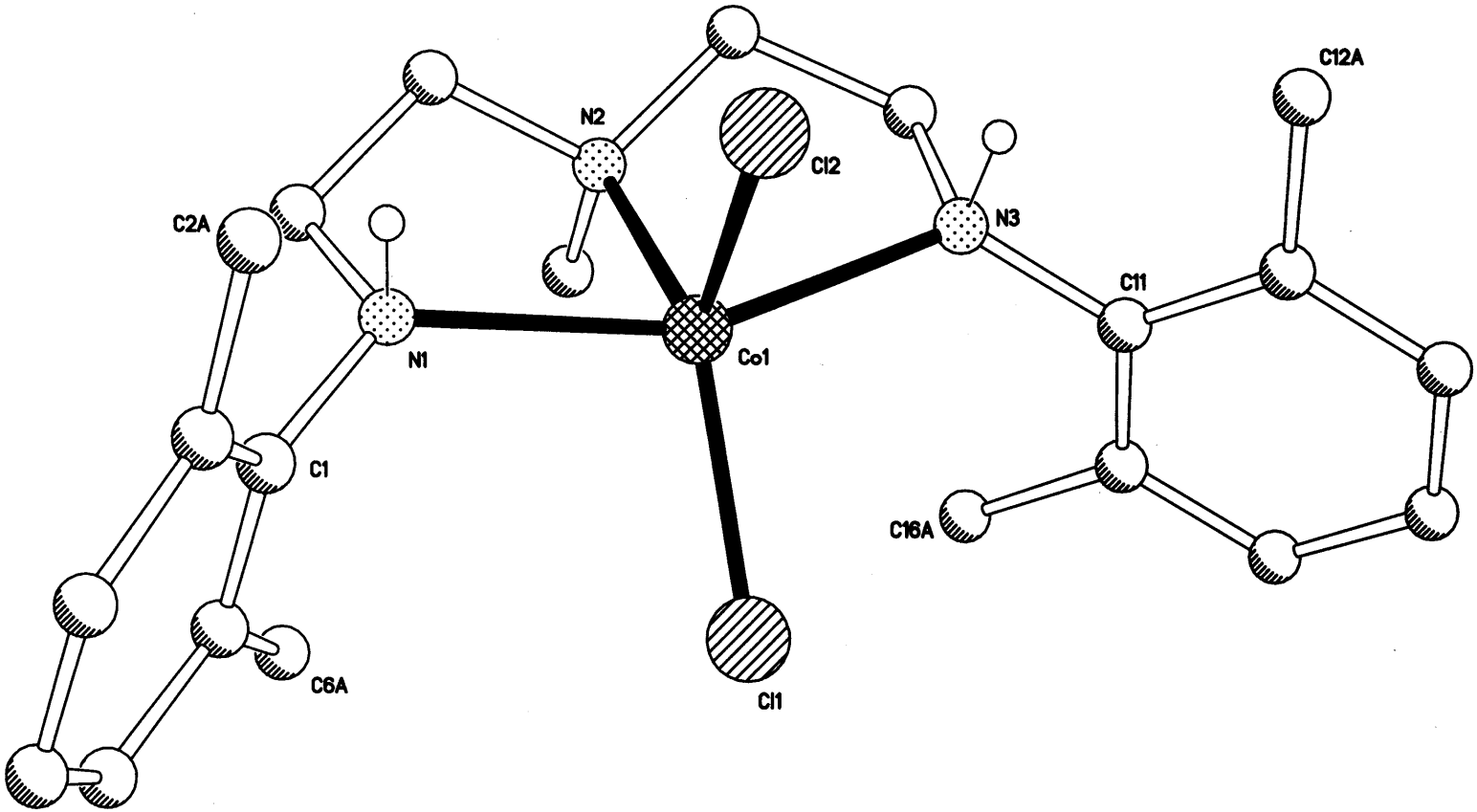

Figure 4 Molecular structure of [{**LVIa**}$CoCl_2$] (**17a**) (All the hydrogen atoms apart from H1 and H3 have been omitted for clarity)

3.4. Reaction of MCl_2 (M = Fe and Co) with LVII

The reaction of $FeCl_2(thf)_{1.5}$ or $CoCl_2.6H_2O$ with 1 equivalent of **LVIIa** under mild reaction conditions gave the complexes [{**LVIIa**}MCl_2] where M = Fe (**18a**) or Co (**19a**), whilst the treatment of anhydrous MCl_2 with 1 equivalent of **LVIIb** in *n*-BuOH at 90 °C afforded the complexes [{**LVIIb**}MCl_2] where M = Fe (**18b**) or Co (**19b** Scheme 5).

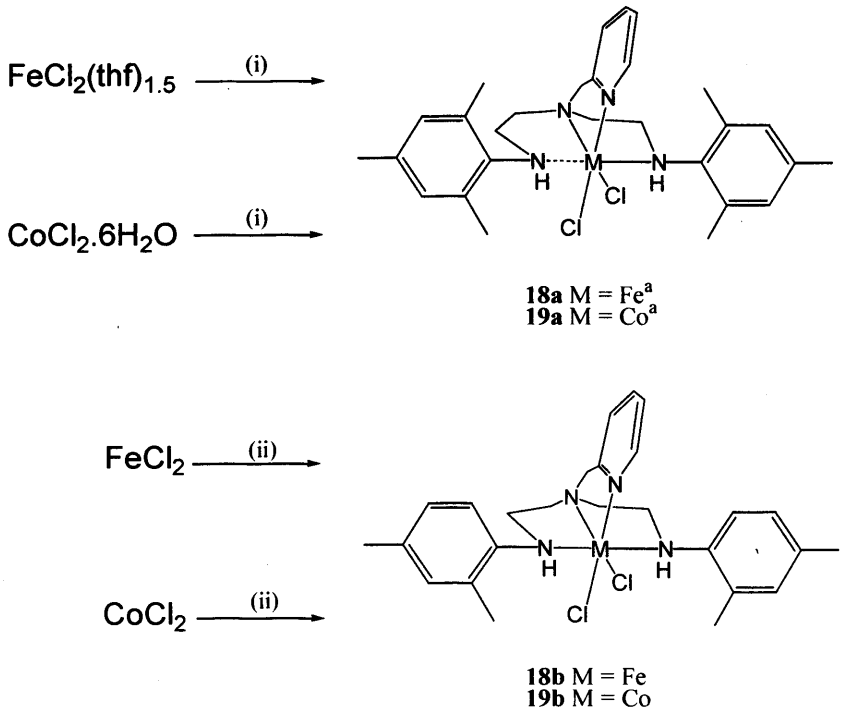

Scheme 5 *Reagents and conditions*: (i) thf, **LVIIa**, rt; (ii) *n*-BuOH, **LVIIb**, heat
[a] Isolated from single crystal X-ray diffraction studies

Evidently, the introduction of the pyridyl nitrogen donor has enabled the formation of a iron(II) species (see section 3.3). Compounds **18** and **19** have been analysed by FAB mass spectrometry, magnetic susceptibility measurements, solid state IR spectroscopy and for **18a** and **19a** elemental analysis. In addition, golden crystals of **18a** and pale blue crystals **19a** suitable for X-ray diffraction studies were grown from the layering of an acetonitrile solution with hexane at rt (**18a**) or the layering of a dichloromethane solution with diethyl ether at rt (**19a**). The molecular structures of **18a** and **19a** are represented in Figure 5 and selected bond distances and bond angles are listed in Table 2. Crystal data and data collection refinement parameters are presented within Chapter 6; section 6.8.

Table 2 Selected bond distances (Å) and angles (°) for **18a**.MeCN and **19a**.CH_2Cl_2

	M = Fe (**18a**.MeCN)	M = Co (**19a**.CH_2Cl_2)
M(1)-N(1)	2.248(4)	2.217(2)
M(1)-N(2)	2.165(5)	2.117(2)
M(1)-N(3)	2.319(4)	2.202(2)
M(1)...N(4)	2.597(4)	2.795(2)
M(1)-Cl(1)	2.322(2)	2.322(1)
M(1)-Cl(2)	2.480(2)	2.424(1)
N(1)-M(1)-N(2)	77.89(18)	78.38(8)
N(1)-M(1)-N(3)	78.13(15)	80.45(8)
N(1)-M(1)...N(4)	74.45(14)	72.78(7)
N(2)-M(1)-N(3)	104.89(16)	109.98(8)
N(2)-M(1)...N(4)	91.57(16)	85.00(7)
N(3)-M(1)...N(4)	144.13(15)	146.02(7)
N(1)-M(1)-Cl(1)	170.73(13)	172.95(6)
N(2)-M(1)-Cl(1)	93.23(14)	94.59(6)
N(3)-M(1)-Cl(1)	101.90(12)	101.65(6)
N(4)...M(1)-Cl(1)	108.86(10)	107.48(5)
N(1)-M(1)-Cl(2)	92.44(13)	91.70(6)
N(2)-M(1)-Cl(2)	166.94(14)	160.27(6)
N(3)-M(1)-Cl(2)	81.31(12)	84.71(6)
N(4)...M(1)-Cl(2)	77.25(11)	75.72(5)
Cl(1)-M(1)-Cl(2)	96.73(6)	95.19(3)

The molecular structures of **18a** and **19a** are essentially the same and only **18a** will be discussed in detail. The iron(II) centre may be regarded as being in a *pseudo*-octahedral environment surrounded by one pyridyl nitrogen, one tertiary amine and one terminal *N*-aryl substituted donor of the tripodal ligand and two chloride donors. In addition, the second *N*-aryl substituted donor atom of **LVIIa** is loosely bound [Fe(1)...N(4) 2.597 Å (**18a**) *cf.* Co(1)...N(4) 2.795(2) Å (**19a**)] to give a *pseudo*-N4Cl2 coordination sphere. Notably, the Fe...N(4) separation is *ca.* 0.3 Å greater than the iron *N*-aryl amine bond distances in complexes **10a**, **10c** and **15b** (Chapter 2; sections 2.5 and 2.7). But comparable to the iron *N*-aryl amine bond separation present in the *pseudo*-octahedral structure of complex **15a** [Fe...N(4) 2.558 Å: Chapter 2; section 2.7]. Evidently, the steric hindrance between one *ortho*-methyl group [C(17)] and the pyridyl moiety is preventing the ligand from acting as a genuine *NNNN*-chelate. The two chlorides are coordinated in a *cis*-disposition [Cl(1)-Fe(1)-Cl(2) 96.73(6)°] with Cl(1) *trans* to the central amine [N(1)-Fe(1)-Cl(1) 170.73(13)°] and

Cl(2) *trans* to the pyridyl moiety N(2) [N(2)-Fe(1)-Cl(2) 166.94(14)°]. Such geometry constraints leave the loosely bound *N*-aryl substituted donor atom [N(4)] *trans* to the coordinated *N*-aryl substituted donor atom [N(3)].

The Fe-N bond distances (>2.0 Å) are characteristic of a HS configuration ranging from 2.165(5) – 2.319(4) Å (if Fe...N(4) is excluded).[25 - 28] As expected the Fe-$N_{pyridyl}$ bond distance is *ca.* 0.1 Å shorter than the Fe-$N_{ave.\ amine}$ bond distance, with Fe-N(3) being the most elongated at 2.319(4) Å. The Fe-Cl bond distances are asymmetric with Fe(1)-Cl(2) bond distance being the most elongated [2.480(2) Å], which is attributable to the differing *trans* configurations of each chloride.

The elucidation of the coordination environment surrounding the metal(II) centres in **18b** and **19b** can be achieved despite the unsuccessful attempts at growing crystals suitable for single crystal X-ray diffraction studies, by applying the knowledge obtained from previously determined molecular structures. Firstly, the assumption that **18b** and **19b** are essentially identical will be applied. The overall geometry surrounding the metal(II) centre may be *pseudo*-octahedral or octahedral with respectively, **LVIIb** acting as a *NNN*-chelate with a *N*-aryl substituted donor atom loosely bound (*cf.* **18a** and **19a**) or as a genuine *NNNN*-chelate (*cf.* **15b** Chapter 2; section 2.7). The latter geometrical arrangement may be favourable upon assumption that the *ortho*-methyl group is pointing away from the pyridyl moiety enabling the ligand to be bound as a genuine *NNNN*-chelate.

The FAB mass spectrometric data for complexes **18** and **19** reveal characteristic mass and isotope distribution patterns for a monomeric species with a fragmentation peak corresponding to the loss of a chloride ion present in each case. The solid state IR spectra for **18** and **19** reflect the coordination modes within the compounds by exhibiting characteristic pyridyl ring deformation bands at *ca.* 1600 cm^{-1}, [25, 29] and N-H stretching frequencies at *ca.* 3200 cm^{-1}.[30] The rt magnetic susceptibility measurements exhibit magnetic moments characteristic of a HS mononuclear iron(II) (**18**: *ca.* 5.0 BM) and cobalt(II) (**19**: *ca.* 4.0 BM) configurations.

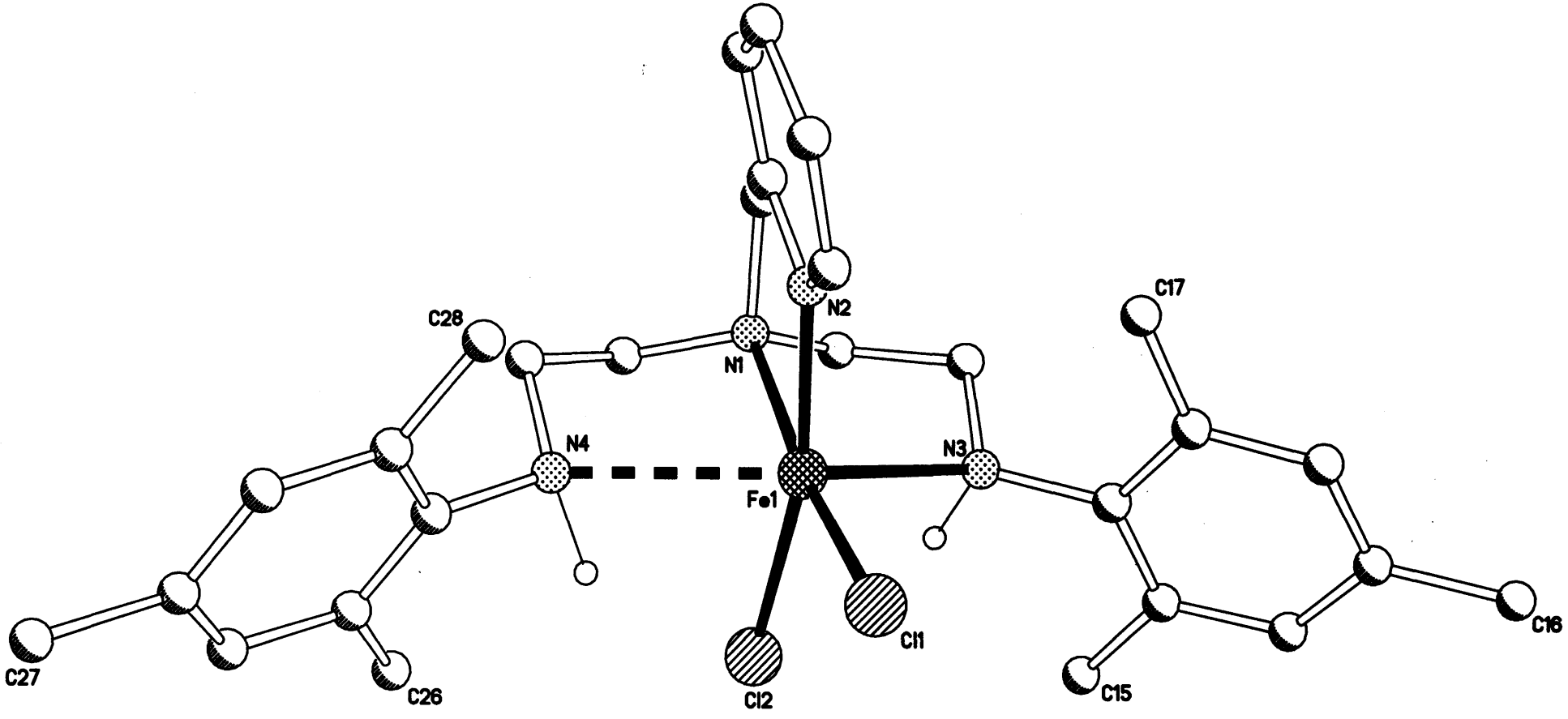

Figure 5 Molecular structure of [{**LVIIa**}$FeCl_2$] (**18a**) (All the hydrogen atoms apart from H4 and H3 have been omitted for clarity). Molecular structure of [{**LVIIa**}$CoCl_2$] (**19a**) reveals a similar coordination geometry

Solution state studies performed on complexes **18a** and **19a** in CD_3CN at rt exhibit broad paramagnetically shifted ^1H NMR spectra in the range of –10 to 130 ppm (Figure 6). Interpretation of the paramagnetic ^1H NMR spectra (Table 3) can be achieved by comparison of chemical shifts and relaxation times to related metal(II) complexes **10c** and **11c** and prior knowledge of polypyridyl metal(II) systems.[26 - 28, 31]

For **18a** the PyCH_α of the coordinated pyridyl arm is shifted downfield the most at δ = 128.3, whilst Py$CH_{\beta/\beta'}$ appear as sharp signals at δ = 53.6 and 52.1 (T_1 = 13.1 and 11.1 ms) and PyCH_γ is the most upfield at δ = 18.2 (T_1 = 42.3 ms). The methylene protons are exceedingly broad and shifted downfield at $\delta \approx$ 115 and 35. The aromatic region can be assigned to give: ArMe_o at δ = 13.3 (T_1 = 40.5 ms), ArCH_m at δ = 12.0 (T_1 = 150 ms) and ArMe_p at δ = 8.7 (T_1 = 3.1 ms). For **19a** the protons of the coordinated pyridyl arm display characteristic chemical shifts and relaxation times [PyCH_α: δ = 97.0; PyCH_β: δ = 50.3 (T_1 = 10.14 ms); Py$CH_{\beta'}$: δ = 46.8 (T_1 = 16.4 ms); PyCH_γ: δ = 0.3 (T_1 = 31.0 ms)]. The methylene protons are not observed and this may be accountable to the significant broadening of the spectrum. The aromatic region can be assigned to afford: ArCH_m at δ = 9.3 (T_1 = 39.4 ms), ArMe_p at δ = 11.5 (T_1 = 135 ms) and ArMe_o at δ = –4.8 (T_1 = 2.8 ms).

Interestingly, for **18a** and **19a** the inequivalence of the *N*-aryl substituted amine arms observed in the solid state does not exist in the solution state. Scheme 6 shows an equilibrium that may explain the apparent solution state behaviour of **18a** and **19a**. The lability of the *N*-aryl amine group (*cf.* Chapter 2; section 2.5) enables the interconversion of species **a** and **b** *via* a 'pendulum mechanism'. At rt the ^1H NMR spectra of **18a** and **19a** are recording the time-average between species **a** and **b** due to their rapid interconversion.

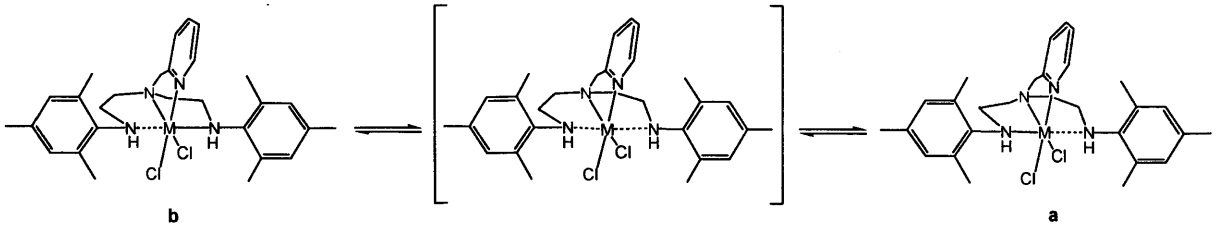

Scheme 6 'Pendulum mechanism'

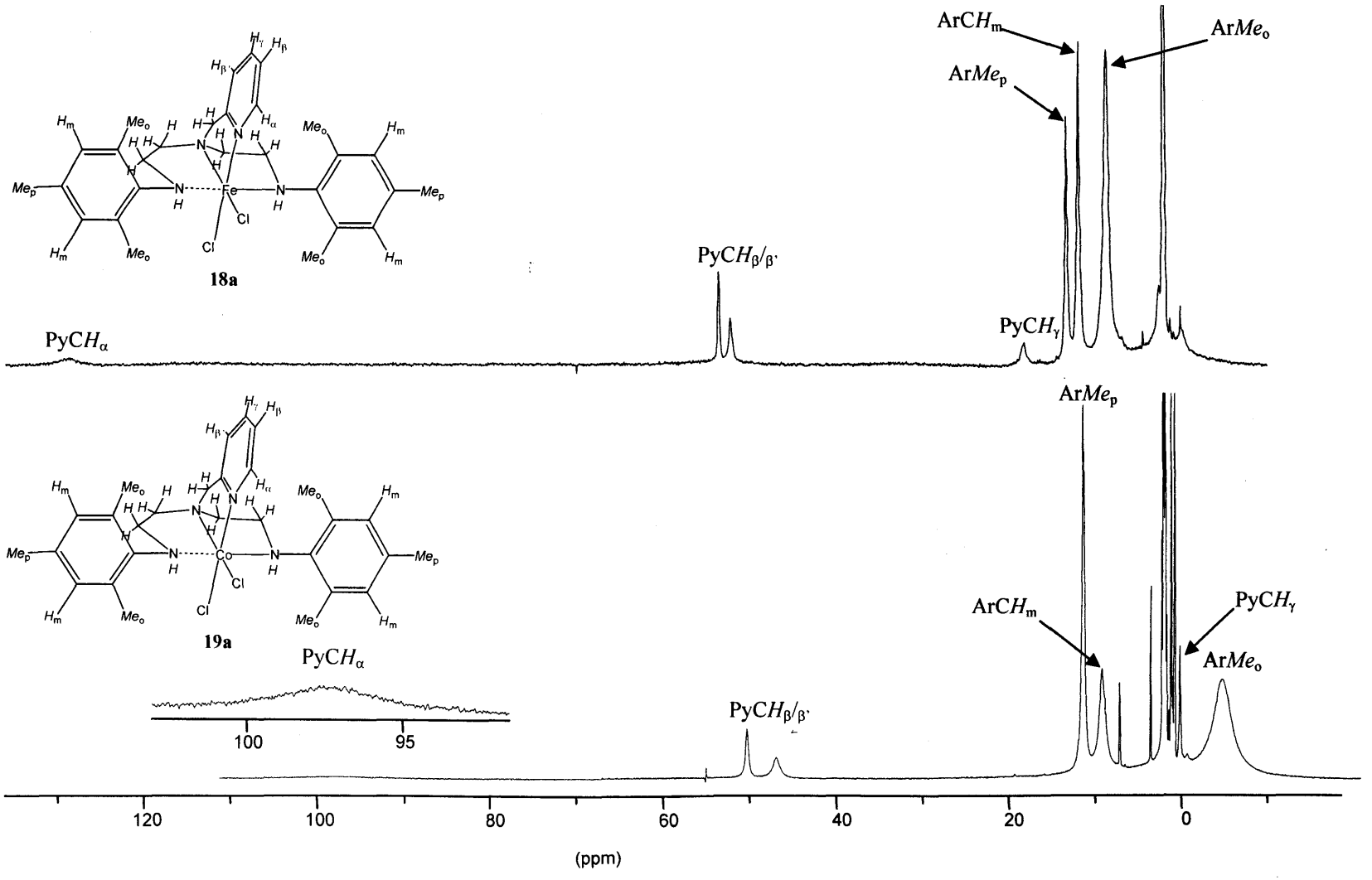

Figure 6 ^{1}H NMR spectra for complexes **18a** and **19a** in CD_3CN at rt

Table 3 ^{1}H NMR chemical shifts (δ) and relaxation times (T_1) for complexes **18a** and **19a** in CD_3CN at rt[a]

	δ / (T_1 ms)						
Complex	PyCH_α	PyC$H_{\beta/\beta'}$	PyCH_γ	CH_2	ArCH	ArMe	NH
10c	129.6 (0.9)	58.6 (13.2), 56.6 (11.2)	16.8 (90.3)	108.1 (1.7), 82.4 (1.1), 63.9 (0.7)	11.6 (27.8, ArCH_m)	15.7 (29.1, ArMe_p), 7.39 (2.5, ArMe_o)	120.0 (1.9), -12.74 (4.0)
18a	128.6	53.6 (13.1), 52.1 (11.1)	18.2 (42.3)	≈ 115 (very broad), ≈ 35 (very broad)	12.0 (150, ArCH_m)	13.3 (40.5, ArMe_p), 8.7 (3.1, ArMe_o)	
11c	116.7 (9.3)	46.6 (15.0), 44.0 (23.2)	-3.0 (52.6)	≈ 90 (very broad), 86.9 (0.9)	12.5 (45.3, ArCH_m)	16.4 (ArMe_p), -11.8 (2.2, ArMe_o)	104.6 (1.5)
19a	97.0	50.3 (10.14), 46.8 (16.4)	0.31 (31.0)		9.3 (39.4, ArCH_m)	11.5 (135, ArMe_p), -4.8 (2.8, ArMe_o)	

[a] Complexes **10c** and **11c** included for comparison

3.5. Conclusions

In summary, the synthesis and characterisation of the sterically variable tri- and *pseudo*-tetradentate ligands **LV**, **LVI** and **LVII** have been reported. Single crystal X-ray diffraction studies reveal the propensity of **LV** and **LVI** to exhibit a *meridional* configuration when coordinated to cobalt(II). The introduction of the pyridyl moiety in **LVII** enables the *pseudo*-tetradentate chelation to iron(II) in addition to that of cobalt(II) in the solid state. Finally, the inequivalence of the *N*-aryl substituted amines observed in the solid state for **18a** and **19a** does not exist in the solution state. This is attributable to the lability of both of the *N*-aryl substituted amines.

References

[1] B.D. Ward, S.R. Dubberley, A. Maisse-Francois, L.H. Gade and P. Mountford, *J. Chem. Soc., Dalton Trans.*, 2002, 4649-4657.
[2] J. B. Love, H. C. S. Clark, F. G. N. Cloke, J. C. Green and P. B. Hitchcock, *J. Am. Chem. Soc.*, 1999, **121**, 6843-6849.
[3] H. C. S. Clark, F. G. N. Cloke, P. B. Hitchcock, J. B. Love and A. P. Wainwright, *J. Organomet. Chem.*, 1995, **501**, 333-340.
[4] F. G. N. Cloke, P. B. Hitchcock, J. B. Love, *J. Chem. Soc., Dalton Trans.*, 1995, 25-30.
[5] L-C. Lang, R. R. Schrock, W. M. Davis and D. H. McConville, *J. Am. Chem. Soc.*, 1999, **121**, 5797-5798.
[6] R.R. Schrock, A. L. Casado, J. T. Goodman, L-C. Liang, P. J. Bonitatebus Jr and W. M. Davis, *Organometallics*, 2000, **19**, 5325-5341.
[7] Y. Schrodi, R. R. Schrock and P. J. Bonitatebus Jr, *Organometallics*, 2001, **20**, 3560-3573.
[8] R. R. Schrock, P. J. Bonitatebus Jr and Y. Schrodi, *Organometallics*, 2001, **20**, 1056-1058.
[9] G. K. B. Clentsmith, V. M. E. Bates, P.B. Hitchcock and F. G. N. Cloke, *J. Am. Chem. Soc.*, 1999, **121**, 10444-10445.
[10] G. P. Clancy, H. C. S. Clark, G. K. B. Clentsmith, F. G. N. Cloke and P. B. Hitchcock, *J. Chem. Soc., Dalton Trans.*, 1999, 3345-3347.
[11] P. E. Collier, S. M. Pugh, H. S. C. Clark, J. B. Love, A. J. Blake, F. G. N. Cloke and P. Mountford, *Inorg. Chem.*, 2000, **39**, 2001-2005.
[12] K. Feghali, D. J. Harding, D. Reardon, S. Gambarotta, G. Yap and Q. Wang, *Organometallics*, 2002, **21**, 968-976.
[13] F. V. Cochran, P. J. Bonitatebus Jr and R. R. Schrock, *Organometallics*, 2000, **19**, 2414-2416.
[14] F. V. Cochran and R. R. Schrock, *Organometallics*, 2001, **20**, 2127-2129.
[15] J. P. Araujo, D. K. Wicht, P. J. Bonitatebus Jr and R. R. Schrock, *Organometallics*, 2001, **20**, 5682-5689.
[16] A. Dumistrescu, B. Martin-Vaca, H. Gornitzka, J-B. Cazaux, D. Bourissou and G. Bertrand, *Eur. J. Inorg. Chem.*, 2002, 1948-1951.
[17] N. Emig, R. Réau, H. Krautscheid, D. Fenske and G. Bertrand, *J. Am. Chem. Soc.*, 1996, **118**, 5822-5823.
[18] N. Emig, H. Nguyen, H. Krautscheid, R. Réau, J. B. Cazaux and G. Bertrand, *Organometallics*, 1998, **17**, 3599-3608.
[19] G. Riggio, W. H. Hopff, A. A Hofmann and P. G., Waser, *Helv. Chim. Acta.*, 1980, **63**, 488-497.
[20] J. P. Wolfe, S. Wagaw and S. L. Buchwald, *J. Am. Chem. Soc.*, 1996, **118**, 7215-7216.
[21] M. E. G. Skinner, D. A. Cowhig and P. Mountford, *Chem. Commun.*, 2000, 1167-1168.
[22] M. E. G. Skinner, Y. Li and P. Mountford, *Inorg. Chem.*, 2002, **41**, 1110-1119.
[23] G. J. P. Britovsek, M. Bruce, V. C. Gibson, B. S. Kimberley, P. J. Maddox, S. Mastroianni, S. J. McTavish, C. Redshaw, G. A. Solan, S. Strömberg, A. J. P. White and D. J. Williams, *J. Am. Chem. Soc.*, 1999, **121**, 8728-8740.
[24] G. J. P. Britovsek, S. Mastroianni, G. A. Solan, S. P. D. Baugh, C. Redshaw, V. C. Gibson, A. J. P. White, D. J. Williams and M. R. J. Elsegood, *Chem. Eur. J.*, 2000, **6**, 2221-2231.
[25] Z. He, D. C. Craig and S. B. Colbran, *J. Chem. Soc., Dalton Trans.*, 2002, 4224-4235.
[26] Y. Zang, J. Kim, Y. Dong, E. C. Wilkinson, E. H. Appelman and L. Que, Jr, *J. Am. Chem. Soc.*, 1997, **119**, 4197-4205.
[27] A. Diebold and K.S. Hagen, *Inorg. Chem.*, 1998, **37**, 215-223.
[28] D. Mandon, A. Machkour, S. Goetz and R. Welter, *Inorg. Chem.*, 2002, **41**, 5364-5372.
[29] M. M. da Mota, J. Rodgers and S. M. Nelson, *J. Chem. Soc. A.*, 1969, 2036-2044.
[30] Upon coordination the N-H stretching frequency decreases by *ca.* 100 cm^{-1}.
[31] T. M. Kooistra, K.F.W. Hekking, Q. Knijnenburg, B. de Bruin, P. H.M. Budzelaar, R. de Gelder, J.M.M. Smits and A. W. Gal, *Eur. J. Inorg. Chem.*, 2003, 648-655.

University *of*
Leicester

Chapter Four

Ethylene Oligomerisation Utilising Flexible *NNN*-Iron(II) and -Cobalt(II) Cationic Catalysts

Abstract

The *NNN*-chelates **10**, **11**, **16** and **17** are activated by the addition of excess MAO for the oligomerisation of ethylene. The activities are low-to-moderate at 1 bar ethylene pressure and the selectivity of the catalysts is dependent on the metal centre with the iron systems (**10**) forming linear α-olefins, while the cobalt systems (**11**, **16** and **17**) give a mixture of linear and branched oligomers.

4.1. Introduction

Oligomers are a necessity of the modern world with linear α-olefins in the range of C_6-C_{20} being used extensively for the preparation of lubricants, detergents, plasticisers and as co-monomers in the polymerisation of ethylene to give LLDPE. Industrial processes predominantly employ alkylaluminium compounds independently or early TM compounds combined with alkylaluminium compounds as co-catalysts or late TM complexes (SHOP process see Chapter 1; section 1.8).[1] These catalytic systems control the chain length *via* altering the reaction temperature or the ethylene pressure.[1, 2] In contrast, the highly active α-diimine nickel(II) and pyridine-diimine iron(II)-based catalysts, are capable of controlling the molecular weight *via* modification of the ligand architecture (see Chapter 1; sections 1.2.1 and 1.3.2).[3 - 6] As a consequence, a program of academic and industrial research into olefin polymerisation/oligomerisation was initiated.

In addition to the catalyst systems reviewed in Chapter 1 both the hetero- and homo-functionalised tridentate systems depicted in Figure 1 have recently been reported.[7 - 10] The *PNP*-based, the *SNS*-based and the *PPP*-based chromium(III) complexes **I-III** exhibit high selectivity for the trimerisation of ethylene into 1-hexene.[7 - 9] Whilst, the *PNP*-based complex **IV** with iron(II) or cobalt(II) as the metal centre affords high selectivity towards C_4-C_{10} oligomers.[10]

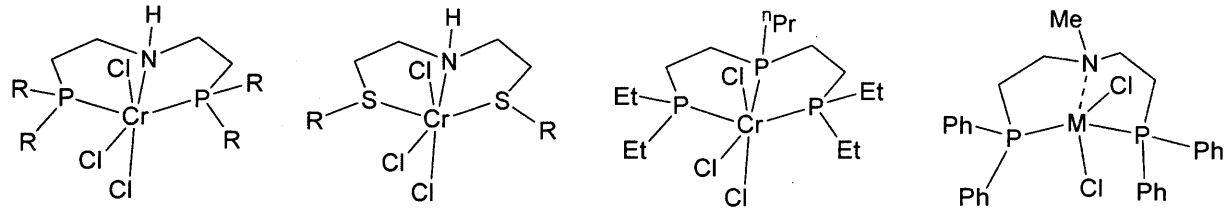

I R = hydrocarbyl **II** R = hydrocarbyl **III** **IV** M = Fe or Co

Figure 1 Tridentate chelates

Herein, we report the oligomerisation behaviour of the flexible *NNN*-based complexes **10**, **11**, **16** and **17** (Chapters **2** and **3**) upon activation with MAO under mild reaction conditions (Figure 2). The selectivity of the catalysts is dependent upon the metal centre with iron systems producing linear α-olefins (**10**) whilst the cobalt systems afford a mixture of linear and branched oligomeric products (**11**, **16** and **17**).

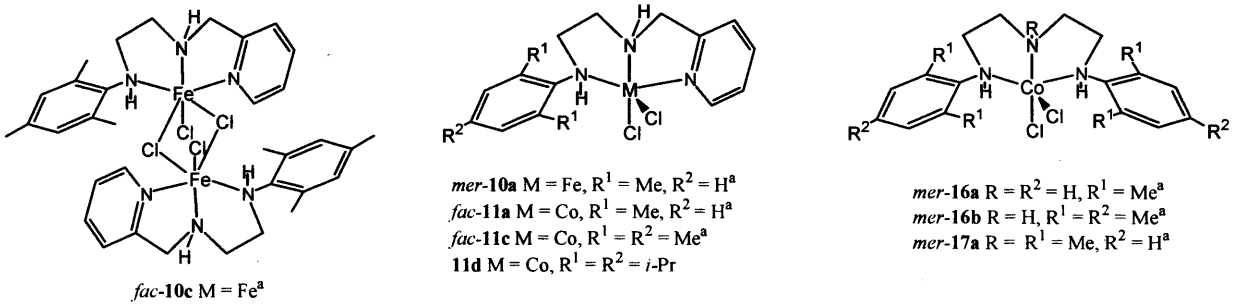

Figure 2 Precatalysts employed in the oligomerisation of ethylene
[a] Isolated from single crystal X-ray diffraction studies

4.2. Ethylene Oligomerisation Results

All the complexes were evaluated for oligomerisation activity by treating them with 400 equivalents of MAO in toluene, 1 bar of ethylene pressure and ambient temperature (Scheme 1). The catalyst activities were calculated from the GC traces in the range of C_6-C_{26}

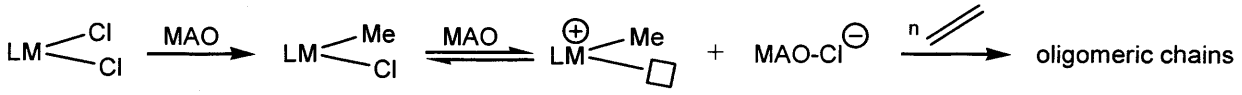

Scheme 1 Postulated activation of the precatalysts **10**, **11**, **16** and **17** with MAO followed by oligomerisation of ethylene

with 1-heptadecene utilised as an internal standard. The results of the evaluation are shown in Table 1. The most active systems contained cobalt as the metal centre (**11**, **16** and **17**) with **11d** displaying the highest activity (run 5: 76 g/mmol/h/bar). Thee activities are comparable with the pyridine-diimine supported cobalt complexes under similar experimental conditions.[11] The iron systems **10a** and **10c** exhibit lower activities than the corresponding cobalt complexes and are three orders of magnitude lower in activity than the most active pyridine-diimine iron systems.[11]

Table 1 Ethylene oligomerisation evaluation employing precatalysts **10, 11, 16** and **17** runs 1-8

Run[a]	Pre-catalyst	Yield (g)[b]	Activity (g/mmol/h/bar)	Internal olefin (%)[c]	Terminal olefin (%)[c]	Branched (%)[c]	Av. chain length[c] C_n	α	β
1	**10a**	0.022	4	1	98.5	0.5	6.5	0.74	0.35
2	**10c**	0.026	5	0.7	99.3	negligible	6.87	0.74	0.35
3	**11a**	0.295	59	63.6	25.5	10.9	12.7	0.76	0.32
4	**11c**	0.131	26	59.7	29.9	10.4	11.7	0.76	0.32
5	**11d**	0.381	76	63.0	25.0	12.0	13.7	0.80	0.25
6	**16a**	0.206	41	61.5	27.3	11.2	11.3	0.74	0.35
7	**16b**	0.198	40	62.2	27.7	10.1	10.6	0.74	0.35
8	**17a**	0.168	34	60.5	30.2	9.3	11.2	0.76	0.32

[a] *General conditions*: 1 bar ethylene Schlenk test carried out in toluene (40 ml) at 20 °C, using 4.0 mmol MAO (Al:M = 400:1), 0.01 mmol precatalyst, over 0.5 h. Reactions terminated by addition of dilute HCl; [b] Determined from GC using 1-heptadecene as an internal standard; [c] Oligomerisation product percentages and average chain length, C_n calculated *via* integration of ^{1}H NMR spectra.

The formation of oligomers for both the iron and cobalt systems is indicative of a mechanism where chain transfer is competitive with chain propagation. In all cases a Schulz-Flory distribution[12 - 15] of oligomers prevails and can be described by α, where α represents the probability of chain propagation (Equation (1)).

$$\alpha = \frac{\text{rate of propagation}}{\text{rate of propagation + rate of chain transfer}} = \frac{\text{moles of } C_{n+2}}{\text{moles of } C_n} \quad (1)$$

The β value is classified as the ratio between the rate of chain transfer and chain propagation as expressed in Equation 2.

$$\beta = \frac{\text{rate of chain transfer}}{\text{rate of propagation}} = \frac{1 - \alpha}{\alpha} \quad (2)$$

The α values for complexes **10, 11, 16** and **17** are approximately 0.8 and are characteristic of a Schulz-Flory distribution. As is observed for the dipyridine-imine iron system, complexes **10** and **11** form oligomers as opposed to polymer.[16] This may be a consequence of inadequate

steric bulk around the metal centre enabling facile a.d. of the oligomeric chain to occur.[16] The presence of di-*ortho* aryl substituted rings on both ends of the *NNN*-ligand architecture in **16** and **17** suggests polymer to be the favoured product. However, the N donors are sp^3, **not** sp^2 hybridised, which may prevent the aryl substituent from imparting steric control around the metal centre. In addition, the formation of oligomers by **16** and **17** is similar to that observed for the *PNP*-based complex **IV**.[10]

The oligomerisation products formed by **10** exhibit a high selectivity for linear α-olefins (≥ 98 %), which is comparable to the pyridine-diimine system.[11] In contrast, the oligomerisation products arising from **11, 16** and **17** reveal extensive isomerisation to give a mixture of terminal, internal and branched olefins consisting of vinylidenes and trisubstituted alkenes (Scheme 2). The extensive isomerism arising from the cobalt systems may be attributable to three factors: (1) chain-walking mechanism, (2) isomerisation of α-olefins and (3) reincorporation of α-olefins into the oligomeric chain.

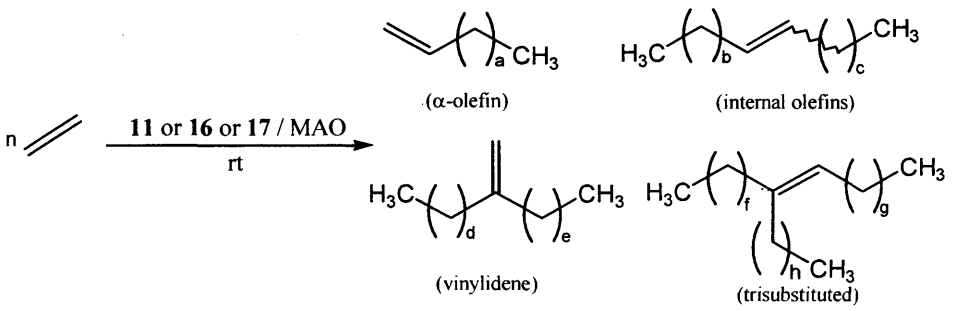

Scheme 2 Mixture of oligomeric product obtained using cobalt catalysts (**11, 16 and 17**)

The oligomer composition was investigated over a time duration of 0.25-1 h for complexes **11a** and **17a** under analogous reaction conditions (Table 2). The relatively constant ratio of terminal to internal olefins is indicative of no significant isomerisation of the α-olefin products occurring over longer time durations. This data is supported by control experiments in which no observable isomerisation of 1-nonene and 1-tridecene occurs during the course of the oligomerisation. In addition, the relative percentage of branched oligomeric products remains constant over the course of 1 h, which is consistent with no reincorporation of α-olefins into the oligomeric chain.

Further assignment of the ^{1}H NMR spectra reveals evidence for 2-alkenes and branching within the oligomeric chain (Appendices: Figures 7-14 and Table 1). In addition, supporting evidence is provided by the ^{13}C and the ^{1}H - ^{13}C COSY NMR spectra. The chain-walking mechanism depicted in Scheme 3 may indeed be accountable for all four classifications of olefin as well as the internal branching.

Table 2 Ethylene oligomerisation evaluation employing precatalysts **11a** and **17a** runs 9-14

Run[a]	Time (h)	Pre-catalyst	Internal olefin (%)[b]	Terminal olefin (%)[b]	Branched (%)[b]	Av. chain length[b], C_n
9	0.25	**11a**	61.1	27.1	11.8	11.7
10	0.5	**11a**	63.6	25.5	10.9	12.7
11	1	**11a**	61.1	27.1	11.8	11.7
12	0.25	**17a**	61.4	27.3	11.3	11.0
13	0.5	**17a**	60.5	30.2	9.3	11.2
14	1	**17a**	60.9	27.0	12.1	10.9

[a] *General conditions*: 1 bar ethylene Schlenk test carried out in toluene (40 ml) at 20 °C, using 4.0 mmol MAO (Al:M = 400:1), 0.01 mmol precatalyst. Reactions terminated by addition of dilute HCl; [b] Oligomerisation product percentages and average chain length, C_n calculated *via* integration of ^{1}H NMR spectra.

The chain propagation is assumed to follow a Cossee-Arlman type mechanism *via* species **a** and **b**.[17 - 19] β-H elimination results in the formation of species **c**, which can follow three alternative pathways: (1) chain transfer to afford regeneration of the catalytic cycle (species **d**) and linear α-olefin, (2) consecutive chain-walking followed by chain transfer to give species **d** and 2-alkene or (3) reinsertion at the opposite carbon atom to form the secondary alkyl species **f**. Insertion of ethylene into the oligomeric chain (species **f**) followed by β-H elimination and chain transfer yields species **d** and olefin with internal branching. Alternatively, species **g** may chain-walk and form species **h**. If the mechanism is assumed to be similar to the α-diimine system ethylene will not insert at a secondary alkyl species adjacent to a tertiary carbon atom or a tertiary alkyl species.[20] Therefore species **h** may

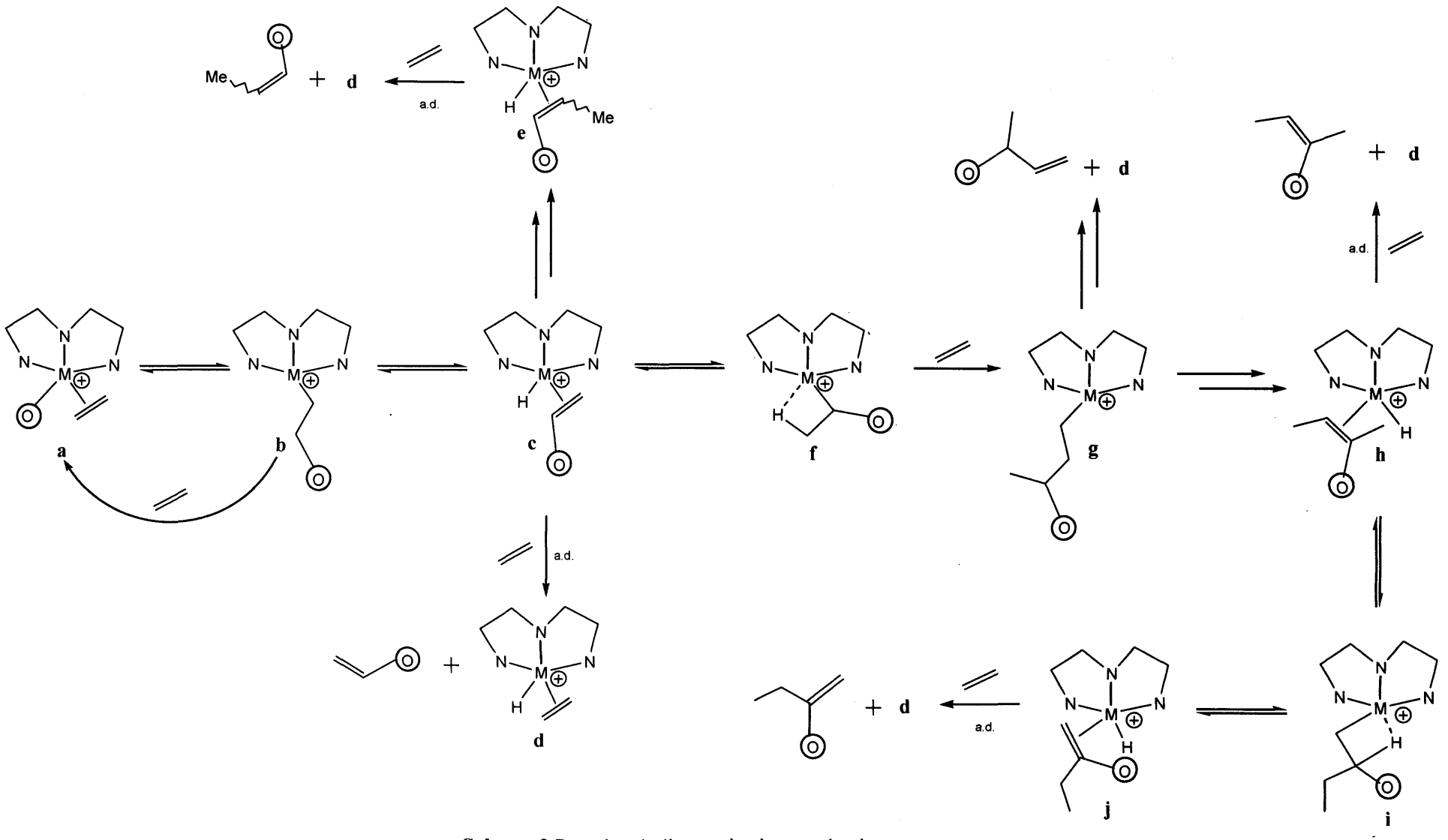

Scheme 3 Postulated oligomerisation mechanism

undergo chain transfer to produce species **d** and trisubstituted olefin or chain-walk to a tertiary alkyl species **i** followed by β-H elimination and chain transfer to produce species **d** and vinylidene.

The absence of steric control may aid the formation of the sterically hindered secondary and tertiary alkyl complexes. Indeed, the bipy nickel system observes a diminished production of linear α-olefins compared to the α-diimine nickel system.[4] However, the differing oligomeric products afforded when iron and cobalt systems are employed implies that electronic effects must also impose a significant role on the catalysis. In the case of iron the electropositivity of the metal centre may compensate for the lack of steric control to give a metal-carbon bond with strong ionic character ($M^{\delta+}$-$C^{\delta-}$). Primary alkyl complexes will now be favoured because of the inductive electron releasing effect of the alkyl group on the α-carbon atom, thereby affording a high selectivity for linear α-olefins.[21] Equally, for the cobalt systems it is plausible that a cumulative effect between sterics and electronics is accountable for the mixture of oligomeric products.

4.3. Conclusions

In summary, the N-picolylethylenediamine and the diethylenetriamine ligand sets have been shown to be compatible supports for iron and cobalt, which can be activated with MAO to produce ethylene oligomerisation catalysts under mild reaction conditions. The activity and the selectivity of the catalysts are found to be dependent upon the metal centre.

References

[1] J. Skupińska, *Chem. Rev.*, 1991, **91**, 613-648.
[2] W. Keim, F. H. Kowaldt, R. Goddard and C. Krüger, *Angew. Chem., Int. Ed. Engl.*, 1978, **17**, 466-467.
[3] L. K. Johnson, M. C. Killian and M. Brookhart, *J. Am. Chem. Soc.*, 1995, **117**, 6414-6415.
[4] M. C. Killian, L. K. Johnson and M. Brookhart, *Organometallics*, 1997, **16**, 2005-2007.
[5] G. J. P. Britovsek, V. C. Gibson, B. S. Kimberley, P. J. Maddox, S. J. McTavish, G. A. Solan, A. J. P. White and D. J. Williams, *Chem. Commun.*, 1998, 849-850
[6] B. L. Small and M. Brookhart, *J. Am. Chem. Soc.*, 1998, **120**, 7143-7144.
[7] D. S. McGuiness, P. Wasserscheid, W. Keim, C. Hu, U. Englert, J. T. Dixon and C. Grove, *Chem. Commun.*, 2003, 334-335.
[8] D. S. McGuiness, P. Wasserscheid, W. Keim, D. Morgan, J. T. Dixon, A. Bollmann, H. Maumela, F. Hess and U. Englert, *J. Am. Chem. Soc.*, 2003, **125**, 5272-5273.
[9] F. J. Wu, *U. S. Patent.*, 1998, 5,550,305.
[10] M. Wang, X. Yu, Z. Shi, M. Qian, K. Jin, J. Chen and R. He, *J. Organomet. Chem.*, 2002, **645**, 127-133.
[11] G. J. P. Britovsek, S. Mastroianni, G. A. Solan, S. P. D. Baugh, C. Redshaw, V. C. Gibson, A. J. P. White, D. J. Williams and M. R. J. Elsegood, *Chem. Eur. J.*, 2000, **6**, 2221-2231.
[12] J. P. Flory, *J. Am. Chem. Soc.*, 1940, **62**, 1561-1565.
[13] G. V. Schulz, *Z. Phys. Chem., Abt. B.* 1935, **30**, 379-398.
[14] G. V. Schulz, *Z. Phys. Chem., Abt. B.* 1939, **43**, 25-46.
[15] G. Henricj-Olivé and S. Olivé, *Adv. Polym. Sci.*, 1974, **15**, 1-30.
[16] G. J. P. Britovsek, S. P. D. Baugh, O. Hoarau, V. C. Gibson, D. F. Wass, A. J. P. White and D. J. Williams, *Inorg. Chim. Acta.*, 2003, **345**, 279-291.
[17] P. Cossee, *J. Catal.*, 1964, **3**, 80-88.
[18] E. J. Arlman, *J. Catal.*, 1964, **3**, 89-98.
[19] E. J. Arlman and P. Cossee, *J. Catal.*, 1964, **3**, 99-104.
[20] S. D. Ittel, L. K. Johnson and M. Brookhart, *Chem. Rev.*, 2000, **100**, 1169-1203.
[21] J. N. Harvey, *Organometallics*, 2001, **20**, 4887-4895.

University of Leicester

Chapter Five

The Synthesis of the Adaptable *NNO*-Ligand Sets Coordination Behaviour of Iron, Cobalt and Aluminium Complexes and the Polymerisation of Ethylene

Abstract

The versatile preparation of the *NNO*-ligand sets 2-{(2'-OMe-3'-R^1-5'-R^2)C_6H_2}-6-{CR^3N(2,6-*i*-$Pr_2C_6H_3$)}C_5H_3N (**LVIIIa**: R^1 = R^2 = H, R^3 = Me; **LVIIIb**: R^1 = Ph, R^2 = H, R^3 = Me), 2-{(2'-OH-3'-R^1-5'-R^2)C_6H_2}-6-{CR^3N(2,6-*i*-$Pr_2C_6H_3$)}C_5H_3N (**LIXa**: R^1 = R^2 = H, R^3 = Me; **LIXb**: R^1 = Ph, R^2 = H, R^3 = Me; **LIXc**: R^1 = R^2 = R^3 = H; **LIXd**: R^1 = R^3 = H, R^2 = *t*-Bu), 2-{(2'-OH)C_6H_4}-6-{CMe_2NH(2,6-*i*-$Pr_2C_6H_3$)}C_5H_3N (**LX**) and 2-{(2'-OH)C_6H_4}-6-{CHMeNH(2,6-*i*-$Pr_2C_6H_3$)}C_5H_3N **(LXI)**, is reported. The single crystal X-ray structure determination of **LVIIIb** and **LIXa** reveal a *transoid* arrangement between the pyridine and imine moieties of the *NNO*-ligand. The aluminium reaction intermediate formed during the synthesis of **LX** has been isolated by single crystal X-ray diffraction studies, [{**LX**$^{-2H}$}AlMe(NCMe)] (**20**). The treatment of **LVIIIa** with MCl_2 in *n*-BuOH at 90 °C affords the distorted tetrahedral complexes [{**LVIIIa**}MCl_2] (M = Fe **21**, Co **22**), with **LVIIIa** acting as a *NN*-chelate, attributable to the pendant nature of the anisole donor, as determined by single crystal X-ray diffraction studies. The reaction of **LIX** with a MCl_2 precursor in thf at room temperature affords the compounds [{**LIXa**}MCl_2] (M = Fe **23a** and Co **24a**) and [{**LIXb**}MCl_2] (M = Fe **23b** and Co **24b**). The addition of NaH converts the phenol donor into a phenolate atom to afford the complexes [{**LIXa**$^{-H}$}MCl]$_2$ (M = Fe **25** and Co **26a**). Employing elevated temperatures in *n*-BuOH yields the complexes [{**LIX**$^{-H}$}CoCl]$_2$ (**LIXc**: **26b** and **LIXd**: **26c**) in the absence of a deprotonating reagent. Single crystal X-ray structure determination of **24a**, **26a**, **26b** and **26c** reveal a distorted square pyramidal environment at each central atom with **LIX** coordinated in a *meridional* configuration. Preliminary catalytic evaluation studies reveal moderate-to-high activities for the polymerisation of ethylene into moderate-to-high molecular weight polyethylene.

5.1. Introduction

Polydentate pyridine/imine phenol *NNO*-chelates have been used in the coordination chemistry of mid-to-late TMs and main group chemistry. For example, phenol-bipyridine an *NNO*-tridentate terpy analogue and derivatives thereof (Figure 1) have formed bis-ligated species with ruthenium(III),[1] cobalt(III)[2] and iron(III)[3] and a mono-ligated species with

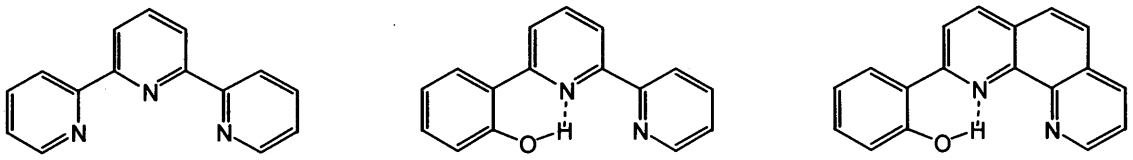

Figure1 terpy and the *NNO*-tridentate analogue phenol-bipyridine and derivatives thereof

palladium(II).[4] In addition, the potentially tridentate Schiff base ligands (Figure 2) have been employed as supports for chromium(III),[5] iron(III)[6, 7] and aluminium(III),[8, 9] while the pyridine-imine-acetyl and the pyridine-imine-methylalcohol ligands afford *cis*-dichloro-iron(II) complexes.[10, 11, 12] Applications of these *NNO*-systems range from studying their redox potentials,[1 - 3] to acting as ethylene polymerisation/oligomerisation catalysts[5, 8 –12] or atom transfer radical polymerisation (ATRP) mediators.[6]

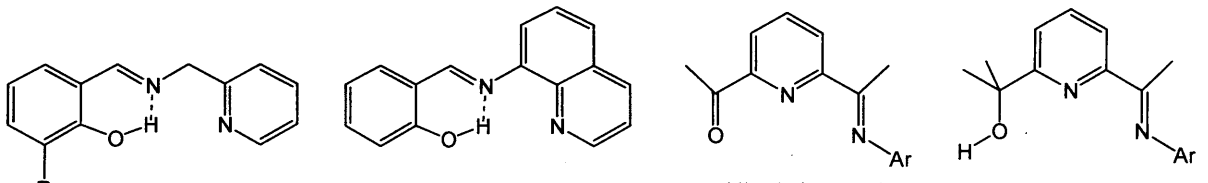

Figure 2 Alternative literature precedent *NNO*-ligands

In a similar manner to the *NNO*-tridentate terpy analogue the pyridine-diimine ligand set may be modified *via* replacing an *N*-aryl-imine substituent with a phenol group to form the novel ligand family **LIX** (Figure 3). The steric hindrance present about the remaining *N*-aryl-imine substituent may enable **LIX** to act as a suitable support for an ethylene polymerisation catalyst.

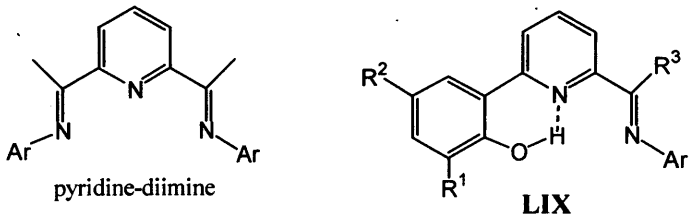

Figure 3 pyridine-diimine *NNO*-tridentate analogue

The versatility of this *NNO*-ligand set can be exploited to afford suitable tridentate donors for early-to-late TMs and aluminium (Figure 4: **LVIII** - **LXI**) with the intended application as ethylene polymerisation catalysts, ROMP catalysts and ATRP mediators.

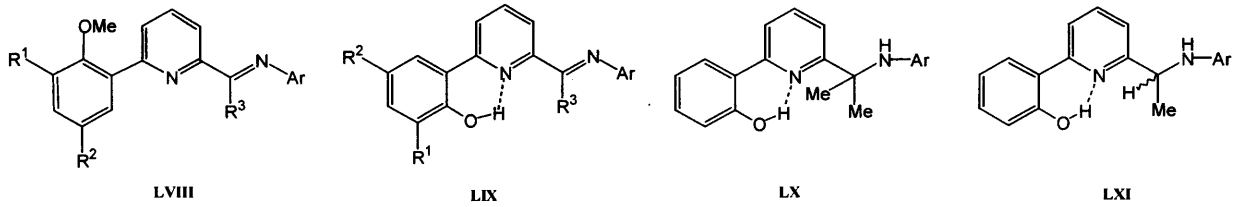

Figure 4 Adaptation of the novel *NNO*-ligand

Herein, we report the synthetic strategies employed for the preparation of the ligand sets **LVIII** - **LXI**. The coordination behaviour of **LVIII** and **LIX** when bound to *cis*-dichloro-iron(II) and -cobalt(II) or mono-halo-iron(II) and -cobalt(II) and that of **LX** when supported by aluminium(III) are discussed. In addition, the propensity for the iron(II) and cobalt(II) systems to act as ethylene polymerisation catalysts is investigated.

5.2. The Versatile Preparation of the *NNO*-Ligand Families

The new *NNO*-chelates **LVIII** and **LIX** were prepared in moderate overall yields *via* the procedures depicted in Scheme 1. Primarily, the anisole-pyridine-acyl precursor (**a**) was prepared in high yield by a palladium catalysed C(aryl)-C(aryl) cross-coupling reaction of 2-bromo-6-acyl-pyridine with 1.2 equivalents of the respective aryl boronic acid using experimental protocol established by Suzuki.[13, 14] The condensation reaction between the respective precursor **a** and 2,6-diisopropylaniline afforded **LVIIIa** and **LVIIIb** without the requirement for further purification. Alternatively, the anisole functionality within **a** can be

removed to yield the phenol-pyridine-acyl precursor (**b**). This demethylation was accomplished *via* two different reaction protocols. Namely, the employment of molten pyridinium chloride under forcing reaction conditions or BBr_3 under milder reaction conditions. Finally, the condensation reaction between the respective precursor **b** and 2,6-diisopropylaniline gave **LIXa-d** without the need for further purification. **LVIII** and **LIX** have been characterised by IR, ^1H and ^{13}C NMR spectroscopy and ES mass spectrometry (see Chapter 6; sections 6.5.1 – 6.5.3).

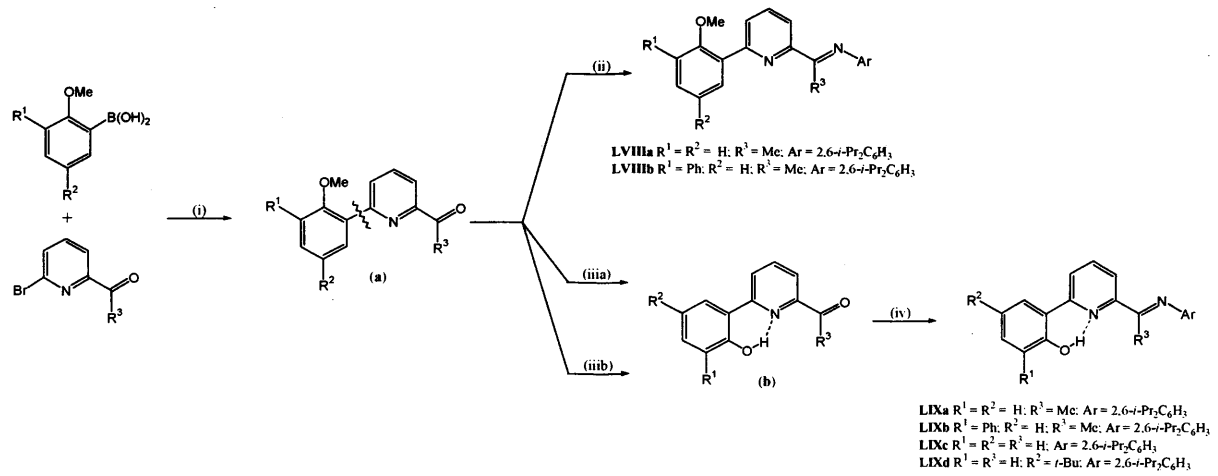

Scheme 1 *Reagents and Conditions*: (i) $Pd(PPh_3)_4$, K_2CO_3 (2 M), toluene, 90 °C; (ii) 2,6-*i*-$Pr_2C_6H_3NH_2$, H^+; (iiia) PyH^+Cl^-, 300 °C; (iiib) BBr_3, CH_2Cl_2, -78°C to rt; (iv) 2,6-*i*-$Pr_2C_6H_3NH_2$, H^+

Insight into the ligand environment in the solid state was provided by single crystal X-ray diffraction studies performed on ligands **LVIIIb** and **LIXa**. Single crystals suitable for the study were grown by layering a solution of dichloromethane with hexane at rt to give yellow crystals of **LVIIIb** and **LIXa**. The molecular structures **LVIIIb** and **LIXa** are depicted in Figures 5 and 6 and selected bond distances and bond angles are listed in Tables 1 and 2. Crystal data and data collection refinement parameters are presented within Chapter 6; section 6.8.

Table 1 Selected bond distances (Å) and angles (°) for **LVIIIb**

N(1)-C(3)	1.345(2)
N(1)-C(7)	1.347(2)
N(2)-C(1)	1.279(2)
N(2)-C(21)	1.418(2)
O(1)-C(13)	1.384(2)
O(1)-C(14)	1.430(2)
C(1)-C(3)	1.494(2)
C(3)-N(1)-C(7)	118.15(11)
C(1)-N(2)-C(21)	121.41(11)
N(2)-C(1)-C(3)	116.31(11)
N(2)-C(1)-C(2)	125.86(12)
C(3)-C(1)-C(2)	117.83(11)
C(13)-O(1)-C(14)	113.63(10)

A single crystal X-ray diffraction study of **LVIIIb** shows the molecule to possess a *transoid* arrangement between the pyridine and imine moieties of the ligand, a geometry which differs to the *cisoid* configuration of the group 8 and 9 complexes within this chapter. The *transoid* arrangement observed here is similar to that observed for related species in the solid state.[15] The anisole substituent is orthogonal to the N(2)-C(1)-C(3)-N(1)-C(7) plane with the methoxy group pointing upwards out of the plane and the phenyl substituent in the 3'-position perpendicular to the anisole ring. The *N*-aryl group is also orthogonal to the plane defined by N(2)-C(1)-C(3)-N(1)-C(7) such that the *ortho*-isopropyl groups are positioned above and below the plane. The double bond character of the C=N bonds is noted by the bond lengths of *ca.* 1.3 Å and the bond angles of *ca.* 120°.[15]

Table 2 Selected bond distances (Å) and angles (°) for **LIXa**.2.2CH_2Cl_2

N(1)-C(7)	1.345(3)
N(1)-C(11)	1.347(3)
N(2)-C(12)	1.274(4)
N(2)-C(14)	1.421(3)
O(1)-C(1)	1.357(3)
C(11)-C(12)	1.497(3)
H(1)---N(1)	1.787
C(7)-N(1)-C(11)	119.8(2)
C(12)-N(2)-C(14)	120.9(2)
N(2)-C(12)-C(11)	116.4(2)
N(2)-C(12)-C(13)	125.8(2)
C(13)-C(12)-C(11)	117.9(2)

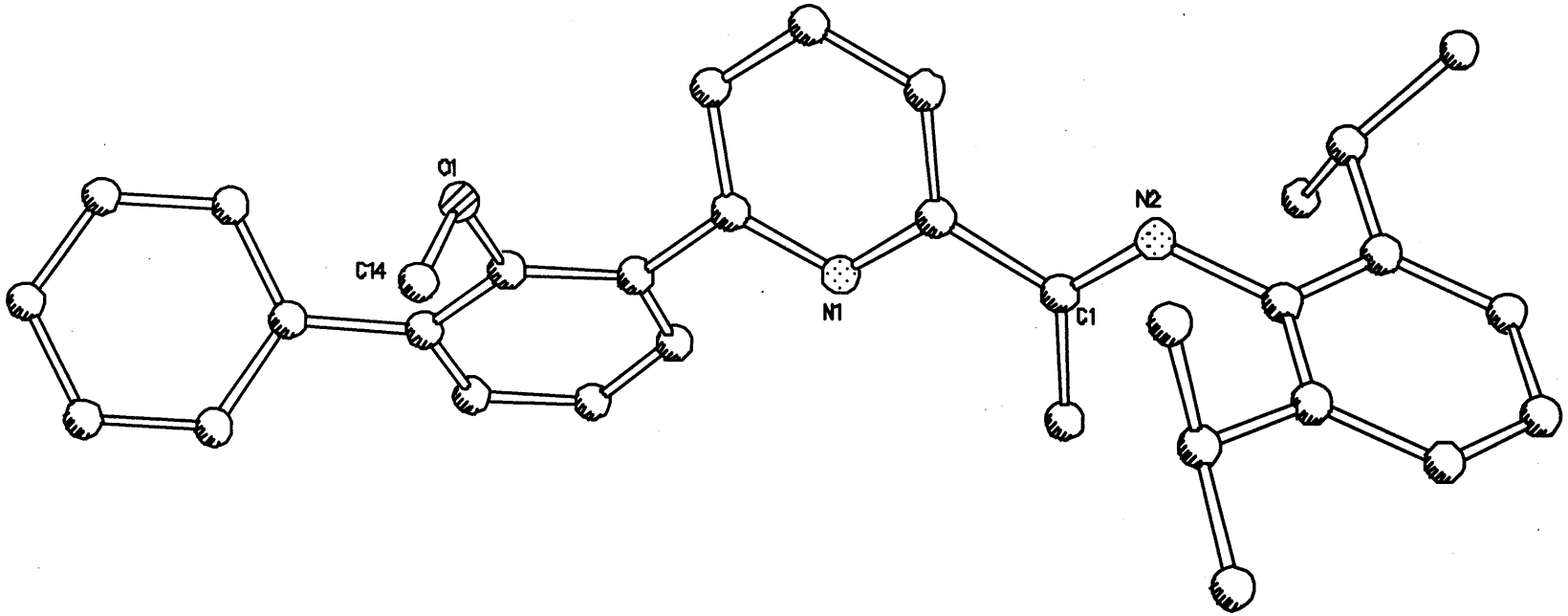

Figure 5 Molecular structure of **LVIIIb** (All the hydrogen atoms have been omitted for clarity)

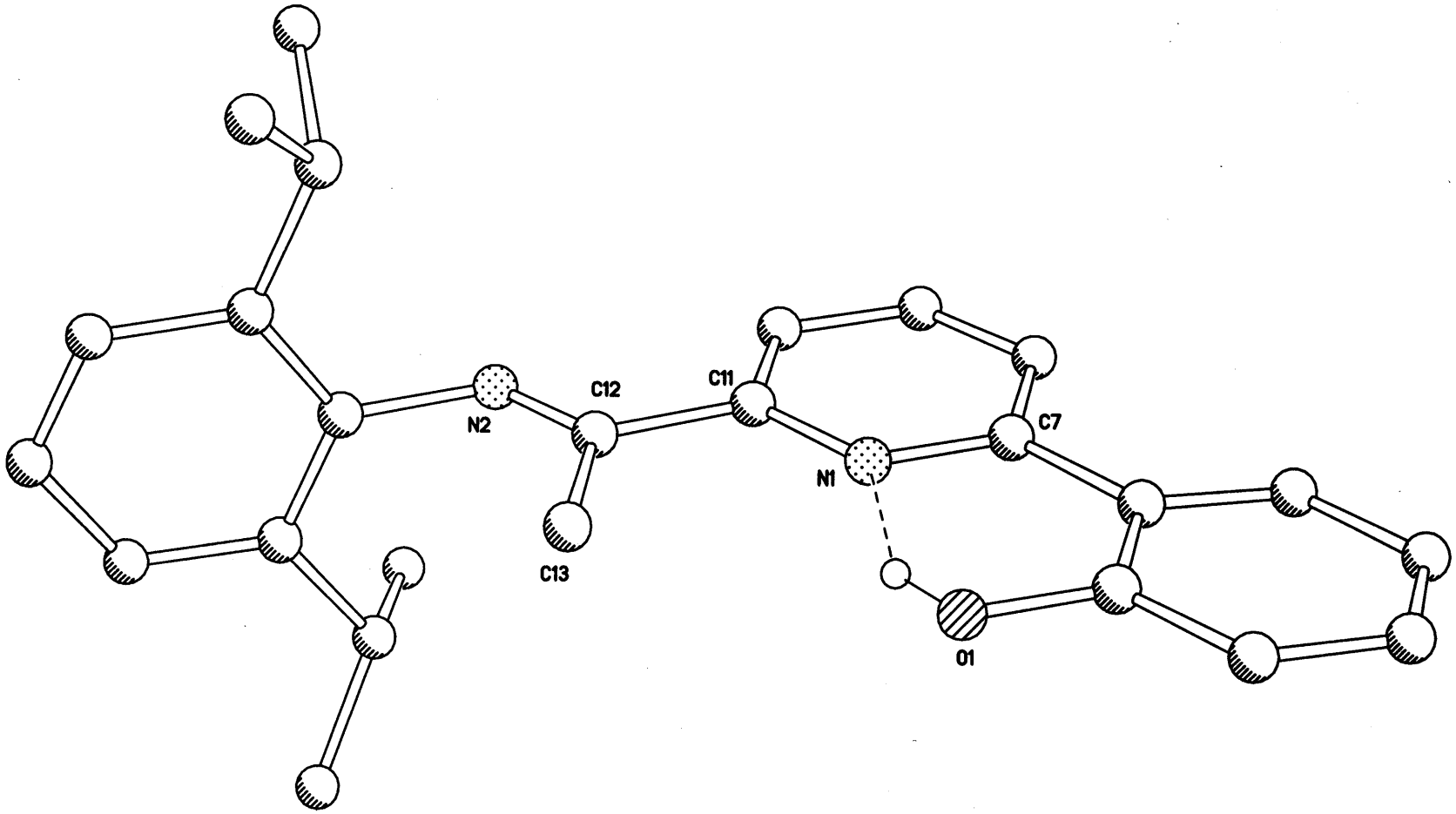

Figure 6 Molecular structure of **LIXa** (All the hydrogen atoms except H(1) have been omitted for clarity

The molecular structure of **LIXa** also exhibits a *transoid* relationship between the pyridine [N(1)] and imine [N(2)] moieties of the ligand, which in turn differs to the *cisoid* configuration of the group 8, 9 and 13 complexes within this chapter. The intramolecular hydrogen-bonding interaction between the hydrogen atom H(1) and N(1) [H(1)---N(1) 1.787 Å] enforces a *cisoid* conformation between O(1) and N(1) [O(1)---N(1) 2.536 Å] and a *transoid* arrangement between O(1) and N(2). The geometrical arrangements observed here are characteristic of those observed by similar species in the solid state.[2, 15 - 17] The *N*-aryl group is orthogonal to the plane defined by N(2)-N(1)-O(1) such that the *ortho*-isopropyl groups are positioned above and below the plane. As for **LVIIIb** the double bond character of the C=N bonds is noted by the bond lengths of *ca.* 1.3 Å and the bond angles of *ca.* 120°.

The ligands **LX** and **LXI** are prepared by exploiting the well-known attack by nucleophilic reagents at imine carbon atoms ($AlMe_3/LiAlH_4$).[18 - 21] Indeed, in refluxing toluene the reaction of $AlMe_3$ with **LIXa** results in the methylation of the imine carbon atom (Scheme 2). The reaction was quenched with water, followed by extraction with pentane and workup to give **LX** in quantitative yield. Notably, if the reaction was performed at rt no methylation of the imine carbon atom was observed. The reduction of **LIXa** by the reducing agent $LiAlH_4$ affords **LXI** in high yield. Compounds **LX** and **LXI** have been characterised by IR, ^1H and ^{13}C NMR spectroscopy and ES mass spectrometry (see Chapter 6; sections 6.5.4 and 6.5.5).

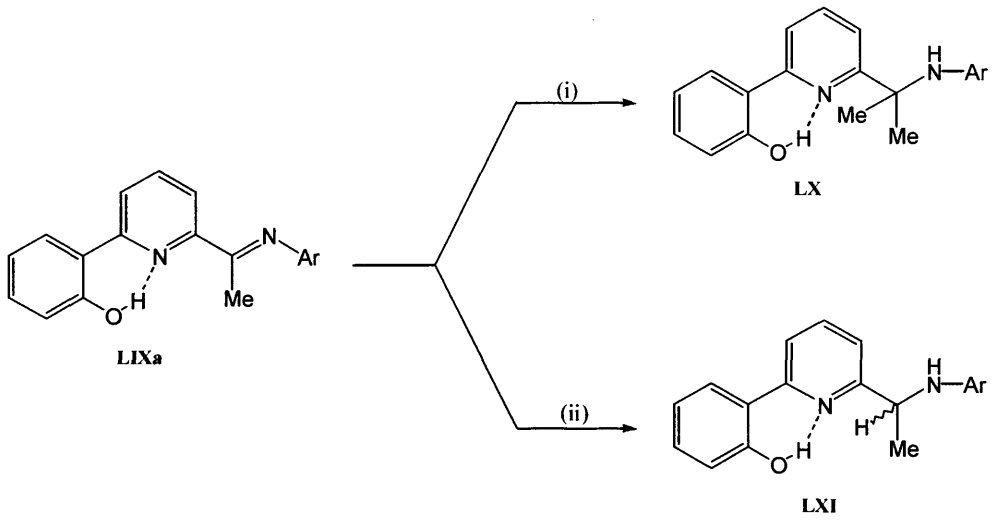

Scheme 2 *Reagents and conditions*: (i) $AlMe_3$, toluene, heat and reaction quenched with H_2O; (ii) $LiAlH_4$, -78 °C to rt and reaction quenched with H_2O

Insight into the reaction between $AlMe_3$ and **LIXa** in refluxing toluene was provided by the isolation of the *NNO*-aluminium(III) intermediate, [{$\mathbf{LX}^{-2H}$}AlMe(NCMe)] (**20**). Crystals of **20** were grown from an acetonitrile solution and subject to a single crystal X-ray diffraction study. The molecular structure of **20** is depicted in Figure 7 and selected bond distances and bond angles are listed in Table 3. Crystal data and data collection refinement parameters are presented within Chapter 6; section 6.8.

Table 3 Selected bond distances (Å) and angles (°) for **20**

Al(1)-O(1)	1.800(4)
Al(1)-N(1)	1.995(5)
Al(1)-N(2)	1.829(5)
Al(1)-N(3)	2.083(6)
Al(1)-C(27)	1.966(7)
N(3)-C(28)	1.146(7)
C(28)-C(29)	1.450(8)
N(1)-C(11)	1.347(7)
O(1)-Al(1)-N(1)	87.4(2)
O(1)-Al(1)-N(2)	129.5(2)
O(1)-Al(1)-N(3)	84.2(2)
O(1)-Al(1)-C(27)	97.2(3)
N(1)-Al(1)-N(2)	82.8(2)
N(1)-Al(1)-N(3)	162.3(2)
N(2)-Al(1)-N(3)	90.5(2)
N(1)-Al(1)-C(27)	100.4(2)
N(2)-Al(1)-C(27)	117.8(3)
N(3)-Al(1)-C(27)	97.2(3)
C(28)-N(3)-Al(1)	169.1(5)
N(3)-C(28)-C(29)	177.6(7)

The geometry at the aluminium(III) centre in complex **20** is best described as being distorted square pyramidal with a N3OC coordination sphere. The square basal plane consists of the *NNO*-chelate [N(1), N(2) and O(1)] and the acetonitrile molecule N(3), with Al(1) deviating out of this plane by 0.543 Å. The apical position is occupied by the methyl donor C(27). The *NNO*-chelate is coordinated in what may be regarded as a *meridional* configuration with a five-and a six-membered chelate. The phenolate ring is twisted by a torsional angle of 20.3° [*tors.*: C(5)-C(6)-C(7)-C(8)] in order to accommodate for the constraints imposed by the six-membered ring and the angular bonding mode of the phenolate

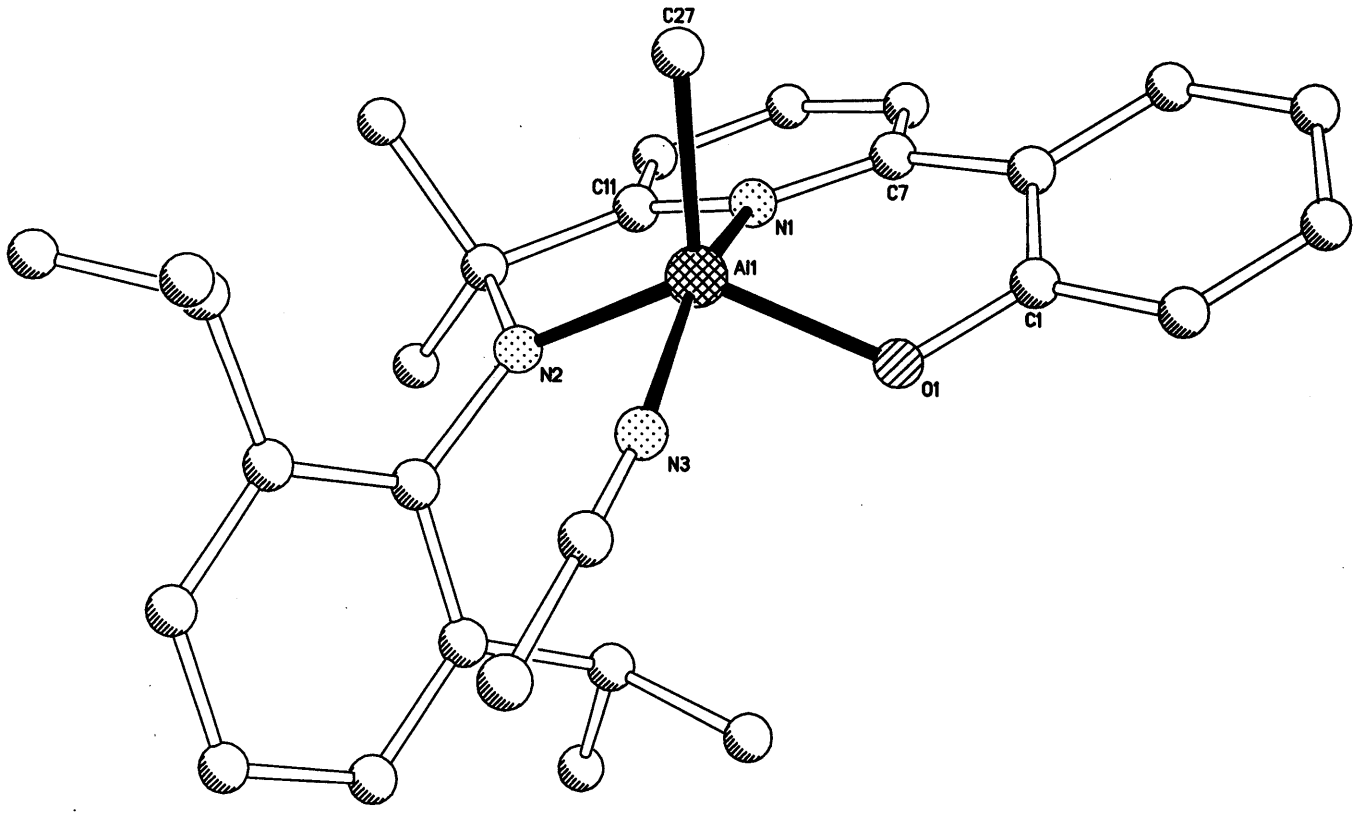

Figure 7 Molecular structure of [{$\mathbf{LX}^{-2H}$}AlMe(NCMe)] (**20**) (All the hydrogen atoms have been omitted for clarity)

donor atom. The 2,6-diisopropylphenyl substituent is oriented such that the *ortho*-substituents are pointing above and below the basal plane. The formal double bond character of the $C{=}N_{pyridine}$ bond is retained [N(1)-C(11) 1.347(7) Å] and is characteristic of related *NNO*-aluminium(III) compounds.[8] As for related aluminium(III) compounds[18] the Al-N bond lengths of the tridentate ligand are inequivalent with the distance to the pyridine donor being the longest [Al(1)-N(1) 1.995(5) Å] and the amide donor the shortest [Al(1)-N(1) 1.829(5) Å]. Furthermore, the Al-O distance of 1.800(4) Å is typical of a phenolate donor in a six-membered chelate ring.[8, 9, 17, 22] The bond length of 1.966(7) Å for the aluminium-methyl distance is similar to that observed for related species in the solid state.[8, 9, 17, 22] The Lewis acidity of the aluminium(III) centre is exhibited by the coordination of the acetonitrile molecule [Al(1)-N(3) 2.083(6) Å] in a *trans* configuration to the pyridine moiety. This strong affinity for Lewis bases may have a profound effect upon the catalytic nature of the aluminium(III) centre.[22]

The rt ^{1}H NMR spectrum arising from **20** dissolved in C_6D_6 reveals the solid state structure to be maintained in solution and is typical of the ^{1}H NMR spectra of related complexes (Figure 8).[8, 9, 18] For example, the resonance at $\delta = 0.51$ is attributable to the coordinated acetonitrile molecule. Notably, a resonance for non-coordinated acetonitrile at $\delta \approx 2$ is absent from the spectrum. The Al-Me resonance is found at $\delta = -0.24$. The methyl groups of the isopropyl substituents are found at $\delta = 1.31 - 1.43$ and the methine protons at $\delta = 3.71$ and 4.40. The two methyl groups of the amide carbon atom resonate at $\delta = 1.55$ and 1.80 and the aromatic protons are found in the region $\delta = 6.8 - 7.7$.

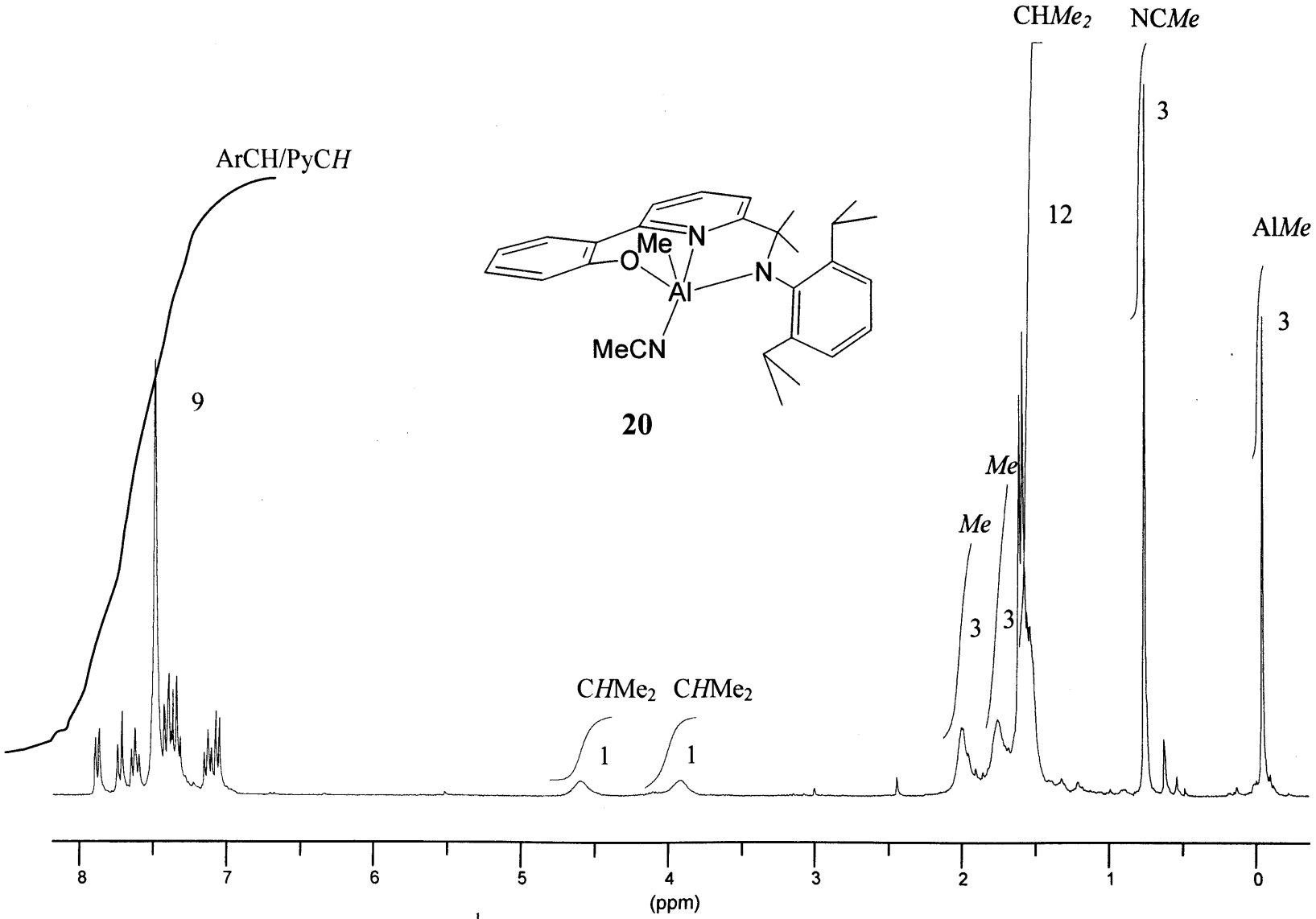

Figure 8 ^{1}H NMR spectrum of complex **20** in C_6D_6 at rt

5.3. Reactions of MCl_2 (M = Fe and Co) with LVIII

The treatment of anhydrous MCl_2 with 1 equivalent of **LVIIIa** in *n*-BuOH at 90 °C afforded the complexes [{**LVIIIa**}MCl_2] (M = Fe **21**, Co **22**) in moderate-to-high yield (Scheme 3). Both compounds have been characterised by FAB mass spectrometry, solid state IR spectroscopy, magnetic susceptibility measurements and elemental analysis. Insight into the coordination geometry around the metal centre and the pendant nature of the anisole donor was provided by single crystal X-ray diffraction studies.

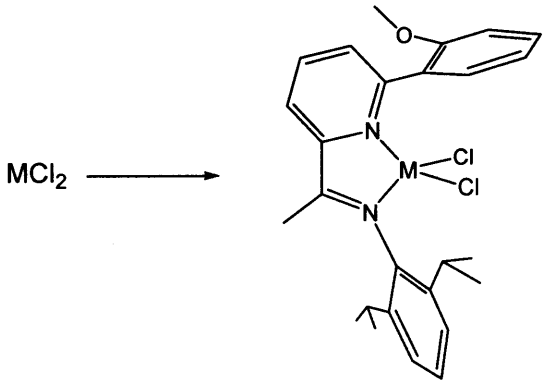

M = Fe **21**[a]
M = Co **22**[a]

Scheme 3 *Reagents and conditions*: **LVIIIa**, *n*-BuOH, 90 °C
[a] Isolated from single crystal X-ray diffraction studies

Red crystals of **21** and green crystals of **22** were grown from a chloroform solution at rt and subject to a single crystal X-ray diffraction study. The molecular structures of **21** and **22** are depicted in Figure 9 and selected bond distances and bond angles are listed in Table 4. Crystal data and data collection refinement parameters are presented within Chapter 6; section 6.8.

The structures of **21** and **22** are essentially identical and will be discussed together. The metal(II) centre is coordinated to two chloride atoms, one pyridine (N1) and one imine (N2) atom of the *NNO*-ligand to give a distorted tetrahedral environment around the metal(II) centre. Notably, the anisole donor is pendant and orthogonal to the N(2)-M(1)-N(1) plane, similar geometrical arrangements are observed in the pyridine-imine-thiophenyl cobalt(II) complexes.[23] In contrast to the molecular structure of the related free ligand **LVIIIb**, N(1) and N(2) possess a *cisoid* configuration. The *N*-aryl substituent is oriented essentially orthogonal

Table 4 Selected bond distances (Å) and angles (°) for **21**.$CHCl_3$ and **22**.$CHCl_3$

	M = Fe (**21**.$CHCl_3$)	M = Co (**22**.$CHCl_3$)
M(1)-N(1)	2.118(3)	2.054(2)
M(1)-N(2)	2.112(3)	2.052(2)
M(1)-Cl(1)	2.224(1)	2.210(1)
M(1)-Cl(2)	2.249(1)	2.235(1)
N(1)-C(11)	1.354(4)	1.360(3)
N(2)-C(12)	1.289(4)	1.281(3)
C(11)-C(12)	1.484(5)	1.488(3)
N(1)-M(1)-N(2)	77.82(11)	81.02(7)
N(1)-M(1)-Cl(1)	113.23(8)	115.32(5)
N(1)-M(1)-Cl(2)	114.56(8)	116.67(5)
N(2)-M(1)-Cl(1)	111.89(8)	112.42(5)
N(2)-M(1)-Cl(2)	107.12(8)	107.99(5)
Cl(1)-M(1)-Cl(2)	122.87(4)	117.30(3)

to the N(2)-M(1)-N(1) plane with the *ortho*-isopropyl groups positioned above and below the plane. The acute N(1)-M(1)-N(2) angle [77.82(11)° (Fe), 81.02(7)° (Co)] is associated with the constraints imposed by the five-membered chelate ring, while the Cl(1)-M(1)-Cl(2) angle is obtuse [122.87(4)° (Fe), 117.30(3)° (Co)]. Comparative inter-bond angles are observed in single crystal X-ray structure determinations of α-diimine iron(II)[24, 25] and cobalt(II)[26] complexes. The formal double bond character of the C=N linkages is retained upon coordination to both iron and cobalt as indicated by the C=N bond lengths [*ca.* 1.3 Å] and the C(11)-C(12) bond distance [*ca.* 1.5 Å]. This is analogous to the α-diimine iron(II)[24, 25] complexes and in contrast to the partial delocalisation of the double bonds exhibited in the α-diimine cobalt(II)[26] compound. Furthermore, the M-N and M-Cl bond distances are similar to those observed in the pyridine-imine-thiophenyl cobalt(II) complexes[23] and the α-diimine iron(II)[24, 25] and cobalt(II)[26] complexes.

The FAB mass spectrometric data exhibits characteristic mass and isotope distribution patterns for a monomeric dichloro complex. The solid state IR spectra reflect the coordination of **LVIIIa** to the metal(II) centre *via* the notable absence of the free-ligand $C{=}N_{imine}$ stretching frequency at 1646 cm^{-1} and the formation of three C=N stretching frequencies in the region of 1620 – 1590 cm^{-1}. The rt magnetic susceptibility measurements are consistent with tetrahedral HS iron(II) and cobalt(II) configurations. For example, **21** reveals a magnetic moment of 4.97

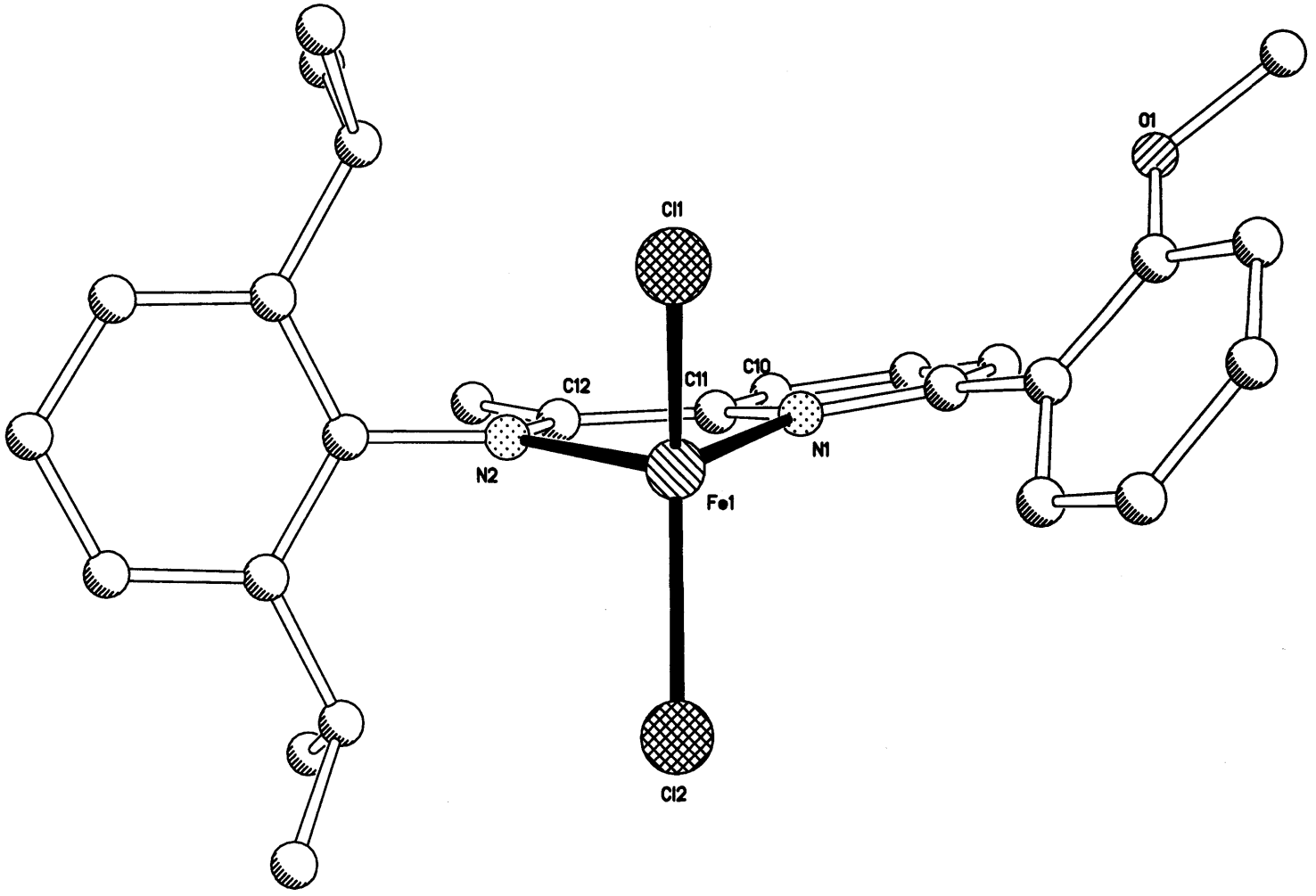

Figure 9 Molecular structure of [{**LVIIIa**}$FeCl_2$] (**21**) (All the hydrogen atoms have been omitted for clarity). Molecular structure of [{**LVIIIa**}$CoCl_2$] (**22**) reveals a similar coordination geometry

BM characteristic of a mononuclear iron(II) HS configuration (S = 2), while **22** shows a magnetic moment of 4.04 BM indicative of a mononuclear cobalt(II) HS configuration (S = 3/2).

5.4. Reactions of MCl_2 (M = Fe and Co) with LIX

The reaction of the MCl_2 precursor with 1 equivalent of **LIX** in thf at rt afforded the complexes [{**LIXa**}MCl_2] (M = Fe **23a**, Co **24a**) and [{**LIXb**}MCl_2] (M = Fe **23b**, Co **24b**) in moderate-to-high yield (Scheme 4). The compounds have been characterised by FAB mass spectrometry, solid state IR spectroscopy and magnetic susceptibility measurements. Insight into the coordination geometry around the metal centre was provided by single crystal X-ray diffraction studies performed on complex **24a**. The molecular structure of **24a** is depicted in Figure 10 and selected bond distances and bond angles are listed in Table 5.

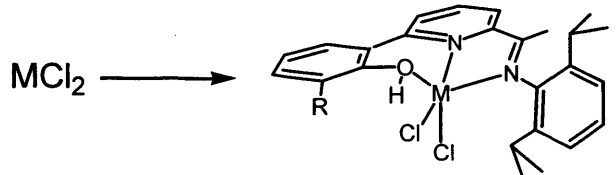

23a M = Fe; R = H
23b M = Fe; R = Ph
24a M = Co; R = H[a]
24b M = Co; R = Ph

Scheme 4 *Reagents and Conditions*: **LIX**, $FeCl_2(thf)_{1.5}$ or $CoCl_2$, thf, rt
[a] Isolated from single crystal X-ray diffraction studies

Green crystals of **24a** were grown from the slow cooling of a hot acetonitrile solution and subject to a single crystal X-ray diffraction study. Crystal data and data collection refinement parameters are presented within Chapter 6; section 6.8. The molecular structure of **24a** possesses a similar overall geometrical arrangement to the aluminium(III) complex **20** and in contrast to the molecular structure of the free ligand **LIXa**, N(1) and N(2) possess a *cisoid* configuration. The cobalt(II) centre is bound to two terminal chlorides and a *NNO*-chelate in a *meridional* configuration with a five-and a six-membered chelate to give a distorted square pyramidal environment. The basal plane consists of the *NNO*-chelate [N(1), N(2) and O(1)] and the chloride atom Cl(2), with Co(1) sitting out of this plane by 0.580 Å.

Table 5 Selected bond distances (Å) and angles (°) for **24a**

Co(1)-O(1)	2.080(2)
Co(1)-N(1)	2.133(2)
Co(1)-N(2)	2.072(2)
Co(1)-Cl(1)	2.269(1)
Co(1)-Cl(2)	2.321(1)
O(1)-C(1)	1.388(2)
N(1)-C(7)	1.351(3)
N(2)-C(12)	1.288(3)
C(11)-C(12)	1.487(3)
O(1)-Co(1)-N(1)	78.53(6)
O(1)-Co(1)-N(2)	128.90(6)
O(1)-Co(1)-Cl(1)	112.68(4)
O(1)-Co(1)-Cl(2)	91.07(4)
N(1)-Co(1)-N(2)	76.86(7)
N(1)-Co(1)-Cl(1)	92.41(5)
N(1)-Co(1)-Cl(2)	162.58(5)
N(2)-Al(1)-Cl(1)	112.44(5)
N(2)-Al(1)-Cl(2)	99.72(5)
Cl(1)-Co(1)-Cl(2)	104.56(2)
C(1)-O(1)-Co(1)	119.81(13)

The apical position is occupied by the chloride ligand Cl(1). The phenol ring is twisted by a torsional angle of 23.0° [*tors.*: C(5)-C(6)-C(7)-C(8)]. The 2,6-diisopropylphenyl group is oriented such that the *ortho*-substituents are pointing above and below the basal plane. Notably, the formal double bond character of the C=N linkages is retained upon coordination as indicated by the C=N bond lengths [*ca.* 1.3 Å] and the C(11)-C(12) bond distance [*ca.* 1.5 Å]. The Co-N bond lengths of the tridentate ligand are inequivalent with the distance to the pyridine donor being the longest [Co(1)-N(1) 2.133(2) Å] and the imine donor the shortest [Co(1)-N(2) 2.072(2) Å]. The Co-O bond distance of 2.080(2) Å is typical of a phenol donor in a six-membered chelate ring.[16] The Co-Cl distances differ by *ca.* 0.05 Å with Co-Cl(2) being the longest [2.321(1) Å]. The Cl-Co-Cl angle at 104.56(2)° lies below the range found in the *NNN*-related pyridine-diimine cobalt(II) complexes,[27, 28] but compares well with the *NNN*-chelates **11a** and **11c** (see Chapter 2; section 2.5).

The FAB mass spectrometric data for complexes **23** and **24** show characteristic mass and isotope distribution patterns consistent with a monomeric species and in the case of **23a**

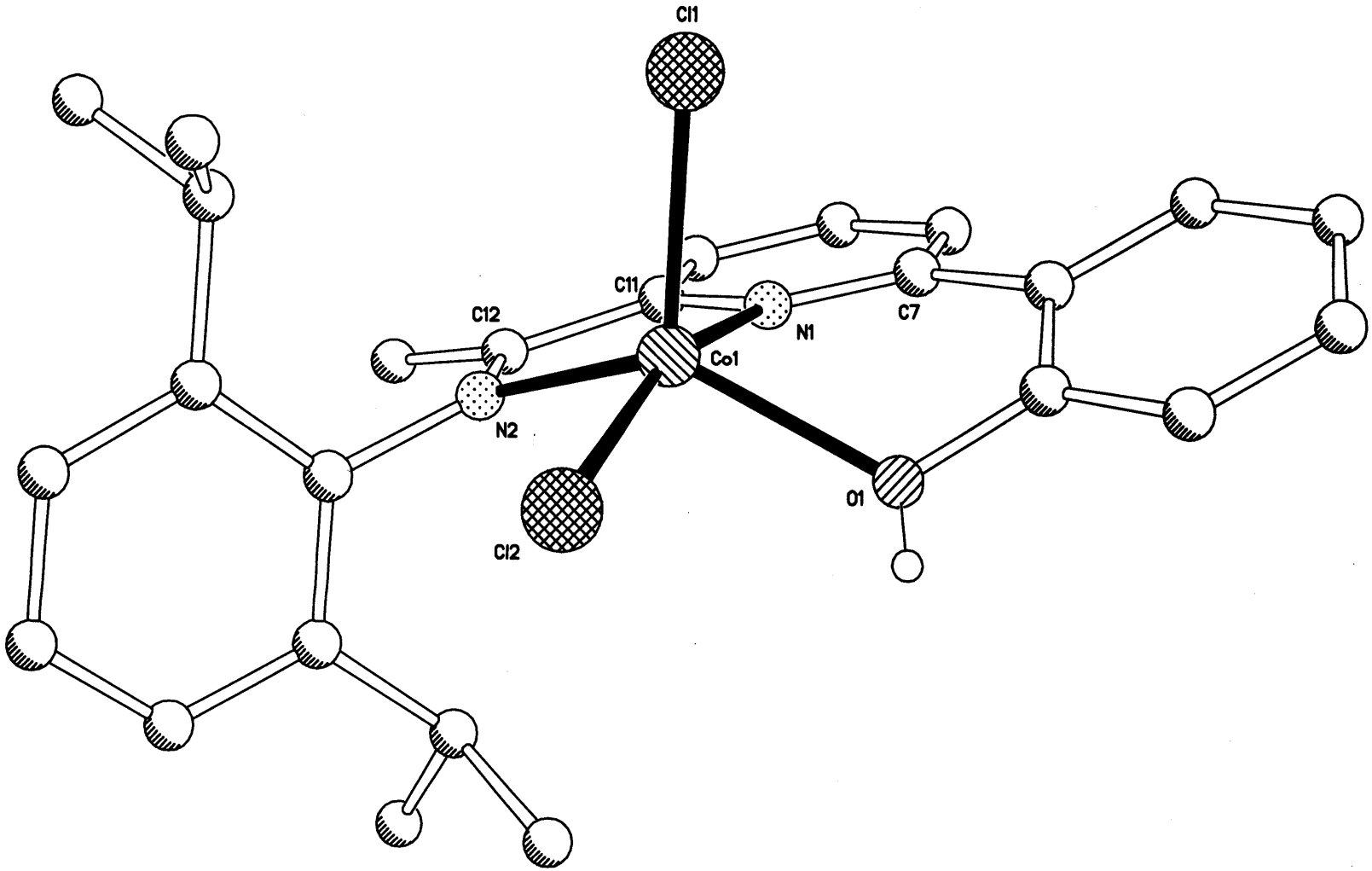

Figure 10 Molecular structure of [{**LIXa**}$CoCl_2$] (**24a**) (All the hydrogen atoms except for H(1) have been omitted for clarity)

and **24a** minor peaks attributable to a dimeric species. The solid state IR spectra reflect the coordination of the *NNO*-chelate to the metal(II) centre *via* the notable absence of the free-ligand $C{=}N_{imine}$ stretching frequency at *ca.* 1640 cm^{-1} and the formation of C=N stretching frequencies in the region of 1610 – 1590 cm^{-1}. The rt magnetic susceptibility measurements gave magnetic moments of *ca.* 5.00 BM, characteristic of a HS iron (II) configuration ($S = 2$) and *ca.* 4.00 BM, characteristic of a HS cobalt(II) configuration ($S = 3/2$).

The treatment of **LIXa** with NaH results in the deprotonation of the *NNO*-ligand at the phenol atom (Scheme 5). The resultant sodium salt undergoes a metathesis reaction with a MCl_2 precursor under mild reaction conditions to afford the dimeric complexes [{**LIXa**$^{-H}$}$MCl]_2$ (M = Fe **25**, Co **26a**). Interestingly, under forcing conditions **LIXc** and **LIXd** yield the bis(μ-phenolate) dimeric complexes [{**LIXc**$^{-H}$}$CoCl]_2$ (**26b**) and [{**LIXd**$^{-H}$}$CoBr]_2$ (**26c**) in the notable absence of a deprotonating reagent. With the exception of complex **25**, all products have been characterised by FAB mass spectrometry, solid state IR spectroscopy, magnetic susceptibility and by elemental analysis.

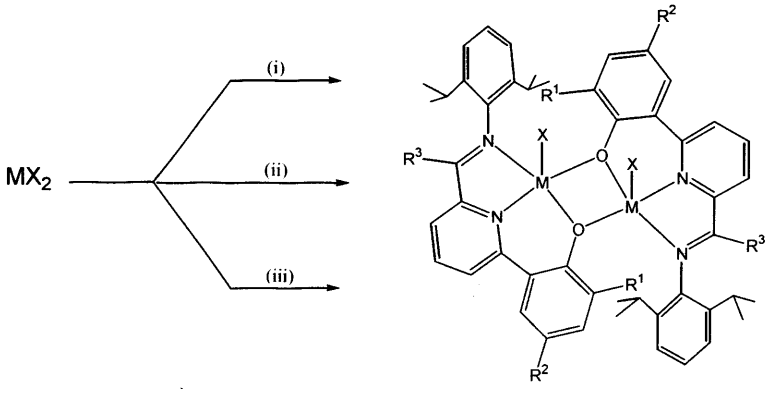

(i): **25** M = Fe; $R^1 = R^2 =$ H; R^3 = Me; X = Cl
(i): **26a** M = Co; $R^1 = R^2 =$ H; R^3 = Me; X = Cl[a]
(ii): **26b** M = Co; $R^1 = R^2 = R^3$ = H; X = Cl[a]
(iii): **26c** M = Co; $R^1 = R^3$ = H; R^2 = *t*-Bu; X = Br[a]

Scheme 5 *Reagents and Conditions*: (ia) **LIXa**, NaH, thf, heat; (ib) $FeCl_2(thf)_{1.5}$ or $CoCl_2$, thf, rt; (ii) $CoCl_2$, *n*-BuOH, **LIXc**, heat; (iii) $CoBr_2$, *n*-BuOH, **LIXd**, heat
[a] Isolated from single crystal X-ray diffraction studies

In addition, red crystals of **26a-c** were grown from the slow cooling of a hot acetonitrile solution and subject to single crystal X-ray diffraction studies. The molecular structures of **26a-c** are represented in Figure 11 and selected bond distances and bond angles are listed in Tables 6 and 7. Crystal data and data collection refinement parameters are presented within Chapter 6; section 6.8. The molecular structure of **26a** is generated *via* C_2 symmetry passing

through the centre of the Co_2O_2 bridging core, while **26b** and **26c** consist of two inequivalent cobalt(II) centres. However, the overall geometry and structural features at each metal centre in **26b** and **26c** are similar to one another and comparable to **26a**. Therefore, only **26a** will be discussed in detail.

Table 6 Selected bond distances (Å) and angles (°) for **26a**.MeCN

Co(1)-O(1)	2.009(1)
Co(1)-N(1)	2.102(2)
Co(1)-N(2)	2.119(2)
Co(1)-Cl(1)	2.299(1)
Co(1)-O(1A)	2.037(1)
O(1)-C(1)	1.350(2)
N(1)-C(7)	1.352(3)
N(2)-C(12)	1.290(3)
C(11)-C(12)	1.485(3)
Co(1)...Co(1A)	3.146
O(1)-Co(1)-N(1)	85.12(6)
O(1)-Co(1)-N(2)	140.77(6)
O(1)-Co(1)-Cl(1)	109.41(4)
O(1)-Co(1)-O(1A)	77.57(6)
O(1A)-Co(1)-N(1)	150.00(6)
O(1A)-Co(1)-N(2)	101.10(6)
O(1A)-Co(1)-Cl(1)	112.22(4)
N(1)-Co(1)-N(2)	77.25(6)
N(1)-Co(1)-Cl(1)	96.52(4)
N(2)-Co(1)-Cl(1)	107.23(5)
C(1)-O(1)-Co(1)	121.55(12)
Co(1)-O(1)-Co(1A)	102.06(6)

The molecular structure of **26a** consists of a dimeric unit in which the cobalt(II) centres are bridged by two phenolate donors, which originate from the *meridionally* coordinated *NNO*-chelates at each cobalt atom. In addition, each cobalt atom is bound to a terminal chloride to give a distorted square pyramidal geometry with an N2O2Cl coordination sphere. The basal plane comprises of the N(1), N(2), O(1) and O(1A), with Co(1) deviating from this plane by 0.686 Å. The apical position is occupied by the chloride donor Cl(1). Interestingly, the two apical chlorides are oriented in a *syn*-arrangement with respect to one another, which is in contrast to literature precedent bis(μ-phenolate) cobalt(II) complexes.[29 - 31] The Co-O distances differ by *ca.* 0.03 Å with Co(1)-O(1A) being the longest [2.037 (1) Å]. Notably, the Co(1)-(O1) distance in **26a** is *ca.* 0.07 Å shorter than that observed in **24a**, this may be

attributable to the π-donor capability of a phenolate *versus* a phenol donor. The Co-N and Co-Cl distances are comparable to those found in the momomeric complex **24a**. Likewise, the formal double bond character of the C=N linkages is retained upon coordination as indicated by the C=N bond lengths [*ca.* 1.3 Å] and the C(11)-C(12) bond distance [*ca.* 1.5 Å]. The Co-O-Co bond angle is 102.06(6)° and the Co...Co bond separation is 3.146 Å, which are similar to those observed in related bis(μ-phenolate) cobalt(II) complexes.[29-31]

Table 7 Selected bond distances (Å) and angles (°) for **26b**.2MeCN and **26c**.3MeCN

	X = Cl (**26b**.2MeCN)	X = Br (**26c**.3MeCN)
Co(1)-O(1)	1.995(2)	1.977(3)
Co(1)-N(1)	2.098(3)	2.094(3)
Co(1)-N(2)	2.115(3)	2.082(3)
Co(1)-X(1)	2.283(1)	2.439(1)
Co(1)-O(2)	2.037(2)	2.034(3)
O(1)-C(1)	1.347(4)	1.347(5)
Co(2)-O(2)	1.994(2)	1.979(3)
Co(2)-N(3)	2.105(3)	2.101(3)
Co(2)-N(4)	2.114(3)	2.111(3)
Co(2)-X(2)	2.305(1)	2.453(1)
Co(2)-O(1)	2.036(2)	2.034(3)
O(2)-C(25)	1.346(4)	NA
O(2)-C(29)	NA	1.348(5)
Co(1)...Co(2)	3.101	3.128
O(1)-Co(1)-N(1)	84.73(10)	84.41(12)
O(1)-Co(1)-N(2)	138.30(11)	137.88(13)
O(1)-Co(1)-X(1)	112.95(8)	119.55(8)
O(1)-Co(1)-O(1A)	79.38(9)	77.43(11)
O(2)-Co(1)-N(1)	153.30(11)	151.60(12)
O(2)-Co(1)-N(2)	100.18(11)	100.52(12)
O(2)-Co(1)-X(1)	109.03(7)	116.12(8)
N(1)-Co(1)-N(2)	77.81(11)	78.62(13)
N(1)-Co(1)-X(1)	96.87(8)	91.79(9)
N(2)-Co(1)-X(1)	106.59(9)	99.40(10)
C(1)-O(1)-Co(1)	123.0(2)	124.3(2)
O(2)-Co(2)-N(3)	83.67(11)	85.84(12)
O(2)-Co(2)-N(4)	139.23(11)	143.68(12)
O(2)-Co(2)-X(2)	115.06(7)	111.97(8)
O(1)-Co(2)-O(1A)	79.42(9)	77.40(11)
O(1)-Co(2)-N(3)	149.86(10)	148.78(12)
O(1)-Co(2)-N(4)	99.68(10)	100.27(12)
O(1)-Co(2)-X(2)	112.92(7)	115.13(8)
N(3)-Co(2)-N(4)	77.43(12)	78.03(13)
N(3)-Co(1)-X(2)	96.81(8)	95.48(9)
N(4)-Co(1)-X(2)	102.91(8)	101.89(9)
C(25)-O(2)-Co(2)	121.5(2)	NA
C(29)-O(2)-Co(2)	NA	125.3(2)

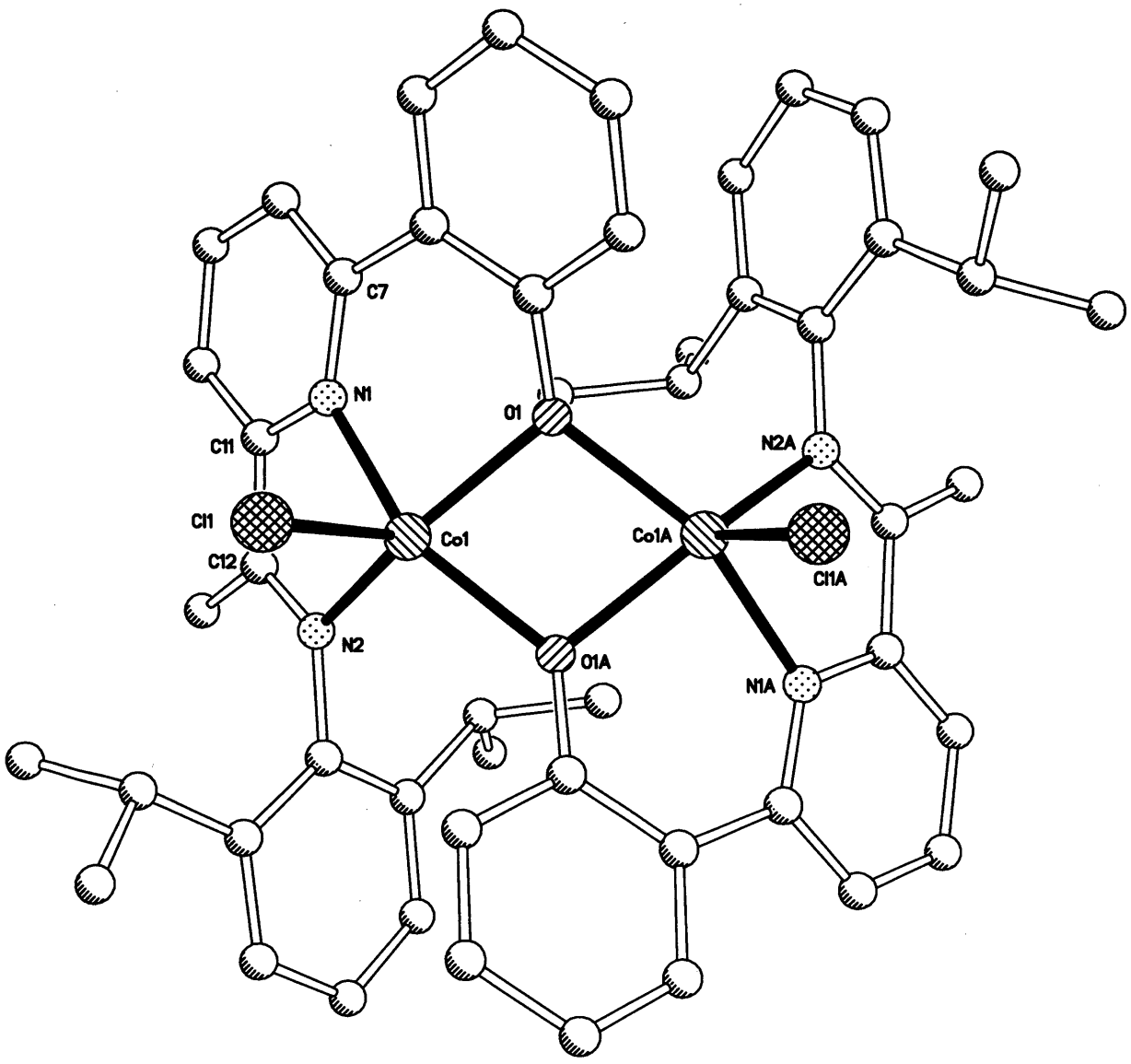

Figure 11 Molecular structure of [{**LIXa**$^{-H}$}CoCl]$_2$ (**26a**) (All the hydrogen atoms have been omitted for clarity). Molecular structure of [{**LIXc**$^{-H}$}CoCl]$_2$ (**26b**) and [{**LIXd**$^{-H}$}CoBr]$_2$ (**26c**) reveal a similar coordination geometry

The FAB mass spectrometric data exhibits characteristic mass and isotope distribution patterns for a dimeric species. The solid state IR spectra reflect the coordination of the *NNO*-chelate to the metal(II) centre *via* the notable absence of the free-ligand $C{=}N_{imine}$ stretching frequency at 1650 - 1630 cm^{-1} and the formation of C=N stretching frequencies in the region of 1630 - 1590 cm^{-1}. The rt magnetic susceptibility measurements are consistent with two non-interacting HS iron(II) or cobalt(II) centres. For example, **25** possess a magnetic moment of 7.1 BM, while **26a-c** show magnetic moments of *ca.* 6.0 BM. In addition, the complexes **25** and **26** may act as suitable precursors for the preparation of a single-component α-olefin polymerisation catalyst. However, attempts to isolate such a species have so far proved unsuccessful.

5.5. Insight into the Polymerisation of Ethylene

Preliminary catalytic evaluation of the pre-catalysts **21, 23a**, **23b** and **24b** treated with 100 equivalents of MAO in toluene, 17.23 bar of ethylene[32] and at 40 °C, showed moderately-to-highly active activities for the polymerisation of ethylene (Table 8).

Table 8 Ethylene polymerisation evaluation employing precatalysts **21, 23a**, **23b** and **24b** runs 1 – 4

Run[a]	Pre-catalyst	Yield (g)[b]	Activity (g/mmol/h/bar)	M_w	M_n	M_w/M_n
1	**21**	0.04	25	325866	120691	2.7
2	**23a**	0.46	975	35834	17917	2.0
3	**23b**	0.34	160	100968	42070	2.4
4	**24b**	0.30	104	105105	45698	2.3

[a] *General conditions*: 0.08 mmol of precatalyst, 80 mmol MAO, toluene, 17.23 bar ethylene, at 40 °C. Reaction quenched with 5 mol% Oxygen in Argon after total duration of 1 h or 1.38 bar of ethylene had been consumed.

The PE produced ranges from moderate-to-high molecular weight with polydispersities typical of a single-site catalytic system (M_w/M_n *ca.* 2). In the pre-catalytic state the iron(II) centre in **21** is bound to a *NN*-chelate with a pendant anisole donor, while **23** contains a *NNO*-

chelate and in a analogous fashion to the α-diimine[33] and the pyridine-diimine iron[27] systems the activity is enhanced upon employing the tridentate coordination mode. Indeed, the highest activity observed to date was with the pre-catalyst **23a** (run 2: 975 g/mmol/h/bar), albeit an order of magnitude lower than the related pyridine-diimine iron system.[27] In contrast, the cobalt system (**24b**) displays a comparable activity to the related pyridine-diimine cobalt system.[27]

5.6. Conclusions

In summary, we have established several synthetic procedures for the novel *NNO*-ligand sets **LVIII – LXI**. Single crystal X-ray diffraction studies have revealed that **LVIII** and **LIX** possess a *transoid* arrangement between the pyridine and imine moieties of the ligand, a geometry, which differs to the *cisoid* configuration of the complexes reported within this Chapter. The functionality of the oxygen donor has been found to have a profound effect upon the nuclearity, the binding mode and the catalytic activity. Finally, the iron systems display higher activities than the cobalt systems.

References

[1] B. M. Holligan, J. C. Jeffery, M. K. Norgett, E. Schatz and M. D. Ward, *J. Chem. Soc., Dalton Trans.*, 1992, 3345-3351.
[2] J. C. Jeffery, E. Schatz and M. D. Ward, *J. Chem. Soc., Dalton Trans.*, 1992, 1921-1927.
[3] J. C. Jeffery, C. S. G. Moore, E. Psillakis and M. D. Ward, *Polyhedron*, 1995, **14**, 599-604.
[4] D. Bradwell, D. Black, J. C. Jeffery and M. D. Ward, *Polyhedron*, 1993, **12**, 1577-1580.
[5] D. J. Jones, V. C. Gibson, S. Green and P. J. Maddox, *Chem. Commun.*, 2002, 1038-1039.
[6] R. K. O'Reilly, V. C. Gibson, A. J. P. White and D. J. Williams, *J. Am. Chem. Soc.*, 2003, **125**, 8450-8451.
[7] R. Viswanathan, M. Palaniandavar, T. Balasubramanian and P. T. Muthiah, *J. Chem. Soc., Dalton Trans.*, 1996, 2519-2525.
[8] P. A. Cameron, V. C. Gibson, C. Redshaw, J. A. Segal, M. D. Bruce, A. J. P. White and D. J. Williams, *Chem. Commun.*, 1999, 1883-1884.
[9] P. A. Cameron, V. C. Gibson, C. Redshaw, J. A. Segal, A. J. P. White and D. J. Williams, *J. Chem. Soc., Dalton Trans.*, 2002, 415-422.
[10] S. Fernandes, R. M. Bellabarba, A. F. G. Ribeiro, P. T. Gomes, J. R. Ascenso, J. F. Mano, A. R. Dias and M. M. Marques, *Polym. Int.*, 2002, **51**, 1301-1303.
[11] V. C. Gibson, C. Redshaw, G. A. Solan, A. Tomov, A. J. P. White and D. J. Williams, 2004 manuscript in preparation.
[12] V. C. Gibson, C. Redshaw and G. A. Solan, 2004 manuscript in preparation.
[13] N. Miyaura, T. Yanagi and A. Suzuki, *Synth. Commun.*, 1981, **11**, 513-519.
[14] N. Miyaura and A. Suzuki, *Chem. Rev.*, 1995, *95*, 2457-2483.
[15] G. J. P. Britovsek, V. C. Gibson, S. Mastroianni, D. C. H. Oakes, C. Redshaw, G. A. Solan, A. J. P. White and D. J. Williams, *Eur. J. Inorg. Chem.*, 2001, 431-437.
[16] L. Wang, W-H. Sun, L. Han, Z. Li, Y. Hu, C. He and C. Yan, *J. Organomet. Chem.*, 2002, **650**, 59-64.
[17] S-F. Liu, C. Seward, H. Aziz, N-X, Hu, Z. Popovic and S. Wang, *Organometallics*, 2000, **19**, 5709-5714.
[18] M. Bruce, V. C. Gibson, C. Redshaw, G. A. Solan, A. J. P. White and D. J. Williams, *Chem. Commun.*, 1998, 2523-2524.
[19] G. van Koten and K. Vrieze, *J. Organomet. Chem.*, 1979, **181**, 271-283.
[20] V. C. Gibson, C. Newton, C. Redshaw, G. A. Solan, A. J. P. White and D. J. Williams, *J. Chem. Soc., Dalton Trans.*, 1999, 827-829.
[21] G. J. P. Britovsek, V. C. Gibson, S. Mastroianni, D. C. H. Oakes, C. Redshaw, G. A. Solan, A. J. P. White and D. J. Williams, *Eur. J. Inorg. Chem.*, 2001, 431-437.
[22] P. A. Cameron, D. Jhurry, V. C. Gibson, A. J. P. White, D. J. Williams and S. Williams, *Macromol. Rapid. Commun.*, 1999, **20**, 616-618.
[23] C. Bianchini, G. Mantovani, A. Meli and F. Migliaci, *Organometallics*, 2003, **22**, 2545-2547.
[24] V. C. Gibson, R. K. O'Reilly, W. Reed, D. F. Wass, A. J. P. White and D. J. Williams, *Chem. Commun.*, 2002, 1850-1851.
[25] J. Breuer, H-W, Frühauf, W. J. J. Smeets and A. L. Spek, *Inorg. Chim. Acta.*, 1999, 438-447.
[26] T. V. Laine, M. Klinga, A. Maaninen, E. Aitola and M. Leskelä, *Acta. Chem. Scand.*, 1999, **53**, 968-973.
[27] G. J. P. Britovsek, M. Bruce, V. C. Gibson, B. S. Kimberley, P. J. Maddox, S. Mastroianni, S. J. McTavish, C. Redhaw, G. A. Solan, S. Strömberg, A. J. P. White and D. J. Williams, *J. Am. Chem. Soc.*, 1999, **121**, 8728-8740.
[28] G. J. P. Britovsek, S. Mastroianni, G. A. Solan, S. P. D. Baugh, C. Redshaw, V. C. Gibson, A. J. P. White, D. J. Williams and M. R. J. Elsegood, *Chem. Eur. J.*, 2000, **6**, 2221-2231.
[29] M. Du, D-L. An, Y-M. Guo and X-H. Bu, *J. Mol. Struct.*, 2002, 641, 193-198.
[30] H. Furutachi, S. Fujinami, M. Suzuki and H. Ōkawa, *J. Chem. Soc., Dalton Trans.*, 2000, 2761-2769.
[31] B. F. Hoskins and G. A. Williams, *Aust. J. Chem.*, 1975, **28**, 2607-2614.
[32] 1 bar = 14.508 psi. Therefore, 17.23 bar = 250 psi.
[33] L. K. Johnson, C. M. Killian, S. D. Arthur, J. Feldman, E. McCord, S. J. McLain, K. A. Kreutzer, M. A. Bennett, E. B. Coughlin, S. D. Ittel, A. Parthasarathy, D. Tempel and M. Brookhart, (UNC-Chapel-Hill/DuPont), WO 9623010, 1996., *Chem. Abstr.*, 1996, **125**, 222773t.

University of Leicester

Chapter Six

Experimental

6.1. General

All operations were carried out under an inert atmosphere of nitrogen using standard Schlenk and cannular techniques or in a nitrogen purged glove box. Solvents were distilled under nitrogen from appropriate drying agents and degassed prior to use.[1] The infrared spectra were recorded as Nujol mulls between 0.5 mm NaCl plates on a Perkin Elmer 1600 series or in the solid state using a Perkin Elmer Spectrum one FT-IR spectrometer. The ES and the FAB mass spectra were recorded using a micromass Quattra LC mass spectrometer and a Kratos Concept spectrometer with methanol or NBA as the matrix respectively. GC mass spectrometry measurements were obtained using a Perkin Elmer Autosystem XL chromatogram and a Perkin Elmer Turbo Mass Spectrometer. ^{1}H and ^{13}C NMR spectra were recorded on a Bruker ARX spectrometer 250 or 300 or 400 MHz; chemical shifts (ppm) are referred to the residual protic solvent peaks. GC mass spectrometry measurements were obtained using a Perkin Elmer Autosystem XL chromatogram and a Perkin Elmer Turbo Mass Spectrometer. Magnetic Susceptibility studies were performed using an Evans Balance (Johnson Matthey) at room temperature and variable temperature measurements were recorded at University of Edinburgh using a SQUID magnetometer in the region of 2-300 K in an applied field of 100 G (0.01 T). The magnetic moment was calculated following standard methods[2] and corrections for underlying diamagnetism were applied to data.[3]

Elemental analyses were performed at the Department of Chemistry, University of North London by Dr S. Boyer.

The reagents, 2-chloroethylamine monohydrochloride, 2-picolylamine, the aryl halides, methyl iodide, 4-(chloromethyl)styrene, 2-picolyl chloride hydrochloride, the metal dichlorides, diethylenetriamine, MAO (10%wt in toluene), 1-heptadecene, 1-nonene, 1-tridecene, 2,6- diisopropylaniline were purchased from Aldrich Chemical Co. and used without further purification (except for 2,6- diisopropylaniline[1]). *rac*-BINAP was purchased from Strem Chemical Co. Ethylene gas (Grade 3.5) was supplied from BOC. The compounds, $Pd_2(dba)_3$,[4] 2,4,6-triisopropylphenyl bromide,[5] bis(2-picolyl)amine (dpa),[6]

aminediethylenediamine(methyl)amine,[7] tris(2-picolyl)amine (tpa),[8] 2-(tosylamino)ethyl-*p*-toluenesulfonate,[9] N-tosylaziridine,[9] were prepared according to previously reported procedures. The reagents, $Pd(PPh_3)_4$,[10] phenyl(2-methoxy)boronic acid,[11] phenyl(2-methoxy,3-phenyl)boronic acid,[11, 12] phenyl(2-methoxy,5-*t*-butyl)boronic acid,[11] 2-bromo-6-acetyl-pyridine,[13] 2-bromo-6-formyl-pyridine[13] and $FeCl_2(thf)_{1.5}$[14] were prepared according to or based upon previously reported procedures. All other chemicals were obtained commercially and used without further purification.

6.2. Experimental for Chapter 2

6.2.1. Synthesis of (2-aminoethyl)(2-picolyl)amine: This preparation was carried out based on a modification of the literature procedure.[7] 2-chloroethylamine monohydrochloride (12.0 g, 103 mmol) was added in portions to an ice-cooled solution of NaOH (2M, 51.5 ml, 103 mmol). This was repeated and the contents of the two flasks (206 mmol) combined. The free 2-chloroethylamine was then added dropwise to a rapidly stirred solution of 2-picolylamine, (44.0 g, 407 mmol) in absolute ethanol (50 ml) and refluxed for 2 h. The volatiles were removed by rotary evaporation, the residue poured onto crushed ice and excess KOH pellets added. The dark orange brown solution was extracted with chloroform (3 x 100 ml). The combined extracts were dried over $MgSO_4$, filtered and taken to dryness to give an oily residue. Distillation of the residue under reduced pressure (3.0 x 10^{-1} mmHg) gave unreacted 2-(aminomethyl)pyridine (44 °C) as the first fraction followed by $(H_2NCH_2CH_2)\{(2\text{-}C_5H_4N)CH_2\}NH$ as a pale yellow liquid (84 °C). Yield: 26 % (9.10 g, 60.3 mmol). FAB mass spectrum: m/z 151 $[M]^+$. ^1H NMR ($CDCl_3$, 300 MHz): δ 1.55 (s, br, 3H, N*H*), 2.74 (m, 2H, CH_2), 2.84 (m, 2H, CH_2), 3.92 (s, 2H, PyCH_2), 7.13-7.18 (m, 1H, PyC*H*), 7.32 (d, 1H, $^3J_{H\text{-}H}$ 7.6 Hz, PyC*H*), 7.64 (dt, 1H, $^3J_{H\text{-}H}$ 7.6 Hz, $^4J_{H\text{-}H}$ 1.8 Hz, PyC*H*), 8.56 (m, 2H, PyC*H*). ^{13}C NMR ($CDCl_3$, 75.5 MHz, ^1H composite pulse decoupled): δ 41.7 (1C, *C*H_2), 50.8 (1C, *C*H_2), 55.2 (1C, Py*C*H_2), 121.9 (1C, Py*C*H), 122.2 (1C, Py*C*H), 136.2 (1C, Py*C*H), 149.0 (1C, Py*C*H), 159.8 (1C, Py*C*).

6.2.2. Syntheses of $(ArNHCH_2CH_2)\{(2\text{-}C_5H_4N)CH_2\}NH$ (LI)

(i) (Ar = 2,6-$Me_2C_6H_3$); (*N*-2,6-dimethylphenyl-2-aminoethyl)(2-picolyl)amine (LIa): An oven-dried Schlenk flask equipped with a magnetic stir bar was evacuated and backfilled with nitrogen. The flask was charged with $(H_2NCH_2CH_2)\{(2\text{-}C_5H_4N)CH_2\}NH$ (1.00 g, 6.62 mmol), 2,6-dimethylphenyl bromide (0.95 ml, 1.47 g, 7.94 mmol), $Pd_2(dba)_3$ (30 mg, 0.033 mmol), *rac*-BINAP (62 mg, 0.10 mmol), NaO^tBu (1.91 g, 19.9 mmol) and toluene (40 ml). The reaction mixture was heated to 120 °C and stirred for a period of 4 days. After cooling to

room temperature, the solvent was removed under reduced pressure to afford an oily residue. The residue was dissolved in diethyl ether (30 ml) and washed with water (3 x 30 ml) and NaCl solution (3 x 30 ml). The organic layer was separated and dried over $MgSO_4$. The volatiles were removed under reduced pressure and the residue left under vacuum at 50 °C for 24 h to give {(2,6-$Me_2C_6H_3$)$HNCH_2CH_2$}{(2-C_5H_4N)CH_2}NH (**LIa**) as a viscous red oil. Yield: 79 % (1.333 g, 5.23 mmol). ES mass spectrum: m/z 256 $[M+H]^+$. IR (nujol mull, cm^{-1}): *v* 3350 (N-H, medium), 1590 ($C=N_{pyridine}$). ^1H NMR ($CDCl_3$, 250 MHz): δ 2.20 (s, 6H, Me_o), 2.77 (t, 2H, $^3J_{H-H}$ 5.7 Hz, CH_2), 3.02 (t, 2H, $^3J_{H-H}$ 5.7 Hz, CH_2), 3.85 (s, 2H, PyCH_2), 6.70 (m, 1H, Ar*CH*), 6.88 (m, 2H, Ar*CH*), 7.06 (m, 1H, Py*CH*), 7.20 (d, 1H, $^3J_{H-H}$ 7.8 Hz, Py*CH*), 7.52 (dt, 1H, $^3J_{H-H}$ 7.8 Hz, Py*CH*), 8.50 (dd, 1H, $^3J_{H-H}$ 4.4 Hz, Py*CH*). ^{13}C NMR ($CDCl_3$, 75 MHz, ^1H composite pulse decoupled): δ 19.0 (2C, Me_o), 48.4 (1C, CH_2), 50.0 (1C, CH_2), 55.4 (1C, PyCH_2), 121.9 (1C, Py*CH*), 122.4 (1C, Py*CH*), 122.6 (1C, Ar*CH*), 129.2 (2C, Ar*CH*), 129.7 (2C, Ar*C*), 136.9 (1C, Py*CH*), 146.8 (1C, Ar*C*), 149.7 (1C, Py*CH*), 160.3 (1C, Py*C*).

(ii) (Ar = 2,4-$Me_2C_6H_3$); (*N*-2,4-dimethylphenyl-2-aminoethyl)(2-picolyl)amine (LIb): Using an analogous route to that outlined in 6.2.2(i) employing ($H_2NCH_2CH_2$){(2-C_5H_4N)CH_2}NH (1.00 g, 6.62 mmol), 2,4-dimethylphenyl bromide (1.1 ml, 1.47 g, 7.94 mmol), $Pd_2(dba)_3$ (30 mg, 0.033 mmol), *rac*-BINAP (62 mg, 0.10 mmol), NaO^tBu (1.91 g, 19.9 mmol) and toluene (40 ml) gave {(2,4 –$Me_2C_6H_3$)$HNCH_2CH_2$}{(2-C_5H_4N)CH_2}NH (**LIb**) as a viscous red oil. Yield: 77 % (1.30 g, 5.10 mmol). ES mass spectrum: m/z 256 $[M+H]^+$. IR (neat, cm^{-1}): *v* 3370 (N-H, medium), 1590 ($C=N_{pyridine}$). ^1H NMR ($CDCl_3$, 250 MHz): δ 2.05 (s, 3H, Me_p), 2.14 (s, 3H, Me_o), 2.86 (t, 2H, $^3J_{H-H}$ 6.0 Hz, CH_2), 2.86 (t, 2H, $^3J_{H-H}$ 6.0 Hz, CH_2), 3.17 (t, 2H, $^3J_{H-H}$ 6.0 Hz, CH_2), 3.85 (s, 2H, PyCH_2), 6.45 (d, 1H, $^3J_{H-H}$ 8.0 Hz, Ar*CH*), 6.82 (m, 2H, Ar*CH*), 7.05 (dt, 1H, $^3J_{H-H}$ 6.0 Hz, Py*CH*), 7.20 (d, 1H, $^3J_{H-H}$ 7.6 Hz, Py*CH*), 7.53 (dt, 1H, $^3J_{H-H}$ 7.8 Hz, $^4J_{H-H}$ 1.8 Hz, Py*CH*), 8.46 (dd, 1H, $^3J_{H-H}$ 4.6 Hz, PyCH). ^{13}C ($CDCl_3$, 75 MHz, ^1H composite pulse decoupled): δ 17.9 (1C, Me_o), 20.7 (1C, Me_p), 44.2 (1C, CH_2), 48.7 (1C, CH_2), 55.2 (1C, PyCH_2), 110.5 (1C, Ar*CH*), 122.4 (1C, Py*CH*), 122.6 (1C,

Py*C*H), 122.8 (1C, Ar*C*), 126.4 (1C, Ar*C*), 127.7 (1C, Ar*C*H), 131.3 (1C, Ar*C*H), 136.8 (1C, Py*C*H), 144.6 (1C, Ar*C*), 149.7 (1C, Py*C*H), 160.3 (1C, Py*C*).

(iii) (Ar = 2,4,6-$Me_3C_6H_2$); (*N*-2,4,6-trimethylphenyl-2-aminoethyl)(2-picolyl)amine (LIc): Using an analogous route to that outlined in 6.2.2(i) employing $(H_2NCH_2CH_2)\{(2\text{-}C_5H_4N)CH_2\}NH$ (1.00 g, 6.62 mmol), 2,4,6-trimethylphenyl bromide (1.02 ml, 1.58 g, 7.94 mmol), $Pd_2(dba)_3$ (30 mg, 0.033 mmol), *rac*-BINAP (62 mg, 0.10 mmol), NaO^tBu (1.91 g, 19.9 mmol) and toluene (40 ml) gave $\{(2,4,6\text{-}Me_3C_6H_2)HNCH_2CH_2\}\{(2\text{-}C_5H_4N)CH_2\}NH$ (**LIc**) as a viscous red oil. Yield: 75 % (1.34 g 4.97 mmol). ES mass spectrum: m/z 270 $[M+H]^+$. IR (neat, cm^{-1}): *v* 3345 (N-H, medium), 1590 ($C{=}N_{pyridine}$). ^1H NMR ($CDCl_3$, 250 MHz): δ 2.21 (s, 3H, *Me*$_p$), 2.29 (s, 6H, *Me*$_o$), 2.89 (t, 2H, $^3J_{H\text{-}H}$ 6.2 Hz, C*H*$_2$), 2.98 (t, 2H, $^3J_{H\text{-}H}$ 6.0 Hz, C*H*$_2$), 3.86 (s, 2H, PyC*H*$_2$), 6.72 (s, 2H, ArC*H*), 7.06 (m, 1H, PyC*H*), 7.25 (d, 1H, $^3J_{H\text{-}H}$ 4.4 Hz, PyC*H*), 7.55 (dt, 1H, $^3J_{H\text{-}H}$ 7.6 Hz, $^4J_{H\text{-}H}$ 1.9 Hz, PyC*H*), 8.47 (dd, 1H, $^3J_{H\text{-}H}$ 4.5 Hz, PyC*H*). ^{13}C NMR ($CDCl_3$, 75 MHz, ^1H composite pulse decoupled): δ 18.8 (2C, *Me*$_o$), 20.9 (1C, *Me*$_p$), 48.7 (1C, *C*H$_2$), 50.0 (1C, *C*H$_2$), 55.5 (1C, Py*C*H$_2$), 122.4 (1C, Py*C*H), 122.6 (1C, Py*C*H), 129.4 (2C, Ar*C*H), 130.0 (2C, Ar*C*), 131.4 (1C, Ar*C*), 136.7 (1C, Py*C*H), 144.1 (1C, Ar*C*), 149.7 (1C, Py*C*H), 160.3 (1C, Py*C*).

(iv) (Ar = 2,4,6-*i*-$Pr_3C_6H_2$); (*N*-2,4,6-triisopropylphenyl-2-aminoethyl)(2-picolyl)amine (LId): Using an analogous route to that outlined in 6.2.2(i) employing $(H_2NCH_2CH_2)\{(2\text{-}C_5H_4N)CH_2\}NH$ (1.00 g, 6.62 mmol), 2,4,6-triisopropylphenyl bromide (2.25 g, 7.94 mmol), $Pd_2(dba)_3$ (30 mg, 0.033 mmol), *rac*-BINAP (62 mg, 0.10 mmol), NaO^tBu (1.91 g, 19.9 mmol) and toluene (40 ml) gave $\{(2,4,6\text{-}i\text{-}Pr_3C_6H_2)HNCH_2CH_2\}\{(2\text{-}C_5H_4N)CH_2\}NH$ (**LId**) as a viscous red oil. Yield: 65 % (1.50 g, 4.25 mmol). ES mass spectrum: m/z 354 $[M+H]^+$. IR (neat, cm^{-1}): *v* 3355 (N-H, medium), 1590 ($C{=}N_{pyridine}$). ^1H NMR ($CDCl_3$, 250 MHz): δ 1.15 (dd, 18H, $^3J_{H\text{-}H}$ 6.9 Hz, CH*Me*$_2$), 2.69-2.97 (m, 5H), 3.24 (septet, 2H, $^3J_{H\text{-}H}$ 7.0 Hz, C*H*Me$_2$), 3.89 (s, 2H, PyC*H*$_2$), 6.85 (s, 2H, ArC*H*), 7.03-7.07 (m, 1H, PyC*H*), 7.25 (d, 2H, $^3J_{H\text{-}H}$ 7.5 Hz,

PyC*H*), 7.54 (dt, 1H, $^{3}J_{H\text{-}H}$ 6.7 Hz, $^{4}J_{H\text{-}H}$ 1.8 Hz, PyC*H*), 8.46-8.48 (m, 1H, PyC*H*). ^{13}C NMR ($CDCl_3$, 75 MHz, ^{1}H composite pulse decoupled): δ 23.1 (2C, CH*Me*$_2$), 24.1 (4C, CH*Me*$_2$), 27.7 (2C, *C*HMe$_2$), 34.0 (1C, *C*HMe$_2$), 49.8 (1C, *C*H$_2$), 51.4 (1C, *C*H$_2$), 55.2 (1C, Py*C*H$_2$), 121.4 (2C, Ar*C*H), 121.9 (1C, Py*C*H), 122.1 (1C, Py*C*H), 136.4 (1C, Py*C*H), 141.1 (1C, Ar*C*), 142.3 (2C, Ar*C*), 143.6 (1C, Ar*C*), 149.4 (1C, Py*C*H), 160.1 (1C, Py*C*).

6.2.3. Synthesis of (*N*-2,4,6-trimethylphenyl-2-aminoethyl)(2-picolyl)(methyl)amine (LII): An oven-dried Schlenk flask equipped with a magnetic stir bar was evacuated and backfilled with nitrogen. The flask was charged with **LIc** (200 mg, 0.74 mmol), K_2CO_3 (154 mg, 1.12 mmol) in MeCN (40 ml) and cooled to -10 °C, followed by the addition of MeI (0.05 ml, 0.82 mmol) in MeCN (40 ml) over the course of 1 h. The reaction mixture was warmed to rt and stirred for an additional 1 h. The reaction mixture was filtered and the solvent removed under reduced pressure to afford an oily residue. The residue was dissolved in dichloromethane (30 ml) and washed with water (3 x 30 ml). The organic layer was separated, dried over $MgSO_4$ and the volatiles were removed under reduced pressure to give a brown oil. The crude product was purified via alumina column chromatography employing ethyl acetate and hexane as the eluting solvent mixture (1:3) to give {(2,4,6-$Me_3C_6H_2$)NHCH_2CH_2}{(2-C_5H_4N)CH_2}NMe (**LII**) as a yellow oil. Yield: 63 % (132 mg, 0.47 mmol). ES mass spectrum: m/z 284 $[M+H]^+$. IR (neat, cm^{-1}): *v* 3356 (N-H, medium), 1589 (C=$N_{pyridine}$). ^{1}H NMR ($CDCl_3$, 300 MHz): δ 2.13 (s, 3H, *Me*$_p$), 2.18 (s, 6H, *Me*$_o$), 2.20 (s, 3H, N-*Me*), 2.61 (t, 2H, $^{3}J_{H\text{-}H}$ 6.0 Hz, C*H*$_2$), 3.00 (t, 2H, $^{3}J_{H\text{-}H}$ 6.0 Hz, C*H*$_2$), 3.65 (s, 2H, PyC*H*$_2$), 6.72 (s, 2H, ArC*H*), 7.07 (m, 1H, PyC*H*), 7.39 (d, 1H, $^{3}J_{H\text{-}H}$ 7.6 Hz, PyC*H*), 7.67 (dt, 1H, $^{3}J_{H\text{-}H}$ 7.5 Hz, $^{4}J_{H\text{-}H}$ 1.6 Hz, PyC*H*), 8.46 (dd, 1H, PyC*H*). ^{13}C NMR ($CDCl_3$, 75 MHz, ^{1}H composite pulse decoupled): δ 17.5 (2C, *Me*$_o$), 19.5 (1C, *Me*$_p$), 40.94 (1C, N-*Me*), 44.9 (1C, C*H*$_2$), 56.67 (1C, C*H*$_2$), 63.26 (1C, PyC*H*$_2$), 121 (1C, PyC*H*), 121.8 (1C, PyC*H*), 127.9 (2C, ArC*H*), 128.4 (2C, Ar*C*), 129.6 (1C, Ar*C*), 135.4 (1C, PyC*H*), 143.0 (1C, Ar*C*), 148.0 (1C, PyC*H*), 158.3 (1C, Py*C*).

6.2.4. Synthesis of (*N*-2,6-dimethylphenyl-2-aminoethyl)(2-picolyl)((methyl)styrene) amine (LIII): An oven-dried Schlenk flask equipped with a magnetic stir bar was evacuated and backfilled with nitrogen. The flask was charged with **LIIa** (0.667 g, 2.62 mmol), 4-(chloromethyl)styrene (0.600 g, 0.55 ml, 3.93 mmol), K_2CO_3 (1.08 g, 7.86 mmol) and acetonitrile (60 ml). The reaction mixture was heated to 80 °C and stirred for a period of 3 days. After cooling to room temperature, the reaction mixture was filtered and the solvent removed under reduced pressure to afford an oily residue. The residue was dissolved in dichloromethane (40 ml) and washed with water (3 x 40 ml). The organic layer was separated, dried over $MgSO_4$ and the volatiles were removed under reduced pressure to give a brown oil. The crude product was purified via alumina column chromatography employing ethyl acetate and hexane as the eluting solvent mixture (1:4) to give $\{(2,6\text{-}Me_2C_6H_3)NHCH_2CH_2\}\{(2\text{-}C_5H_4N)CH_2\}N(CH_2C_6H_4CH{=}CH_2)$ (**LIII**) as a yellow oil. Yield: 41 % (0. 401 g, 1.08 mmol). ES mass spectrum: m/z 372 $[M+H]^+$. IR (neat, cm^{-1}): *v* 3361 (NH, medium), 1628 (C=C), 1590 ($C{=}N_{pyridine}$). ^1H NMR ($CDCl_3$, 300 MHz): δ 2.15 (s, 6H, Me_o), 2.70 (t, 2H, $^3J_{H\text{-}H}$ 6.2 Hz, CH_2), 3.07 (t, 2H, $^3J_{H\text{-}H}$ 6.0 Hz, CH_2), 3.62 (s, 2H, PyCH_2), 3.73 (s, 2H, StyCH_2), 5.15 (d, 1H, $^3J_{H\text{-}H}$ 11 Hz, vinylCH), 5.65 (d, 1H, $^3J_{H\text{-}H}$ 17 Hz, vinylCH), 6.6-6.7 (m, 2H, Ar-CH and vinylCH), 6.87 (d, 2H, $^3J_{H\text{-}H}$ 7.6 Hz, ArCH), 7.07 (m, 1H, PyCH), 7.27 (m, 4H, ArCH), 7.4 (d, 1H, $^3J_{H\text{-}H}$ 7.9 Hz, Py-CH), 7.57 (dt, 1H, $^3J_{H\text{-}H}$ 7.6 Hz, $^4J_{H\text{-}H}$ 1.8 Hz, PyCH), 8.45 (d, 1H, $^3J_{H\text{-}H}$ 5 Hz, PyCH). ^{13}C NMR ($CDCl_3$, 75 MHz, ^1H composite pulse decoupled): δ 17.8 (2C, Me_o), 44.7 (1C, CH_2), 53.3 (1C, CH_2), 57.4 (1C, CH_2), 58.9 (1C, PyCH_2), 112.5 (1C, vinylCH_2), 120.0 (1C, PyCH), 121.0 (1C, PyCH), 122.0 (1C, ArCH), 125.2 (2C, ArCH), 127.3 (2C, ArC), 127.8 (2C, ArCH), 128.2 (2C, ArCH), 135.4 (1C, PyCH), 135.5 (1C, vinylCH) 137.3 (1C, ArC), 145.5 (1C, ArC), 147.9 (1C, PyCH), 158.5 (1C, PyC).

6.2.5. Synthesis of $(ArNHCH_2CH_2)\{(2\text{-}C_5H_4N)CH_2\}_2N$ (LIV)

(i) (Ar = 2,6-$Me_2C_6H_3$); (*N*-2,6-dimethylphenyl-2-aminoethyl)bis(2-picolyl)amine (LIVa): An oven-dried Schlenk flask equipped with a magnetic stir bar was evacuated and backfilled with nitrogen. The flask was charged with **LIa** (1.0 g, 3.92 mmol), 2-picolyl chloride hydrochloride (0.965 g, 5.88 mmol), K_2CO_3 (1.628 g, 11.8 mmol) and acetonitrile (80 ml). The reaction mixture was heated to 55 °C and stirred for a period of 3 days. After cooling to room temperature, the reaction mixture was filtered and the solvent removed under reduced pressure to afford an oily residue. The residue was dissolved in dichloromethane (50 ml) and washed with water (3 x 50 ml). The organic layer was separated, dried over $MgSO_4$ and the volatiles were removed under reduced pressure to give a brown oil. The crude product was purified via alumina column chromatography employing ethyl acetate and hexane as the eluting solvent mixture (1:4) to give $\{(2,6\text{-}Me_2C_6H_3)NHCH_2CH_2\}\{(2\text{-}C_5H_4N)CH_2\}_2N$ (**LIVa**) as a yellow oil. Yield: 35 % (0.48 g, 1.4 mmol). ES mass spectrum: m/z 347 $[M+H]^+$. IR (nujol mull, cm^{-1}): ν 3354 (N-H, medium), 1591 ($C{=}N_{pyridine}$). ^1H NMR ($CDCl_3$, 250 MHz): δ 2.2 (s, 6H, Me_o), 2.8 (t, 2H, $^3J_{H\text{-}H}$ 6 Hz, CH_2), 3.1 (t, 2H, $^3J_{H\text{-}H}$ 6 Hz, CH_2), 3.8 (s, 4H, PyCH_2), 6.68 (m, 1H, $^3J_{H\text{-}H}$ 7.56, 7.12 Hz, ArC*H*), 6.87 (d, 1H, $^3J_{H\text{-}H}$ 7.37 Hz, ArC*H*), 7.07 (m, 2H, $^3J_{H\text{-}H}$ 4.8, 6 Hz, PyC*H*), 7.42 (d, 2H, $^3J_{H\text{-}H}$ 8.1 Hz, PyC*H*), 7.6 (dt, 2H, $^3J_{H\text{-}H}$ 6, 7.8 Hz, $^4J_{H\text{-}H}$ 1.09 Hz, PyC*H*), 8.47 (dd, 2H, $^3J_{H\text{-}H}$ 4.8 Hz, $^4J_{H\text{-}H}$ 1.6 Hz, PyC*H*). ^{13}C NMR ($CDCl_3$, 75 MHz, ^1H composite pulse decoupled): δ 19.2 (2C, Me_o), 46.2 (1C, CH_2), 55.0 (1C, CH_2), 60.8 (2C, PyCH_2), 121.5 (1C, ArCH), 122.5 (2C, PyCH), 123.5 (2C, PyCH), 129.2 (2C, ArCH), 136.8 (2C, PyCH), 138.9 (2C, Ar*C*), 147.0 (1C, Ar*C*), 149.6 (2C, PyCH), 159.7 (2C, Py*C*).

(ii) (Ar = 2,4-$Me_2C_6H_3$); (*N*-2,4-dimethylphenyl-2-aminoethyl)bis(2-picolyl)amine (LIVb): Using an analogous route to that outlined in 6.2.5(i) employing **LIb** (1.0 g, 3.92 mmol), 2-picolyl chloride hydrochloride (0.965 g, 5.88 mmol), K_2CO_3 (1.628 g, 11.8 mmol) and acetonitrile (80 ml) gave $\{(2,4\text{-}Me_2C_6H_3)NHCH_2CH_2\}\{(2\text{-}C_5H_4N)CH_2\}_2N$ (**LIVb**) as a yellow oil. Yield: 38 % (0.515 g, 1.49mmol). ES mass spectrum: m/z 347 $[M+H]^+$. IR (nujol

mull, cm^{-1}): ν 3331 (N-H, medium), 1589 ($C=N_{pyridine}$). ^1H NMR ($CDCl_3$, 250 MHz): δ 2.10 (s, 3H, Me_p), 2.13 (s, 3H, Me_o), 2.83 (t, 2H, $^3J_{H-H}$ 6 Hz, CH_2), 3.12 (t, 2H, $^3J_{H-H}$ 6 Hz, CH_2), 3.79 (s, 4H, PyCH_2), 6.35 (d, 1H, $^3J_{H-H}$ 8.47 Hz, ArCH), 6.79 (m, 2H, $^3J_{H-H}$ 6 Hz, ArCH), 7.05 (t, 2H, $^3J_{H-H}$ 7, 6, 5 Hz, PyCH), 7.37 (d, 2H, $^3J_{H-H}$ 7.8 Hz, PyCH), 7.53 (dt, 2H, $^3J_{H-H}$ 7.5 Hz, $^3J_{H-H}$ 1.6 Hz, PyCH), 8.45 (d, 2H, $^3J_{H-H}$ 4.8 Hz, PyCH). ^{13}C NMR ($CDCl_3$, 75 MHz, ^1H composite pulse decoupled): δ 17.9 (1C, Me_o), 20.73 (1C, Me_p), 41.7 (1C, CH_2), 53.1 (1C, CH_2), 60.6 (2C, PyCH_2), 110.3 (1C, ArCH), 122.45 (1C, ArC), 122.5 (2C, PyCH), 123.4 (2C, PyCH), 126.1 (1C, ArC), 127.7 (1C, ArCH), 131.2 (1C, ArCH), 136.8 (2C, PyCH), 144.7 (1C, Ar-C), 149.6 (2C, PyCH), 159.8 (2C, PyC).

6.2.6. Synthesis of bis(2-picolyl)(2-aminoethyl) amine (dpea)

Prepared *via* two-step procedure:

(a) (*N*-tosyl-2-aminoethyl)bis(2-picolyl)amine. To a 3-necked round bottom flask equipped with a reflux condenser, dropping funnel and a magnetic stirrer was added dpa (19.900 g, 100 mmol) dissolved in acetonetrile (250 ml). The yellow solution was brought to reflux and N-tosylaziridine in acetonitrile (200 ml) was added dropwise over 1 h, to give a dark red solution, which was heated to reflux for an additional 5 h. The dark red solution was concentrated on a rotary evaporator and dried under reduced pressure overnight to give $(TsNHCH_2CH_2)\{(2\text{-}C_5H_4N)CH_2\}_2N$ as a dark red oil. Yield: 99 % (39.204 g, 99.0 mmol). ES mass spectrum: m/z 397 $[M+H]^+$. ^1H NMR ($CDCl_3$, 250 MHz): δ 2.36 (s, 3H, *Me*), 2.77 (t, 2H, $^3J_{H-H}$ 5.25 Hz, CH_2), 3.03 (q, 2H, $^3J_{H-H}$ 5.25 Hz, CH_2), 3.76 (s, 4H, PyCH_2), 7.16 (m, 6H, CH), 7.57 (m, 2H, $^3J_{H-H}$ 6 Hz, PyCH), 7.71 (d, 2H, $^3J_{H-H}$ 8 Hz, PyCH), 8.58 (d, 2H, $^3J_{H-H}$ 4.6 Hz, PyCH).

(b) *bis*(2-picolyl)(2-aminoethyl)amine (dpea). To (*N*-tosyl-2-aminoethyl)bis(2-picolyl)amine (39.204 g, 99.0 mmol) was added concentrated H_2SO_4 (300 ml). The dark red solution was heated at 130 °C. After 3 days the reaction mixture was cooled in an ice bath. The dropwise addition of diethyl ether (4000 ml) and absolute ethanol (3000 ml) gave a dark brown precipitate. *Caution! The brown precipitate is hydroscopic.* The brown precipitate was filtered and immediately dissolved in saturated NaOH. The organic layer was extracted by washing with chloroform, the resulting red organic phase was dried over $MgSO_4$ and concentrated on a rotary evaporator, to give $\{(2\text{-}C_5H_4N)CH_2\}_2(H_2NCH_2CH_2)N$ as a red oil. Yield: 73 % (17.449 g, 72.0 mmol). ES mass spectrum: m/z 243, $[M+H]^+$. IR (CH_2Cl_2, cm^{-1}): *v* 3360 (N-H, medium), 1590 ($C{=}N_{pyridine}$). ^1H NMR ($CDCl_3$, 250 MHz): δ 1.65 (s, 2H, N*H*$_2$), 2.67 (t, 2H, $^3J_{H\text{-}H}$ 5.7 Hz, C*H*$_2$), 2.80 (t, 2H, $^3J_{H\text{-}H}$ 5.6 Hz, C*H*$_2$), 3.85 (s, 4H, PyC*H*$_2$), 7.14 (dt, 2H, $^3J_{H\text{-}H}$ 7.5, 5 Hz, $^4J_{H\text{-}H}$ 1.4 Hz, PyC*H*), 7.49 (d, 2H, $^3J_{H\text{-}H}$ 7.75 Hz, PyC*H*), 7.65 (dt, 2H, $^3J_{H\text{-}H}$ 7.5 Hz, $^4J_{H\text{-}H}$ 1.6 Hz, PyC*H*), 8.53 (d, 2H, $^3J_{H\text{-}H}$ 5 Hz, $^4J_{H\text{-}H}$ 1.6 Hz, PyC*H*). ^{13}C NMR ($CDCl_3$, 63 MHz, ^1H composite pulse decoupled): δ 39.9 (1C, *C*H$_2$), 57.8 (1C, *C*H$_2$), 61.1 (2C, Py*C*H$_2$), 122.4 (2C, Py*C*H), 123.4 (2C, Py*C*H), 136.8 (2C, Py*C*H), 149.4 (2C, Py*C*H), 160.0 (2C, Py*C*).

6.2.7. Alternative Synthesis of $(ArNHCH_2CH_2)\{(2\text{-}C_5H_4N)CH_2\}_2N$ (LIV)

(i) (Ar = 2,6-$Me_2C_6H_3$); (*N*-2,6-dimethylphenyl-2-aminoethyl)bis(2-picolyl)amine (LIVa): An oven-dried Schlenk flask equipped with a magnetic stir bar was evacuated and backfilled with nitrogen. The flask was charged with dpea (4.00 g, 16.5 mmol), 2,6-dimethylphenyl bromide (2.42 ml, 3.36 g, 18.2 mmol), $Pd_2(dba)_3$ (32 mg, 0.034 mmol), *rac*-BINAP (64 mg, 0.11 mmol), NaO^tBu (1.982 g, 21.0 mmol) and toluene (30 ml). The reaction mixture was heated to 120 °C in an oil bath and stirred for 4 days. After cooling to room temperature the solvent was removed under reduced pressure to afford an oil residue. The residue was dissolved in diethyl ether, washed with water and saturated NaCl solution. The organic layer was separated and dried over $MgSO_4$. The volatiles were removed under reduced pressure and

the residue left under vacuum at 50 °C for 24 h to give {(2,6-$Me_2C_6H_3$)$NHCH_2CH_2$}{(2-C_5H_4N)CH_2}$_2$N (**LIVa**) as a viscous oil. Yield: 85 % (4.864 g, 14.0 mmol). ES mass spectrum: m/z 347 $[M+H]^+$. IR (nujol mull, cm^{-1}): *v* 3354 (N-H, medium), 1591 ($C=N_{pyridine}$). ^1H NMR ($CDCl_3$, 250 MHz): δ 2.2 (s, 6H, *Me*$_o$), 2.8 (t, 2H, $^3J_{H-H}$ 6 Hz, C*H*$_2$), 3.1 (t, 2H, $^3J_{H-H}$ 6 Hz, C*H*$_2$), 3.8 (s, 4H, PyC*H*$_2$), 6.68 (m, 1H, $^3J_{H-H}$ 7.56, 7.12 Hz, ArC*H*), 6.87 (d, 1H, $^3J_{H-H}$ 7.37 Hz, ArC*H*), 7.07 (m, 2H, $^3J_{H-H}$ 4.8, 6 Hz, PyC*H*), 7.42 (d, 2H, $^3J_{H-H}$ 8.1 Hz, PyC*H*), 7.6 (dt, 2H, $^3J_{H-H}$ 6, 7.8 Hz, $^4J_{H-H}$ 1.09 Hz, PyC*H*), 8.47 (dd, 2H, $^3J_{H-H}$ 4.8 Hz, $^4J_{H-H}$ 1.6 Hz, PyC*H*). ^{13}C NMR ($CDCl_3$, 63 MHz, ^1H composite pulse decoupled): δ 19.2 (2C, *Me*$_o$), 46.2 (1C, *C*H$_2$), 55.0 (1C, *C*H$_2$), 60.8 (2C, Py*C*H$_2$), 121.5 (1C, Ar*C*H), 122.5 (2C, Py*C*H), 123.5 (2C, Py*C*H), 129.2 (2C, Ar*C*H), 136.8 (2C, Py*C*H), 138.9 (2C, Ar*C*), 147.0 (1C, Ar*C*), 149.6 (2C, Py*C*H), 159.7 (2C, Py*C*).

(ii) (Ar = 2,4-$Me_2C_6H_3$); (*N*-2,4-dimethylphenyl-2-aminoethyl)bis(2-picolyl)amine (LIVb): Using an analogous route to that outlined in 6.2.7(i) employing dpea (3.68 g, 15.2 mmol), 2,4-dimethylphenyl bromide (2.5 ml, 3.36 g, 18.2 mmol), $Pd_2(dba)_3$ (28 mg, 0.030 mmol), *rac*-BINAP (61 mg, 0.10 mmol), NaO^tBu (1.90 g, 20 mmol) and toluene (30 ml) gave {(2,4-$Me_2C_6H_3$)$NHCH_2CH_2$}{(2-C_5H_4N)CH_2}$_2$N (**LIVb**) as a viscous brown oil. Yield: 74 % (4.237 g, 12.25 mmol). ES mass spectrum: m/z 347 $[M+H]^+$. IR (nujol mull, cm^{-1}): *v* 3331 (N-H, medium), 1589 ($C=N_{pyridine}$). ^1H NMR ($CDCl_3$, 250 MHz): δ 2.10 (s, 3H, *Me*$_p$), 2.13 (s, 3H, *Me*$_o$), 2.83 (t, 2H, $^3J_{H-H}$ 6 Hz, C*H*$_2$), 3.12 (t, 2H, $^3J_{H-H}$ 6 Hz, C*H*$_2$), 3.79 (s, 4H, PyC*H*$_2$), 6.35 (d, 1H, $^3J_{H-H}$ 8.47 Hz, ArC*H*), 6.79 (m, 2H, $^3J_{H-H}$ 6 Hz, ArC*H*), 7.05 (t, 2H, $^3J_{H-H}$ 7, 6, 5 Hz, PyC*H*), 7.37 (d, 2H, $^3J_{H-H}$ 7.8 Hz, PyC*H*), 7.53 (dt, 2H, $^3J_{H-H}$ 7.5 Hz, $^3J_{H-H}$ 1.6 Hz, PyC*H*), 8.45 (d, 2H, $^3J_{H-H}$ 4.8 Hz, PyC*H*). ^{13}C NMR ($CDCl_3$, 63 MHz, ^1H composite pulse decoupled): δ 17.9 (1C, *Me*$_o$), 20.73 (1C, *Me*$_p$), 41.7 (1C, *C*H$_2$), 53.1 (1C, *C*H$_2$), 60.6 (2C, Py*C*H$_2$), 110.3 (1C, Ar*C*H), 122.45 (1C, Ar*C*), 122.5 (2C, Py*C*H), 123.4 (2C, Py*C*H), 126.1 (1C, Ar*C*), 127.7 (1C, Ar*C*H), 131.2 (1C, Ar*C*H), 136.8 (2C, Py*C*H), 144.7 (1C, Ar*C*), 149.6 (2C, Py*C*H), 159.8 (2C, Py*C*).

(iii) (Ar = 2,4,6-$Me_3C_6H_2$); (*N*-2,4,6-trimethylphenyl-2-aminoethyl)bis(2-picolyl)amine (LIVc): Using an analogous route to that outlined in 6.2.7(i) employing dpea (4.00 g, 16.5 mmol), 2,4,6-trimethylphenyl bromide (3.0 ml, 3.94 g, 19.8 mmol), $Pd_2(dba)_3$ (32 mg, 0.034 mmol), *rac*-BINAP (64 mg, 0.11 mmol), NaO^tBu (1.982 g, 21.0 mmol) and toluene (30 ml) gave $\{(2,4,6\text{-}Me_3C_6H_2)NHCH_2CH_2\}\{(2\text{-}C_5H_4N)CH_2\}_2N$ (**LIVc**) as a viscous brown oil. Yield: 47 % (2.831 g, 7.86 mmol). ES mass spectrum: m/z 383 $[N+Na]^+$, 361 $[M+H]^+$. IR (nujol, cm^{-1}): *v* 3355 (N-H, medium), 1589 ($C=N_{pyridine}$). ^1H NMR ($CDCl_3$, 250 MHz): δ 2.12 (s, 9H, *Me*), 2.76 (t, 2H, $^3J_{H\text{-}H}$ 6 Hz, CH_2), 3.02 (t, 2H, $^3J_{H\text{-}H}$ 6 Hz, CH_2), 3.81 (s, 4H, PyCH_2), 6.69 (s, 2H, Ar*CH*), 7.06 (m, 2H, $^3J_{H\text{-}H}$ 7.5, 5 Hz, Py*CH*), 7.42 (d, 2H, $^3J_{H\text{-}H}$ 8 Hz, Py*CH*), 7.56 (dt, 2H, $^3J_{H\text{-}H}$ 7.5 Hz, $^4J_{H\text{-}H}$ 1.8 Hz, Py*CH*), 8.46 (d, 2H, $^3J_{H\text{-}H}$ 5 Hz, Py*CH*). ^{13}C NMR ($CDCl_3$, 63 MHz, ^1H composite pulse decoupled): δ 17.6 (2C, Me_o), 19.5 (1C, Me_p), 45.1 (1C, CH_2), 53.6 (1C, CH_2), 59.3 (2C, PyCH_2), 121.0 (2C, Py*C*H), 122.1 (2C, Py*C*H), 127.9 (2C, Ar*C*), 128.4 (2C, Ar*C*H), 129.5 (1C, Ar*C*), 135.3 (2C, Py*C*H), 142.9 (1C, Ar*C*), 148.1 (2C, Py*C*H), 158.3 (2C, Py*C*).

6.2.8. Syntheses of $[\{dpa\}FeCl(\mu\text{-}Cl)]_2$ (1) and $[\{dpa\}_2Fe][Cl]_2$ (2):

(a) An oven-dried Schlenk flask equipped with a magnetic stir bar was evacuated and backfilled with nitrogen. The flask was charged with $FeCl_2$ (60 mg, 0.47 mmol) in *n*-butanol (10 ml) at 90 °C and a solution of dpa (94 mg, 0.47 mmol) in *n*-butanol was introduced to form a yellow solution. After being stirred at 90 °C for 1 h, the reaction was allowed to cool to room temperature. The reaction mixture was concentrated and hexane was added to induce precipitation of $[\{dpa\}FeCl(\mu\text{-}Cl)]_2$ (**1**) as a yellow solid. The suspension was stirred overnight, filtered, washed with hexane (2 x 30 ml) and dried under reduced pressure. Recrystallisation from slow cooling of a hot acetonitrile solution or dichloromethane at rt gave yellow crystals yellow crystals of **1** suitable for single crystal X-ray structure determination. Yield: 70 % (120 mg, 0.18 mmol).

(b) An oven-dried Schlenk flask equipped with a magnetic stir bar was evacuated and backfilled with nitrogen. The flask was charged with $FeCl_2$ (60 mg, 0.47 mmol) in *n*-butanol (10 ml) at 90 °C and a solution of dpa (140 mg, 0.71 mmol) in *n*-butanol was introduced to form an orange solution. After being stirred at 90 °C for 1 h, the reaction was allowed to cool to room temperature. The reaction mixture was concentrated and hexane was added to induce precipitation of a mixture of $[\{dpa\}FeCl(\mu\text{-}Cl)]_2$ (**1**) and $[\{dpa\}_2Fe][Cl]_2$ (**2**) as an orange solid. The suspension was stirred overnight, filtered, washed with hexane (2 x 30 ml) and dried under reduced pressure. Recrystallisation from slow cooling of a hot acetonitrile solution or dichloromethane at rt gave yellow crystals of **1** (40 %) and red crystals of **2** (30 %) suitable for single crystal X-ray structure determination.

(c) An oven-dried Schlenk flask equipped with a magnetic stir bar was evacuated and backfilled with nitrogen. The flask was charged with $FeCl_2$ (60 mg, 0.47 mmol) in *n*-butanol (10 ml) at 90 °C and a solution of dpa (187 mg, 0.94 mmol) in *n*-butanol was introduced to form a red solution. After being stirred at 90 °C for 1 h, the reaction was allowed to cool to room temperature. The reaction mixture was concentrated and hexane was added to induce precipitation of $[\{dpa\}_2Fe][Cl]_2$ (**2**) as a red solid. The suspension was stirred overnight, filtered, washed with hexane (2 x 30 ml) and dried under reduced pressure. Recrystallisation from slow cooling of a hot acetonitrile solution gave red crystals of **2** suitable for single crystal X-ray structure determination. Yield: 91 % (225 mg, 0.43 mmol).

6.2.9. Syntheses of $[\{dpa\}CoCl(\mu\text{-}Cl)]_2$ (3) and $[\{dpa\}_2Co][Cl]_2$ (4):

(a) Using an analogous procedure and molar quantities of reagents as above in 6.2.8a employing dpa (100 mg, 0.5 mmol) and $CoCl_2$ (65 mg, 0.5 mmol) gave $[\{dpa\}CoCl(\mu\text{-}Cl)]_2$ (**3**) as a purple solid. Yield: 75 % (125 mg, 0.19 mmol).

(b) Using an analogous procedure and molar quantities of reagents as above in 6.2.8c employing dpa (242 mg, 1.56 mmol) and $CoCl_2$ (100 mg, 0.78 mmol) gave [{dpa}CoCl][Cl]$_2$ (**4**) as a blue solid. Recrystallisation from a hot acetonitrile solution gave golden crystals of **4** suitable for single crystal X-ray structure determination. Yield: 50 % (205 mg, 0.39 mmol).

6.2.10. Synthesis of [{tpa}$MnCl_2$] (5): An oven-dried Schlenk flask equipped with a magnetic stir bar was evacuated and backfilled with nitrogen. The flask was charged with $MnCl_2$ (40 mg, 0.32 mmol) in *n*-butanol (10 ml) at 90 °C and tpa (87 mg, 0.30 mmol) was added to form a white solution. After being stirred at 90 °C for 1 h, the reaction was allowed to cool to room temperature. The reaction mixture was concentrated and hexane added to induce precipitation of [{tpa}$MnCl_2$] (**5**) as a white solid. The suspension was stirred overnight, filtered, washed with hexane (2 x 30 ml) and dried under reduced pressure. Layering of an acetonitrile solution of **5** with hexane gave clear crystals of **5** suitable for single crystal X-ray structure determination. Yield: 75 % (100 mg, 0.24 mmol).

6.2.11. Synthesis of [{tpa}$FeCl_2$] (6): Using an analogous procedure and molar ratios of reagents as above in 6.2.10 employing tpa (70 mg, 0.24 mmol) and $FeCl_2$ (30 mg, 0.24 mmol), gave [{tpa}$FeCl_2$] (**6**) as an orange powder. Recrystallisation from a hot acetonitrile gave orange crystals of **6** suitable for single crystal X-ray structure determination. Yield: 81% (91 mg, 0.23 mmol).

6.2.12. Synthesis of [{tpa}$CoCl_2$] (7) and [{tpa}CoCl][Cl] (8): Using an analogous procedure and molar ratios of reagents as above in 6.2.10 employing tpa (79 mg, 0.27 mmol) and $CoCl_2$ (35 mg, 0.27 mmol), gave a mixture of [{tpa}$CoCl_2$] (**7**) and [{tpa}CoCl][Cl] (**8**) as a blue powder. Recrystallisation from a hot acetonitrile solution gave dark green crystals of **7** and purple crystals of **8** suitable for single crystal X-ray structure determination. Yield **7**: 41% (46 mg, 0.11 mmol). Yield **8**: 34 % (38 mg, 0.09 mmol).

6.2.13. Synthesis of [{tpa}CoCl]$_2$[CoCl$_4$] (9): An oven-dried Schlenk flask equipped with a magnetic stir bar was evacuated and backfilled with nitrogen. The flask was charged with 1.5 equivalents of $CoCl_2$ (50 mg, 0.41 mmol) in *n*-butanol (10 ml) at 90 °C and tpa (79 mg, 0.27 mmol) was introduced to form a blue solution. After being stirred at 90 °C for 1 h, the reaction was allowed to cool to room temperature. The reaction mixture was concentrated and hexane added to induce precipitation of [{tpa}CoCl]$_2$[CoCl$_4$] (**9**) as a blue solid. The suspension was stirred overnight, filtered, washed with hexane (2 x 30 ml) and dried under reduced pressure. Recrystallisation from a hot acetontrile solution gave blue crystals of **9** suitable for single crystal X-ray structure determination. Yield: 78 % (75 mg, 0.18 mmol).

6.2.14. Synthesis of [{(ArHNCH$_2$CH$_2$)((2-C$_5$H$_4$N)CH$_2$)NH}FeCl$_2$]n (10)

(i) (n = 1, Ar = 2,6-Me$_2$C$_6$H$_3$); 10a: An oven-dried Schlenk flask equipped with a magnetic stir bar was evacuated and backfilled with nitrogen. The flask was charged with $FeCl_2$ (36 mg, 0.28 mmol) in *n*-butanol (5 ml) at 90 °C and a solution of **LIa** (71 mg, 0.28 mmol) in *n*-butanol was introduced to form a yellow solution. After being stirred at 90 °C for 1 h, the reaction was allowed to cool to room temperature. The reaction mixture was concentrated and hexane added to induce precipitation of [{**LIa**}FeCl$_2$] (**10a**) as a yellow powder. The suspension was stirred overnight, filtered, washed with hexane (2 x 30 ml) and dried under reduced pressure. Yield: 77 % (84 mg, 0.22 mmol). Recrystallisation from hot acetonitrile gave golden crystals of **10a** suitable for single crystal X-ray structure determination.

(ii) (n = 1, Ar = 2,4-Me$_2$C$_6$H$_3$); 10b: Using an analogous procedure and molar quantities of reagents as above in 6.2.14(i) employing **LIb** (64 mg, 0.28 mmol) and $FeCl_2$ (32 mg, 0.25 mmol), in *n*-butanol gave [{**LIb**}FeCl$_2$] (**10b**) as a yellow powder. Yield 75 % (72 mg, 0.19 mmol).

(iii) (n = 2, Ar = 2,4,6-$Me_3C_6H_2$); 10c: Using an analogous procedure and molar quantities of reagents as above in 6.2.14(i) employing **LIc** (75 mg, 0.28 mmol) and $FeCl_2$ (36 mg, 0.28 mmol), gave [{**LIc**}FeCl(μ-Cl)]$_2$ (**10c**) as a yellow-brown powder. Layering of an acetonitrile solution of **10c** with hexane gave golden crystals of **10c** suitable for single crystal X-ray structure determination. Yield: 71 % (79 mg, 0.10 mmol).

6.2.15. Synthesis of [{(ArNHCH$_2$CH$_2$)((2-C$_5$H$_4$N)CH$_2$)NH}CoCl$_2$] (11)

(i) (Ar = 2,6-$Me_2C_6H_3$); 11a: Using an analogous procedure and molar quantities of reagents as above in 6.2.14(i) employing **LIa** (100 mg, 0.39 mmol) and $CoCl_2$ (51 mg, 0.39 mmol), gave [{**LIa**}$CoCl_2$] (**11a**) as a green solid. The suspension was stirred overnight, filtered, washed with hexane (2 x 30 ml) and dried under reduced pressure. Layering of an acetonitrile solution of **11a** with hexane gave dark blue crystals of **11a** suitable for single crystal X-ray structure determination. Yield 80 % (119 mg, 0.31 mmol).

(ii) (Ar = 2,4-$Me_2C_6H_3$); 11b: Using an analogous procedure and molar quantities of reagents as above in 6.2.14(i) employing **LIb** (100 mg, 0.39 mmol) and $CoCl_2$ (51 mg, 0.39 mmol), gave [{**LIb**}$CoCl_2$] (**11b**) as a green powder. Yield 85 % (127 mg, 0.33 mmol).

(iii) (Ar = 2,4,6-$Me_3C_6H_2$); 11c: Using an analogous procedure and molar quantities of reagents as above in 6.2.14(i) employing **LIc** (105 mg, 0.39 mmol) and $CoCl_2$ (51 mg, 0.39 mmol), gave [{**LIc**}$CoCl_2$] (**11c**) as a green powder. Layering of an acetonitrile solution of **11c** with hexane gave dark blue crystals of **11c** suitable for single crystal X-ray structure determination. Yield 75 % (115 mg, 0.29 mmol).

(iv) (Ar = 2,4,6-*i*-$Pr_3C_6H_2$); 11d: Using an analogous procedure and molar quantities of reagents as above in 6.2.14(i) employing **LId** (150 mg, 0.39 mmol) and $CoCl_2$ (51 mg, 0.39 mmol), gave [{**LId**}$CoCl_2$] (**11d**) as a pale green powder. Yield 60 % (118 mg, 0.23 mmol).

6.2.16. Synthesis of [{((2,4,6-$Me_3C_6H_2$)NHCH_2CH_2)((2-C_5H_4N)CH_2)NMe}$CoCl_2$] (12): An oven-dried Schlenk flask equipped with a magnetic stir bar was evacuated and backfilled with nitrogen. The flask was charged with $CoCl_2.6H_2O$ (66 mg, 0.28 mmol) in THF (5 ml) at rt and **LII** (80 mg, 0.28 mmol) was introduced to form a purple solution. After being stirred at rt for 24 h, the reaction mixture was concentrated and hexane added to induce precipitation of [{**LII**}$CoCl_2$] (**12**) as a purple solid. The suspension was stirred overnight, filtered, washed with hexane (2 x 30 ml) and dried under reduced pressure. Yield: 72 % (87 mg, 0.21 mmol). Recrystallisation from hot acetonitrile gave purple crystals of **12** suitable for single crystal X-ray structure determination.

6.2.17. Synthesis of [{((2,6-$Me_2C_6H_3$)NHCH_2CH_2)((2-C_5H_4N)CH_2)N($CH_2C_6H_4CH=CH_2$)}$CoCl_2$] (13): An oven-dried Schlenk flask equipped with a magnetic stir bar was evacuated and backfilled with nitrogen. The flask was charged with $CoCl_2.6H_2O$ (22 mg, 0.09 mmol) in THF (5 ml) at rt and **LIII** (33 mg, 0.09 mmol) was introduced to form a blue solution. After being stirred at rt for 24 h, the reaction mixture was concentrated and hexane added to induce precipitation of [{**LIII**}$CoCl_2$] (**13**) as a blue solid. The suspension was stirred overnight, filtered, washed with hexane (2 x 30 ml) and dried under reduced pressure. Yield: 65 % (30 mg, 0.06 mmol). IR (neat, cm^{-1}): ν 1629 (C=C).

6.2.18. Synthesis of [{(ArNHCH_2CH_2){(2-C_5H_4N)CH_2}$_2$N}$MnCl_2$]$_n$ (14)

(i) (n = 2, Ar = 2,6-$Me_2C_6H_3$); 14a: An oven-dried Schlenk flask equipped with a magnetic stir bar was evacuated and backfilled with nitrogen. The flask was charged with $MnCl_2$ (76 mg, 0.60 mmol) in *n*-butanol (10 ml) at 90 °C and **LIVa** (208 mg, 0.60 mmol) was introduced to form a yellow solution. After being stirred at 90 °C for 1 h, the reaction was allowed to cool to room temperature. The reaction mixture was concentrated and hexane added to induce precipitation of [{**LIVa**}MnCl(μ-Cl)]$_2$ (**14a**) as a white solid. The suspension was stirred overnight, filtered, washed with hexane (2 x 30 ml) and dried under reduced pressure.

Layering of an acetonitrile solution of **14a** with hexane gave clear crystals of **14a** suitable for single crystal X-ray structure determination. Yield: 71 % (198 mg, 0.21 mmol).

(ii) (n = 1, Ar = 2,4-$Me_2C_6H_3$); 14b: Using an analogous procedure and molar ratios of reagents as above in 6.2.18(i) employing **LIVb** (194 mg, 0.56 mmol) and $MnCl_2$ (70 mg, 0.56 mmol), gave [{**LIVb**}$MnCl_2$] (**14b**) as a white powder. Layering of an acetonitrile solution of **14b** with hexane gave clear crystals of **14b** suitable for single crystal X-ray structure determination. Yield: 65 % (170 mg, 0.36 mmol).

(iii) (n = 2, Ar = 2,4,6-$Me_3C_6H_2$); 14c: Using an analogous procedure and molar ratios of reagents as above in 6.2.18(i) employing **LIVc** (100 mg, 0.28 mmol) and $MnCl_2$ (35 mg, 0.28 mmol), gave [{**LIVc**}$MnCl(\mu\text{-}Cl)]_2$ (**14c**) as a white powder. Yield: 84 % (115 mg, 0.12 mmol).

6.2.19. Synthesis of [{(ArNHCH$_2$CH$_2$){(2-C_5H_4N)CH$_2$}$_2$N}FeCl$_2$] (15)

(i) (Ar = 2,6-$Me_2C_6H_3$); 15a: Using an analogous procedure and molar ratios of reagents as above in 6.2.18(i) employing **LIVa** (59 mg, 0.17 mmol) and $FeCl_2$ (22 mg, 0.17 mmol), gave [{**LIVa**}$FeCl_2$] (**15a**) as a yellow powder. Layering of an acetonitrile solution of **15a** with hexane gave yellow crystals of **15a** on prolonged standing suitable for X-ray structure determination. Yield: 65% (57 mg, 0.11 mmol).

(ii) (Ar = 2,4-$Me_2C_6H_3$); 15b: Using an analogous procedure and molar ratios of reagents as above in 6.2.18(i) employing **LIVb** (138 mg, 0.40 mmol) and $FeCl_2$ (50 mg, 0.40 mmol), gave [{**LIVb**}$FeCl_2$] (**15b**) as a yellow powder. Recrystallisation from a hot acetonitrile solution gave yellow crystals of **15b** suitable for single crystal X-ray structure determination upon cooling to room temperature. Yield: 79 % (151 mg, 0.32 mmol).

(iii) (Ar = 2,4,6-$Me_3C_6H_2$); 15c: Using an analogous procedure and molar ratios of reagents as above in 6.2.18(i) employing **LIVc** (140 mg, 0.40 mmol) and $FeCl_2$ (50 mg, 0.4 mmol), gave [{**LIVc**}$FeCl_2$] (**15c**) as a yellow powder. Yield: 87 % (170 mg, 0.18 mmol).

Table 1 Elemental analysis results for complexes **1–15**

Compound	Microanalysis (%)[a]		
	C	H	N
$C_{24}H_{26}N_6Fe_2Cl_4$ (**1**)	44.15 (44.21)	3.95 (4.02)	12.87 (12.89)
$C_{24}H_{26}N_6FeCl_2$ (**2**)	54.88 (54.95)	4.99 (4.94)	16.00 (15.90)
$C_{24}H_{26}N_6CoCl_2$ (**4**)	54.34 (54.56)	4.96 (4.96)	15.81 (15.91)
$C_{18}H_{18}N_4MnCl_2$ (**5**)	52.35 (51.94)	4.35 (4.36)	13.48 (13.46)
$C_{18}H_{18}N_4FeCl_2$ (**6**)	51.97 (51.8)	4.39 (4.32)	13.3% (13.43)
$C_{18}H_{18}N_4CoCl_2$ (**7**)	51.31 (51.45)	4.25 (4.32)	13.27 (13.33)
$C_{18}H_{18}N_4CoCl_2$ (**8**)	51.39 (51.45)	4.40 (4.32)	13.40 (13.33)
$C_{36}H_{36}N_8Co_3Cl_6$ (**9**)	44.48 (44.57)	3.82 (3.74)	11.51 (11.55)
$C_{16}H_{21}N_3FeCl_2$ (**10a**)	49.65 (50.29)	5.62 (5.53)	10.62 (10.98)
$C_{16}H_{21}N_3FeCl_2$ (**10b**)	49.97 (50.29)	5.41 (5.53)	10.79 (10.98)
$C_{34}H_{44}N_6Fe_2Cl_4$ (**10c**)	51.59 (51.68)	5.51 (5.61)	10.77 (10.63)
$C_{16}H_{21}N_3CoCl_2$ (**11a**)	50.01 (49.89)	5.61 (5.49)	10.80 (10.91)
$C_{16}H_{21}N_3CoCl_2$ (**11b**)	49.97 (49.89)	5.55 (5.49)	10.73 (10.91)
$C_{17}H_{23}N_3CoCl_2.CH_3CN$ (**11c**)	51.84 (51.83)	5.97 (5.95)	12.61 (12.73)
$C_{44}H_{52}N_8Mn_2Cl_4$ (**14a**)	55.81 (55.95)	5.37 (5.55)	11.88 (11.86)
$C_{22}H_{26}N_4MnCl_2$ (**14b**)	55.73 (55.95)	5.67 (5.55)	11.67 (11.86)

$C_{22}H_{26}N_4FeCl_2$ (**15a**)	55.67 (55.84)	5.46 (5.54)	12.00 (11.84)
$C_{22}H_{26}N_4FeCl_2$ (**15b**)	55.80 (55.84)	5.59 (5.54)	11.67 (11.84)

[a] calculated values in parentheses.

Table 2 FAB MS, IR and rt magnetic moment data for complexes **1-15**

Compound[a]	FAB mass spectrum (m/z)	ν(N-H) (cm^{-1})[b]	ν(C=$N_{pyridine}$) (cm^{-1})[b]	μ_{eff} (BM)
$C_{24}H_{26}N_6Fe_2Cl_4$ (**1**)	615 $[M-Cl]^+$, 290 $[M/2-Cl]^+$	3238w	1601	7.4[d]
$C_{24}H_{26}N_6FeCl_2$ (**2**)	489 $[M-Cl]^+$, 453$[M-2Cl-H]^+$	-	1604	1.17[c] 0.98[d]
$C_{24}H_{26}N_6Co_2Cl_4$ (**3**)	621 $[M-Cl]^+$, 292 $[M/2-Cl]^+$	3242w	1606	5.73
$C_{24}H_{26}N_6CoCl_2$ (**4**)	492 $[M]^+$, 456 $[M-2Cl-H]^+$	-	1603	4.44[c]
$C_{18}H_{18}N_4MnCl_2$ (**5**)	415 $[M]^+$, 380 $[M-Cl]^+$	-	1601	5.52[c]
$C_{18}H_{18}N_4FeCl_2$ (**6**)	417 $[M]^+$, 381 $[M-Cl]^+$	-	1602	4.82[c] 5.07[d]
$C_{18}H_{18}N_4CoCl_2$ (**7**)	384 $[M-Cl]^+$	-	1605	4.39[c]
$C_{18}H_{18}N_4CoCl_2$ (**8**)	384 $[M-Cl]^+$	-	1608	4.10[c]
$C_{36}H_{36}N_8Co_3Cl_6$ (**9**)	384 $[M-Cl]^+$	-	1608	3.70[c]
$C_{16}H_{21}N_3FeCl_2$ (**10a**)	729 $[2M-Cl]^+$, 381 $[M]^+$ 347 $[M-Cl]^+$	3238w	1605	4.89[c]
$C_{16}H_{21}N_3FeCl_2$ (**10b**)	729 $[2M-Cl]^+$, 381 $[M]^+$, 346 [M-Cl]	3234w	1605	4.95[c]
$C_{34}H_{44}N_6Fe_2Cl_4$ (**10c**)	755 $[M-Cl]^+$, 395 $[M/2]^+$, 360 $[M/2-Cl]^+$	3188w	1605	7.76[d]
$C_{16}H_{21}N_3CoCl_2$ (**11a**)	733 $[2M-Cl]^+$, 384 $[M]^+$, 349 $[M-Cl]^+$	3227w	1607	3.80[c]
$C_{16}H_{21}N_3CoCl_2$ (**11b**)	733 $[2M-Cl]^+$, 384 $[M]^+$, 349 $[M-Cl]^+$	3218w	1609	4.40[c]
$C_{17}H_{23}N_3CoCl_2.CH_3CN$ (**11c**)	763 $[2M-Cl]^+$, 398 $[M]^+$,	3223w	1608	3.70[c]

	363 $[M\text{-}Cl]^+$			
$C_{23}H_{35}N_3CoCl_2$ (**11d**)	931 $[2M\text{-}Cl]^+$, 483 $[M]^+$, 447 $[M\text{-}Cl]^+$	3218w	1610	3.82[c]
$C_{18}H_{25}N_3CoCl_2$ (**12**)	789 $[2M\text{-}Cl]^+$, 412 $[M]^+$, 377 $[M\text{-}Cl]^+$	3278w	1606	4.09[c]
$C_{25}H_{29}N_3CoCl_2$ (**13**)	967 $[2M\text{-}Cl]^+$ 465 $[M\text{-}Cl]^+$	3263w	1607	4.16[c]
$C_{44}H_{52}N_8Mn_2Cl_4$ (**14a**)	909 $[M\text{-}Cl]^+$, 436 $[M/2\text{-}Cl]^+$	3312w 3261w	1603	8.04[c]
$C_{22}H_{26}N_4MnCl_2$ (**14b**)	909 $[2M\text{-}Cl]^+$, 436 $[M\text{-}Cl]^+$	3311w 3261w	1602	5.46[c]
$C_{46}H_{56}N_8Mn_2Cl_4$ (**14c**)	937 $[M\text{-}Cl]^+$, 450 $[M/2\text{-}Cl]^+$	3343w 3274w	1604	8.50[c]
$C_{22}H_{26}N_4FeCl_2$ (**15a**)	909 $[2M\text{-}Cl]^+$ 472 $[M]^+$ 437 $[M\text{-}Cl]^+$	3238w	1604	6.2[d]
$C_{22}H_{26}N_4FeCl_2$ (**15b**)	910 $[2M\text{-}Cl]^+$, 472 $[M]^+$, 437 $[M\text{-}Cl]^+$	3279w	1603	5.22[d]
$C_{23}H_{28}N_4FeCl_2$ (**15c**)	939 $[2M\text{-}Cl]^+$, 487 $[M]^+$, 452 $[M\text{-}Cl]^+$	3257w	1604	4.96[c]

[a] Molecular Formula obtained from elemental analysis with the exception of **3**, **11d**, **12**, **13**, **14c** and **15c**; [b] Recorded in the solid state; [c] Analysed using an Evans Balance; [d] Analysed using a SQUID.

Table 3 ^{1}H NMR resonance assignments for complexes **1, 6-11** and **15** in CD_3CN at rt

Compound	^{1}H NMR chemical shifts (ppm), relaxation times (T_1) and assignment
1	116.5 (poor data set 0.4 ms, PyCH_α), 107.0 (1.3 ms, NH), 70.8 (1.1 ms, CH_2), 54.7 (10.1 ms, PyCH_β), 51.8 (9.1 ms, PyC$H_{\beta'}$), 7.8 (PyCH_γ)
3	122.8 (1.3 ms, PyCH_α), 118.0 (1.9 ms, NH), 110.6 (2.0 ms, CH_2), 54.5 (30.4 ms, PyCH_β), 43.1 (19.7 ms, PyC$H_{\beta'}$), -0.9 (PyCH_γ)
6	127.8 (poor data set 0.5 ms, PyCH_α), 50.5 (9.8 ms, PyCH_β), 45.8 (8.1 ms, PyC$H_{\beta'}$), 24.5 (25.0 ms, PyCH_γ), -10 to 10 (very broad, CH_2)
7	130.8 (poor data set 0.6 ms, PyCH_α), 105.3 (1.1 ms, CH_2), 58.3 (17.9 ms, PyCH_β), 46.2 (10.0 ms, PyC$H_{\beta'}$), -2.7 (29.3 ms, PyCH_γ)
8	130.8 (poor data set 0.6 ms, PyCH_α), 105.2 (1.1 ms, CH_2), 58.3 (16.2 ms, PyCH_β), 46.0 (10.6 ms, PyC$H_{\beta'}$), -2.6 (30.2 ms, PyCH_γ)
9	131.1 (poor data set 0.5 ms, PyCH_α), 104.3 (1.0 ms, CH_2), 59.3 (16.6 ms, PyCH_β), 45.4 (9.5

	ms, Py$CH_{\beta'}$), -3.2 (22.7 ms, PyCH_{γ})
10a	130.4 (poor data set 65.6 ms, PyCH_{α}), 124.1 (3.8 ms, N*H*), 104.9 (0.96 ms, CH_2), 80.9 (0.73 ms, CH_2), 62.9 (0.9 ms, CH_2), 58.8 (16.4 ms, PyCH_{β}), 57.4 (14.6 ms, Py$CH_{\beta'}$), 15. 8 (37.1 ms, PyCH_{γ}), 12.3 (34.2 ms, ArCH_m), 6.6 (2.0 ms, ArMe_o), -5.4 (poor data set 143 ms, ArCH_p), -15.01 (15.3 ms, N*H*)
10c	129.6 (0.9 ms, PyCH_{α}), 120.0 (1.9 ms, N*H*), 108.1 (1.7 ms, CH_2), 82.4 (1.1 ms, CH_2), 63.9 (0.7 ms, CH_2), 58.6 (13.2 ms, PyCH_{β}), 56.6 (11.2 ms, Py$CH_{\beta'}$), 16.8 (90.3 ms, PyCH_{χ}), 15.7 (29.1 ms, ArMe_p), 11.6 (27.8 ms, ArCH_m), 7.39 (2.5 ms, ArMe_o), -12.74 (4.0 ms, N*H*)
11a	113.8 (4.1 ms, PyCH_{α}), 110.1 (1.0 ms, N*H*), 97.0 (0.8 ms, CH_2), 87.3 (1.1 ms, CH_2), 45.7 (15.9 ms, PyCH_{β}), 42.5 (25.9 ms, Py$CH_{\beta'}$), 13.5 (2.9 ms, CH_2), 11.8 (43.2 ms, ArCH_m), -3.6 (poor data set 52.8 ms, PyCH_{χ}), -9.1 (poor data set 3588 s, ArCH_p), -14.1 (poor data set 5.3 ms, ArMe_o), -40 (N*H*)
11c	116.7(9.3 ms, PyCH_{α}), 104.6 (1.5 ms, N*H*), ≈ 90 (CH_2), 86.9 (0.9 ms, CH_2), 46.6 (15.0 ms, PyCH_{β}), 44.0 (τ_1 23.2 ms, Py$CH_{\beta'}$), 16.4 (poor data set 135.4 ms, ArMe_p), 12.5 (45.3 ms, ArCH_m), -3.0 (52.6 ms, PyCH_{χ}), -11.8 (2.2ms, ArMe_o)
15a	120.2 (poor data set 32.6 ms, PyCH_{α}), 73.5 (1.3 ms, CH_2), 51.9 (11.4 ms, PyCH_{β}), 51.1 (9.3 ms, Py$CH_{\beta'}$), 28.7 (1.0 ms, CH_2), 19.3 (26.3 ms, PyCH_{γ}), 14.5 (31.9 ms, ArCH_m), 12.2 (1.7 ms, CH_2), 9.7 (3.1 ms, ArMe_o), 0.62 (ArCH_p), -42.5 (poor data set 15.2 ms, N*H*)
15b	139.1 (0.5 ms, PyCH_{α}), 53.0 (11.7 ms, PyCH_{β}), 45.5 (poor data set 7.2 ms, Py$CH_{\beta'}$), 27.6 (37.9 ms, PyCH_{γ}), 21.9 (poor data set 117 ms, ArCH_m), 19.1 (2.0 ms, ArMe_p), 16.1 (poor data set 52.3 ms, ArMe_o), 15.1 (29.6 ms, ArCH_o), -3.4 (poor data set 38.9 ms, N*H*)

6.3. Experimental for Chapter 3

6.3.1. Syntheses of $(ArNHCH_2CH_2)_2NH$ (LV)

(i) (Ar = 2,6-$Me_2C_6H_3$); bis(*N*-*N*-2,6-dimethylphenyl-2-aminoethyl)amine (LVa): An oven-dried Schlenk flask equipped with a magnetic stir bar was evacuated and backfilled with nitrogen. The flask was charged with $(H_2NCH_2CH_2)_2NH$ (1.06 g, 10.3 mmol), 2,6-dimethylphenyl bromide (2.74 ml, 3.81 g, 20.6 mmol), $Pd_2(dba)_3$ (47 mg, 0.052 mmol), *rac*-BINAP (96 mg, 0.155 mmol), $NaOBu^t$ (2.97 g, 30.9 mmol) and toluene (40 ml). The reaction mixture was heated to 120 °C and stirred for a period of 4 days. After cooling to room temperature, the solvent was removed under reduced pressure to afford an oily residue. The residue was dissolved in diethyl ether (30 ml) and washed with water (3 x 30 ml) and saturated NaCl solution (3 x 30 ml). The organic layer was separated and dried over $MgSO_4$. The solvent was removed under reduced pressure and the residue left under vacuum at 50 °C for 24 h to give $\{(2,6\text{-}Me_2C_6H_3)HNCH_2CH_2\}_2NH$ (**LVa**) as a viscous red oil. Yield: 75 % (2.40 g, 7.73 mmol). ES mass spectrum: m/z 312 $[M+H]^+$. IR (nujol mull, cm^{-1}): *v* 3358 (N-H, medium). ^1H NMR ($CDCl_3$, 300 MHz): δ 2.22 (s, 12H, Me_o), 2.76 (t, 4H, $^3J_{H\text{-}H}$ 5.8 Hz, CH_2), 3.00 (t, 4H, $^3J_{H\text{-}H}$ 6 Hz, CH_2), 6.72 (t, 2H, $^3J_{H\text{-}H}$ 7.6 Hz, $ArCH_p$), 6.89 (d, 4H, $^3J_{H\text{-}H}$ 7.3 Hz, $ArCH_m$). ^{13}C NMR ($CDCl_3$, 75 MHz, ^1H composite pulse decoupled): δ 18.7 (4C, Me_o), 48.3 (2C, CH_2), 50.1 (2C, CH_2), 121.8 (2C, $ArCH_p$), 128.9 (4C, $ArCH_m$), 129.4 (4C, ArC), 146.4 (2C, ArC).

(ii) (Ar = 2,4,6-$Me_3C_6H_2$); bis(*N*-*N*-2,4,6-trimethylphenyl-2-aminoethyl)amine (LVb): Using an analogous route to that outlined in 6.3.1(i) employing $(H_2NCH_2CH_2)_2NH$ (1.06 g, 10.3 mmol), 2,4,6-trimethylphenyl bromide (3.15 ml, 4.10 g, 20.6 mmol), $Pd_2(dba)_3$ (30 mg, 0.033 mmol), *rac*-BINAP (62 mg, 0.10 mmol), NaO^tBu (1.91 g, 19.9 mmol) and toluene (40 ml) gave $\{(2,4,6\text{-}Me_3C_6H_2)HNCH_2CH_2\}_2NH$ (**LVb**) as a viscous red oil. Yield: 73 % (2.444 g, 7.52 mmol). ES mass spectrum: m/z 340 $[M+H]^+$. IR (neat, cm^{-1}): *v* 3359 (N-H, medium). ^1H NMR ($CDCl_3$, 300 MHz): δ 2.13 (s, 6H, Me_p), 2.18 (s, 12H, Me_o), 2.67 (br s, 3H, NH),

2.76 (t, 4H, $^3J_{H-H}$ 6 Hz, CH_2), 2.95 (t, 4H, $^3J_{H-H}$ 6 Hz, CH_2), 6.72 (s, 4H, ArCH_m). ^{13}C NMR ($CDCl_3$, 75 MHz, ^{1}H composite pulse decoupled): δ 18.5 (4C, Me_o), 20.7 (2C, Me_p), 48.5 (2C, CH_2), 50.1 (2C, CH_2), 129.5 (4C, ArCH_m), 129.8 (4C, Ar*C*), 131.0 (2C, Ar*C*), 143.7 (2C, Ar*C*).

(iii) (Ar = 2,4-$Me_2C_6H_3$); bis(*N*-*N*-2,4-dimethylphenyl-2-aminoethyl)amine (LVc): Using an analogous route to that outlined in 6.3.1(i) employing $(H_2NCH_2CH_2)_2NH$ (1.06 g, 10.3 mmol), 2,4-dimethylphenyl bromide (2.78 ml, 3.81 g, 20.6 mmol), $Pd_2(dba)_3$ (47 mg, 0.052 mmol), *rac*-BINAP (96 mg, 0.155 mmol), NaO^{t}Bu (2.97 g, 30.9 mmol) and toluene (40 ml) gave $\{(2,4\text{-}Me_2C_6H_3)HNCH_2CH_2\}_2NH$ (**LVc**) as a viscous red oil. Yield: 68% (2.27 g, 6.97 mmol). ES mass spectrum, *m/z* 312 $[M+H]^+$. IR (neat, cm^{-1}): *v* 3347 (NH, medium). ^{1}H NMR ($CDCl_3$, 300 MHz): δ 2.10 (s, 6H, Me_p), 2.14 (s, 6H, Me_o), 2.71 (t, 4H, $^3J_{H-H}$ 6.0 Hz, CH_2), 3.20 (t, 4H, $^3J_{H-H}$ 6.0 Hz, CH_2), 6.45 (d, 2H, $^3J_{H-H}$ 8.1 Hz, Ar-H), 6.82 (m, 4H, Ar-H). ^{13}C NMR ($CDCl_3$, 75 MHz, ^{1}H composite pulse decoupled): δ 17.9 (2C, Me_o), 20.7 (2C, Me_p), 44.2 (2C, CH_2), 48.7 (2C, CH_2), 110.5 (2C, ArCH_o), 122.8 (2C, Ar*C*), 126.4 (2C, ArCH_m), 127.7 (2C, ArCH_m), 131.3 (2C, Ar*C*), 144.6 (2C, Ar*C*).

6.3.2. Syntheses of $(ArNHCH_2CH_2)_2NMe$ (LVI)

(i) (Ar = 2,6-$Me_2C_6H_3$); bis(*N*-*N*-2,6-dimethylphenyl-2-aminoethyl)(methyl)amine (LVIa): An oven-dried Schlenk flask equipped with a magnetic stir bar was evacuated and backfilled with nitrogen. The flask was charged with $(H_2NCH_2CH_2)_2NMe$ (1.20 g, 10.3 mmol), 2,6-dimethylphenyl bromide (2.74 ml, 3.81 g, 20.6 mmol), $Pd_2(dba)_3$ (30 mg, 0.033 mmol), *rac*-BINAP (62 mg, 0.10 mmol), NaO^{t}Bu (1.91 g, 19.9 mmol) and toluene (40 ml). The reaction mixture was heated to 120 °C and stirred for a period of 4 days. After cooling to room temperature, the solvent was removed under reduced pressure to afford an oily residue. The residue was dissolved in diethyl ether (30 ml) and washed with water (3 x 30 ml) and saturated NaCl solution (3 x 30 ml). The organic layer was separated and dried over $MgSO_4$.

The solvent was removed under reduced pressure and the residue left under vacuum at 50 °C for 24 h to give {(2,6-$Me_2C_6H_3$)$HNCH_2CH_2$}$_2$NMe (**LVIa**) as a viscous red oil. Yield: 81 % (2.71 g, 8.34 mmol). ES mass spectrum: m/z 326 $[M+H]^+$. IR (neat, cm^{-1}): *v* 3364 (N-H, medium). ^{1}H NMR ($CDCl_3$, 300 MHz): δ 2.19 (s, 3H, N-*Me*), 2.20 (s, 12H, Me_o), 2.53 (t, 4H, $^3J_{H-H}$ 6 Hz, CH_2), 3.02 (t, 4H, $^3J_{H-H}$ 6 Hz, CH_2), 3.66 (br s, 2H, N*H*), 6.69 (t, 2H, $^3J_{H-H}$ 7.6 Hz, ArCH_p), 6.88 (d, 4H, $^3J_{H-H}$ 7.3 Hz, ArCH_m). ^{13}C NMR ($CDCl_3$, 75 MHz, ^{1}H composite pulse decoupled): δ 18.8 (4C, Me_o), 41.4 (1C, N-*Me*), 45.8 (2C, *C*H_2), 58.4 (2C, *C*H_2), 121.6 (2C, Ar*C*H_p), 128.9 (4C, Ar*C*H_m), 129.0 (4C, Ar*C*), 146.6 (2C, Ar*C*).

(ii) (Ar = 2,4,6-$Me_3C_6H_2$); bis(*N*-*N*-2,4,6-trimethylphenyl-2-aminoethyl) (methyl)amine (LVIb): Using an analogous route to that outlined in 6.3.2(i) employing ($H_2NCH_2CH_2)_2$NMe (1.20 g, 10.3 mmol), 2,4,6-trimethylphenyl bromide (3.15 ml, 4.10 g, 20.6 mmol), $Pd_2(dba)_3$ (30 mg, 0.033 mmol), *rac*-BINAP (62 mg, 0.10 mmol), NaO^tBu (1.91 g, 19.9 mmol) and toluene (40 ml) gave {(2,4,6-$Me_3C_6H_2$)$HNCH_2CH_2$}$_2$NMe (**LVIb**) as a viscous red oil. Yield: 79 % (2.88 g, 8.16 mmol). ES mass spectrum: m/z 354 $[M+H]^+$. IR (nujol mull, cm^{-1}): *v* 3362 (N-H, medium); ^{1}H NMR ($CDCl_3$, 300 MHz): δ 2.14 (s, 6H, Me_p), 2.18 (s, 12H, Me_o), 2.20 (s, 3H, N-*Me*), 2.54 (t, 4H, $^3J_{H-H}$ 6 Hz, CH_2), 2.98 (t, 4H, $^3J_{H-H}$ 6 Hz, CH_2), 6.72 (s, 4H, Ar-CH_m). ^{13}C NMR ($CDCl_3$, 75 MHz, ^{1}H composite pulse decoupled): δ 18.5 (4C, Me_o), 20.6 (2C, Me_p), 41.4 (1C, N-*Me*), 46.0 (2C, *C*H_2), 58.4 (2C, *C*H_2), 129.3 (4C, Ar*C*), 129.5 (4C, Ar*C*H_m), 130.9 (2C, Ar*C*), 143.9 (2C, Ar*C*).

6.3.3. Syntheses of (ArNH$CH_2CH_2)_2${(2-C_5H_4N)CH_2}N (LVII)

(i) (Ar = 2,4,6-$Me_3C_6H_2$); bis(*N*-*N*-2,4,6-trimethylphenyl-2-aminoethyl)(2-picolyl)amine (LVIIa): An oven dried Schlenk flask was charged with **LVb** (0.50 g, 1.54 mmol), 2-picolyl chloride hydrochloride (0.380 g, 2.31 mmol), K_2CO_3 (0.457 g, 4.62 mmol) and acetonitrile (40 ml). The reaction mixture was heated to 55 °C and stirred for a period of three days. After cooling to room temperature, the solution was filtered and the solvent removed under reduced

pressure to afford an oily residue. The residue was dissolved in diethyl ether (30 ml) and washed with water (3 x 30 ml). The organic phases were combined and concentrated on a rotary evaporator to give a brown oil. The crude product was purified via alumina column chromatography employing ethyl acetate and hexane as the eluting solvents (1:4) to give $\{(2,4,6\text{-}Me_3C_6H_2)NHCH_2CH_2\}_2\{(2\text{-}C_5H_4N)CH_2\}N$ **(LVIIa)** as a yellow oil. Yield: 31 % (0.202 g, 0.48 mmol). ES mass spectrum: m/z 431 $[M+H]^+$. IR (neat, cm^{-1}): *v* 3356 (N-H, medium), 1590 ($C{=}N_{pyridine}$). ^1H NMR ($CDCl_3$, 300 MHz): δ 2.13 (s, 18H, *Me*), 2.74 (t, 4H, $^3J_{H\text{-}H}$ 6 Hz, C*H*$_2$), 3.0 (t, 4H, $^3J_{H\text{-}H}$ 6 Hz, C*H*$_2$), 3.22 (br s, 2H, N-*H*), 3.8 (s, 2H, PyC*H*$_2$), 6.7 (s, 4H, ArC*H*$_m$), 7.07 (m, 1H, PyC*H*), 7.39 (d, 1H, $^3J_{H\text{-}H}$ 7.9 Hz, PyC*H*), 7.55 (dt, 1H, $^3J_{H\text{-}H}$ 7 Hz, $^4J_{H\text{-}H}$ 1.8 Hz, PyC*H*), 8.45 (dd, 1H, $^3J_{H\text{-}H}$ 5 Hz, $^4J_{H\text{-}H}$ 1 Hz, PyC*H*). ^{13}C NMR ($CDCl_3$, 75 MHz, ^1H composite pulse decoupled): δ 18.5 (4C, *Me*$_o$), 20.6 (2C, *Me*$_p$), 46.1 (2C, *C*H$_2$), 55.1 (2C, *C*H$_2$), 60.5 (1C, Py*C*H$_2$), 122.1 (1C, Py*C*H), 123 (1C, Py*C*H), 129.3 (4C, Ar*C*), 129.4 (4C, Ar*C*H$_m$), 130.9 (2C, Ar*C*), 136.4 (1C, Py*C*H), 143.7 (2C, Ar*C*), 149.2 (1C, Py*C*H), 159.4 (1C, Py*C*).

(ii) (Ar = 2,4-$Me_2C_6H_3$); bis(*N*-*N*-2,4-dimethylphenyl-2-aminoethyl)(2-picolyl)amine (LVIIb): Using the same procedure and molar quantities of reagents as above in 6.3.3(i) using **LVc** (0.49 g, 1.54 mmol), 2-picolyl chloride hydrochloride (0.380 g, 2.31 mmol), K_2CO_3 (0.457 g, 4.62 mmol) gave $\{(2,4\text{-}Me_2C_6H_3)NHCH_2CH_2\}_2\{(2\text{-}C_5H_4N)CH_2\}N$ (**LVIIb**) as a yellow oil. Yield: 29% (0.184 g, 0.47 mmol). ES mass spectrum: m/z 403 $[M+H]^+$. IR (neat, cm^{-1}): *v* 3371 (N-H, medium). ^1H NMR ($CDCl_3$, 300 MHz): δ 2.00 (s, 6H, *Me*$_p$), 2.12 (s, 6H, *Me*$_o$), 3.20 (t, 4H, $^3J_{H\text{-}H}$ 6 Hz, C*H*$_2$), 3.55 (t, 4H, $^3J_{H\text{-}H}$ 6 Hz, C*H*$_2$), 3.86 (s, 2H, PyC*H*$_2$), 6.45 (d, 2H, $^3J_{H\text{-}H}$ 8.1 Hz, ArC*H*$_o$), 6.90 (m, 4H, ArC*H*$_m$), 7.05 (m, 1H, PyC*H*), 7.46 (d, 1H, $^3J_{H\text{-}H}$ 7.9 Hz, PyC*H*), 7.51 (dt, 1H, $^3J_{H\text{-}H}$ 7.0, $^4J_{H\text{-}H}$ 1.8 Hz, PyC*H*), 8.61 (dd, 1H, $^3J_{H\text{-}H}$ 5.8, $^4J_{H\text{-}H}$ 1.1 Hz, PyC*H*). ^{13}C NMR ($CDCl_3$, 75 MHz, ^1H composite pulse decoupled): δ 17.9 (1C, *Me*$_o$), 20.7 (1C, *Me*$_p$), 44.2 (2C, *C*H$_2$), 48.7 (2C, *C*H$_2$), 59.9 (1C, Py*C*H$_2$), 110.5 (2C, Ar*C*H), 122.5 (1C, Py*C*H), 122.8 (1C, Py*C*H), 126.4 (2C, Ar*C*), 127.7 (2C, Ar*C*H), 131.3 (2C,

ArCH), 136.4 (1C, PyCH), 143.9 (2C, ArC), 144.6 (2C, ArC), 149.5 (1C, PyCH), 160.2 (1C, PyC).

6.3.4. Synthesis of [{(ArNHCH$_2$CH$_2$)$_2$NH}CoCl$_2$] (16)

(i) (Ar = 2,6-Me$_2$C$_6$H$_3$); 16a: An oven-dried Schlenk flask equipped with a magnetic stir bar was evacuated and backfilled with nitrogen. The flask was charged with $CoCl_2$ (42 mg, 0.32 mmol) in *n*-butanol (5 ml) at 90 °C and a solution of **LVa** (100 mg, 0.32 mmol) in *n*-butanol was introduced to form a green solution. After being stirred at 90 °C for 1 h, the reaction was allowed to cool to room temperature. The reaction mixture was concentrated and hexane added to induce precipitation of [{**LVa**}$CoCl_2$] (**16a**) as a pale blue solid. The suspension was stirred overnight, filtered, washed with hexane (2 x 30 ml) and dried under reduced pressure. Layering of an acetonitrile solution of **16a** with hexane gave **16a** as pale blue crystals suitable for single crystal X-ray structure determination. Yield: 80 % (114 mg, 0.26 mmol).

(ii) (Ar = 2,4,6-Me$_3$C$_6$H$_2$); 16b: Using an analogous route to that outlined in 6.3.4(i) employing **LVb** (105 mg, 0.32 mmol) and $CoCl_2$ (40 mg, 0.32 mmol), gave [{**LVb**}$CoCl_2$] (**16b**) as a pale blue solid. Layering of an acetonitrile solution of **16b** with hexane gave **16b** as pale blue crystals suitable for single crystal X-ray structure determination. Yield: 85 % (124 mg, 0.27 mmol).

6.3.5. Synthesis of [{(ArNHCH$_2$CH$_2$)$_2$NMe}CoCl$_2$] (17)

(i) (Ar = 2,6-Me$_2$C$_6$H$_3$); 17a: An oven-dried Schlenk flask equipped with a magnetic stir bar was evacuated and backfilled with nitrogen. The flask was charged with $CoCl_2$ (40 mg, 0.32 mmol) in *n*-butanol (5 ml) at 90 °C and a solution of **LVIa** (105 mg, 0.32 mmol) in *n*-butanol was introduced to form a green solution. After being stirred at 90 °C for 1 h, the reaction was allowed to cool to room temperature. The reaction mixture was concentrated and hexane added to induce precipitation of [{**LVIa**}$CoCl_2$] (**17a**) as a pale blue solid. The suspension was stirred

overnight, filtered, washed with hexane (2 x 30 ml) and dried under reduced pressure. Layering of an acetonitrile solution of **17a** with hexane gave **17a** as pale blue crystals suitable for single crystal X-ray structure determination. Yield: 75 % (110 mg, 0.24 mmol).

(ii) (Ar = 2,4,6-$Me_3C_6H_2$); 17b: Using the same procedure and molar quantities of reagents as above in 6.3.5(i) using **LVIb** (113 mg, 0.32 mmol) and $CoCl_2$ (40 mg, 0.32 mmol), gave [{**LVIb**}$CoCl_2$] (**17b**) as a pale blue solid. Yield: 71% (110 mg, 0.23 mmol).

6.3.6. Synthesis of [{(ArNHCH$_2$CH$_2$)$_2$((2-C$_5$H$_4$N)CH$_2$)N}FeCl$_2$] (18)

(i) (Ar = 2,4,6-$Me_3C_6H_2$); 18a: An oven-dried Schlenk flask equipped with a magnetic stir bar was evacuated and backfilled with nitrogen. The flask was charged with $FeCl_2(thf)_{1.5}$ (108 mg, 0.47 mmol) in thf (10 ml) and a solution of **LVIIa** (200 mg, 0.47 mmol) in thf (5 ml) was introduced to form a yellow solution. After being stirred at rt for 24 h, the reaction mixture was concentrated and hexane added to induce precipitation of [{**LVIIa**}$FeCl_2$] (**18a**) as a yellow solid. The suspension was stirred overnight, filtered, washed with hexane (2 x 30 ml) and dried under reduced pressure. Layering of an acetonitrile solution of **18a** with hexane gave **18a** as golden crystals suitable for single crystal X-ray structure determination. Yield: 80 % (212 mg, 0.38 mmol).

(ii) (Ar = 2,4-$Me_2C_6H_3$); 18b: An oven-dried Schlenk flask equipped with a magnetic stir bar was evacuated and backfilled with nitrogen. The flask was charged with $FeCl_2$ (19 mg, 0.15 mmol) in *n*-BuOH (5 ml) and the reaction stirred at 90 °C and **LVIIb** (63 mg, 0.15 mmol) in *n*-BuOH (2 ml) was introduced to form a yellow solution. After being stirred at 90 °C for and 20 min, the reaction mixture was allowed to cool to rt. The reaction mixture was concentrated and hexane added to induce precipitation of [{**LVIIb**}$FeCl_2$] (**18b**) as a yellow solid. The suspension was stirred overnight, filtered, washed with hexane (2 x 30 ml) and dried under reduced pressure. Yield: 65 % (0.053 g, 0.10 mmol).

6.3.7. Synthesis of [{(ArNHCH$_2$CH$_2$)$_2$((2-C$_5$H$_4$N)CH$_2$)N}CoCl$_2$] (19)

(i) (Ar = 2,4,6-Me$_3$C$_6$H$_2$); 19a: Using the same procedure and molar quantities of reagents as above in 6.3.6(i) using **LVIIa** (50 mg, 0.12 mmol) and $CoCl_2.6H_2O$ (30 mg, 0.12 mmol), gave [{**LVIIa**}$CoCl_2$] (**19a**) as a pale blue solid. Layering of a dichloromethane solution of **19a** with diethyl ether gave pale blue crystals suitable for a single crystal X-ray diffraction study. Yield: 71 % (0.13 g, 0.23 mmol).

(ii) Ar = 2,4-Me$_2$C$_6$H$_3$; 19b: Using the same procedure and molar quantities of reagents as above in 6.3.6(ii) using **LVIIb** (61 mg, 0.15 mmol) and $CoCl_2$ (20 mg, 0.15 mmol), gave [{**LVIIb**}$CoCl_2$] (**19b**) as a pale blue solid. Yield: 65% (0.052 g, 0.10 mmol).

Table 4 Elemental analysis results for complexes **16–19**

Compound	Microanalysis (%)[a]		
	C	H	N
$C_{20}H_{29}N_3CoCl_2$ (**16a**)	54.07 (54.43)	6.53 (6.62)	9.15 (9.52)
$C_{22}H_{33}N_3CoCl_2$ (**16b**)	56.11 (56.29)	6.99 (7.09)	8.88 (8.95)
$C_{21}H_{31}N_3CoCl_2$ (**17a**)	55.65 (55.39)	7.02 (6.86)	9.11 (9.23)
$C_{28}H_{38}N_4FeCl_2$ (**18a**)	57.57 (60.34)	6.32 (6.87)	9.51 (10.05)
$C_{28}H_{38}N_4CoCl_2$ (**19a**)	60.13 (60.00)	6.94 (6.76)	10.14 (10.00)

[a] calculated values in parentheses.

Table 5 FAB MS, IR spectra and rt magnetic moments for complexes **16-19**

Compound[a]	FAB mass spectrum (m/z)	ν(N-H) (cm^{-1})[b]	ν(C=$N_{pyridine}$) (cm^{-1})[b]	μ_{eff} (BM)[c]
$C_{20}H_{29}N_3CoCl_2$ (**16a**)	440 $[M]^+$, 405 $[M\text{-}Cl]^+$	3292w	-	3.90
$C_{22}H_{33}N_3CoCl_2$(**16b**)	468 $[M]^+$, 433 $[M\text{-}Cl]^+$	3290w	-	3.90
$C_{21}H_{31}N_3CoCl_2$ (**17a**)	454 $[M]^+$, 419 $[M\text{-}Cl]^+$	3286w	-	4.00
$C_{23}H_{35}N_3CoCl_2$(**17b**)	483 $[M]^+$, 447 $[M\text{-}Cl]^+$	3294w	-	3.80
$C_{28}H_{38}N_4FeCl_2$ (**18a**)	556 $[M]^+$, 521 $[M\text{-}Cl]^+$	3209w	1605	4.88
$C_{26}H_{34}N_4FeCl_2$ (**18b**)	493 $[M\text{-}Cl]^+$	3233w	1603	5.11
$C_{28}H_{38}N_4CoCl_2$ (**19a**)	524 $[M\text{-}Cl]^+$	3245w	1608	3.8
$C_{26}H_{34}N_4CoCl_2$ (**19b**)	496 $[M\text{-}Cl]^+$	3190w	1608	4.10

[a] Molecular Formula obtained from elemental analysis except for **17b**, **18b** and **19b**; [b] Recorded in the sold state; [c] Analysed using an Evans Balance

Table 6 ^{1}H NMR resonance assignments for complexes **18a** and **19a** in CD_3CN at rt

Compound	^{1}H NMR chemical shifts (ppm), relaxation times (τ_1) and assignment
18a	128.6 (poor data set 6.0 ms, PyCH_α), 53.6 (13.1 ms, PyCH_β), 52.1 (11.1 ms, PyC$H_{\beta'}$), 18.2 (42.3 ms, PyCH_γ), 13.3 (40.5 ms, ArMe_p), 12.0 (150 ms, ArCH_m), 8.7 (3.1 ms, ArMe_o)
19a	97.0 (poor data set 0.5 ms, PyCH_α), 50.3 (10.14 ms, PyCH_β), 46.8 (16.4 ms, PyC$H_{\beta'}$), 11.5 (135 ms, ArMe_p), 9.3 (39.4 ms, ArCH_m), 0.3 (31.0 ms, PyCH_γ), -4.8 (2.8 ms, ArMe_o)

6.4. Experimental for Chapter 4

6.4.1. Schlenk test: An oven-dried Schlenk flask equipped with a magnetic stir bar was evacuated and backfilled with nitrogen. The flask was charged with the precatalyst (0.01 mmol) dissolved in toluene (40 ml) and MAO (10%wt in toluene) was introduced. Upon the addition of MAO the colour of the solution intensified. The Schlenk tube was purged with ethylene and magnetically stirred at a constant rate under one bar of ethylene at 25 °C. After 0.5 h the polymerisation/oligomerisation was terminated by the addition of aqueous hydrogen chloride. The toluene layer was dried over $MgSO_4$, transferred to a volumetric flask with 1-heptadecene present as an internal standard and analysed by GC mass spectrometry. The catalysts were validated with the literature precedent [{2-(2'-$MeC_6H_4N)_2C_5H_3N$}$FeCl_2$] complex and MAO as activator.

6.4.2. 1-Nonene and 1-Tridecene isomerisation control experiment

(i) An oven-dried Schlenk flask equipped with a magnetic stir bar was evacuated and backfilled with nitrogen. The flask was charged with the precatalyst (0.01 mmol) dissolved in toluene (40 ml) and MAO (10%wt in toluene, 4.0 mmol, 2.65 ml) followed by the introduction of 1-nonene (50 μl) and 1-tridecene (50 μl). Upon the addition of MAO the colour of the solution intensified. The Schlenk tube was purged with ethylene and magnetically stirred at a constant rate under one bar of ethylene at 25 °C. After 0.5 h the oligomerisation was terminated by the addition of aqueous hydrogen chloride. The oligomers were extracted by 2 x 25 ml of toluene dried over $MgSO_4$ and diluted to 100 ml in a volumetric flask with 1-heptadecene (50 μl) present as an internal standard and analysed by GC mass spectrometry.

(ii) An oven-dried Schlenk flask equipped with a magnetic stir bar was evacuated and backfilled with nitrogen. The flask was charged with the precatalyst (0.01 mmol) dissolved in toluene (40 ml) and MAO (10%wt in toluene, 4.0 mmol, 2.65 ml) followed by the

introduction of 1-nonene (50 μl) and 1-tridecene (50 μl). Upon the addition of MAO the colour of the solution intensified. The Schlenk tube was magnetically stirred at a constant rate at 25 °C. After 0.5 h the control experiment was terminated by the addition of aqueous hydrogen chloride. The organic phase was extracted with 2 x 25 ml of toluene dried over $MgSO_4$ and diluted to 100 ml in a volumetric flask with 1-heptadecene (50 μl) present as an internal standard and analysed by GC mass spectrometry.

(iii) 1-nonene (50 μl), 1-tridecene (50 μl), 1-heptadecene (50 μl) were diluted with toluene to 100 ml in a volumetric flask. The resulting solution was analysed by GC mass spectrometry and the relative areas of each respective α-olefin were compared to those present in examples 6.4.2(i) and 6.4.2(ii).

6.5. Experimental for Chapter 5

6.5.1. Synthesis of 2-{(2'-OMe-3'-R^1-5'-R^2)C_6H_3}-6-(COR^3)C_5H_3N

(i) (R^1 = R^2 = H, R^3 = Me); 2-phenyl(2'-methoxy)-6-acetyl-pyridine: An oven-dried Schlenk flask equipped with a magnetic stir bar was evacuated and backfilled with nitrogen. The flask was charged with $Pd(PPh_3)_4$ (361 mg, 0.31 mmol), 2-bromo-6-acetyl-pyridine (2.072 g, 10.4 mmol), toluene (22 ml) and an aqueous solution of K_2CO_3 (2M, 10.4 ml, 20.8 mmol). The solution was stirred for 15 min followed by the addition of (2-methoxyphenyl)boronic acid (1.889 g, 12.4 mmol) in ethanol (11 ml). After heating the reaction mixture at 90 °C in an oil bath for 24 h, the residual 2-methoxyphenylboronic acid was oxidized by 30%-H_2O_2 at room temperature for 1 h. The product was extracted with diethyl ether, washed with saturated NaCl solution and water. The aqueous layer was washed repeatedly with chloroform to ensure extraction of organic phase was complete. The organic extracts were combined, dried over $MgSO_4$ and the volatiles removed under reduced pressure to form a yellow solid. The crude product was purified via column chromatography employing dichloromethane and hexane as the eluting solvent mixture (1:1) to give 2-{(2'-OMe)C_6H_4}-6-(COMe)C_5H_3N as a yellow solid. Yield: 78 % (1.841 g, 8.1 mmol). Mp: 62-64 °C. ES mass spectrum: m/z 228 $[M+H]^+$. IR (nujol mull, cm^{-1}): ν 1692 (CMe=O), 1578 ($C=N_{pyridine}$). ^1H NMR ($CDCl_3$, 250 MHz): δ 2.72 (s, 3H, C*Me*=O), 3.81 (s, 3H, O*Me*), 6.95 (d, 1H, $^3J_{H-H}$ 8.3 Hz, ArC*H*), 7.05 (dt, 1H, $^3J_{H-H}$ 7.6 Hz, $^4J_{H-H}$ 0.9 Hz, ArC*H*), 7.35 (dt, 1H, $^3J_{H-H}$ 8.3 Hz, $^4J_{H-H}$ 1.9 Hz, ArC*H*), 7.75 (t, 1H, $^3J_{H-H}$ 7.8 Hz, ArC*H*), 7.86-7.91 (m, 2H, PyC*H*), 8.02 (dd, 1H, $^3J_{H-H}$ 7.8 Hz, $^4J_{H-H}$ 0.9 Hz, PyC*H*). ^{13}C NMR ($CDCl_3$, 63 MHz, ^1H composite pulse decoupled): δ 26.2 (1C, C*Me*=O), 56.0 (1C, O*Me*), 112.0 (1C, Ar*C*H), 119.8 (1C, Ar*C*H), 121.5 (1C, Py*C*H), 128.6 (1C, Ar*C*), 128.9 (1C, Py*C*H), 130.8 (1C, Py*C*H), 131.7(1C, Ar*C*H), 136.8 (1C, Ar*C*H), 153.7 (1C, Py*C*), 155.5 (1C, Ar*C*), 157.7 (1C, Py*C*), 201.2 (1C, *C*Me=O).

(ii) (R^1 = Ph, R^2 = H, R^3 = Me); 2-phenyl(2'-methoxy-3'-phenyl)-6-acetyl-pyridine: Using an analogous procedure and molar ratios of reagents as above in 6.5.1(i) employing $Pd(PPh_3)_4$ (231 mg, 0.20 mmol), 2-bromo-6-acetyl-pyridine (1.320 g, 6.6 mmol), K_2CO_3 (2M, 6.6 ml, 13.2 mmol), phenyl(2-methoxy-3-phenyl) boronic acid (1.81 g, 7.92 mmol). After refluxing for 3 days followed by purification *via* column chromatography (eluting solvents: dichloromethane and hexane, 1:1) formed 2-{(2'OMe-3'-Ph)C_6H_3}-6-(COMe)C_5H_3N as a white solid. Yield: 89 % (1.763 g, 5.81 mmol). Mp: 62-64 °C. ES mass spectrum: m/z 304 $[M+H]^+$. IR (nujol mull, cm^{-1}): *v* 1692 (CMe=O), 1578 ($C=N_{pyridine}$). ^1H NMR ($CDCl_3$, 300 MHz): δ 2.70 (s, 3H, C*Me*=O), 3.17 (s, 3H, O*Me*), 7.2-7.38 (m, 5H, ArC*H*), 7.50-7.53 (m, 2H, ArC*H*), 7.75-7.82 (m, 2H, PyC*H*), 7.93 (dd, 1H, $^3J_{H-H}$ 7 Hz, $^4J_{H-H}$ 0.9 Hz, ArC*H*), 8.06 (dd, 1H, $^3J_{H-H}$ 7.8 Hz, $^4J_{H-H}$ 0.9 Hz, PyC*H*). ^{13}C NMR ($CDCl_3$, 75 MHz, ^1H composite pulse decoupled): δ 24.8 (1C, C*Me*=O), 59.9 (1C, O*Me*), 118.7 (1C, ArCH), 123.5 (1C, PyCH), 126.3 (1C, ArCH), 127.2 (1C, ArCH), 127.3 (2C, ArCH), 128.2 (2C, ArCH), 129.6 (1C, ArCH), 131.1 (1C, PyCH), 132.4 (1C, Ar*C*), 134.9 (1C, Ar*C*), 135.8 (1C, PyCH), 137.3 (1C, Py*C*), 152.4 (1C, Ar*C*), 154.5 (1C, Py*C*), 154.6 (1C, Ar*C*), 199.5 (1C, *C*Me=O).

(iii) (R^1 = R^2 = R^3 = H); 2-phenyl(2'-methoxy)-6-formyl-pyridine: An oven-dried Schlenk flask equipped with a magnetic stir bar was evacuated and backfilled with nitrogen. The flask was charged with $Pd(PPh_3)_4$ (295 mg, 0.22 mmol), 2-bromo-6-formyl-pyridine (2.08 g, 11.2 mmol), toluene (20 ml) and an aqueous solution of K_2CO_3 (2M, 11.2 ml, 22.4 mmol). The solution was stirred for 15 min followed by the addition of (2-methoxyphenyl)boronic acid (1.889 g, 12.4 mmol) in ethanol (11 ml). After heating the reaction mixture at 90 °C in an oil bath for 42 h, the residual 2-methoxyphenylboronic acid was oxidized by 30%-H_2O_2 at room temperature for 1 h. The product was extracted with diethyl ether, washed with saturated NaCl solution and water. The aqueous layer was washed repeatedly with chloroform to ensure extraction of organic phase was complete. The organic extracts were combined, dried over $MgSO_4$ and the volatiles removed under reduced pressure to form a yellow solid. The crude

product was purified via column chromatography employing dichloromethane and hexane (4:1) as the eluting solvent mixture to give 2-{(2'-OMe)C_6H_4}-6-(CHO)C_5H_3N as a yellow solid. Yield: 84 % (2.01 g, 9.4 mmol). ES mass spectrum: m/z 214 $[M+H]^+$. IR (neat, cm^{-1}): *v* 1703 (CH=O), 1597 ($C=N_{pyridine}$). ^1H NMR ($CDCl_3$, 300 MHz): δ 3.79 (s, 3H, O*Me*), 6.95 (d, 1H, $^3J_{H-H}$ 8.5 Hz, ArC*H*), 7.04 (dt, 1H, $^3J_{H-H}$ 7.6 Hz, $^4J_{H-H}$ 1.2 Hz, ArC*H*), 7.34 (dt, 1H, $^3J_{H-H}$ 7.7 Hz, $^4J_{H-H}$ 1.7 Hz, ArC*H*), 7.75-7.84 (m, 3H, ArC*H*/PyC*H*), 8.01 (dd, 1H, $^3J_{H-H}$ 6.4 Hz, $^4J_{H-H}$ 2.6 Hz, PyC*H*), 10.07 (s, 1H, C*H*=O). ^{13}C NMR ($CDCl_3$, 75 MHz, ^1H composite pulse decoupled): δ 54.6 (1C, O*Me*), 110.5 (1C, Ar*C*H), 118.4 (1C, Py*C*H), 120.2 (1C, Ar*C*H), 126.8 (1C, Py*C*), 128.4 (1C, Py*C*H), 129.6 (1C, Py*C*H), 130.1 (1C, Ar*C*H), 138.3 (1C, Ar*C*H), 151.6 (1C, Py*C*), 155.6 (1C, Ar*C*), 156.1 (1C, Ar*C*), 193.1 (1C, *C*H=O).

(iv) ($R^1 = R^3 = H$; $R^2 = t$-Bu); 2-phenyl(2'-hydroxy-5'-*t*-butyl)-6-acetyl-pyridine: Using an analogous procedure and molar ratios of reagents as above in 6.5.1(iii) employing $Pd(PPh_3)_4$ (130 mg, 0.11 mmol), 2-bromo-6-formyl-pyridine (1.04 g, 5.6 mmol), K_2CO_3 (2M, 5.6 ml, 11.2 mmol), phenyl(2-methoxy-5-*t*-butyl) boronic acid (1.39 g, 6.7 mmol). After refluxing for 42 h followed by purification *via* column chromatography (eluting solvents: dichloromethane and hexane, 1:1) formed 2-{(2'OMe-5'-*t*-Bu)C_6H_3}-6-(CHO)C_5H_3N as a pale yellow solid. Yield: 74 % (1.12 g, 4.14 mmol). ES mass spectrum: m/z 270 $[M+H]^+$. IR (nujol mull, cm^{-1}): *v* 1710 (CH=O), 1584 ($C=N_{pyridine}$). ^1H NMR ($CDCl_3$, 300 MHz): δ 1.29 (s, 9H, C*Me*$_3$), 3.77 (s, 3H, O*Me*), 6.89 (d, 1H, $^3J_{H-H}$ 8.8 Hz, ArC*H*), 7.36 (dd, 1H, $^3J_{H-H}$ 8.8 Hz, $^4J_{H-H}$ 2.6 Hz, ArC*H*), 7.77-7.82 (m, 3H, ArC*H*/PyC*H*), 7.75-7.84 (m, 3H, ArC*H*/PyC*H*), 8.00 (dd, 1H, $^3J_{H-H}$ 6.4 Hz, $^4J_{H-H}$ 2.6 Hz, PyC*H*), 10.09 (s, 1H, C*H*=O). ^{13}C NMR ($CDCl_3$, 75 MHz, ^1H composite pulse decoupled): δ 30.5 (9C, C*Me*$_3$), 33.2 (1C, *C*Me$_3$), 54.7 (1C, O*Me*), 110.2 (1C, Ar*C*H), 118.3 (1C, Py*C*H), 126.1 (1C, Py*C*), 126.5 (1C, Py*C*H), 127.1 (1C, Py*C*H), 128.5 (1C, Ar*C*H), 135.4 (1C, Ar*C*H), 142.8 (1C, Ar*C*), 151.6 (1C, Py*C*), 153.93 (1C, Ar*C*), 156.1 (1C, Ar*C*), 193.2 (1C, *C*H=O).

6.5.2. Synthesis of 2-{(2'-OMe-3'-R^1-5'-R^2)C_6H_2}6-{CR^3N(2,6-*i*-$Pr_2C_6H_3$)}C_5H_3N (LVIII)

(i) (R^1 = R^2 = H, R^3 = Me); 2-phenyl(2'-methoxy)-6-acetyl(2,6-diisopropylanil)-pyridine (LVIIIa): To a solution of 2-phenyl(2'-methoxy)-6-acetyl-pyridine (500 mg, 2.2 mmol) in the minimum volume of absolute ethanol was added 1.5 equivalents of 2,6-diisopropylaniline (0.62 ml, 3.3 mmol). After the addition of a few drops of formic acid, the solution was refluxed overnight. Upon cooling to room temperature the product recrystallised from the ethanol. After filtration the yellow solid was washed with cold ethanol to give 2-{(2'-OMe)C_6H_4}6-{CMeN(2,6-*i*-$Pr_2C_6H_3$)}C_5H_3N (**LVIIIa**) as a yellow solid. Yield: 66 % (565 mg, 1.46 mmol). ES mass spectrum: *m/z* 387 $[M+H]^+$. IR (neat, cm^{-1}): *v* 1646 ($C=N_{imine}$), 1575 ($C=N_{pyridine}$). ^1H NMR ($CDCl_3$, 250 MHz): δ 1.44 (dd, 12H, $^3J_{H-H}$ 6.8 Hz, $^2J_{H-H}$ 1.9 Hz, CH*Me*$_2$), 2.55 (s, 3H, C*Me*=N), 3.05 (septet, 2H, $^3J_{H-H}$ 7 Hz, C*H*Me$_2$), 4.15 (s, 3H, O*Me*), 7.25-7.5 (m, 5H, ArC*H*), 7.65 (dt, 1H, $^3J_{H-H}$ 7.6 Hz, $^4J_{H-H}$ 1.8 Hz, ArC*H*), 8.07 (t, 1H, $^3J_{H-H}$ 7.8 Hz, ArC*H*), 8.27 (m, 2H, PyC*H*), 8.55 (dd, 1H, $^3J_{H-H}$ 7.8 Hz, $^4J_{H-H}$ 0.8 Hz, PyC*H*). ^{13}C NMR ($CDCl_3$, 63 MHz, ^1H composite pulse decoupled): δ 17.8 (1C, C*Me*=N), 23.3 (2C, CH*Me*$_2$), 23.7 (2C, CH*Me*$_2$), 28.7, (2C, *C*HMe$_2$), 56.1 (1C, O*Me*), 112.0 (1C, Ar*C*H), 119.6 (1C, Ar*C*H), 121.5 (1C, Py*C*H), 123.4 (2C, Ar*C*H), 123.9 (1C, Ar*C*H), 126.6 (1C, Ar*C*H), 129.3 (1C, Ar*C*), 130.5 (1C, Py*C*H), 131.8 (1C, Py*C*H), 136.3 (1C, Ar*C*H), 136.5 (2C, Ar*C*), 147.1 (1C, Py*C*), 154.9 (1C, Py*C*), 156.4 (1C, Ar*C*), 157.7 (1C, Ar*C*) 168.0 (1C, *C*Me=N).

(ii) (R^1 = Ph, R^2 = H, R^3 = Me); 2-phenyl(2'-methoxy-3'-phenyl)-6-acetyl(2,6-diisopropylanil)-pyridine (LVIIIb): Using an analogous procedure and molar ratios of reagents as 6.5.2(i) employing 2-phenyl(2'-methoxy-3'-phenyl)-6-acetyl-pyridine (115 mg, 0.38 mmol) and 1.5 equivalents of 2,6-diisopropylaniline (0.10 ml, 0.57 mmol) to give 2-{(2'-OMe-3'-Ph)C_6H_3}6-{CMeN(2,6-*i*-$Pr_2C_6H_3$)}C_5H_3N (**LVIIIb**) as a brown solid. Layering of a dichloromethane solution of **LVIIIb** with hexane gave yellow crystals of **LVIIIb** suitable for a single crystal X-ray diffraction study. Yield: 82 % (145 mg, 0.31 mmol). ES mass spectrum: *m/z* 463 $[M+H]^+$. IR (nujol mull, cm^{-1}): *v* 1631 ($C=N_{imine}$), 1590 ($C=N_{pyridine}$). ^1H NMR

($CDCl_3$, 250 MHz): δ 1.38 (dd, 12H, $^3J_{H-H}$ 6.9 Hz, $^2J_{H-H}$ 1.8 Hz, CH*Me*$_2$), 2.51 (s, 3H, C*Me*=N), 2.99 (septet, 2H, $^3J_{H-H}$ 7 Hz, C*H*Me$_2$), 3.54 (s, 3H, O*Me*), 7.29-7.71 (m, 8H, ArCH), 7.83 (dd, 2H, ArC*H*), 8.10 (m, 2H, C*H*), 8.3 (dd, 1H, PyC*H*), 8.55 (dd, 1H, PyC*H*). ^{13}C NMR ($CDCl_3$, 63 MHz, ^{1}H composite pulse decoupled): δ 16.4 (1C, C*Me*=N), 21.9 (2C, CH*Me*$_2$), 22.3 (2C, CH*Me*$_2$), 27.2 (2C, C*H*Me$_2$), 60.0 (1C, O*Me*), 118.4 (1C, Ar*C*H), 122.0 (2C, Ar*C*H), 122.5 (1C, Ar*C*H), 123.5 (1C, Py*C*H), 124.8 (1C, Ar*C*H), 126.2 (1C, Ar*C*H), 127.3 (2C, Ar*C*H), 128.3 (2C, ArCH), 129.7 (1C, Ar*C*H), 130.8 (1C, Py*C*H), 133.0 (1C, ArC), 134.8 (1C, Ar*C*), 134.9 (2C, Ar*C*), 135.5 (1C, Py*C*H), 137.6 (1C, Py*C*), 145.6 (1C, Ar*C*), 153.9 (1C, Ar*C*), 154.7 (1C, Py*C*), 155.1 (1C, Ar*C*), 166.4 (1C, *C*Me=N).

6.5.3. Synthesis of 2-{(2'-OH-3'-R^1-5'-R^2)C_6H_2}6-{CR^3N(2,6-*i*-$Pr_2C_6H_3$)}C_5H_3N (LIX)

(i) (R^1 = R^2 = H, R^3 = Me); 2-phenyl(2'-hydroxy)-6-acetyl(2,6-diisopropylanil)-pyridine (LIXa):

Prepared *via* a two-step procedure:

(a) To a 25 ml round bottom flask equipped with a stir bar and distillation apparatus, concentrated HCl (9.7 ml, 308 mmol) was added to technical grade pyridine (9 ml, 110 mmol). Water was distilled from the mixture at 300 °C for 3 h to give molten pyridinium chloride upon cooling to 140 °C. To the round bottom flask was added 2-phenyl(2'-methoxy)-6-acetyl-pyridine (1.00 g, 4.4 mmol) and the reaction mixture was heated at 300 °C for 4 h. After cooling to room temperature, the solution was diluted with an equal volume of water and the pH adjusted to 7 with aqueous NaOH. The aqueous phase was extracted by washing with chloroform (3 x 50 ml) and dried over $MgSO_4$. The volatiles were removed under reduced pressure to give 2-{(2'-OH)C_6H_4}6-(COMe)C_5H_3N as a red solid. Yield: 90 % (42 mg, 1.98 mmol). ES mass spectrum: m/z 214 $[M+H]^+$. IR (nujol mull, cm^{-1}): *v* 3330 (O-H), 1692 (CMe=O), 1586 (C=$N_{pyridine}$). ^{1}H NMR ($CDCl_3$, 300 MHz): δ 2.66 (s, 3H, C*Me*=O), 6.84-6.98 (m, 1H, ArC*H*), 6.96 (dd, 1H, $^3J_{H-H}$ 8.1 Hz, $^4J_{H-H}$ 1.2 Hz, ArC*H*), 7.24-7.29 (m, 1H, ArC*H*), 7.73(dd, 1H, $^3J_{H-H}$ 8.1 Hz, $^4J_{H-H}$ 1.1 Hz, ArC*H*), 7.88-7.90 (m, 1H, PyC*H*), 8.0 (dd,

1H, $^{3}J_{H\text{-}H}$ 6.4 Hz, $^{4}J_{H\text{-}H}$ 2.6 Hz, PyC*H*). ^{13}C NMR ($CDCl_3$, 75 MHz, ^{1}H composite pulse decoupled): δ 25.1 (1C, C*Me*=O), 117.2 (1C, Ar*C*), 117.5 (1C, ArC*H*), 118.3 (1C, Ar*C*H), 118.8 (1C, Ar*C*H), 121.8 (1C, Py*C*H), 125.5 (1C, Ar*C*H), 131.1 (1C, Py*C*H), 137.7 (1C, Py*C*H), 148.9 (1C, Py*C*), 156.2 (1C, Py*C*), 158.5 (1C, Ar*C*), 196.5 (1C, *C*Me=O).

(b) To a solution of 2-phenyl(2'-hydroxy)-6-acetyl-pyridine (1.874 g, 8.8 mmol) in the minimum volume of absolute ethanol was added 1.5 equivalents of 2,6-diisopropylaniline (2.5 ml, 13.0 mmol). After the addition of a few drops of formic acid, the solution was refluxed for 48 h. Upon cooling to room temperature the product crystallized from the ethanol. After filtration the yellow solid was washed with cold ethanol to give 2-{(2'-OH)C_6H_4}-6-{CMeN(2,6-*i*-$Pr_2C_6H_3$)}C_5H_3N (**LIXa**). Layering of a dichloromethane solution of **LIXa** with hexane gave yellow crystals of **LIXa** suitable for a single crystal X-ray diffraction study. Yield: 80 % (2.6 g, 7.0 mmol). Mp: 190-192 °C. ES mass spectrum: m/z 373 $[M+H]^+$. IR (neat, cm^{-1}): *v* 3381 (O-H), 1644 ($C=N_{imine}$), 1588 ($C=N_{pyridine}$). ^{1}H NMR ($CDCl_3$, 250 MHz): δ 1.08 (dd, 12H, $^{3}J_{H\text{-}H}$ 6.9 Hz, $^{2}J_{H\text{-}H}$ 1.7 Hz, CH*Me*$_2$), 2.18 (s, 3H, C*Me*=N), 1.54 (broad s, 1H, O*H*), 2.65 (septet, 2H, $^{3}J_{H\text{-}H}$ 6.9Hz, C*H*Me$_2$), 6.88 (dt, 1H, $^{3}J_{H\text{-}H}$ 6.3 Hz, $^{4}J_{H\text{-}H}$ 0.73 Hz, ArC*H*), 6.97 (dd, 3H, $^{3}J_{H\text{-}H}$ 6.5 Hz, $^{4}J_{H\text{-}H}$ 0.75 Hz, ArC*H*), 7.11-7.15 (m, 3H, ArC*H*), 7.28 (dt, 1H, $^{3}J_{H\text{-}H}$ 6.6 Hz, $^{4}J_{H\text{-}H}$ 0.98 Hz, ArC*H*), 7.79 (dd, 1H, $^{3}J_{H\text{-}H}$ 6.9 Hz, $^{4}J_{H\text{-}H}$ 1.4 Hz, ArC*H*), 7.85-8.00 (m, 2H, PyC*H*), 8.23 (dd, $^{3}J_{H\text{-}H}$ 7.1 Hz, $^{4}J_{H\text{-}H}$ 1.2 Hz, PyC*H*). ^{1}H NMR ($CDCl_3$:D_2O, 250 MHz): δ 1.08 (dd, 12H, $^{3}J_{H\text{-}H}$ 6.9 Hz, CH*Me*$_2$), 2.18 (s, 3H, C*Me*=N), 2.65 (septet, 2H, $^{3}J_{H\text{-}H}$ 6.9Hz, C*H*Me$_2$), 6.88 (dt, 1H, $^{3}J_{H\text{-}H}$ 6.3 Hz, $^{4}J_{H\text{-}H}$ 0.73 Hz, ArC*H*), 6.97 (dd, 3H, $^{3}J_{H\text{-}H}$ 6.5 Hz, $^{4}J_{H\text{-}H}$ 0.75 Hz, ArC*H*), 7.11-7.15 (m, 3H, ArC*H*), 7.28 (dt, 1H, $^{3}J_{H\text{-}H}$ 6.6 Hz, $^{4}J_{H\text{-}H}$ 0.98 Hz, ArC*H*), 7.79 (dd, 1H, $^{3}J_{H\text{-}H}$ 6.9 Hz, $^{4}J_{H\text{-}H}$ 1.4 Hz, ArC*H*), 7.85-8.00 (m, 2H, PyC*H*), 8.23 (dd, $^{3}J_{H\text{-}H}$ 7.1 Hz, $^{4}J_{H\text{-}H}$ 1.2 Hz, PyC*H*). ^{13}C NMR ($CDCl_3$, 75 MHz, ^{1}H composite pulse decoupled): δ 16.2 (1C, C*Me*=N), 21.7 (2C, CH*Me*$_2$), 22.0 (2C, CH*Me*$_2$), 27.2 (2C, *C*HMe$_2$), 117.3 (1C, Ar*C*H), 117.6 (1C, Ar*C*), 118.0 (1C, Ar*C*H), 118.2 (1C, Ar*C*H), 119.2 (1C, Py*C*H), 121.9 (2C, Ar*C*H), 122.8 (1C, Ar*C*H), 125.3 (1C, Ar*C*H), 130.6 (1C, Py*C*H), 134.5

(2C, Ar*C*), 137.3 (1C, PyCH), 144.8 (1C, Py*C*), 151.9 (1C, Ar*C*), 155.6(1C, Py*C*), 158.4 (1C, Ar*C*), 163.6 (1C, *C*Me=N).

(ii) (R^1 = Ph, R^2 = H, R^3 = Me); 2-phenyl(2'-hydroxy-3'-phenyl)-6-acetyl(2,6-diisopropylanil)-pyridine (LIXb):

Prepared *via* a two-step procedure:

(a) Using an analogous procedure and molar ratios of reagents as 6.5.3(ia) employing concentrated HCl (3.6 ml, 116 mmol), pyridine (3.3 ml, 41 mmol) and 2-phenyl(2'-methoxy-3'-phenyl)6-acetyl-pyridine (500 mg, 1.65 mmol) to form 2-{(2'-OH-3'-Ph)C_6H_3}6-(COMe)C_5H_3N as a brown oil after heating at 210 °C for 6 h. Yield: 75 % (358 mg, 1.24 mmol). ES mass spectrum: m/z 290 $[M+H]^+$. ^{1}H NMR ($CDCl_3$, 300 MHz): δ 2.65 (s, 3H, C*Me*=O), 6.93 (t, 1H, ArC*H*), 7.25-7.40 (m, 5H, ArC*H*), 7.58 (d, 2H, $^3J_{H-H}$ 7.3 Hz, ArC*H*), 7.72-7.75 (m, 1H, PyC*H*), 7.88-7.90 (m, 1H, PyC*H*), 8.03-8.07 (m, 1H, PyC*H*). ^{13}C NMR ($CDCl_3$, 75 MHz, ^{1}H composite pulse decoupled): δ 25.3 (1C, C*Me*=O), 117.6 (1C, Ar*C*), 118.1 (1C, Ar*C*H), 118.8 (1C, Ar*C*H), 122.3 (1C, Py*C*H), 125.1 (1C, Ar*C*H), 126.2 (1C, Ar*C*H), 127.1 (2C, Ar*C*H), 128.5 (2C, Ar*C*H), 130.3 (1C, Ar*C*), 132.3 (1C, Py*C*H), 137.2 (1C, Py*C*), 137.8 (1C, Py*C*H), 148.9 (1C, Ar*C*), 155.8 (1C, Ar*C*), 156.5 (1C, Py*C*), 196.6 (1C, *C*Me=O).

(b) Using an analogous procedure and molar ratios of reagents as 6.5.3(ib) employing 2-phenyl(2'-hydroxy-3'-phenyl)-6-acetyl(2,6-diisopropylanil)-pyridine (358 mg, 1.24 mmol) and 1.5 equivalents of 2,6-diisopropylaniline (0.35 ml, 1.86 mmol) to give 2-{(2'-OH-3'-Ph)C_6H_3}6-{CMeN(2,6-*i*-$Pr_2C_6H_3$)}C_5H_3N (**LIXb**) as a brown solid. Yield: 61 % (339 mg, 0.76 mmol). Mp: 197-199 °C. ES mass spectrum: m/z 449 $[M+H]^+$. IR (nujol mull, cm^{-1}): *v* 3387 (O-H), 1632 ($C=N_{imine}$), 1588 ($C=N_{pyridine}$). ^{1}H NMR ($CDCl_3$, 300 MHz): δ 1.06 (dd, 12H, $^3J_{H-H}$ 6.9 Hz, CH*Me*$_2$), 2.16 (s, 3H, C*Me*=N), 2.63 (septet, 2H, $^3J_{H-H}$ 7.0 Hz, C*H*Me$_2$), 6.94 (t, 1H, $^3J_{H-H}$ 7.9 Hz, ArC*H*), 6.97-7.11 (m, 3H, ArC*H*), 7.23-7.38 (m, 4H, ArC*H*), 7.59

(dd, 2H, $^3J_{H-H}$ 7.1 Hz, ArC*H*), 7.79 (dd, 1H, $^3J_{H-H}$ 8.2 Hz, ArC*H*), 7.90 (t, 1H $^3J_{H-H}$ 7.9 Hz, PyC*H*), 8.00 (d, 1H, $^3J_{H-H}$ 7.6 Hz, PyC*H*), 8.28 (dd, 1H, $^3J_{H-H}$ 7.3 Hz, PyC*H*). ^{13}C NMR ($CDCl_3$, 75 MHz, ^{1}H composite pulse decoupled): δ 17.6 (1C, C*Me*=N), 22.9 (2C, CH*Me*$_2$), 23.2 (2C, CH*Me*$_2$), 28.4 (2C, *C*HMe$_2$), 118.9 (1C, Ar*C*H), 119.1 (1C, Ar*C*), 119.5 (1C, Ar*C*H), 120.9 (1C, Py*C*H), 123.1 (2C, Ar*C*H), 123.9 (1C, Ar*C*H), 126.1 (1C, Ar*C*H), 127.1 (1C, Ar*C*H), 128.1 (2C, Ar*C*H), 129.6 (2C, Ar*C*H), 131.2 (1C, Ar*C*), 132.9 (1C, Py*C*H), 135.7 (2C, Ar*C*), 138.5 (1C, Py*C*H), 146.0 (1C, Py*C*), 153.1 (1C, Ar*C*), 156.9 (1C, Ar*C*), 157.1 (1C, Py*C*), 164.9 (1C, *C*Me=N).

(iii) (R^1 = R^2 = R^3 = H); 2-phenyl(2'-hydroxy)-6-formyl(2,6-diisopropylanil)-pyridine (LIXc):

Prepared *via* a two-step procedure:

(a) 2-phenyl(2'-methoxy)-6-formyl-pyridine (200 mg, 0.939 mmol) was dissolved in dry dichloromethane (10 ml) in an oven-dried Schlenk. Boron tribromide (1.0 M in CH_2Cl_2, 1.98 ml, 1.98 mmol) was added to the solution at –78 °C to afford a dark brown solution. The solution was allowed to warm to room temperature and left to stir for 4 h. Water (10 ml) was carefully added to the solution and the mixture neutralised (with 2M K_2CO_3) and then stirred overnight. The organic phase was separated and the aqueous layer washed with chloroform several times until the extracts became colourless. The combined organic layers were dried over $MgSO_4$ and the solvent removed under reduced pressure to give 2-{(2'-OH)C_6H_4}-6-(CH=O)C_5H_3N as an orange/brown solid. Yield: 63 % (117 mg, 0.588 mmol). ES mass spectrum: *m/z* 200 $[M+H]^+$. ^{1}H NMR ($CDCl_3$, 300 MHz): δ 1.51 (s, br, 1H, OH), 6.89 (t, 1H, $^3J_{H-H}$ 7.3 Hz, ArC*H*), 6.99 (d, 1H, $^3J_{H-H}$ 7.9 Hz, ArC*H*), 7.29 (t, 1H, $^3J_{H-H}$ 7.0 Hz, ArC*H*), 7.72 (d, 1H, $^3J_{H-H}$ 7.3 Hz, ArC*H*), 7.80 (d, 1H, $^3J_{H-H}$ 7.3 Hz, PyC*H*), 7.91 (t, 1H, $^3J_{H-H}$ 7.6 Hz, PyC*H*), 8.05 (d, 1H, $^3J_{H-H}$ 7.0 Hz, PyC*H*), 10.02 (s, 1H, *C*H=O).

(b) Using an analogous procedure and molar ratios of reagents as in 6.5.3(ib) but with 2-phenyl(2'-methoxy)-6-formyl-pyridine (100 mg, 0.50 mmol) and 1.2 equivalents of 2,6-diisopropylaniline (106 mg, 0.60 mmol). to give 2-{(2'-OH)C_6H_4}-6-{CHN(2,6-*i*-$Pr_2C_6H_3$)}C_5H_3N (**LIXc**) as a pale yellow solid. Yield: 67 % (120 mg, 0.34 mmol). ES mass spectrum: *m/z* 359 $[M+H]^+$. IR (neat, cm^{-1}): *v* 1647 ($C=N_{imine}$), 1592 ($C=N_{pyridine}$). ^1H NMR ($CDCl_3$, 300 MHz): δ 1.08 (d, 12H, $^3J_{H-H}$ 6.7 Hz, *Me*), 2.89 (septet, 2H, $^3J_{H-H}$ 6.7 Hz, C*H*), 6.87 (t, 1H, $^3J_{H-H}$ 7.3 Hz, ArC*H*), 6.96 (d, 1H, $^3J_{H-H}$ 7.9 Hz, ArC*H*), 7.04-7.16 (m, 3H, ArC*H*), 7.25 (t, 1H, $^3J_{H-H}$ 7.0 Hz, ArC*H*), 7.76 (d, 1H, $^3J_{H-H}$ 7.3 Hz, ArC*H*), 7.89-7.97 (m, 2H, PyC*H*), 8.07 (d, 1H, $^3J_{H-H}$ 7.0 Hz, PyC*H*), 8.26 (s, 1H, C*H*=N). ^{13}C NMR ($CDCl_3$, 75 MHz, ^1H composite pulse decoupled): δ 23.5 (4C, CH(*Me*)$_2$), 28.1 (2C, CH), 118.6 (1C, Ar*C*), 118.7 (1C, Ar*C*H), 119.2 (1C, Ar*C*H), 119.4 (1C, Ar*C*H), 121.0 (1C, Py*C*H), 123.2 (2C, Ar*C*H), 124.8 (1C, Ar*C*H), 126.5 (1C, Ar*C*H), 131.9 (1C, Py*C*H), 137.2 (2C, Ar*C*), 138.6 (1C, Py*C*H), 148.3 (1C, Ar*C*), 151.0 (1C, Py*C*), 158.1 (1C, Ar*C*), 159.8 (1C, Py*C*), 161.1 (1C, *C*H=N).

(iv) (R^1 =R^3 = H, R^2 = *t*-Bu); 2-phenyl(2'-hydroxy-5'-*t*-butyl)-6-formyl(2,6-diisopropylanil)-pyridine (LIXd):

Prepared *via* a two-step procedure:

(a) Using an analogous procedure as in 6.5.3(iiia) but with 2-phenyl(2'-methoxy-5'-*t*-butyl)-6-formyl-pyridine (410 mg, 1.53 mmol) and boron tribromide (1.0 M in CH_2Cl_2, 3.10 ml, 3.10 mmol,). After stirring for 4 h the reaction mixture was worked up to give 2-{(2'-OH-5'-*t*-Bu)C_6H_3}-6-(CH=O)C_5H_3N as an orange/brown solid. Yield: 59 % (230 mg, 0.902 mmol). ES mass spectrum: *m/z* 256 $[M+H]^+$. ^1H NMR ($CDCl_3$, 300 MHz): δ 1.29 (s, 9H, C(*Me*)$_3$), 6.91 (d, 1H, $^3J_{H-H}$ 8.5 Hz, ArC*H*), 7.35 (dd, 1H, $^3J_{H-H}$ 8.8 Hz, $^4J_{H-H}$ 2.3 Hz, ArC*H*), 7.71 (d, 1H, $^4J_{H-H}$ 2.3 Hz, ArC*H*), 7.80 (d, 1H, $^3J_{H-H}$ 7.3 Hz, PyC*H*), 7.92 (t, 1H, $^3J_{H-H}$ 7.6 Hz, PyC*H*), 8.10 (d, 1H, $^3J_{H-H}$ 7.3 Hz, PyC*H*), 10.01 (s, 1H, C*H*O). ^{13}C NMR ($CDCl_3$, 75 MHz, ^1H composite pulse decoupled): δ 30.5 (3C, C(*Me*)$_3$), 33.2 (1C, *C*(Me$_3$)$_3$), 116.3 (1C, Ar*C*),

117.4 (1C, ArCH), 118.6 (1C, ArCH), 121.8 (1C, PyCH), 122.6 (1C, ArCH), 128.8 (1C, PyCH), 137.7 (1C, PyCH), 140.9 (1C, PyC), 148.4 (1C, ArC), 156.3 (1C, PyC), 158.0 (1C, ArC), 190.1 (C, CH=O).

(b) Using an analogous procedure and molar ratios of reagents as in 5.5.3(ib) employing 2-phenyl(2'-hydroxy-5'-*t*-butyl)-6-formyl-pyridine (100 mg, 0.39 mmol) and 1.2 equivalents of 2,6-diisopropylaniline (83 mg, 0.47 mmol) to give 2-{(2'-OH-5'-*t*-Bu)C_6H_3}-6-{CHN(2,6-*i*-$Pr_2C_6H_3$)}C_5H_3N **(LIXd)** as pale yellow solid Yield: 67 % (101 mg, 0.26 mmol). ES mass spectrum: *m/z* 415 $[M+H]^+$. IR (neat, cm^{-1}): *v* 1648 ($C=N_{imine}$), 1592 ($C=N_{pyridine}$). ^1H NMR ($CDCl_3$, 300 MHz): δ 1.11 (d, 12H, $^3J_{H-H}$ 7.0 Hz, Me_3), 1.28 (s, 9H, $C(Me)_3$), 2.88 (septet, 2H, $^3J_{H-H}$ 7.0 Hz, CH), 6.90 (d, 1H, $^3J_{H-H}$ 8.5 Hz, ArCH), 7.02-7.15 (m, 3H, ArCH), 7.30 (dd, 1H, $^3J_{H-H}$ 8.8 Hz, $^4J_{H-H}$ 2.3 Hz, ArCH), 7.73 (d, 1H, $^4J_{H-H}$ 2.3 Hz, ArCH), 7.88-7.98 (m, 2H, PyCH), 8.06 (d, 1H, $^3J_{H-H}$ 7.3 Hz, PyCH), 8.25 (s, 1H, CH=N). ^{13}C NMR ($CDCl_3$, 75 MHz, ^1H composite pulse decoupled): δ 23.5 (4C, $CH(Me)_2$), 28.1 (2C, CH), 31.6 (3C, $C(Me)_3$), 34.2 (1C, $C(Me)_3$), 117.8 (1C, ArC), 118.2 (1C, ArCH), 119.1 (1C, ArCH), 120.9 (1C, PyCH), 122.9 (1C, ArCH), 123.2 (2C, ArCH), 124.8 (1C, ArCH), 129.3 (1C, PyCH), 137.2 (2C, ArC), 138.5 (1C, PyCH), 141.7 (1C, PyC), 148.3 (1C, ArC), 151.1 (1C, ArC), 157.4 (1C, PyC), 158.1 (1C, ArC), 161.2 (1C, CH=N).

6.5.4. Synthesis of 2-phenyl(2'-hydroxy)-6-(2,6-diisopropylphenyl)amino(dimethyl)methyl-pyridine (LX):

Prepared *via* a two-step procedure:

(a) An oven-dried Schlenk flask equipped with a magnetic stir bar was evacuated and backfilled with nitrogen. To the flask charged with **LIXa** (150 mg, 0.40 mmol) dissolved in toluene (15 ml) were introduced 2 equivalents of $AlMe_3$ (2M, 0.4 ml, 0.81 mmol). The reaction mixture was stirred at reflux for 12 h. After removal of the volatiles acetonitrile (18 ml) was added and refluxed until dissolution. Upon filtration and cooling to room temperature

clear crystals of [{$\mathbf{LX}^{-2H}$}AlMe(NCMe)] (**20**) were formed, which were suitable for single crystal X-ray structure determination. ^{1}H NMR (C_6D_6, 400 MHz): δ -0.24 (s, 3H, Al*Me*), 0.51 (s, 3H, NC*Me*), 1.31-1.43 (m, 12H, CH*Me*$_2$), 1.55 (s, 3H, *Me*), 1.80 (s, 3H, *Me*), 3.71 (s, 1H, C*H*Me$_2$), 4.40 (s, 1H, C*H*Me$_2$), 6.84 (dd, 1H, $^3J_{H-H}$ 7.6 Hz, $^4J_{H-H}$ 1.0 Hz, ArC*H*), 6.9 (dt, 1H, $^3J_{H-H}$ 7.6 Hz, $^4J_{H-H}$ 1.4 Hz, ArC*H*), 7.10-7.19 (m, 4H, ArC*H*), 7.41 (dt, 1H, $^3J_{H-H}$ 7.7 Hz, $^4J_{H-H}$ 1.8 Hz, PyC*H*), 7.53 (dd, 1H, $^3J_{H-H}$ 8 Hz, $^4J_{H-H}$ 1.2 Hz, PyC*H*), 7.67 (dd, 1H, $^3J_{H-H}$ 8 Hz, $^4J_{H-H}$ 1.8 Hz, PyC*H*).

(b) Pentane (10 ml) was added to **20** followed by the dropwise addition of an equal volume of water. After stirring for a further three hours, the aqueous phase was extracted into chloroform (3 x 20 ml) and dried over $MgSO_4$. The volatiles were removed under reduced pressure to give 2-{(2'-OH)C_6H_4}-6-{CMe_2NH(2,6-*i*-$Pr_2C_6H_3$)}C_5H_3N (**LX**) as a brown oil. Yield: 80 % (125 mg, 0.32 mmol). ES mass spectrum: m/z 389 $[M+H]^+$. IR (nujol mull, cm^{-1}): *v* 1596 ($C{=}N_{pyridine}$). ^{1}H NMR ($CDCl_3$, 300 MHz): δ 0.98 (d, 12H, $^3J_{H-H}$ 7.0 Hz, CH*Me*$_2$), 1.48 (s, 6H, NC*Me*$_2$), 2.94 (septet, 2H, $^3J_{H-H}$ 7.0 Hz, C*H*Me$_2$), 3.35 (broad s, 1H, O*H*), 6.85 (dt, 1H, $^3J_{H-H}$ 7.6 Hz, $^4J_{H-H}$ 1.2 Hz, C*H*), 6.92-6.98 (m, 4H, C*H*), 7.22 (dt, 1H, $^3J_{H-H}$ 7.7 Hz, $^4J_{H-H}$ 1.7 Hz, C*H*), 7.59 (dd, 1H, $^3J_{H-H}$ 7.3 Hz, $^4J_{H-H}$ 1.4 Hz, C*H*), 7.70-7.76 (m, 3H, C*H*). ^{1}H NMR ($CDCl_3$:D_2O, 250 MHz): δ 0.98 (d, 12H, $^3J_{H-H}$ 7.0 Hz, CH*Me*$_2$), 1.48 (s, 6H, NC*Me*$_2$), 2.94 (septet, 2H, $^3J_{H-H}$ 7.0 Hz, C*H*Me$_2$), 6.85 (dt, 1H, $^3J_{H-H}$ 7.6 Hz, $^4J_{H-H}$ 1.2 Hz, C*H*), 6.92-6.98 (m, 4H, C*H*), 7.22 (dt, 1H, $^3J_{H-H}$ 7.7 Hz, $^4J_{H-H}$ 1.7 Hz, C*H*), 7.59 (dd, 1H, $^3J_{H-H}$ 7.3 Hz, $^4J_{H-H}$ 1.4 Hz, C*H*), 7.70-7.76 (m, 3H, C*H*). ^{13}C NMR ($CDCl_3$, 75 MHz, ^{1}H composite pulse decoupled): δ 22.8 (4C, CH*Me*$_2$), 27.4 (2C, C*H*Me$_2$), 28.2 (2C, NC*Me*$_2$), 58.1 (1C, N*C*Me$_2$), 115.7 (1C, Ar*C*H), 117.2 (1C, Ar*C*H), 117.4 (1C, Ar*C*H), 117.7 (1C, Ar*C*H), 118.1 (1C, Ar*C*), 122.1 (2C, Ar*C*H), 123.5, (1C, Py*C*H), 125.3 (1C, Ar*C*H), 130.3 (1C, Py*C*H), 137.0 (1C, Py*C*H), 138.7 (1C, Py*C*), 144.3 (2C, Ar*C*), 155.5 (1C, Py*C*), 159.0 (1C, Ar*C*), 165.1 (1C, Ar*C*).

6.5.5. Synthesis of 2-phenyl(2'-hydroxy)-6-(2,6-diisopropylphenyl)amino(methyl)methyl-pyridine (LXI): An oven dried Schlenk flask equipped with a magnetic stir bar was evacuated and backfilled with nitrogen. The flask was charged with lithium aluminium hydride (4.05 ml, 4.05 mmol) and diethyl ether (10 ml) at –78 °C. A suspension of **LIXa** (50 mg, 1.35 mmol) in diethyl ether (15 ml) was added dropwise, followed by warming to rt. After 30 min. the reaction was quenched at 0 °C with 5 ml of water and the pH adjusted to 7 with aqueous NaOH. The aqueous phase was extracted into dichloromethane (3 x 50 ml) and dried over $MgSO_4$. The volatiles were removed under reduced pressure to give 2-{(2'-OH)C_6H_4}-6-{CHMeNH(2,6-*i*-$Pr_2C_6H_3$)}C_5H_3N (**LXI**) as a yellow solid. Yield 84 % (421 mg, 1.13 mmol). ES mass spectrum: m/z 375 $[M+H]^+$. IR (nujol mull, cm^{-1}): *v* 3363 (N-H, medium), 1591 ($C=N_{pyridine}$). ^1H NMR ($CDCl_3$, 300 MHz): δ 0.93 (d, 6H, $^3J_{H-H}$ 7.0 Hz, CH*Me*$_2$), 1.13 (d, 6H, $^3J_{H-H}$ 7.0 Hz, CH*Me*$_2$), 1.59 (d, 3H, $^3J_{H-H}$ 7.0 Hz, NCH*Me*), 3.01 (septet, 2H, $^3J_{H-H}$ 6.8 Hz, C*H*Me$_2$), 4.16 (q, 1H, $^3J_{H-H}$ 6.8 Hz, NC*H*Me), 6.85-6.89 (m, 2H, C*H*), 6.93 (m, 4H, C*H*), 7.22-7.28 (m, 1H, C*H*), 7.61 (m, 1H, C*H*), 7.70-7.78 (m, 2H, C*H*). ^{13}C NMR ($CDCl_3$, 75 MHz, ^1H composite pulse decoupled): 19.6 (1C, NCH*Me*), 23.0 (2C, CH*Me*$_2$), 23.2 (2C, CH*Me*$_2$), 26.7 (2C, C*H*Me$_2$), 59.5 (1C, N*C*HMe), 116.6 (1C, Ar*C*H), 117.4 (1C, Ar*C*H), 117.8 (1C, Ar*C*H), 117.9 (1C, Ar*C*), 118.8 (1C, Py*C*H), 122.5 (2C, Ar*C*H), 122.6 (1C, Ar*C*H), 125.3 (1C, Ar*C*H), 130.5 (1C, Py*C*H), 137.0 (1C, Py*C*H), 139.9 (1C, Py*C*), 141.2 (2C, Ar*C*), 156.7 (1C, Py*C*), 158.9 (1C, Ar*C*), 159.0 (1C, Ar*C*).

6.5.6. Synthesis of [{2-((2'-OMe)C_6H_4)-6-(CMeN(2,6-*i*-$Pr_2C_6H_3$))C_5H_3N}$FeCl_2$] (21): An oven-dried Schlenk flask equipped with a magnetic stir bar was evacuated and backfilled with nitrogen. The flask was charged with $FeCl_2$ (221 mg, 1.74 mmol) in *n*-butanol (20 ml) at 90 °C and **LVIIIa** (673 mg, 1.74 mmol) was introduced to form a red solution. After being stirred at 90 °C for 1 h, the reaction was allowed to cool to room temperature. The reaction mixture was concentrated and hexane added to induce precipitation of [{**LVIIIa**}$FeCl_2$] (**21**) as a red solid. The suspension was stirred overnight, filtered, washed with hexane (2 x 30 ml)

and dried under reduced pressure. Crystals of **21** suitable for single crystal X-ray diffraction study were obtained from a chloroform solution. Yield: 78 % (700 mg, 1.40 mmol).

6.5.7. Synthesis of [{6-((2'-OMe)C_6H_4)-2-(CMeN(2,6-*i*-$Pr_2C_6H_3$))C_5H_3N}$CoCl_2$] (22): Using an analogous procedure and molar quantities of reagents as in 6.5.6 employing **LVIIIa** (92 mg, 0.23 mmol) and $CoCl_2$ (30 mg, 0.23 mmol), gave [{**LVIIIa**}$CoCl_2$] (**22**) as a green powder. Crystals of **22** suitable for single crystal X-ray diffraction study were obtained from a chloroform solution. Yield: 64 % (77 mg, 0.15 mmol).

6.5.8. Synthesis of [{2-((2'-OH-3'-R^1-5'-R^2)C_6H_2)-6-(CR^3N(2,6-*i*-$Pr_2C_6H_3$))C_5H_3N}$FeCl_2$] (23)

(i) (R^1 = R^2 = H, R^3 = Me); 23a: An oven-dried Schlenk flask equipped with a magnetic stir bar was evacuated and backfilled with nitrogen. The flask was charged with $FeCl_2(thf)_{1.5}$ (92 mg, 0.40 mmol) in thf (10 ml) at rt and **LIXa** (149 mg, 0.40 mmol) was added to form a dark red solution. After being stirred at rt for 24 h, the reaction was concentrated and hexane added to induce precipitation of [{**LIXa**}$FeCl_2$] (**23a**) as a red/brown solid. The suspension was stirred overnight, filtered, washed with hexane (2 x 30 ml) and dried under reduced pressure. Yield: 66% (132 mg, 0.26 mmol).

(ii) (R^1 = Ph, R^2 = H, R^3 = Me); 23b: Using an analogous procedure and molar quantities of reagents as in 6.5.8(i) employing **LIXb** (99 mg, 0.22 mmol) and $FeCl_2(thf)_{1.5}$ (55 mg, 0.22 mmol), gave [{**LIXb**}$FeCl_2$] (**23b**) as a dark red powder. Yield: 83 % (105 mg, 0.18 mmol).

6.5.9. Synthesis of [{2-((2'-OH-3'-R^1-5'-R^2)C_6H_2)-6-(CR^3N(2,6-*i*-$Pr_2C_6H_3$))C_5H_3N}$CoCl_2$] (24)

(i) (R^1 = R^2 = H, R^3 = Me); 24a: Using an analogous procedure and molar quantities of reagents as in 6.5.8(i) using **LIXa** (149 mg, 0.40 mmol) and $CoCl_2$ (52 mg, 0.40 mmol), gave [{**LIXa**}$CoCl_2$] (**24a**) as a green powder. Recrystallisation from a hot acetonitrile gave green crystals of **24a** suitable for single crystal X-ray structure determination. Yield: 83 % (112 mg, 0.22 mmol).

(ii) (R^1 = Ph, R^2 = H, R^3 = Me); 24b: Using an analogous procedure and molar quantities of reagents as in 6.5.8(i) using **LIXb** (99 mg, 0.22 mmol) and $CoCl_2$ (29 mg, 0.22 mmol), gave [{**LIXb**}$FeCl_2$] (**24b**) as a green powder. Yield: 85 % (108 mg, 0.19 mmol).

6.5.10. Synthesis of [{2-((2'-O)C_6H_4)-6-(CMeN(2,6-*i*-$Pr_2C_6H_3$))C_5H_3N}FeCl]$_n$ (25): An oven-dried Schlenk flask equipped with a magnetic stir bar was evacuated and backfilled with nitrogen. The flask was charged with **LIXa** (100 mg, 0.27 mmol) and sodium hydride (13 mg, 0.54 mmol) in thf (10 ml). The resulting suspension was refluxed for 48 h, followed by cannular filtration into a Schlenk flask containing $FeCl_2(thf)_{1.5}$ (75 mg, 0.32 mmol) and stirred at rt for 24 h. The reaction mixture was concentrated and hexane added to induce precipitation of [{**LIXa**$^{-H}$}FeCl]$_2$ (**25**) as a dark red solid. The suspension was stirred overnight, filtered, washed with hexane (2 x 30 ml) and dried under reduced pressure. Yield: 68 % (83 mg, 0.18 mmol).

6.5.11. Synthesis of [{2-((2'-O-3'-R^1-5'-R^2)C_6H_2)-6-(CR^3N(2,6-*i*-$Pr_2C_6H_3$))C_5H_3N}CoX]$_2$ (26)

(i) (R^1 = R^2 = H, R^3 = Me, X = Cl); 26a: Using the same procedure and molar quantities of reagents as in 6.5.10 using **LIXa** (100 mg, 0.27 mmol), sodium hydride (13 mg, 0.54 mmol), $CoCl_2$ (35 mg, 0.27 mmol) and thf as the solvent, gave [{**LIXa**$^{-H}$}CoCl]$_2$ (**26a**) as a green solid. The suspension was stirred overnight, filtered, washed with hexane (2 x 30 ml) and dried under reduced pressure. Recrystallisation from a hot acetonitrile gave red crystals of **26a** suitable for single crystal X-ray structure determination. Yield: 79 % (98 mg, 0.21 mmol).

(ii) (R^1 = R^2 = R^3 = H, X = Cl); 26b: An oven-dried Schlenk flask equipped with a magnetic stir bar was evacuated and backfilled with nitrogen. The flask was charged with $CoCl_2$ (36 mg, 0.28 mmol) and dissolved in *n*-butanol (10 ml) at 90 °C. **LIXc** (90 mg, 0.25 mmol) was introduced and the reaction mixture stirred at 90 °C for 30 min. The reaction mixture was concentrated and hexane added to induce precipitation of [{**LIXc**$^{-H}$}CoCl]$_2$ (**26b**) as a green powder. The green suspension was stirred overnight, filtered, washed with hexane (2 x 30 ml) and dried under reduced pressure. Red crystals of **26b** suitable for a single crystal X-ray diffraction study were obtained from the slow cooling of a hot acetonitrile solution. Yield: 80 % (98 mg, 0.11 mmol).

(iii) (R^1 = R^3 = H; R^2 = *t*-Bu; X = Br); 26c: An oven-dried Schlenk flask equipped with a magnetic stir bar was evacuated and backfilled with nitrogen. The flask was charged with $CoBr_2$ (94 mg, 0.43 mmol) and dissolved in *n*-butanol (10 ml) at 90 °C. **LIXd** (150 mg, 0.35 mmol) was introduced and the reaction mixture stirred at 90 °C for 30 min. The reaction mixture was concentrated and hexane added to induce precipitation of [{**LIXd**$^{-H}$}CoBr]$_2$ (**26c**) as a green solid. The green suspension was stirred overnight, filtered, washed with hexane (2 x 30 ml) and dried under reduced pressure. Red crystals of **26c** suitable for a single crystal X-

ray diffraction study were obtained from the slow cooling of a hot acetonitrile solution. Yield: 75 % (145 mg, 0.13 mmol).

6.5.12. Ethylene Polymerisation Screening

Polymerisations were performed in glass-lined 23.5 ml reactors equipped with disposable PEEK mechanical stirrers, an external heater for temperature control, septum inlet regulated supply of nitrogen and ethylene, in a nitrogen purged glove box. The complexes **21**, **23a**, **23b** and **24b** were employed. The reactor was dried and degassed at 115°C for 5 h and then purged with nitrogen at room temperature for another 5 h. It was finally purged with ethylene. A mixture of toluene and MAO (100 eq, source Albamarle 10% wt in toluene, % wt altered when necessary) was added at rt, followed by heating the reactor to process temperature (40 °C) while stirring at 800 rpm. The pre-catalyst dissolved in chlorobenzene (0.1 ml, 0.2 mM), was injected at process conditions. Ethylene was fed to the reactor on demand to keep pressure constant at 17.23 bar.[15] The reaction was quenched with 5 mol% Oxygen in Argon after the total duration of 1 h or a predetermined amount of ethylene had been consumed (1.38 bar). The reactor was then cooled, vented and the polymer recovered by vacuum centrifugation of the reaction mixture. The catalysts were validated with the literature precedent [{2,6-*i*-$Pr_2C_6H_3N$=C(Me)-C(Me)=N2,6-*i*-$Pr_2C_6H_3$}$NiBr_2$] and [{2,6-(2',6',-*i*-$Pr_2C_6H_3N)_2C_5H_3N$}$FeCl_2$] complexes and MAO as activator.

Table 7 Elemental analysis results for complexes **21**, **22**, **24a** and **26**

Compound	Microanalysis (%)[a]		
	C	H	N
$C_{26}H_{30}N_2OFeCl_2$ (**21**)	60.94 (60.83)	5.69 (5.90)	5.35 (5.46)
$C_{26}H_{30}N_2OCoCl_2.¾CHCl_3$(**22**)	53.07 (53.03)	4.69 (5.12)	4.09 (4.62)
$C_{25}H_{28}N_2OCoCl_2$ (**24a**)	59.72 (59.77)	5.60 (5.62)	5.72 (5.58)
$C_{50}H_{54}N_4O_2Co_2Cl_2$ (**26a**)	64.52	5.83	6.01

	(64.45)	(5.83)	(6.01)
$C_{48}H_{50}N_4O_2Co_2Cl_2$ (**26b**)	63.40 (63.8)	5.85 (5.58)	6.26 (6.20)
$C_{56}H_{66}N_4O_2Co_2Br_2$ (**26c**)	56.42 (60.88)	5.27 (6.02)	5.56 (5.07)

[a] calculated values in parentheses.

Table 8 FAB MS, IR and rt magnetic moments for complexes **21-26**

Compound[a]	FAB mass spectrum (m/z)	ν(C=N) (cm^{-1})[b]	μ_{eff} (BM)
$C_{26}H_{30}N_2OFeCl_2$ (**21**)	512 $[M]^+$, 477 $[M\text{-}Cl]^+$	1614, 1602, 1588	4.97[b]
$C_{26}H_{30}N_2OCoCl_2.¾CHCl_3$(**22**)	480 $[M\text{-}Cl]^+$	1618, 1606, 1592	4.04[b]
$C_{25}H_{28}N_2OFeCl_2$ (**23a**)	893$[2M\text{-}3Cl]^+$, 497 $[M]^+$, 462 $[M\text{-}Cl]^+$	1604, 1592	5.00[b]
$C_{31}H_{32}N_2OFeCl_2$ (**23b**)	538 $[M\text{-}Cl]^+$, 503 $[M\text{-}2Cl]^+$,	-	5.20[b]
$C_{25}H_{28}N_2OCoCl_2$ (**24a**)	895 $[2M\text{-}3Cl]^+$ 465 $[M\text{-}Cl]^+$ 430 $[M\text{-}2Cl]^+$	1609, 1590	3.98[b]
$C_{31}H_{32}N_2OCoCl_2$ (**24b**)	544 $[M\text{-}Cl]^+$	1589	3.99[b]
$C_{50}H_{54}N_4O_2Fe_2Cl_2$ (**25**)	889 $[M\text{-}Cl]^+$, 462 $[M/2]^+$ 427 $[M/2\text{-}Cl]^+$	1613, 1586	7.1[b]
$C_{50}H_{54}N_4O_2Co_2Cl_2$ (**26a**)	895 $[M\text{-}Cl]^+$ 430 $[M/2\text{-}Cl]^+$	1619, 1591	6.36[c]
$C_{48}H_{50}N_4O_2Co_2Cl_2$ (**26b**)	867 $[M\text{-}Cl]^+$ 416 $[M/2\text{-}Cl]^+$	1628, 1591	5.97[b]
$C_{56}H_{66}N_4O_2Co_2Br_2$ (**26c**)	1036 $[M\text{-}Br]^+$	1627, 1591	5.80[b]

[a] Molecular Formula obtained from elemental analysis except for **23a**, **23b**, **24b** and **25**; [b] Analysed using an Evans Balance; [c] Analysed using a SQUID.

6.6. Density Functional Calculations

Quantum mechanical calculations have been carried out using the Gaussian 98 package of programs. [23] The density functional theory (DFT) was applied, in particular the functional Becke's three-parameter hybrid exchange method combined with LYP correlation functional (B3LYP).[24] The method was used in its unrestricted implementation.

The quasi-relativistic effective core potential (ECP) LANL2DZ was used for the metal atoms (iron and cobalt).[25] The basis set for both atoms is the valence double-ζ contraction associated to this ECP. [23,25] The valence double-ζ with polarisation 6-31G(d)[26,27] basis was used for nitrogen and chlorine and the valence double-ζ 6-31G for carbon and hydrogen.[26] In all cases, the spin contamination, evaluated from the computed value of S^2, was found to be small.

6.7. Variable temperature magnetochemical studies (SQUID) The variable temperature magnetic susceptibility data recorded for 1, 2, 6, 10a, 15a, 15b and 26a were measured in the temperature range 2 - 300 K with a Quantum Design MPMS2 SQUID magnetometer at the University of Edinburgh, operating at 100 G (0.01 T). Data were corrected for magnetisation of the sample holder and for diamagnetic contributions, which were estimated from Pascal constants.[3]

6.8. Crystallography

Data for **1**, **2**, **4**, **5**, **6**, **7**, **8**, **9**, **10c**, **11a**, **11c**, **12**, **14a**, **14b**, **15a**, **15b**, **17a**, **19a**, **LVIIIb**, **LIXa**, **20**, **21**, **22**, **24a**, **26b** and **26c** were collected on a Bruker APEX 2000 CCD diffractometer, data for **16a** and **16b** were collected on a Bruker/Siemens P4 diffractometer and data for **10a**, **18a** and **26a** were collected on a Bruker-NoniasKappa CCD diffractometer. Details of data collection, refinement and crystal data are listed in Tables 9-16. The diffractometers used a graphite-monochromated molybdenum Kα radiation; λ = 0.7107 Å. The data were corrected for Lorenz-polarisation effects and empirical absorption corrections were based on ψ scans.

Structure solution by Patterson methods and structure refinement on F^2 employed SHELXTL version 6.10.[16, 17] Hydrogen atoms were included in calculated positions (C-H = 0.96 Å) riding on the bonded atom with isotropic displacement parameters set to 1.5 U_{eq}(C) for methyl hydrogen atoms and 1.2 U_{eq}(C) for all other hydrogen atoms. All non-hydrogen atoms were refined with anisotropic displacement parameters.

Table 9 Crystallographic and data processing parameters for complexes **1**, **2**, **4** and **5**

Data	1	2	4	5
Empirical formula	$C_{38.5}H_{44}Cl_{11}Fe_3N_9$	$C_{30}H_{35}Cl_2FeN_9$	$C_{30}H_{35}Cl_2CoN_9$	$C_{18}H_{18}Cl_2MnN_4$
Formula weight	1190.34	648.42	651.50	416.20
Temperature (K)	160(2)	150(2)	150(2)	160(2)
Wavelength (Å)	0.71073	0.71073	0.71073	0.71073
Crystal system	Monoclinic	Monoclinic	Monoclinic	Monoclinic
Space group	C2/c	C2/c	C2/c	P2(1)/n
Unit cell dimensions				
a (Å)	40.645(6)	20.425(5)	20.4934(11)	9.017(3)
b (Å)	10.5792(15)	9.535(2)	9.5181(5)	15.865(6)
c (Å)	22.098(3)	16.656(4)	16.8644(9)	13.257(5)
α (°)	90	90	90	90
β (°)	100.410(4)	107.384(4)	105.7270(10)	98.723(5)
γ (°)	90	90	90	90
Volume ($Å^3$)	9346(2)	3095.8(13)	3166.4(3)	1874.7(11)
Z	8	4	4	4
Density (calculated) (Mg/m^3)	1.692	1.391	1.367	1.475
Absorption coefficient (mm^{-1})	1.590	0.696	0.746	0.997
F(000)	4824	1352	1356	852
Crystal size (mm^3)	0.28 x 0.24 x 0.07	0.17 x 0.16 x 0.03	0.24 x 0.24 x 0.07	0.33 x 0.24 x 0.19
Theta range for data collection (°)	1.87 to 27.00	2.09 to 25.00	2.06 to 26.00	2.02 to 26.50
Index ranges	-51<=h<=51 -13<=k<=13 -28<=l<=27	-24<=h<=24 11<=k<=11 19<=l<=19	-25<=h<=25 11<=k<=11 -20<=l<=20	-11<=h<=11 -19<=k<=19 -16<=l<=16
Reflections collected	38649	10766	12058	14112
Independent reflections	10196 [R(int) = 0.0422]	2729 [R(int) = 0.0471]	3108 [R(int) = 0.0192]	3868 [R(int) = 0.1658]
Completeness to max theta (%)	100.0	99.8	99.9	99.5
Absorption correction	Empirical	Empirical	Empirical	Empirical
Max. and min. transmission	0.928 and 0.767	0.93 and 0.85	0.928 and 0.685	0.831 and 0.364
Refinement method	Full-matrix least-squares on F^2	Full-matrix least-squares on F^2	Full-matrix least-squares on F^2	Full-matrix least-squares on F^2
Data / restraints / parameters	10196 / 0 / 555	2729 / 0 / 229	3108 / 0 / 229	3868 / 0 / 226
Goodness-of-fit on F^2	0.944	1.067	1.083	1.022
Final R indices [I>2sigma(I)]	R1 = 0.0423 wR2 = 0.1027	R1 = 0.0485 wR2 = 0.1304	R1 = 0.0294 wR2 = 0.0884	R1 = 0.0419 wR2 = 0.0990
R indices (all data)	R1 = 0.0611 wR2 = 0.1064	R1 = 0.0584 wR2 = 0.1356	R1 = 0.0325 wR2 = 0.0898	R1 = 0.0484 wR2 = 0.1013
Largest diff. peak and hole ($e.Å^{-3}$)	1.016 and -1.030	0.780 and -0.339	0.404 and -0.305	0.898 and -0.610

Table 10 Crystallographic and data processing parameters for complexes **6**, **7**, **8** and **9**

Data	6	7	8	9
Empirical formula	$C_{20}H_{21}Cl_2FeN_5$	$C_{18}H_{18}Cl_2CoN_4$	$C_{18}H_{18}Cl_2CoN_4$	$C_{20}H_{21}Cl_3Co_{1.5}N_5$
Formula weight	458.17	420.19	420.19	526.16
Temperature (K)	160(2)	150(2)	150(2)	160(2)
Wavelength (Å)	0.71073	0.71073	0.71073	0.71073
Crystal system	Orthorhombic	Monoclinic	Cubic	Monoclinic
Space group	Pnn2	P2(1)/c	P2(1)3	Cc
Unit cell dimensions				
a (Å)	14.984(3)	13.1037(8)	12.3978(3)	12.0204(6)
b (Å)	15.312(3)	9.1929(5)	12.3978(3)	7.3573(15)
c (Å)	9.1634(17)	15.7386(9)	12.3978(3)	14.0893(7)
α (°)	90	90	90	90
β (°)	90	92.5490(10)	90	94.0500(10)
γ (°)	90	90	90	90
Volume(Å^3)	2102.3(7)	1894.01(19)	1905.61(8)	4621.6(4)
Z	4	4	4	8
Density (calculated) (Mg/m^3)	1.448	1.474	1.465	1.512
Absorption coefficient (mm^{-1})	0.987	1.196	1.189	1.452
F(000)	944	860	860	2140
Crystal size (mm^3)	0.08 x 0.12 x 0.16	0.14 x 0.15 x 0.05	0.29 x 0.34 x 0.37	0.24 x 0.24 x 0.06
Theta range for data collection (°)	1.90 to 27.00	1.56 to 26.99	2.32 to 26.95	1.49 to 27.00
Index ranges	-19<=h<=19 -19<=k<=19 -11<=l<=11	-16<=h<=16 -11<=k<=11 -20<=l<=20	-15<=h<=15 -15<=k<=15 -15<=l<=15	-15<=h<=15 -34<=k<=34 -17<=l<=17
Reflections collected	16933	15544	16095	19165
Independent reflections	4578 [R(int) = 0.0320]	4130 [R(int) = 0.0336]	1400 [R(int) = 0.0299]	9575 [R(int) = 0.0325]
Completeness to max theta (%)	100.0	99.9	100.0	99.9
Absorption correction	Empirical	Empirical	Empirical	Empirical
Max. and min. transmission	0.91 and 0.83	0.862 and 0.223	0.862 and 0.506	0.928 and 0.714
Refinement method	Full-matrix least-squares on F^2	Full-matrix least-squares on F^2	Full-matrix least-squares on F^2	Full-matrix least-squares on F^2
Data / restraints / parameters	4578 / 1 / 254	4130 / 0 / 226	1400 / 0 / 76	9575 / 2 / 534
Goodness-of-fit on F^2	0.911	0.947	1.095	0.899
Final R indices [I>2sigma(I)]	R1 = 0.0247 wR2 = 0.0507	R1 = 0.0290 wR2 = 0.0744	R1 = 0.0166 wR2 = 0.0448	R1 = 0.0296 wR2 = 0.0602
R indices (all data)	R1 = 0.0288 wR2 = 0.0512	R1 = 0.0351 wR2 = 0.0757	R1 = 0.0167 wR2 = 0.0448	R1 = 0.0341 wR2 = 0.0609
Largest diff. peak and hole (e.Å^{-3})	0.380 and -0.225	0.449 and -0.212	0.172 and -0.174	0.557 and -0.346

Table 11 Crystallographic and data processing parameters for complexes **10a**, **10c**, **11a** and **11c**

Data	10a	10c	11a	11c
Empirical formula	$C_{16}H_{21}Cl_2FeN_3$	$C_{34}H_{56}Cl_4Fe_2N_6$	$C_{16}H_{21}Cl_2CoN_3$	$C_{19}H_{26}Cl_2CoN_4$
Formula weight	382.11	792.26	385.19	440.27
Temperature (K)	120(2)	150(2)	150(2)	150(2)
Wavelength (Å)	0.71073	0.71073	0.71073	0.71073
Crystal system	Orthorhombic	Monoclinic	Monoclinic	Triclinic
Space group	Pbca	C2/c	P2(1)/c	P-1
Unit cell dimensions				
a (Å)	16.1515(2)	28.7059(19)	14.5732(7)	8.6478(8)
b (Å)	12.92940(10)	9.5482(6)	7.5761(4)	10.6957(10)
c (Å)	16.3990(2)	14.2018(10)	16.3162(8)	11.9131(11)
α (°)	90	90	90	82.715(2)
β (°)	90	112.2260(10)	108.4810(10)	68.821(2)
γ (°)	90	100.35(3)	90	85.749(2)
Volume($Å^3$)	3424.59(7)	3603.3(4)	1708.54(15)	1018.70(16)
Z	8	4	4	2
Density (calculated) (Mg/m^3)	1.482	1.460	1.497	1.435
Absorption coefficient (mm^{-1})	1.192	1.136	1.316	1.115
F(000)	1584	1648	796	458
Crystal size (mm^3)	0.66 x 0.32 x 0.28	0.34 x 0.11 x 0.04	0.28 x 0.24 x 0.21	0.24 x 0.15 x 0.07
Theta range for data collection (°)	2.97 to 25.00	1.53 to 25.00	1.47 to 27.00	1.84 to 27.00
Index ranges	-19<=h<=16 -15<=k<=12 -19<=l<=17	-34<=h<=34 -11<=k<=11 -16<=l<=16	-18<=h<=18 -9<=k<=9 -20<=l<=20	-10<=h<=11 -13<=k<=13 -15<=l<=15
Reflections collected	21314	12725	13898	8606
Independent reflections	3013 [R(int) = 0.0473]	3170 [R(int) = 0.0393]	3716 [R(int) = 0.0206]	4357 [R(int) = 0.0342]
Completeness to max theta (%)	99.8	99.9	99.7	98.3
Absorption correction	Empirical	Empirical	Empirical	Empirical
Max. and min. transmission	0.640 and 0.557	0.93 and 0.80	0.862 and 0.767	0.928 and 0.783
Refinement method	Full-matrix least-squares on F^2	Full-matrix least-squares on F^2	Full-matrix least-squares on F^2	Full-matrix least-squares on F^2
Data / restraints / parameters	3013 / 0 / 201	3170 / 0 / 211	3716 / 0 / 201	4357 / 0 / 239
Goodness-of-fit on F^2	1.146	0.990	1.039	0.862
Final R indices [I>2sigma(I)]	R1 = 0.0255 wR2 = 0.0689	R1 = 0.0331 wR2 = 0.0711	R1 = 0.0257 wR2 = 0.0681	R1 = 0.0329 wR2 = 0.0651
R indices (all data)	R1 = 0.0281 wR2 = 0.0701	R1 = 0.0427 wR2 = 0.0741	R1 = 0.0291 wR2 = 0.0689	R1 = 0.0476 wR2 = 0.0671
Largest diff. peak and hole ($e.Å^{-3}$)	0.388 and -0.362	0.363 and -0.243	0.477 and -0.204	0.544 and -0.233

Table 12 Crystallographic and data processing parameters for complexes **12**, **14a**, **14b** and **15a**

Data	12	14a	14b	15a
Empirical formula	$C_{18}H_{25}Cl_2CoN_3$	$C_{44}H_{52}Cl_4Mn_2N_8$	$C_{24}H_{28}Cl_2MnN_5$	$C_{24}H_{29}Cl_2FeN_5$
Formula weight	413.24	944.62	512.35	514.27
Temperature (K)	150(2)	160(2)	150(2)	150(2)
Wavelength (Å)	0.71073	0.71073	0.71073	0.71073
Crystal system	Monoclinic	Monoclinic	Monoclinic	Triclinic
Space group	P2(1)/c	P2(1)/n	P2(1)/c	P-1
Unit cell dimensions				
a (Å)	15.410(3)	12.0717(6)	19.337(3)	7.5084(13)
b (Å)	7.4772(14)	14.9732(8)	14.843(2)	12.873(2)
c (Å)	16.863(3)	13.6389(7)	17.351(3)	12.978(2)
α (°)	90	90	90	82.257(3)
β (°)	94.761(3)	116.121(1)	99.618(3)	86.705(3)
γ (°)	90	90	90	83.201(3)
Volume(Å^3)	1936.2(6)	2213.5(2)	4910.0(13)	1233.1(4)
Z	4	2	8	2
Density (calculated) (Mg/m^3)	1.418	1.417	1.386	1.385
Absorption coefficient (mm^{-1})	1.167	0.854	0.777	0.850
F(000)	860	980	2128	536
Crystal size (mm^3)	0.30 x 0.19 x 0.06	0.26 x 0.21 x 0.04	0.34 x 0.30 x 0.04	0.32 x 0.25 x 0.08
Theta range for data collection (°)	1.33 to 26.00	1.88 to 26.50	1.07 to 25.00	1.58 to 26.00
Index ranges	-18<=h<=19 -9<=k<=9 -20<=l<=20	-15<=h<=15 -18<=k<=18 -17<=l<=17	-22<=h<=22 -17<=k<=17 -20<=l<=20	-9<=h<=9 -15<=k<=15 -15<=l<=15
Reflections collected	13964	17770	34315	9702
Independent reflections	3785 [R(int) = 0.0809]	4587 [R(int) = 0.0384]	8554 [R(int) = 0.0788	4770 [R(int) = 0.0231]
Completeness to max theta (%)	99.4 %	100.0 %	99.0 %	98.7 %
Absorption correction	Empirical	Empirical	Empirical	Empirical
Max. and min. transmission	0.86 and 0.57	0.974 and 0.847	0.86 and 0.74	0.928 and 0.710
Refinement method	Full-matrix least-squares on F^2	Full-matrix least-squares on F^2	Full-matrix least-squares on F^2	Full-matrix least-squares on F^2
Data / restraints / parameters	3785 / 0 / 221	4587 / 0 / 268	8554 / 0 / 583	4770 / 0 / 292
Goodness-of-fit on F^2	1.039	1.054	1.096	1.031
Final R indices [I>2sigma(I)]	R1 = 0.0689 wR2 = 0.1574	R1 = 0.0273 wR2 = 0.0735	R1 = 0.1028 wR2 = 0.2577	R1 = 0.0349, wR2 = 0.0849
R indices (all data)	R1 = 0.1024 wR2 = 0.1751	R1 = 0.0311 wR2 = 0.0749	R1 = 0.1265 wR2 = 0.2695	R1 = 0.0407, wR2 = 0.0883
Largest diff. peak and hole (e.Å^{-3})	0.867 and -0.746	0.431 and -0.240	1.875 and -0.877	0.366 and -0.219

Table 13 Crystallographic and data processing parameters for complexes **15b**, **16a**, **16b** and **17a**

Data	15b	16a	16b	17a
Empirical formula	$C_{24}H_{29}Cl_2FeN_5$	$C_{20}H_{29}Cl_2CoN_3$	$C_{22}H_{33}Cl_2CoN_3$	$C_{21}H_{31}Cl_2CoN_3$
Formula weight	514.27	441.29	469.34	455.32
Temperature (K)	150(2)	200(2) K	200(2) K	200(2) K
Wavelength (Å)	0.71073	0.71073 Å	0.71073 Å	0.71073 Å
Crystal system	Monoclinic	Triclinic	monoclinic	monoclinic
Space group	P2(1)/c	P-1	P2(1)/c	P2(1)/n
Unit cell dimensions				
a (Å)	19.206(4)	6.484(3)	13.143(5)	12.727(8)
b (Å)	14.800(3)	10.962(6)	15.618(6)	13.796(8)
c (Å)	17.270(4)	15.778(5)	11.783(8)	13.816(8)
α (°)	90	103.21(5)	90	90.00
β (°)	99.752(4)	96.16(4)	102.07(5)	112.66(4)
γ (°)	90	100.35(3)	90	90.00
Volume($Å^3$)	4838.1(18)	1061.1(8)	2365(2)	2239(2)
Z	8	2	4	4
Density (calculated) (Mg/m^3)	1.412	1.381	1.318	1.351
Absorption coefficient (mm^{-1})	0.866	1.069	0.964	1.016
F(000)	2144	462	988	956
Crystal size (mm^3)	0.47 x 0.21 x 0.04	0.56 x 0.32 x 0.14	0.52 x 0.12 x 0.09	0.52 x 0.33 x 0.14
Theta range for data collection (°)	1.75 to 25.00	1.95 to 25.48	2.05 to 25.01	2.18 to 26.01
Index ranges	-22<=h<=22 -13<=k<=17 -20<=l<=20	-7<=h<=1 -12<=k<=12 -18<=l<=19	-15<=h<=15 -1<=k<=18 0<=l<=12	0 <=h<= 15 -1<=h<=17 -17<=h<=15
Reflections collected	26576	4388	4674	4377
Independent reflections	8503 [R(int) = 0.1551]	3859 [R(int) = 0.0252]	4083 [R(int) = 0.0480]	4814 [R(int) = 0.0489]
Completeness to max theta (%)	99.8	97.9	97.7	99.6
Absorption correction	Empirical	Psi-scan	Analytical	Empirical
Max. and min. transmission	0.93 and 0.59	0.667 and 0.507	0.908 and 0.836	0.897 and 0.74
Refinement method	Full-matrix least-squares on F^2	Full-matrix least-squares on F^2	Full-matrix least-squares on F^2	Full-matrix least-squares on F^2
Data / restraints / parameters	8503 / 0 / 584	3859 / 0 / 235	4083 / 0 / 253	4377/0/249
Goodness-of-fit on F^2	0.882	1.061	0.966	1.019
Final R indices [I>2sigma(I)]	R1 = 0.0787 wR2 = 0.1608	R1 = 0.0329 wR2 = 0.0774	R1 = 0.0610 wR2 = 0.1165	R1 = 0.0555 wR2 = 0.1220
R indices (all data)	R1 = 0.1670 wR2 = 0.1970	R1 = 0.0421 wR2 = 0.0824	R1 = 0.1312 wR2 = 0.1405	R1 = 0.0906 wR2 = 0.1399
Largest diff. peak and hole ($e.Å^{-3}$)	0.995 and -0.857	0.319 and -0.293	0.413 and -0.368	0.622 and -0.372

Table 14 Crystallographic and data processing parameters for complexes **18a**, **19a** and ligands **LVIIIb** and **LIXa**

Data	18a	19a	LVIIIb	LIXa
Empirical formula	$C_{30}H_{41}Cl_2FeN_5$	$C_{29}H_{40}Cl_4CoN_4$	$C_{32}H_{34}N_2O$	$C_{27}H_{30}Cl_{4.50}N_2O$
Formula weight	598.43	645.38	462.61	558.05
Temperature (K)	120(2)	150(2)	150(2) K	150(2) K
Wavelength (Å)	0.71073	0.71073	0.71073 Å	0.71073 Å
Crystal system	Triclinic	Triclinic	Triclinic	Monoclinic
Space group	P-1	P-1	P-1	C2/c
Unit cell dimensions				
a (Å)	7.4106(15)	7.3225(12)	9.8646(12)	16.7938(10)
b (Å)	15.244(3)	15.150(3)	11.3359(14)	20.9298(10)
c (Å)	15.311(3)	15.669(3)	12.2859(15)	16.4977(8)
α (°)	115.74(3)	114.669(3)	102.516(2)	90
β (°)	97.86(3)	99.627(3)	91.539(2)	110.7790(10)
γ (°)	99.89(3)	97.162(3)	100.520(2)	90
Volume($Å^3$)	1490.7(5)	1520.2(4)	1315.5(3)	5421.6(5)
Z	2	2	2	8
Density (calculated) (Mg/m^3)	1.333	1.410	1.168	1.367
Absorption coefficient (mm^{-1})	0.713	0.942	0.07	0.509
F(000)	632	674	496	2324
Crystal size (mm^3)	0.15 x 0.03 x 0.03	0.11 x 0.18 x 0.32	0.403 x 0.228 x 0.107	0.42 x 0.29 x 0.20
Theta range for data collection (°)	2.91 to 26.00	1.47 to 23.29	1.70 to 27.00	1.62 to 27.00
Index ranges	-8<=h<=9 -18<=k<=18 -18<=l<=18	-8<=h<=8 -16<=k<=16 -17<=l<=16	-12<=h<=12 -14<=k<=14 -15<=l<=15	-21<=h<=21 -26<=k<=26 -21<=l<=20
Reflections collected	10326	9555	11208	22590
Independent reflections	5606 [R(int) = 0.1691]	4362 [R(int) = 0.0241]	5661 [R(int) = 0.0226]	5903 [R(int) = 0.0236]
Completeness to max theta (%)	95.9	99.5	98.4	99.9
Absorption correction	Empirical	Empirical	Empirical	Empirical
Max. and min. transmission	0.911 and 0.887	0.93 and 0.80	0.928 and 0.780	0.93 and 0.12
Refinement method	Full-matrix least-squares on F^2	Full-matrix least-squares on F^2	Full-matrix least-squares on F^2	Full-matrix least-squares on F^2
Data / restraints / parameters	5606 / 0 / 343	4362 / 0 / 349	5661 / 0 / 322	5903 / 0 / 318
Goodness-of-fit on F^2	0.870	0.961	0.830	1.102
Final R indices [I>2sigma(I)]	R_1 = 0.0607 wR_2 = 0.0945	R_1 = 0.0318 wR_2 = 0.0746	R1 = 0.0394 wR2 = 0.0807	R1 = 0.0824 wR2 = 0.2487
R indices (all data)	R_1 = 0.2275, wR_2 = 0.1298	R_1 = 0.0463 wR_2 = 0.0789	R1 = 0.0650 wR2 = 0.0849	R1 = 0.0984 wR2 = 0.2621
Largest diff. peak and hole ($e.Å^{-3}$)	0.410 and -0.536	0.253 and -0.226	0.199 and -0.172	1.284 and -1.308

Table 15 Crystallographic and data processing parameters for complexes **20**, **21**, **22** and **24a**

Data	20	21	22	24a
Empirical formula	$C_{29}H_{36}AlN_3O$	$C_{27}H_{31}Cl_5FeN_2O$	$C_{27}H_{31}Cl_5CoN_2O$	$C_{25}H_{28}Cl_2CoN_2O$
Formula weight	469.59	632.64	635.72	502.32
Temperature (K)	150(2) K	150(2) K	150(2) K	150(2) K
Wavelength (Å)	0.71073 Å	0.71073 Å	0.71073 Å	0.71073 Å
Crystal system	Orthorhombic	Monoclinic	Monoclinic	Monoclinic
Space group	Pbca	P2(1)/n	P2(1)/n	P2(1)/n
Unit cell dimensions				
a (Å)	15.399(14)	8.9967(11)	9.0275(7)	10.0852(7)
b (Å)	16.370(15)	23.154(3)	23.0743(18)	15.7138(11)
c (Å)	20.187(18)	13.8554(17)	13.7964(11)	15.3532(11)
α (°)	90	90	90	90
β (°)	90	94.077(2)	93.9820(10)	102.5540(10)
γ (°)	90	90	90	90
Volume($Å^3$)	5089(8)	2878.9(6)	2866.9(4)	2375.0(3)
Z	8	4	4	4
Density (calculated) (Mg/m^3)	1.226	1.460	1.473	1.405
Absorption coefficient (mm^{-1})	0.106	1.012	1.089	0.967
F(000)	2016	1304	1308	1044
Crystal size (mm^3)	0.39 x 0.12 x 0.11	0.29 x 0.12 x 0.12	0.47 x 0.09 x 0.04	0.36 x 0.16 x 0.10
Theta range for data collection (°)	2.02 to 25.00	1.72 to 26.00	1.72 to 27.00	1.88 to 26.00
Index ranges	-18<=h<=18 -19<=k<=19 -24<=l<=24	-11<=h<=10 -28<=k<=28 -17<=l<=16	-11<=h<=11 -29<=k<=29 -17<=l<=17	-11<=h<=12 -19<=k<=19 -18<=l<=18
Reflections collected	28652	20173	23938	18281
Independent reflections	4470 [R(int) = 0.2247]	5641 [R(int) = 0.0794]	6258 [R(int) = 0.0611]	4631 [R(int) = 0.0331]
Completeness to max theta (%)	99.8	99.9	99.9	99.3
Absorption correction	Empirical	Empirical	Empirical	Empirical
Max. and min. transmission	0.962 and 0.688	0.928 and 0.803	0.802 and 0.611	0.89 and 0.74
Refinement method	Full-matrix least-squares on F^2	Full-matrix least-squares on F^2	Full-matrix least-squares on F^2	Full-matrix least-squares on F^2
Data / restraints / parameters	4470 / 0 / 316	5641 / 0 / 331	6258 / 0 / 331	4631 / 0 / 285
Goodness-of-fit on F^2	0.951	0.904	0.904	1.011
Final R indices [I>2sigma(I)]	R1 = 0.0947 wR2 = 0.1935	R1 = 0.0535 wR2 = 0.1232	R1 = 0.0380 wR2 = 0.0805	R1 = 0.0365 wR2 = 0.0865
R indices (all data)	R1 = 0.1935 wR2 = 0.2431	R1 = 0.0779 wR2 = 0.1309	R1 = 0.0518 wR2 = 0.0826	R1 = 0.0451 wR2= 0.0905
Largest diff. peak and hole ($e.Å^{-3}$)	0.460 and -0.389	1.137 and -0.709	0.840 and -0.438	0.474 and -0.254

Table 16 Crystallographic and data processing parameters for complexes **26a**, **26b** and **26c**

Data	26a	26b	26c
Empirical formula	$C_{52}H_{57}Cl_2Co_2N_5O_2$	$C_{52}H_{56}Cl_2Co_2N_6O_2$	$C_{62}H_{75}Br_2Co_2N_7O_2$
Formula weight	972.78	985.78	1227.96
Temperature (K)	120(2)	150(2)	150(2)
Wavelength (Å)	0.71073	0.71073	0.71073
Crystal system	Monoclinic	Triclinic	Triclinic
Space group	C2/c	P-1	P-1
Unit cell dimensions			
a (Å)	16.0804(3)	16.053(2)	10.8999(6)
b (Å)	16.4777(3)	16.379(2)	14.9607(8)
c (Å)	19.2336(3)	19.884(3)	18.8201(10)
α (°)	90	76.074(3)	83.3610(10)
β (°)	109.5070(10)	79.267(2)	86.4200(10)
γ (°)	90	82.758(3)	88.1550(10)
Volume($Å^3$)	4803.76(15)	4967.6(12)	3041.5(3)
Z	4	4	2
Density (calculated) (Mg/m^3)	1.345	1.318	1.341
Absorption coefficient (mm^{-1})	0.847	0.821	1.906
F(000)	2032	2056	1272
Crystal size (mm^3)	0.40 x 0.38 x 0.10	0.19 x 0.18 x 0.06	0.25 x 0.20 x 0.15
Theta range for data collection (°)	3.23 to 25.00	1.29 to 26.00	1.37 to 26.00
Index ranges	-19<=h<=19 -19<=k<=19 -22<=l<=22	-19<=h<=19 -20<=k<=20 -24<=l<=24	-13<=h<=13 -18<=k<=18 -23<=l<=23
Reflections collected	31909	39368	23389
Independent reflections	4190 [R(int) = 0.0523]	19313 [R(int) = 0.0554]	11620 [R(int) = 0.0361]
Completeness to max theta (%)	98.8	98.9	97.0
Absorption correction	Empirical	Empirical	Empirical
Max. and min. transmission	0.709 and 0.663	0.89 and 0.63	0.89 and 0.74
Refinement method	Full-matrix least-squares on F^2	Full-matrix least-squares on F^2	Full-matrix least-squares on F^2
Data / restraints / parameters	4190 / 0 / 299	19313 / 0 / 1167	11620 / 0 / 679
Goodness-of-fit on F^2	1.026	0.901	0.957
Final R indices [I>2sigma(I)]	R1 = 0.0309 wR2 = 0.0763	R1 = 0.0538 wR2 = 0.1088	R1 = 0.0481 wR2 = 0.1200
R indices (all data)	R1 = 0.0355 wR2 = 0.0789	R1 = 0.0852 wR2 = 0.1185	R1 = 0.0687 wR2 = 0.1267
Largest diff. peak and hole ($e.Å^{-3}$)	0.629 and -0.346	1.115 and -0.474	1.638 and -0.632

References

[1] D. D. Perrin and W. L. I. Armarego, Purification of Laboratory Chemicals., 3rd Ed, 1994.
[2] R. S. Drago, Physical Methods in Chemistry; 1st Ed; W. B. Saunders, Co, USA: London 1977.
[3] Magnetic Susceptibility Balance Instruction Manual; J. M. Inc, Ed: Wayne, PA, 1991.
[4] T. Ukai, H. Kawazura, Y. Ishii, J. Bonnet, and J. A. Ibers, *J. Organomet. Chem.*, 1974, **65**, 253-266.
[5] G. M. Whitesides, M. Eisenhut and W.M. Bunting, *J. Am. Chem. Soc.*, 1974, **96**, 5398-5407.
[6] H. J. Horn, P. de Joode, W. L. Driessen and J. Reedijk, *Recueil des Travaux. Chim. Des. Pays-Bas.*, 1996, **115**, 191.
[7] G. Riggio, W. H. Hopff, A. A Hofmann and P. G., Waser, *Helv. Chim. Acta.*, 1980, **63**, 488-497.
[8] (a) Z. Tyeklar, R. R. Jacobson, N. Wei, N. N. Murthy, J. Zubieta and K. D. Karlin, *J. Am. Chem. Soc.*, 1993, **115**, 2677-2689; (b) B. G. Gafford and R. A. Holwerda, *Inorg. Chem.*, 1989, **28**, 60-66.
[9] B. Dietrich, M. W. Hosseini, J. M. Lehn and R. B. Sessions, *Helv. Chim. Acta.*, 1985, **68**, 289-299.
[10] F. Tellier, R. Sauvetre and J-F. Normant, *J. Organomet. Chem.*, 1985, **292**, 19-28.
[11] P. Baret, V. Beaujolais, C. Beguin, D. Gaude, J. L. Pierre and G. Serratric, *Eur. J. Inorg. Chem.*, 1998, 613-619-.
[12] R. Kadyrov, Detlef and R. Selke, *Tetrahedron: Asymmetry.*, 1998, **9**, 329-340.
[13] J. E. Parks, B. E. Wagner and R. H. Holm, *J. Organomet. Chem.*, 1973, **56**, 53-66.
[14] D. Astruc and J. R. Morow, *Bull. Chem. Soc. Fr.*, 1992, **129**, 319-328.
[15] 1 bar = 14.508 psi. Therefore 17.23 bar = 250 psi.
[16] G.M. Sheldrick, SHELXS97, program for crystal structure solution, University of Göttingen, Germany, 1993.
[17] G.M. Sheldrick, SHELXL97, program for crystal structure refinement, University of Göttingen, Germany, 1993.

7. Appendices

Calculations 1 Interpretation of rt Evans Balance Magnetochemical Data

$$\textbf{1.}\quad \chi_g = c \cdot l/10^9 \cdot m \cdot (R-R_o)$$

Where:

χ_g = magnetic susceptibility

c = constant 1.030

l = length of Evans tube (cm)

m = mass of sample (g)

R = final Evans balance reading

R_o = initial Evans balance reading

$$\textbf{2.}\quad \chi_{m'} = (\chi_g/MW)+\chi_a$$

Where:

$\chi_{m'}$ = molar magnetic susceptibility plus diamagnetic corrections (χ_a)

MW = molecular weight of sample

Diamagnetic corrections (x 10^{-6} mol^{-1}) = pyridine (-49)

= NH_3 (-18)

= OH^- (-12)

= First Row TM (-12.8)

= Cl^- (-23)

= Br^- (-34)

$$\textbf{3.}\quad \mu eff = 2.828\sqrt{(\chi_t)}$$

Where:

μeff = effective magnetic moment (BM)

Calculations 2 Interpretation of Variable Temperature Magnetochemical Data

1. $\chi_{m'} = (0.5 \cdot M/H) \cdot 1000 \cdot (MW/m) + \chi_a$

Where:

$\chi_{m'}$ = molar magnetic susceptibility plus diamagnetic corrections (χ_a)

M = magnetisation

H = magnetic field (G)

MW = molecular weight of sample

m = mass of sample (mg)

Diamagnetic corrections (x 10^{-6} mol^{-1}) = pyridine (-49)

= NH_3 (-18)

= OH^- (-12)

= First Row TM (-12.8)

= Cl^- (-23)

= Capsule (-2)

2. $1/\chi_{m'}$

3. $\chi_{m'} \cdot T$

Where:

T = Temperature (K)

4. $\mu eff = \sqrt{(8 \cdot \chi_{m'} \cdot T)}$

Where:

μeff = effective magnetic moment (BM)

Calculations 3 Ideal Effective Magnetic Moments (μeff) for manganese(II), iron(II) and cobalt(II) centres

$$\mu eff = \sqrt{(n(n+2)}$$

$$= 2.828\sqrt{(\chi_m \cdot T)}$$

$$\text{and } \chi_m.T = g^2/8 \cdot N \cdot S(S+1)$$

Where:

g = gyromagnetic ratio

N = the number of metal centres

S = the spin state

n = number of unpaired electrons

(**ia**) manganese(II) mononuclear complex [g = 2, S = 5/2]

$$\mu eff = 2.828\sqrt{[4/8 \cdot 1 \cdot (2.5(2.5+1))]}$$

$$= 5.92 \text{ BM}$$

(**ib**) manganese(II) dimer in which the metal centres are non-interacting

$$\mu eff = 2.828\sqrt{[4/8 \cdot 2 \cdot (2.5(2.5+1))]}$$

$$= 8.36 \text{ BM}$$

(**ic**) manganese(II) dimer in which the metal centres are ferromagnetically coupled [S_T = 5]

$$\mu eff = 2.828\sqrt{[4/8 \cdot 1 \cdot (5(5+1))]}$$

$$= 10.95 \text{ BM}$$

(**id**) manganese(II) dimer in which the metal centres are antiferromagnetically coupled [S_T = 0]

$$\mu eff = 0 \text{ BM}$$

(**iia**) iron(II) mononuclear complex [g = 2, S = 2]

$$\mu eff = 2.828\sqrt{[4/8 \cdot 1 \cdot (2(2+1))]}$$

$$= 4.90 \text{ BM}$$

iron(II) mononuclear complex [g = 2, S = 0]

$$\mu eff = 0 \text{ BM}$$

(iib) iron(II) dimer in which the metal centres are non-interacting

$$\mu eff = 2.828\sqrt{[4/8 \cdot 2 \cdot (2(2+1))]}$$

$$= 6.93 \text{ BM}$$

(iic) iron(II) dimer in which the metal centres are ferromagnetically coupled [S_T = 4]

$$\mu eff = 2.828\sqrt{[4/8 \cdot 1 \cdot (4(4+1))]}$$

$$= 8.94 \text{ BM}$$

(iid) iron(II) dimer in which the metal centres are antiferromagnetically coupled [S_T = 0]

$$\mu eff = 0 \text{ BM}$$

(iiia) cobalt(II) mononuclear complex [g = 2, S = 3/2]

$$\mu eff = 2.828\sqrt{[4/8 \cdot 1 \cdot (1.5(1.5+1))]}$$

$$= 3.87 \text{ BM}$$

(iiib) cobalt(II) dimer in which the metal centres are non-interacting

$$\mu eff = 2.828\sqrt{[4/8 \cdot 2 \cdot (1.5(1.5+1))]}$$

$$= 5.48 \text{ BM}$$

(iiic) cobalt(II) dimer in which the metal centres are ferromagnetically coupled [S_T = 3]

$$\mu eff = 2.828\sqrt{[4/8 \cdot 1 \cdot (3(3+1))]}$$

$$= 6.93 \text{ BM}$$

(iiid) cobalt(II) dimer in which the metal centres are antiferromagnetically coupled [S_T = 0]

$$\mu eff = 0 \text{ BM}$$

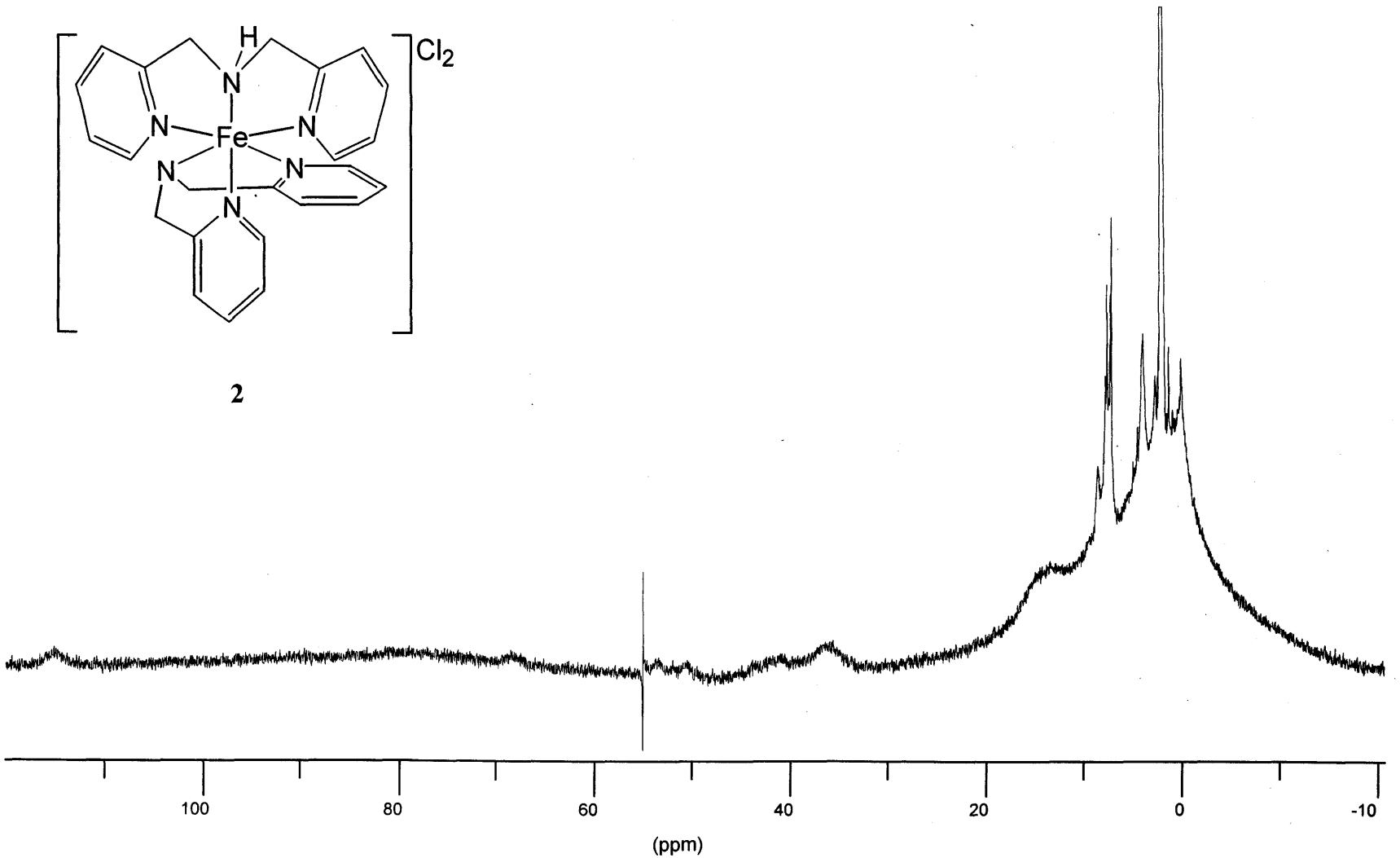

2

Figure 1 ^{1}H NMR spectrum of $[(dpa)_2Fe]Cl_2$ (**2**) in CD_3CN at rt

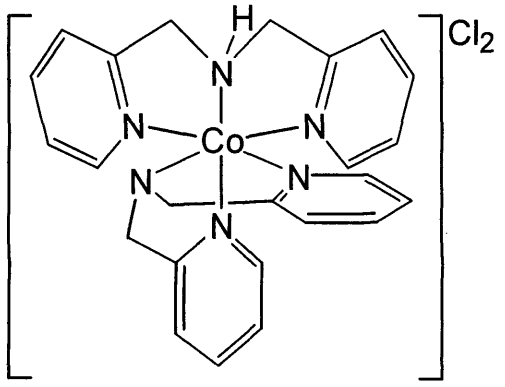

4

Figure 2 ^{1}H NMR spectrum of $[(dpa)_2Co]Cl_2$ (**4**) in CD_3CN at rt

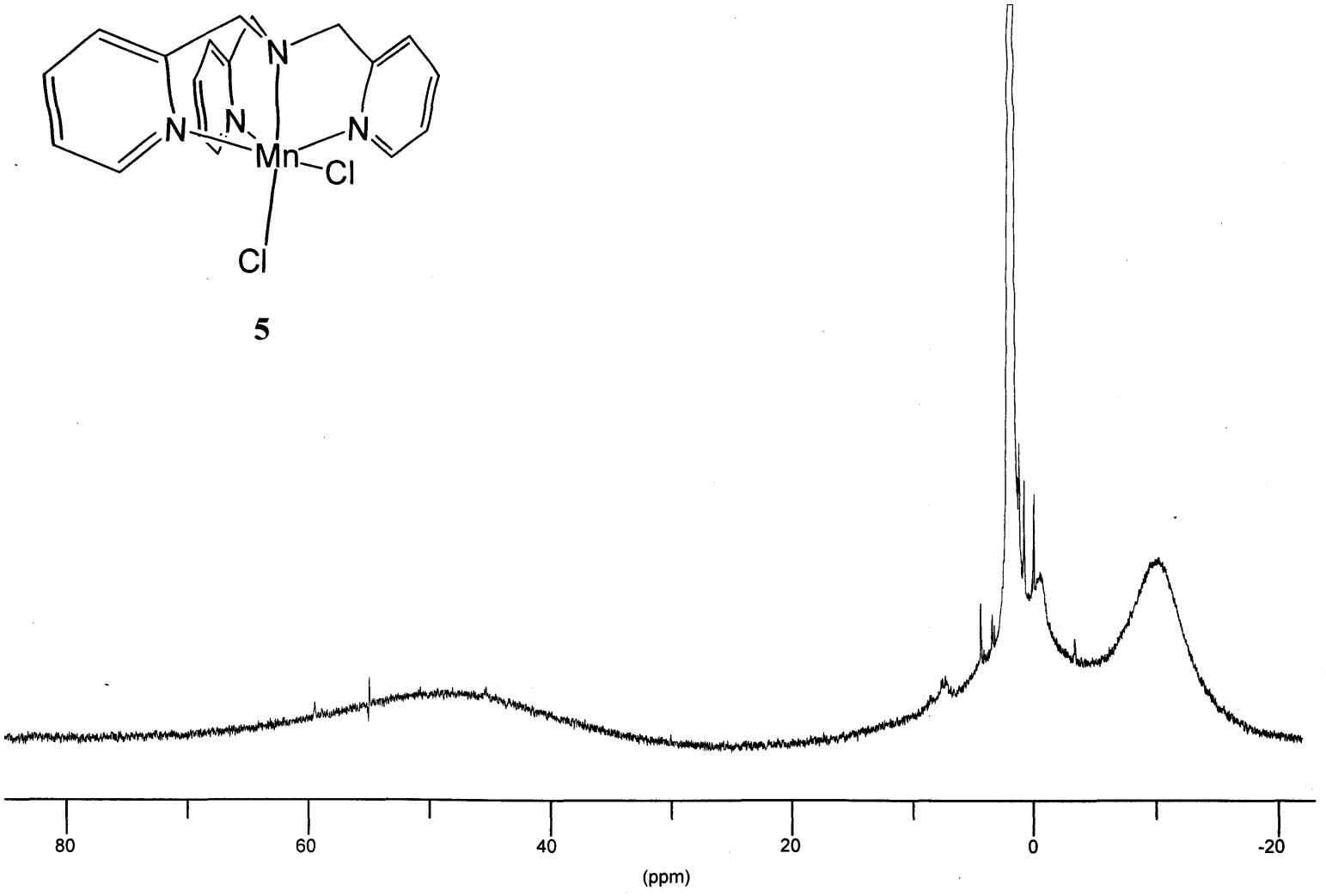

5

Figure 3 ^{1}H NMR spectrum of [{tpa}$MnCl_2$] (**5**) in CD_3CN at rt

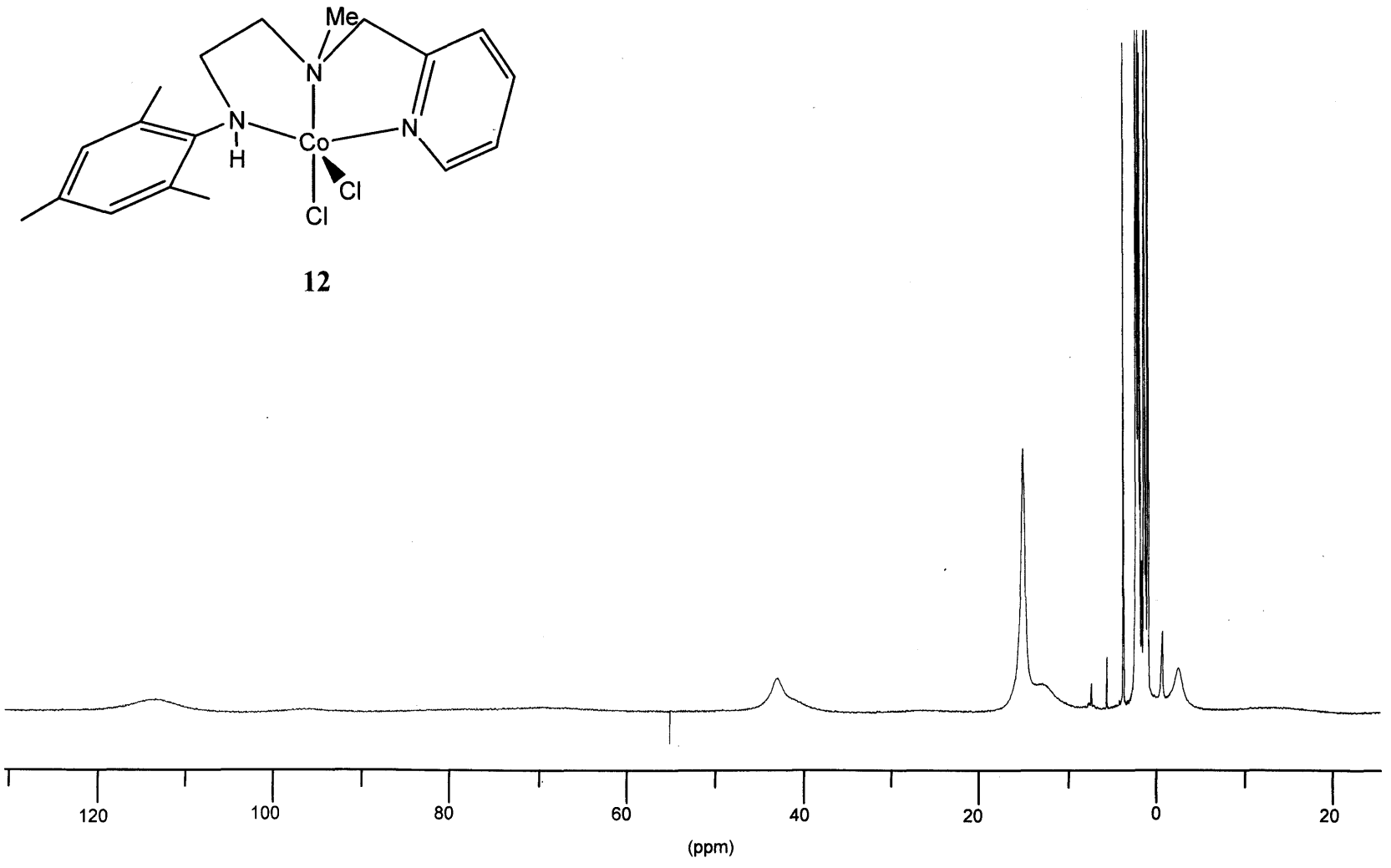

Figure 4 ^{1}H NMR spectrum of [{**LII**}$CoCl_2$] (**12**) in CD_3CN at rt

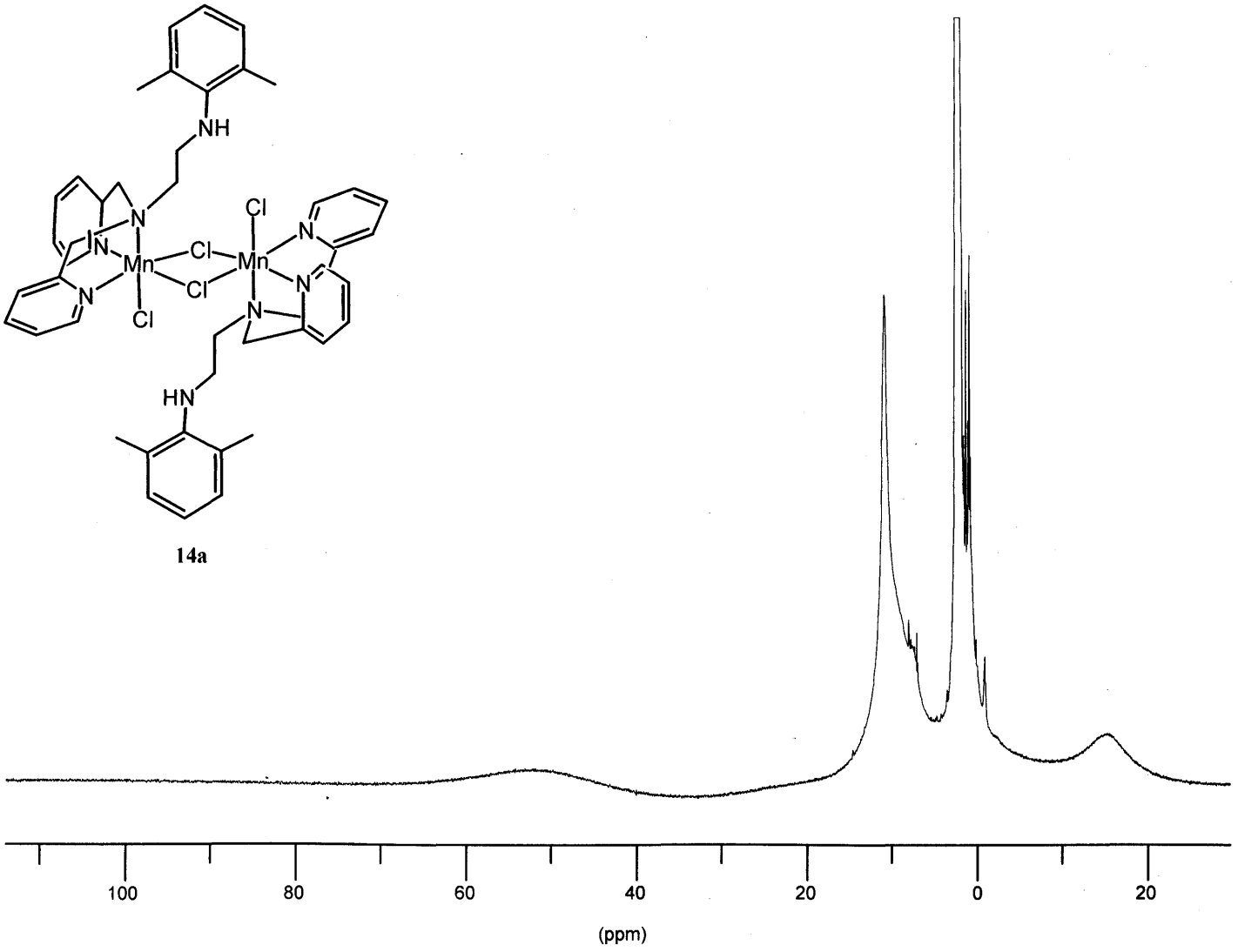

14a

Figure 5 ^{1}H NMR spectrum of [{**LIVa**}$MnCl_2$)]$_2$ (**14a**) in CD_3CN at rt

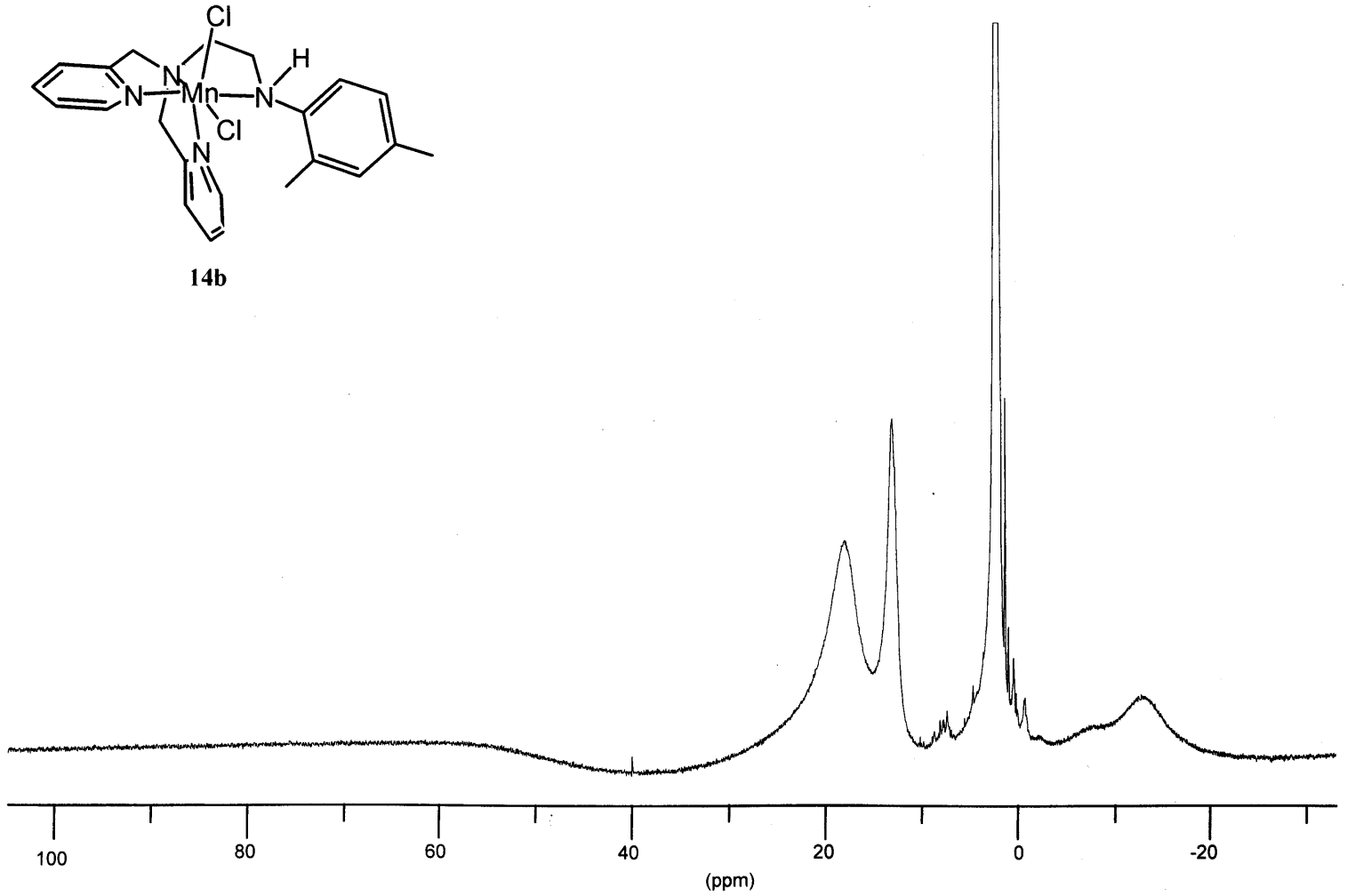

Figure 6 ^{1}H NMR spectrum of [{**LIVb**}$MnCl_2$)]$_2$ (**14b**) in CD_3CN at rt

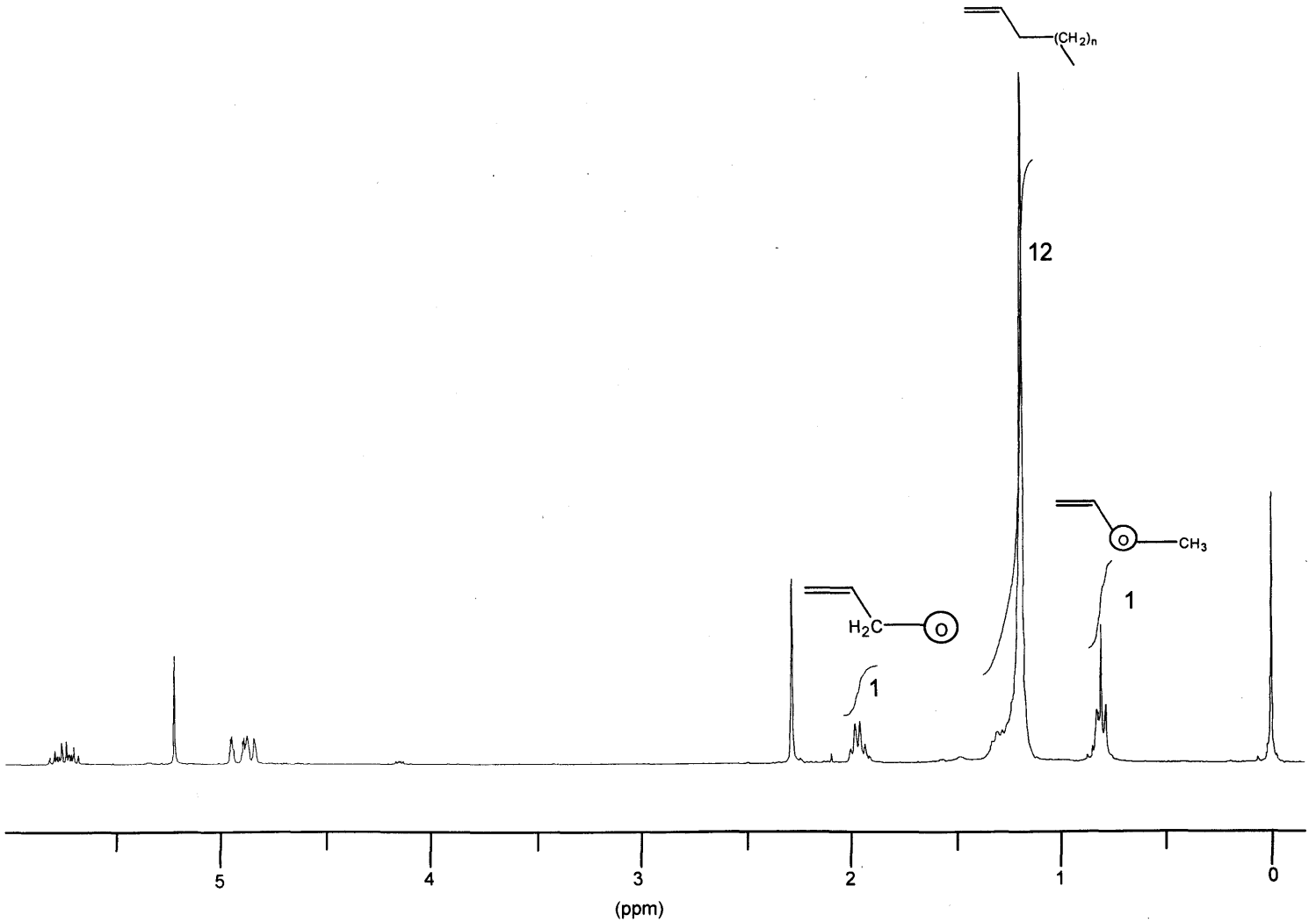

Figure 7 ^{1}H NMR spectrum of oligomers in $CDCl_3$ at rt: **10a**/MAO, 1 bar ethylene pressure, 20 °C, integration per H

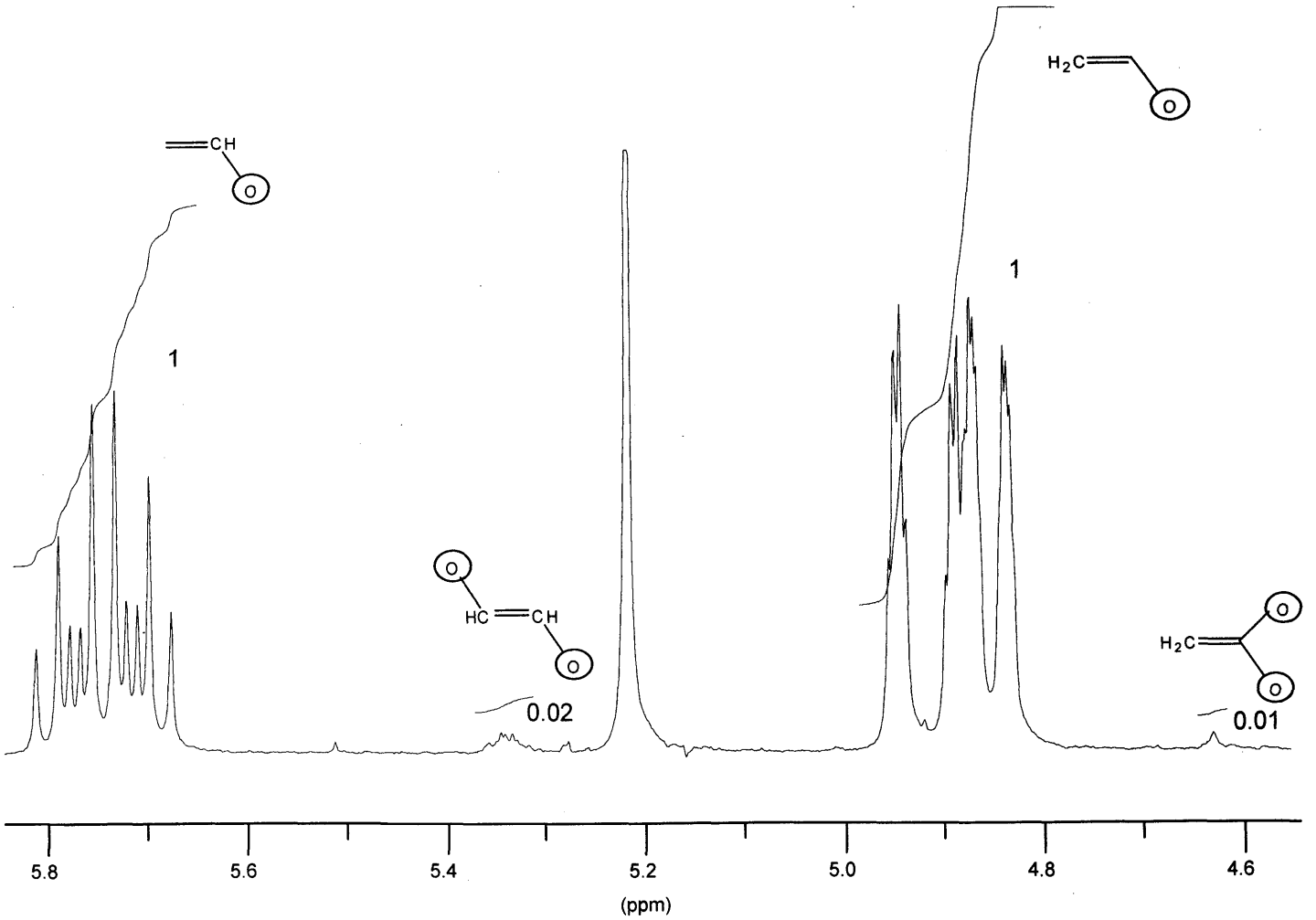

Figure 8 ^{1}H NMR spectrum of oligomers in $CDCl_3$ at rt: **10a**/MAO, 1 bar ethylene pressure, 20 °C, integration per H

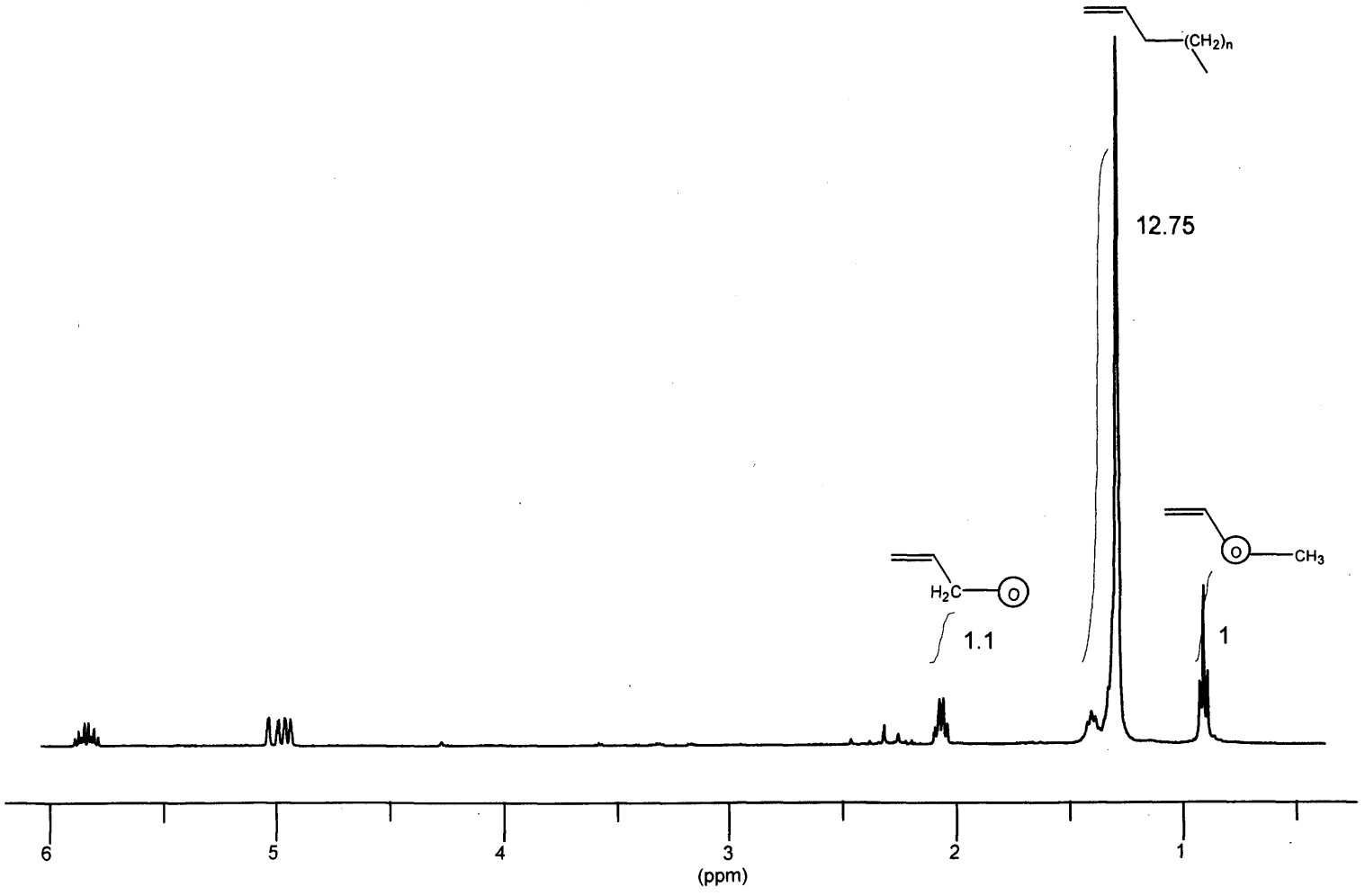

Figure 9 ^{1}H NMR spectrum of oligomers in $CDCl_3$ at rt: **10c**/MAO, 1 bar ethylene pressure, 20 °C, integration per H

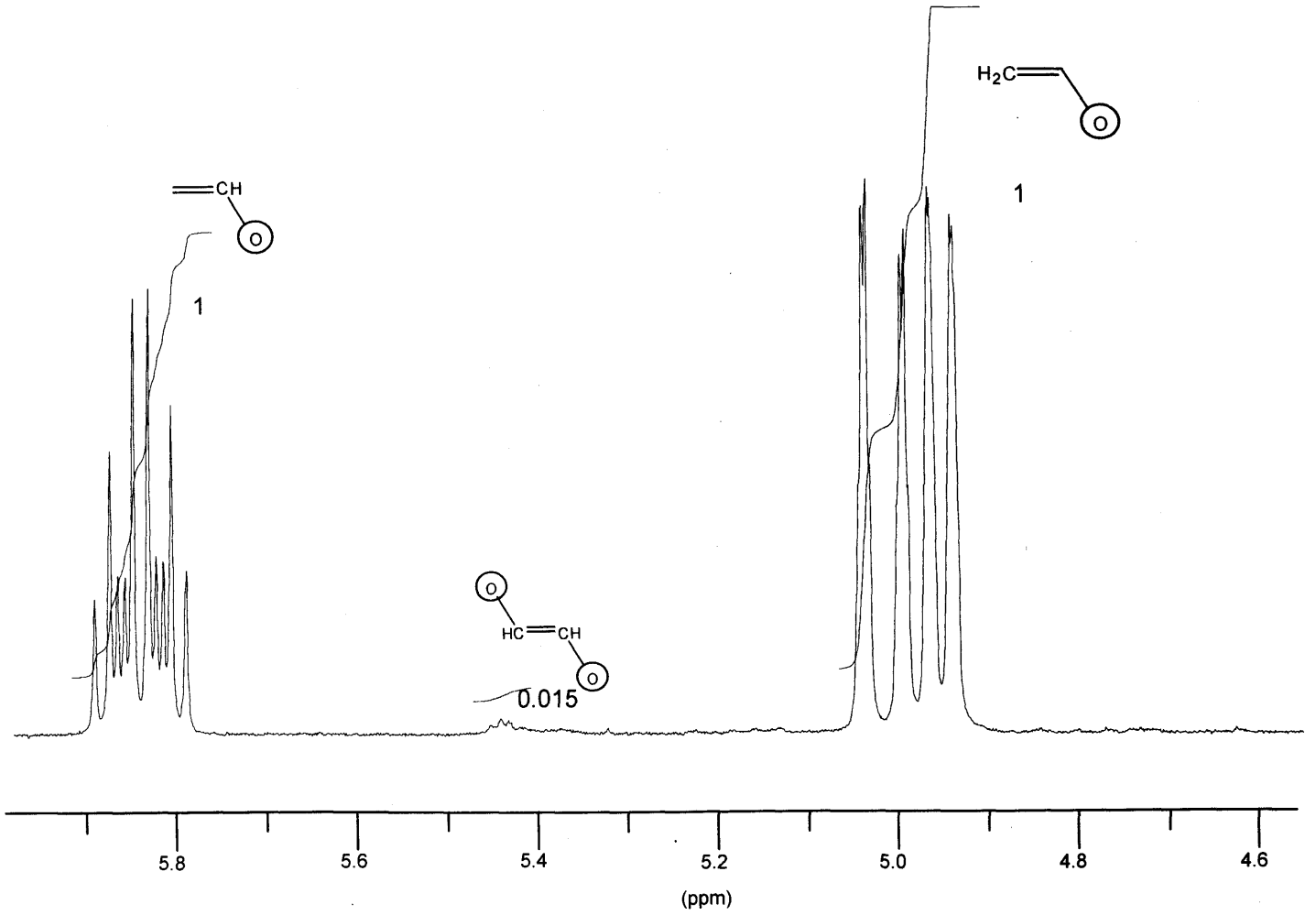

Figure 10 ^{1}H NMR spectrum of oligomers in $CDCl_3$ at rt: **10c**/MAO, 1 bar ethylene pressure, 20 ^{o}C, integration per H

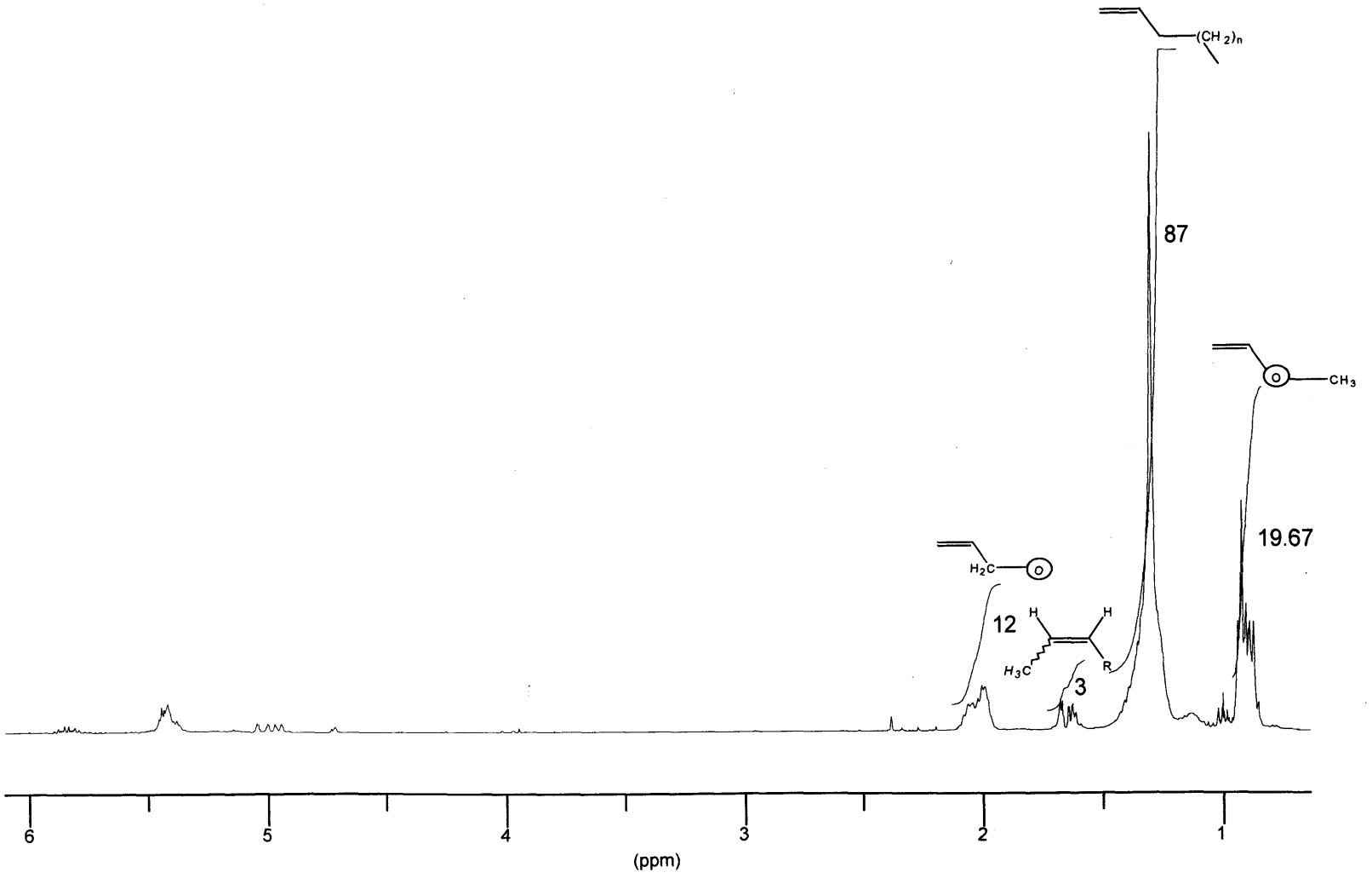

Figure 11 ^{1}H NMR spectrum of oligomers in $CDCl_3$ at rt: **11a**/MAO, 1 bar ethylene pressure, 20 °C, integration per H

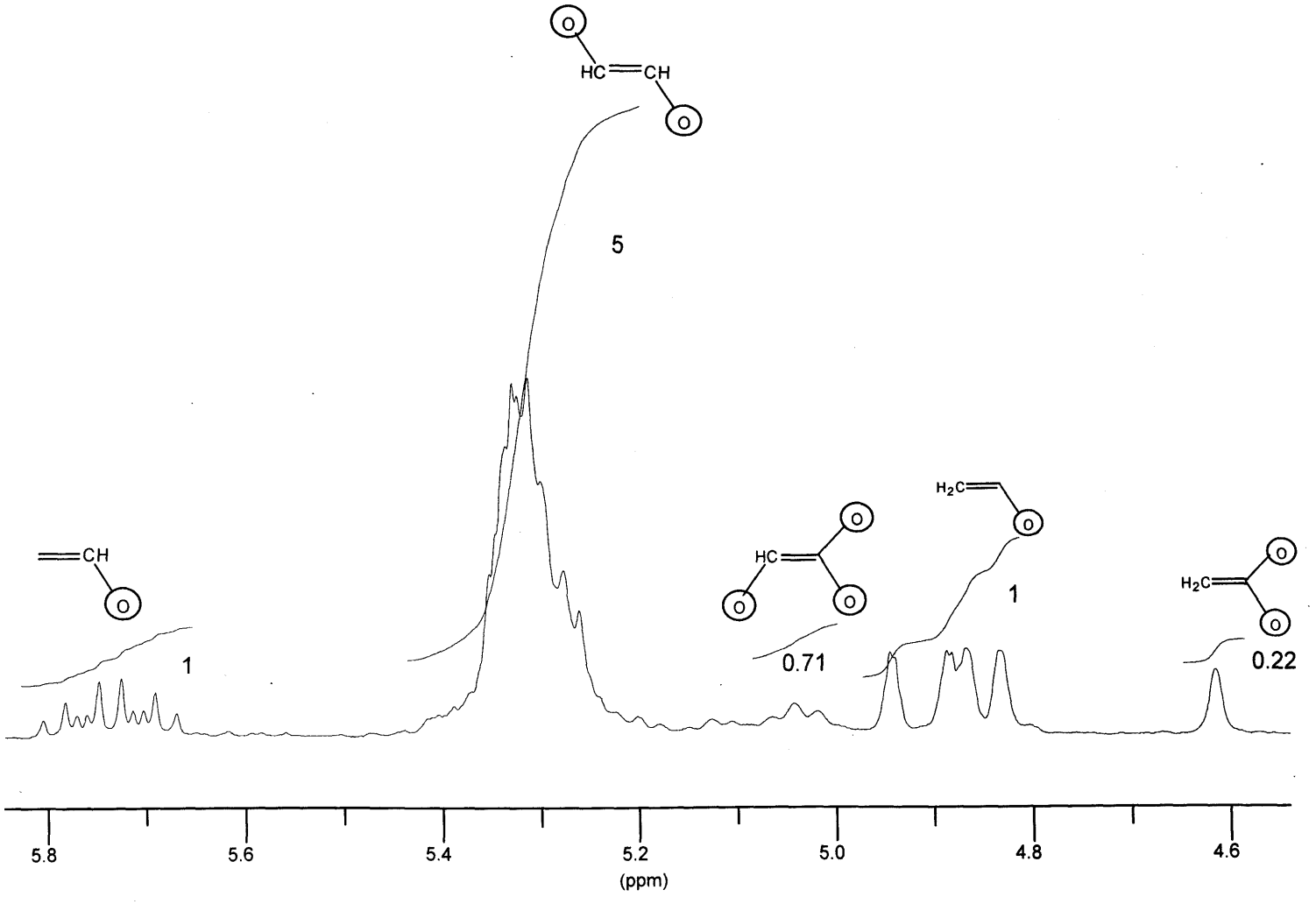

Figure 12 ^{1}H NMR spectrum of oligomers in $CDCl_3$ at rt: **11a**/MAO, 1 bar ethylene pressure, 20 ^{o}C, integration per H

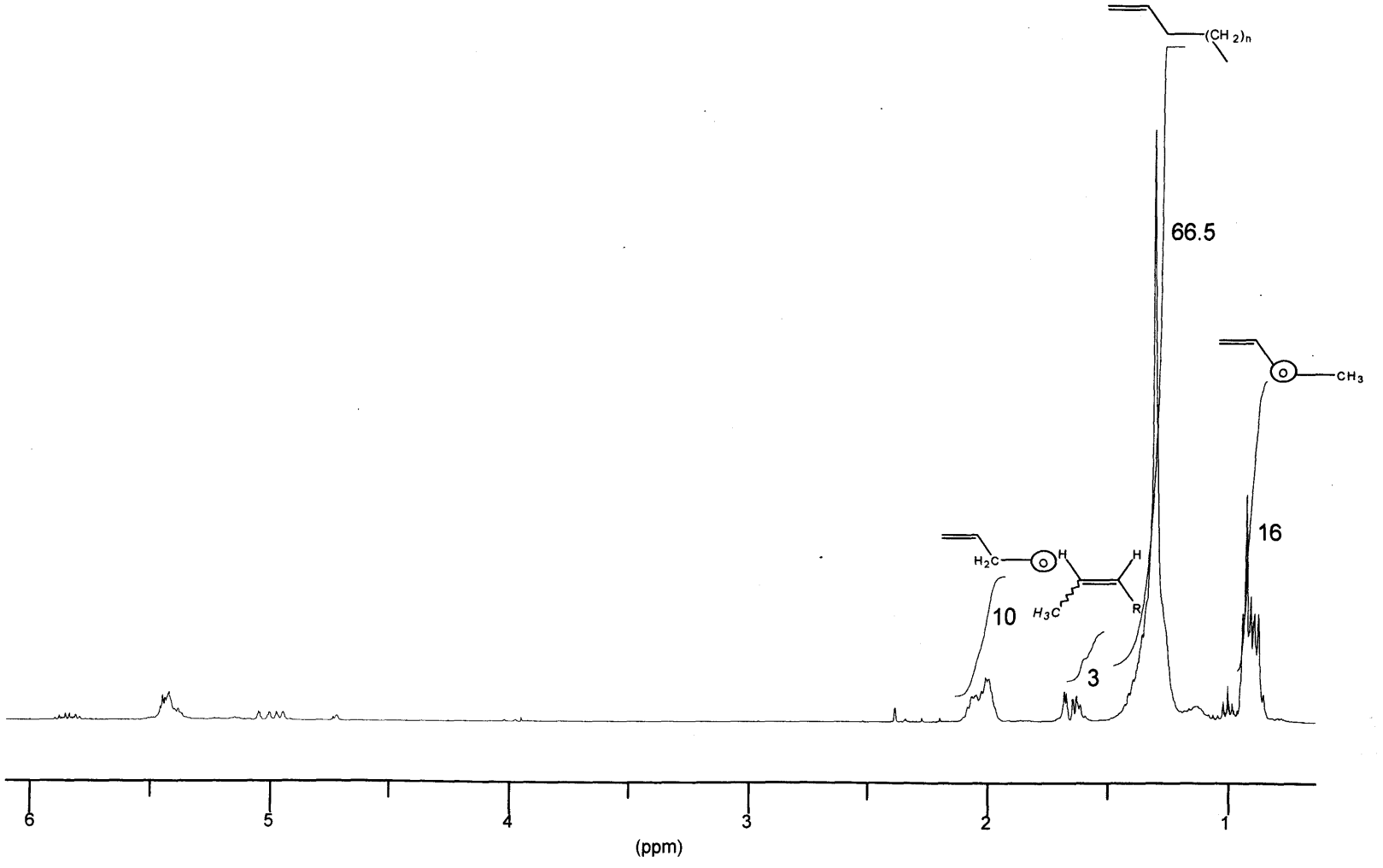

Figure 13 ^{1}H NMR spectrum of oligomers in $CDCl_3$ at rt: **16b**/MAO, 1 bar ethylene pressure, 20 ^{o}C, integration per H

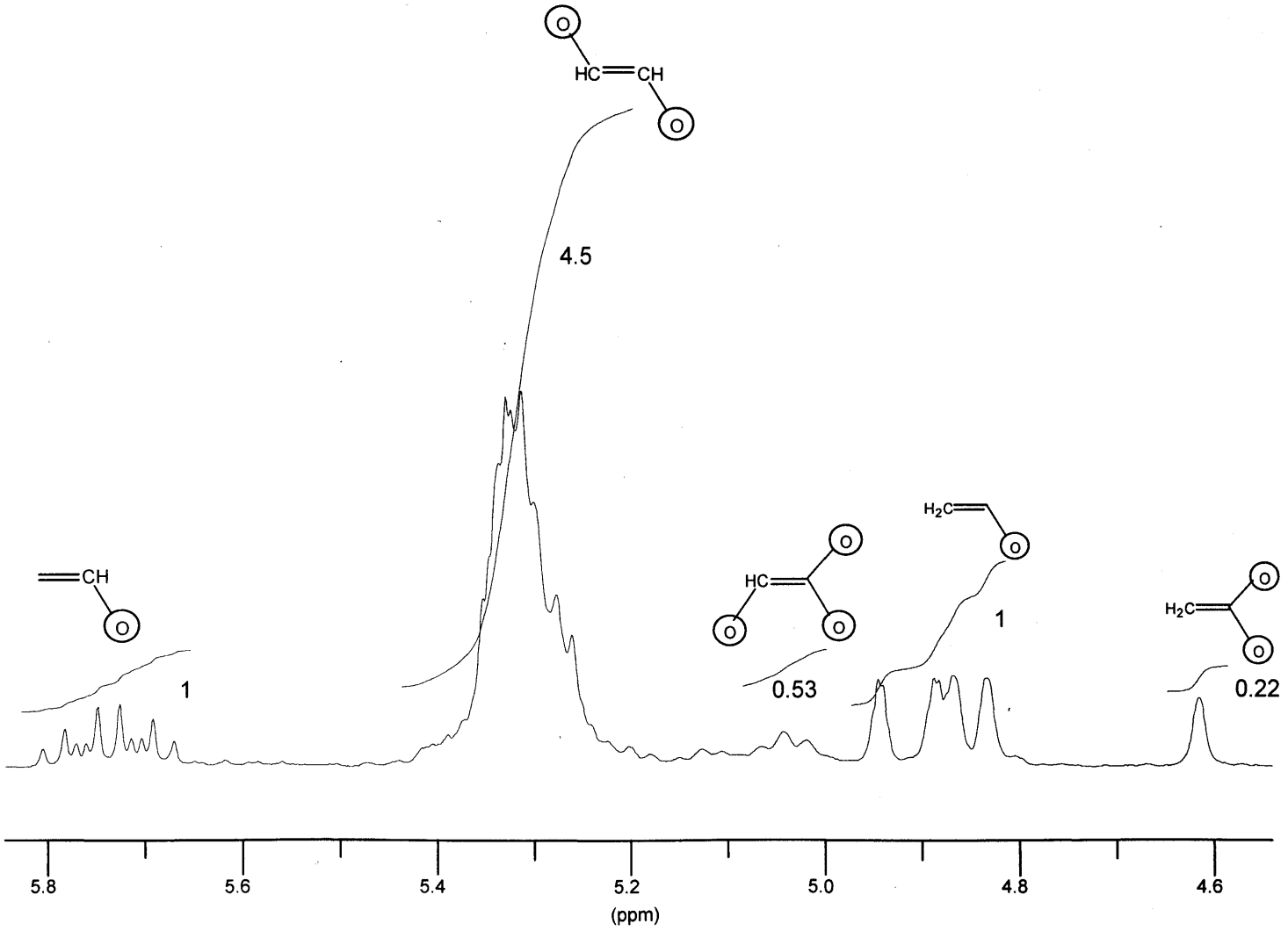

Figure 14 ^{1}H NMR spectrum of oligomers in $CDCl_3$ at rt: **16b**/MAO, 1 bar ethylene pressure, 20 °C, integration per H

Table 1 Ratio of Me:olefinic H

Precatalyst[a]	Time (h)	$Ratio_{exp}$ of Me:olefinic H[b]	$Ratio_{calc}$ of Me:olefinic H[c]
10a	0.5	1:1	1:1
10c	0.5	1:1	1:1
11a	0.25	≈2:1	2.7:1
11a	0.5	≈2:1	2.93:1
11a	1	≈2:1	3:1
11c	0.5	≈2:1	3:1
11d	0.5	≈2:1	3:1
16a	0.5	≈2:1	2.69:1
16b	0.5	≈2:1	2.6:1
17a	0.25	≈2:1	2.64:1
17a	0.5	≈2:1	2.67:1
17a	1	≈2:1	2.66:1

[a] *General conditions*: 1 bar ethylene Schlenk test carried out in toluene (40 ml) at 20 °C, using 4.0 mmol MAO (Al:M = 400:1), 0.01 mmol precatalyst. Reactions terminated by addition of dilute HCl; [b] Ratio of Me:olefinic H *if* no internal branching was present.

8. Postgraduate Record

Attended and participated conferences

22-26/04/01	Catalysis Summer School Leverhulme Centre for Applied Catalysis Liverpool University, UK	**Presented Poster**
5-6/07/01	RSC Coordination Chemistry Discussion Group Annual Conference University of York, UK	**Presented Poster**
8-12/07/02	XXth International Conference of OrganoMetallic Chemistry (ICOMC) Corfu Imperial Hotel, Corfu, Greece	**Presented Poster**
23-27/03/03	*225th American Chemical Society (ACS) National Meeting* Ernest N. Morial Convention Centre, New Orleans, USA	**Presented Poster**
9-11/07/03	RSC Coordination Chemistry Discussion Group Annual Conference University of Manchester, UK	**Presented Seminar**

ExxonMobil project reports

		Attendees
Nov. 2000	Project report I Oral Presentation and Written Report University of Leicester	Dr R. Shutt
Feb. 2001	Project report Ia Oral Presentation and Written Report University of Leicester	Dr R. Shutt, Dr J. P. Stokes and Dr R. J. Wittenbrink
Aug. 2001	Project report II Oral Presentation and Written Report University of Leicester	Dr R. Shutt
Dec. 2001	Project report III Oral Presentation and Written Report University of Leicester	Dr R. Shutt
Sep. 2002	Project report IV Oral Presentation and Written Report ExxonMobil, Notre-Dame de Gravenchon, Normandie, France	Dr R. Shutt
Oct. 2002	Project report IVa Oral Presentation and Written Report University of Leicester	Dr R. Shutt and Dr D. McConville
Mar. 2003	Project report V Oral Presentation and Written Report University of Leicester	Dr R. Shutt
Sep. 2003	Project report VI Oral Presentation and Written Report University of Leicester	Dr R. Shutt